



University of  
**Salford**  
MANCHESTER

Defining the Role of Endonuclease VIII-Like 1 and 3 in the Repair of Interstrand Crosslinks in  
Cancer Cells.

Graham Asher Burberry

Supervisor: Dr Rhoderick Elder

School of Science, Engineering and Environment,  
University of Salford.

Submitted in Partial Fulfilment of the Requirements of the Degree of Doctor of  
Philosophy,  
July 2022.

## Table of Contents

<b>List of Figures .....</b>	<b>iv</b>
<b>List of Tables .....</b>	<b>x</b>
<b>Acknowledgements .....</b>	<b>xii</b>
<b>Abbreviations .....</b>	<b>xiv</b>
<b>Abstract .....</b>	<b>xvii</b>
<b>Chapter 1 Introduction .....</b>	<b>1</b>
<b>1.1. Cancer .....</b>	<b>2</b>
<b>1.2. DNA Stability .....</b>	<b>3</b>
1.2.1. DNA Oxidation.....	3
1.2.2. Interstrand Crosslinks .....	8
<b>1.3. DNA Repair.....</b>	<b>11</b>
<b>1.4. Fanconi Anaemia Pathway .....</b>	<b>12</b>
<b>1.5. Base Excision Repair .....</b>	<b>18</b>
1.5.1. DNA Glycosylases .....	21
1.5.1.1. NEIL1 .....	24
1.5.1.2. NEIL2 .....	26
1.5.1.3. NEIL3 .....	26
<b>1.6. Hypothesis .....</b>	<b>28</b>
<b>Chapter 2 Materials and Methods .....</b>	<b>31</b>
<b>2.1 Materials.....</b>	<b>31</b>
2.1.1. Cell lines .....	31
2.1.2. Cell Culture Reagents .....	33
2.1.3. Microbiology and Molecular Biology Reagents .....	35
2.1.4. Buffers .....	36
2.1.5. Plasmids.....	38
2.1.6. Nucleotide Sequences.....	39
<b>2.2. Plasmid Sub-Cloning Methods.....</b>	<b>41</b>
2.2.1. Agarose Gel Electrophoresis .....	41

2.2.2. Polymerase Chain Reaction (PCR).....	42
2.2.3. ZeroBlunt Cloning .....	43
2.2.4. Plasmid Purification: Mini-Prep .....	44
2.2.5. Restriction Double-Digest .....	45
2.2.6. Purification of DNA Fragments .....	46
2.2.7. T4 DNA Ligation.....	47
2.2.8. Sanger DNA Sequencing.....	48
<b>2.3. Cell Culture Methods .....</b>	<b>48</b>
2.3.1. Cell Counting.....	49
2.3.2. Freeze/Thaw Protocol for Cell Lines.....	50
2.3.3. Mycoplasma Contamination Detection and Treatment .....	51
2.3.4. MTT/MTS Assay.....	53
2.3.5. Determination of Cell Growth Rate.....	54
2.3.6. The Effect of Genotoxic Agents on Cell Growth .....	55
2.3.7. Plasmid Transfection .....	56
2.3.8. Antibiotic-Selection.....	57
2.3.9. Short Interfering RNA (siRNA) Transfection .....	58
<b>2.4. Determination of Gene Expression by Reverse Transcription PCR (RT-PCR)</b> .....	<b>58</b>
2.4.1. RNA Extraction .....	59
2.4.2. Reverse Transcription and RT-PCR .....	60
<b>2.5. Protein Expression and Detection .....</b>	<b>61</b>
2.5.1. Protein Extraction and Quantification .....	62
2.5.2. Sodium Dodecyl Sulfate–Polyacrylamide Gel Electrophoresis (SDS-PAGE) .	62
2.5.3. Western Blotting.....	64
<b>Chapter 3 Results.....</b>	<b>66</b>
<b>3.1. Initial Cell Culture Experiments.....</b>	<b>66</b>
3.1.1. Cell Growth Analysis .....	69
3.1.2. Cell Growth after Genotoxin Treatment.....	73
3.1.3. Gene Expression Studies .....	75
<b>3.2. Cell Culture of the FANCD2-related Cell lines .....</b>	<b>76</b>
3.2.1. Cell Growth Analysis .....	78

3.2.2. Cell Growth after Genotoxin Treatment.....	83
3.2.3. Gene and Protein Expression Studies .....	90
<b>3.3. Generating pcDNA3.1-hNEIL3<sup>FL</sup>-FLAG and pcDNA3.1-hNEIL3<sup>1506</sup>-FLAG..</b>	<b>98</b>
3.3.1. Preparation of pcDNA3.1-hNEIL3 <sup>FL</sup> -FLAG Plasmid.....	100
3.3.2. Cloning and Purification of the hNEIL3 <sup>FL</sup> -FLAG Insert .....	102
3.3.3. Isolation and Purification of the pcDNA3.1 Vector .....	105
3.3.4. Confirmation of pcDNA3.1-NEIL3 <sup>FL</sup> -FLAG plasmid .....	105
3.3.5. Isolation, Cloning and Purification of the hNEIL3 <sup>1506</sup> -FLAG Insert .....	108
3.3.6. Confirmation of pcDNA3.1-hNEIL3 <sup>1506</sup> -FLAG plasmid.....	110
<b>3.4. Survival of FANCD2-Related Cells when Expressing Recombinant Proteins</b>	<b>112</b>
3.4.1. Evidence of Recombinant Protein Expression .....	114
3.4.2. Survival of Plasmid-Transfected Cells .....	120
3.4.3. Evidence of Recombinant Protein Expression after Antibiotic-selection .....	132
3.4.4. Survival of Plasmid-Transfected Cells after Antibiotic-selection.....	140
<b>3.5. Survival of PD20 and 3.15 Cells after Gene-Specific Knockdown.....</b>	<b>151</b>
3.5.1. Evidence of NEIL3 and TRIM26 Protein and mRNA Knockdown.....	153
3.5.2. Survival of siRNA-Transfected Cells Following Treatment with Genotoxic Agents.....	157
<b>Chapter 4 Discussion.....</b>	<b>163</b>
4.1. NEIL1, NEIL3 <sup>FL</sup> , and NEIL3 <sup>1506</sup> Overexpression in FA cells .....	168
4.2. NEIL3 and TRIM26 Knockdown in PD20 and 3.15 Cells.....	175
<b>Chapter 5 Conclusion and Future Work.....</b>	<b>178</b>
<b>References.....</b>	<b>180</b>
<b>Appendix.....</b>	<b>193</b>

## List of Figures

Figure 1.1: Products of Guanine oxidation.....	5
Figure 1.2: Products of adenine oxidation.....	5
Figure 1.3: Products of thymine and cytosine oxidation.....	6
Figure 1.4: DNA crosslinking agents and the structure of the interstrand crosslinks (ICL) produced.....	9
Figure 1.5: ICL unhooking and repair through the Fanconi Anaemia pathway.....	16
Figure 1.6: Activity of mono- and bi-functional DNA glycosylases showing the different ends produced.....	18
Figure 1.7: Base excision repair.....	20
Figure 1.8: Conserved domains of the DNA glycosylase NEIL1.....	25
Figure 1.9: Conserved domains of the DNA glycosylase NEIL2.....	26
Figure 1.10: Conserved domains of the DNA glycosylase NEIL3.....	27
Figure 1.11: Overall flowchart of the thesis project.....	29
Figure 2.1: Vector map of pcDNA3.1 with restriction digest sites in forward (+) or reverse (-).....	48
Figure 2.2: Neubauer haemocytometer grid with grid sections highlighted in red for cell counting.....	50
Figure 2.3: Mathematical formulas for calculating the cell concentration (cells/ml) and percentage cell viability.....	50
Figure 3.1: Flowchart on the approach to cell line analysis work.....	67
Figure 3.2: Mycoplasma detection from cultured cells before (A) and after (B) Plasmocin (InvivoGen) treatment.....	68
Figure 3.3: Growth of HSC-93 (green), HSC-72 (red) and HSC-72-Corrected (blue), determined using MTS assay.....	70
Figure 3.4: MTS assay to determine the growth characteristics of HSC-93 (green), HSC-72 (red) and HSC-72-Corrected (blue) cells.....	72

Figure 3.5: Growth inhibition of HSC-93 (WT, green), HSC-72 (FANCA deficient, red) and HSC-72-Corrected (blue) following treatment with A) mitomycin C (MMC), B) cisplatin, and C) TBHP.....	74
Figure 3.6: Expression of <i>GAPDH</i> , <i>NEIL1</i> and <i>NEIL3</i> from cell lines U2OS (WT, grey), HSC-93 (WT, green), HSC-72 (FANCA deficient, red) and HSC-72-Corrected (blue) by RT-PCR. ....	76
Figure 3.7: Refined flowchart on the approach to cell line analysis work. ....	78
Figure 3.8: Growth of PD20 (FAND2 deficient, red) and 3.15 (PD20 corrected, blue) determined using the MTT assay.....	80
Figure 3.9: Growth of U2OS (WT, blue) and U2OS-D2 (FANCD2 deficient, red) determined using the MTT assay.....	81
Figure 3.10: Growth of HeLa (WT, blue) and HeLa-D2 (FANCD2 deficient, red) determined using the MTT assay.....	82
Figure 3.11: Growth inhibition of PD20 (FANCD2 deficient, red) and 3.15 (PD20 Corrected, blue) following treatment with A) mitomycin C (MMC), B) cisplatin, and C) TBHP. ....	85
Figure 3.12: Growth inhibition of U2OS (WT, blue) and U2OS-D2 (FANCD2 deficient, red) following treatment with A) mitomycin C (MMC), B) cisplatin and C) TBHP. ....	87
Figure 3.13: Growth inhibition of HeLa (WT, blue) and HeLa-D2 (FANCD2 deficient, red) following treatment with A) mitomycin C (MMC), B) cisplatin and C) TBHP. ....	89
Figure 3.14: Expression of <i>GAPDH</i> , <i>NEIL1</i> , <i>NEIL2</i> , <i>NEIL3</i> , <i>FANCA</i> , <i>FANCD2</i> , <i>ERCC1</i> , and $\beta$ -Actin from cell lines A(i) 3.15 (PD20 corrected) and A(ii) PD20 (FANCD2 deficient), by RT-PCR.....	92
Figure 3.15: Expression of <i>GAPDH</i> , <i>NEIL1</i> , <i>NEIL2</i> , <i>NEIL3</i> , <i>FANCD2</i> and <i>FANCA</i> from cell-lines A(i) U2OS (WT) and A(ii) U2OS-D2 (FANCD2 deficient), by RT-PCR..	94
Figure 3.16: Expression of <i>GAPDH</i> , <i>NEIL1</i> , <i>NEIL2</i> , <i>NEIL3</i> , <i>FANCD2</i> and <i>FANCA</i> from cell-lines A(i) HeLa (WT) and A(ii) HeLa-D2 (FANCD2 deficient), by RT-PCR. ...	96
Figure 3.17: Western blots of PD20 (FANCD2 Deficient), 3.15 (PD20 corrected), HeLa (WT), HeLa-D2 (FANCD2 deficient), U2OS (WT) and U2OS-D2 (FANCD2 deficient) cell extracts. (A) FANCD2, (B) NEIL3, (C) NEIL1, and (D) $\beta$ -Actin. ....	97

Figure 3.18: Flowchart on the approach to plasmid generation work. ....	99
Figure 3.19: Amplification of hNEIL3 <sup>FL</sup> -FLAG and hNEIL3 <sup>843</sup> -FLAG from pETDUET2-hNEIL3. ....	100
Figure 3.20: Amplification of hNEIL3 <sup>FL</sup> -FLAG from pETDUET2-hNEIL3. ....	101
Figure 3.21: Analysis of hNEIL3 <sup>FL</sup> -FLAG insert in pCR-Blunt II-TOPO-hNEIL3 <sup>FL</sup> -FLAG, using EcoRI or XbaI.....	103
Figure 3.22: Sequential digestion of pCR-Blunt II-TOPO-hNEIL3 <sup>FL</sup> -FLAG using restriction enzymes EcoRI and XbaI. ....	104
Figure 3.23: Digestion of pcDNA3.1-hNEIL1-FLAG using XbaI and EcoRI. ....	105
Figure 3.24: Confirmation of hNEIL3 <sup>FL</sup> -FLAG insert in pcDNA3.1-hNEIL3 <sup>FL</sup> -FLAG, using XbaI and EcoRI. ....	106
Figure 3.25: Confirmation of pcDNA3.1-hNEIL3 <sup>FL</sup> -FLAG through Sanger-sequencing.	107
Figure 3.26: Amplification of the hNEIL3 <sup>1506</sup> -FLAG insert from pcDNA3.1-hNEIL3 <sup>FL</sup> -FLAG.....	108
Figure 3.27: Analysis of hNEIL3 <sup>1506</sup> -FLAG insert from pCR-Blunt II-TOPO-hNEIL3 <sup>1506</sup> -FLAG, with XbaI (A) followed by EcoRI (B). ....	109
Figure 3.28: Confirmation of the hNEIL3 <sup>1506</sup> -FLAG insert in pcDNA3.1-hNEIL3 <sup>1506</sup> -FLAG, using XbaI and EcoRI. ....	110
Figure 3.29: Confirmation of pcDNA3.1-hNEIL3 <sup>1506</sup> -FLAG through Sanger-sequencing. ....	111
Figure 3.30: Flowchart on the approach to plasmid transfection and cell survivability work. ....	113
Figure 3.31: Western blots of PD20 (FANCD2 Deficient, A[i – iv]) and 3.15 (PD20 corrected, B[i – iv]) cell extracts following transfection with different plasmids. (A, B) i) NEIL3, ii) NEIL1, iii) FLAG-tag, and iv) $\beta$ -Actin. ....	116
Figure 3.32: Western blots of plasmid-transfected HeLa (WT) and U2OS (WT) cell extracts for FLAG-tag.....	117
Figure 3.33: Western blots of plasmid-transfected HeLa (WT, A[i – iv]), HeLa-D2 (FANCD2 deficient, B[i – iv]), U2OS (WT, C[i – iv]) and U2OS-D2 (FANCD2	

deficient, D[i – iv]) cell extracts. (A – D) i) NEIL3, ii) NEIL1, iii) FLAG-tag, and iv) $\beta$ -Actin. ....	119
Figure 3.34: Growth inhibition of plasmid transfected A) PD20 (FANCD2 deficient) following mitomycin C (MMC) treatment based on initial western blot confirmation. ....	121
Figure 3.35: Growth inhibition comparison of plasmid transfected A) 3.15 (PD20 Corrected, blue) and PD20 (FANCD2 deficient, red), following treatment with mitomycin C (MMC).....	123
Figure 3.36: Growth inhibition comparison of plasmid transfected A) 3.15 (PD20 Corrected, blue) and PD20 (FANCD2 deficient, red), following treatment with cisplatin. ....	124
Figure 3.37: Growth inhibition of plasmid transfected (A) 3.15 (PD20 Corrected, blue) and (B) PD20 (FANCD2 deficient, red), and their comparison (C), following treatment with TBHP. ....	125
Figure 3.38: Growth inhibition of plasmid transfected HeLa (WT, blue) and HeLa-D2 (FANCD2 deficient, red), following treatment with mitomycin C (MMC, A), cisplatin (B), and TBHP (C).....	127
Figure 3.39: Growth inhibition of plasmid transfected A) U2OS (WT, blue) and U2OS-D2 (FANCD2 deficient, red), following treatment with mitomycin C. ....	129
Figure 3.40: Growth inhibition of plasmid transfected A) U2OS (WT, blue) and U2OS-D2 (FANCD2 deficient, red), following treatment with cisplatin.....	130
Figure 3.41: Growth inhibition of plasmid transfected (A) U2OS (WT, blue) and (B) U2OS-D2 (FANCD2 deficient, red), and their comparison (C), following treatment with TBHP.....	131
Figure 3.42: Antibiotic titration of HEK293T (WT), HeLa (WT) and HeLa-D2 (FANCD2 deficient) with antibiotic selector G418. ....	134
Figure 3.43: Antibiotic-selection (A) and western blots on cell extracts (B) of plasmid-transfected HeLa (WT) and HeLa-D2 (FANCD2 deficient). (B) i) NEIL3, ii) NEIL1, iii) FLAG-tag, and iv) $\beta$ -Actin. ....	136
Figure 3.44: Antibiotic-selection (A) and western blots on cell extracts (B) of plasmid-transfected HEK293T (WT). (B) i) FLAG-tag, and ii) $\beta$ -Actin. ....	138

Figure 3.45: Growth inhibition of antibiotic selected (A) U2OS (WT, blue) and (B) U2OS-D2 (FANCD2 deficient, red), and their comparison (C), following treatment with mitomycin C. ....	142
Figure 3.46: Growth inhibition of antibiotic selected (A) U2OS (WT, blue) and (B) U2OS-D2 (FANCD2 deficient, red), and their comparison (C), following treatment with cisplatin.....	143
Figure 3.47: Growth inhibition of antibiotic selected (A) U2OS (WT, blue) and (B) U2OS-D2 (FANCD2 deficient, red), and their comparison (C), following treatment with TBHP.....	145
Figure 3.48: Growth inhibition of antibiotic selected HeLa (WT, blue) and HeLa-D2 (FANCD2 deficient, red), following treatment with mitomycin C. ....	147
Figure 3.49: Growth inhibition of antibiotic selected HeLa (WT, blue) and HeLa-D2 (FANCD2 deficient, red), following treatment with cisplatin.....	149
Figure 3.50: Growth inhibition of antibiotic selected HeLa (WT, blue) and HeLa-D2 (FANCD2 deficient, red), following treatment with TBHP.....	150
Figure 3.51: Flowchart on the approach to siRNA transfection and cell survivability work. ....	152
Figure 3.52: Western blots of siRNA-transfected A) PD20 (FANCD2 Deficient) and B) 3.15 (PD20 corrected) cell extracts. (A, B) (i) TRIM26, (ii) GAPDH, and (iii) $\beta$ -Actin..	154
Figure 3.53: RT-PCR of siRNA reverse-transfected PD20 (FANCD2 deficient). Expression of <i><math>\beta</math>-Actin</i> , <i>NEIL1</i> and <i>NEIL3</i> after siRNA transfection targeting A) control (no transfection, lanes 2 – 4), control (non-specific siRNA, lanes 5 – 7), NEIL3 (NEIL3 siRNA, lanes 8 – 10), and TRIM26 (TRIM26 siRNA, lanes 11 – 13).....	156
Figure 3.54: RT-PCR of siRNA reverse-transfected 3.15 (PD20 corrected). Amplification of $\beta$ -Actin, NEIL1 and NEIL3 after siRNA transfection targeting control (no transfection, lanes 2 – 4), control (non-specific siRNA, lanes 5 – 7), NEIL3 (NEIL3 siRNA, lanes 8 – 10), and TRIM26 (TRIM26 siRNA, lanes 11 – 13). ....	157
Figure 3.55: Growth inhibition of siRNA transfected (A) 3.15 (PD20 Corrected, blue) and (B) PD20 (FANCD2 deficient, red), and their comparison (C), following treatment with mitomycin C (MMC).....	159

Figure 3.56: Growth inhibition of siRNA transfected (A) 3.15 (PD20 Corrected, blue) and (B) PD20 (FANCD2 deficient, red), and their comparison (C), following treatment with cisplatin..... 160

Figure 3.57: Growth inhibition of siRNA transfected (A) 3.15 (PD20 Corrected, blue) and (B) PD20 (FANCD2 deficient, red), and their comparison (C), following treatment with TBHP..... 162

## List of Tables

Table 1.1: Radical and nonradical reactive oxygen species (ROS).....	4
Table 1.2: Gene names and molecular function of the Fanconi Anaemia complementation groups (FANCs) in the Fanconi Anaemia (FA) pathway.....	14
Table 1.3: General summary of the structural motif superfamilies, name, class and common lesions targeted by mammalian DNA glycosylases. ....	22
Table 2.1: Fanconi anaemia cell line information. ....	32
Table 2.2: Cell lines and culture media. ....	33
Table 2.3: Cell culture reagents. ....	34
Table 2.4: Details of the genotoxic agents. ....	34
Table 2.5: Microbiology Reagents .....	35
Table 2.6: LB medium and LB-agar.....	35
Table 2.7: Primary and secondary antibodies used for probing proteins $\beta$ -Actin, FANCD2, FLAG-tag, GAPDH, NEIL1, NEIL3, and TRIM26.....	36
Table 2.8: List of pre-prepared buffers.....	37
Table 2.9: Lysis buffer for protein extraction.....	37
Table 2.10: 10x SDS-PAGE running buffer and 10x western blot (WB) transfer buffer. ..	37
Table 2.11: 3x SDS-PAGE loading buffer. ....	38
Table 2.12: Western blot blocking buffer and wash buffer. ....	38
Table 2.13: List of PCR primers for amplification of hNEIL3 <sup>843</sup> , hNEIL3 <sup>1506</sup> and hNEIL3 <sup>FL</sup> inserts.....	39
Table 2.14: Primers for amplification of $\beta$ -Actin, ERCC1, FANCA, FANCD2, GAPDH, NEIL1, NEIL2, and NEIL3, and their expected PCR product size. ....	40
Table 2.15: siRNA for targeted knockdown.....	41
Table 2.16: Phusion and Q5 PCR reaction mixture.....	42
Table 2.17: Thermocycling conditions for Phusion or Q5 PCR.....	43
Table 2.18: Ligation reaction mixture. ....	44

Table 2.19: Restriction double-digest reaction mixture. ....	45
Table 2.20: T4 ligation reaction mixture. ....	47
Table 2.21: PCR reaction mixtures for mycoplasma detection (Sigma-Aldrich kit). ....	51
Table 2.22: Thermocycling conditions for mycoplasma detection (Sigma-Aldrich kit)....	52
Table 2.23: PCR reaction mixtures for mycoplasma detection (ABM kit). ....	52
Table 2.24: Thermocycling conditions for mycoplasma detection (ABM kit). ....	53
Table 2.25: Genomic DNA removal reaction mixture. ....	60
Table 2.26: RT-PCR reaction mixture.....	60
Table 2.27: PCR conditions for RT-PCR. ....	61
Table 2.28: Components required for producing a 4% stacking gel and 12% separating gel for three 1.0 mm or two 1.5 mm SDS-PAGE Mini-gels. ....	63
Table 4.1: Growth inhibition summary of FANCD2-deficient (PD20, U2OS-D2 and HeLa- D2) and WT/FANCD2 corrected (3.15, U2OS and HeLa) cell lines, following treatment with mitomycin C (MMC), cisplatin and TBHP. ....	169
Table 4.2: Growth inhibition summary of plasmid transfected FANCD2-deficient (PD20, U2OS-D2 and HeLa-D2) and WT/FANCD2 corrected (3.15, U2OS and HeLa) cell lines, following treatment with mitomycin C (MMC), cisplatin and TBHP. ....	170
Table 4.3: Growth inhibition summary of antibiotic-selected and plasmid transfected FANCD2-deficient (U2OS-D2 and HeLa-D2) and WT/FANCD2 corrected (U2OS and HeLa) cell lines, following treatment with mitomycin C (MMC), cisplatin and TBHP. .....	172
Table 4.4: Growth inhibition summary of siRNA transfected FANCD2-deficient (U2OS-D2 and HeLa-D2) and WT/FANCD2 corrected (U2OS and HeLa) cell lines, following treatment with mitomycin C (MMC), cisplatin and TBHP. ....	176

## Acknowledgements

I would like to thank my supervisor, Dr. Rhoderick H. Elder, for giving me the chance to carry out this project, for providing professional development and advice during my PhD study, and for inspiring me to continue working in DNA repair research. I would also like to thank him for his support over the past four years during the difficulties of the research and the COVID-19 pandemic.

Through the University of Salford, I would like to thank the UK Lighthouse Labs Network and Catapult Medicines Discovery at Alderley Park, Cheshire, for the opportunity to deploy, improve and advance my laboratory skills and for the professional work experience during the lockdown phase of the COVID-19 pandemic. Through them, I met a range of workers from various academic fields who also motivated and inspired me to pursue work in science and contribute to our shared world.

Throughout my PhD years, I worked closely with other colleagues and became friends with many with whom I look forward to staying connected. I would like to thank Dr. Peter Martin and Dr. Mustafa Albelazi for their friendship and for sharing their experience, advice and criticism during the PhD project. Their timely support with materials and contributions helped move the project forward. I would like to thank my colleague Mr. Stephen Austin for his friendship and continual support, his field of study helping me to see my project from a different perspective. I would like to thank Ms. Adesuwa Iseghohimen for her collaboration and clarification of the project details. I would like to thank Dr. David Greensmith for allowing me to continue work in his group's cell culture laboratory during the closure of my assigned laboratory. I want to thank the Translational Medicine department, especially Ms. Sonia Morlando and lab technician Ms. Rumana Rafiq, for their continual assistance. I am more than grateful to Dr. Camillo Sargiacomo for his support, because his exceptional experience, advice and criticism regarding scientific research helped me to regain confidence in my abilities.

I would also like to thank the laboratory technicians, including Dr. Anthony Bodell, Helen Bradshaw, Marian Denson, Manishadevi Patel, Andrew Martin, and Sally Shepherd, for their support. I especially would like to thank Dr. Muna Abubaker for her practical and moral support throughout the hard times in cell culture.

I would like to thank Dr. Soran Mohammed, Dr. Firozeh Ashtian, Dr. Natalie Barnes, Dr. Oluwasegun Abraham Iwakun, Dr. Henry Madubuike, Mr. Arvind Swamy, and Dr. Mudaser Zafar for their support, good humour and friendship.

Finally, I would thank my parents for encouraging me and supporting me. Their example has inspired me and kept me going during these many years of study.

## Abbreviations

3'-OH	3'-hydroxyl
5'-dRP	5'-deoxyribose phosphate
5-OHC	5-hydroxycytosine
5-OHU	5-hydroxyuracil
8-oxoG	8-oxo-7,8-dihydroguanine
aa	Amino acid
AP	Apurinic or apyrimidinic
APE1	AP-endonuclease 1
ATM	Ataxia-telangiectasia mutated
ATR	ATM- and Rad3-related
BER	Base excision repair
bp	Base pairs
cDNA	Complementary DNA
DDR	DNA damage response
DMSO	Dimethyl sulfoxide
DNA	Deoxyribonucleic acid
DSB	Double strand break
EDTA	Ethylenediaminetetraacetic acid
FA	Fanconi Anaemia
FANC	Fanconi Anaemia complementation group
FapyA	4,6-diamino-5-formamidopyrimidine
FapyG	2,6-diamino-4-hydroxy-5-formamidopyrimidine
FBS	Foetal bovine serum
FL	Full length
Fpg	Formamidopyrimidine DNA glycosylase
GAPDH	Glyceraldehyde 3-phosphate dehydrogenase
Gh	Guanidinohydantoin
H2tH	Helix two-turn helix
HhH	Helix-hairpin-helix
HR	Homologous recombination
hNEIL1	human NEIL1

hNEIL3	human NEIL3
ICL	Interstrand crosslink
IC <sub>50</sub>	Half-maximal inhibitory concentration
LB	Lysogeny broth
MBD4	Methyl-binding domain glycosylase 4
MGMT	<i>O</i> <sup>6</sup> -methylguanine-DNA-methyltransferase
MMC	Mitomycin C
MPG	3-methyl-purine glycosylase
MTS	3-(4,5-dimethylthiazol-2-yl)-5-(3-carboxymethoxyphenyl)-2-(4-sulfophenyl)-2H-tetrazolium, inner salt
MTT	(3-(4,5-dimethylthiazol-2-yl)-2,5-diphenyltetrazolium bromide
MUTYH	MutY homolog DNA glycosylase
Nei	Endonuclease VIII
NEIL1	Endonuclease VIII-Like 1
NEIL2	Endonuclease VIII-Like 2
NEIL3	Endonuclease VIII-Like 3
NER	Nucleotide excision repair
NS	Non-specific
NTHL1	Endonuclease III-like 1
OGG1	8-oxoguanine DNA glycosylase
PBS	Phosphate-buffered saline
PCR	Polymerase chain reaction
Pen/Strep	Penicillin and streptomycin
Pol β	DNA polymerase β
RNA	Ribonucleic acid
ROS	Reactive oxygen species
RPMI	Roswell Park Memorial Institute
RT	Reverse transcription
SMUG1	Single-strand-specific monofunctional uracil DNA glycosylase 1
S-phase	Synthesis phase

Sp	Spiroiminodihydantoin
SSB	Single-strand break
TBE	Tris base, boric acid and EDTA
TBHP	<i>tert</i> -butyl hydroperoxide
TDG	Thymine DNA glycosylase
Tg	Thymine glycol
TRAIP	RING-Type E3 ubiquitin ligase TRAIP
TRIM26	E3-ubiquitin ligase tripartite motif-containing protein 26
UNG	Uracil-N glycosylase
UV	Ultraviolet
WT	Wild type
zf-GRF	Zinc finger GRF

## Abstract

Fanconi Anaemia (FA) is an inherited autosomal-recessive disorder that can lead to abnormal development, bone-marrow failure, and an increased vulnerability to carcinogenesis. Cells derived from FA patients are unusually sensitive to DNA crosslinking agents and it is now known that FA cells lack one of twenty-two known different FA complementation group (FANC) proteins involved in the repair of DNA interstrand crosslinks (ICLs). More recently, two DNA glycosylases (endonuclease VIII – like 1 & 3 [NEIL1 & NEIL3]) that excise oxidised bases from DNA, thus initiating base excision repair, have been found to participate in the resolution of psoralen induced ICLs. Therefore, this project set out to determine whether the modulation of NEIL1 or NEIL3 expression in cell lines lacking FANCD2, of the monoubiquitinated DNA-heterodimer protein complex FANCD2/FANCI, could significantly affect their sensitivity to ICL-inducing agents, such as mitomycin C and cisplatin. An FA original and two FA-generated cancerous cell model systems representing FA and equivalent wildtype cells were then transfected with plasmids expressing FLAG-tagged NEIL1 or NEIL3 and challenged with the crosslinking agents or the oxidising agent *tert*-butyl hydroperoxide, and any differences in sensitivity to these agents determined. Similarly, siRNAs were designed against NEIL3 and the E3-ubiquitin ligase tripartite motif-containing protein 26 (TRIM26), that has been shown to ubiquitinate both NEIL1 and NEIL3 for proteasomal degradation and similar cell growth analyses performed using the MTT assay. Recombinant NEIL1 expression was confirmed by western blotting but had little effect on resistance to crosslinking and oxidising agents. Overexpression of NEIL3, either a truncated version lacking the C-terminal GRF domains (NEIL3<sup>1506</sup>), or the full-length protein, proved more difficult to confirm by western blotting, possibly due to antibody specificities to recombinant and non-recombinant NEIL3. However, MTT assays generally indicated a small increase in resistance irrespective of FA background, suggesting that NEIL3 overexpression was achieved in these cells. Unexpectedly, compared to literature and Elder laboratory results, knockdown of NEIL3 showed increased resistance against ICL and oxidative agents independent of FA phenotype, while knockdown of TRIM26 showed no clear effect on the sensitivity of the FA cell line to the genotoxic agents tested. In conclusion, the results indicate that the overexpression of NEIL1 or NEIL3 could not compensate for the loss of the FA pathway of ICL repair and had little reproducible effect on the resistance of these cell lines to crosslinking and oxidizing agents.

## Chapter 1 Introduction

Cancers are caused by simple or multifactorial factors, of which environmental factors, ageing, genetic mutations, or a combination of all these factors could lead to an increased chance of carcinogenesis (Jorde *et al.*, 2016, Chapter 11 and 12; Hassanpour and Dehghani, 2017). They can also occur at an increased rate when a patient is diagnosed with another disease or disorder with contributing genetic mutations, such as Fanconi Anaemia (Cheung and Taniguchi, 2017). Fanconi Anaemia (FA) is an inherited autosomal-recessive disorder that due to the deficiency of one of twenty-two known FA complementation group (FANC) genes, can lead to the phenotypes of abnormal development, bone-marrow failure, aplastic anaemia and an increased vulnerability to blood-related carcinogenesis and solid tumours (Mehta and Ebens, 2002; Garaycochea *et al.*, 2018). The FA pathway, also known as the interstrand crosslink (ICL) repair pathway, is a DNA repair pathway involved in targeting and excising ICLs using the affected FANC genes during DNA replication (Cheung and Taniguchi, 2017; Garaycochea *et al.*, 2018). Base excision repair (BER) is responsible for repairing chemically modified DNA bases and single-strand breaks often induced by oxidation, deamination, alkylation or hydrolysis (Bosshard *et al.*, 2012; Iyama and Wilson, 2014).

From the BER pathway the DNA glycosylases endonuclease VIII-like (NEIL)-1 (NEIL1), NEIL2 and NEIL3 specifically target multiple oxidative lesions, including in a supportive or backup role for other DNA glycosylases and themselves, in both single- and double-stranded DNA (Jacobs and Schär, 2012). However, NEIL3 knockout mouse embryonic fibroblasts (MEF) have been shown to be sensitised to an ICL-inducing agent cisplatin (Rolseth *et al.*, 2013), and the overexpression of NEIL1 increased resistance to the ICL-inducing agent mitomycin C (MMC, Macé-Aimé *et al.*, 2010). Furthermore, it was recently shown that hNEIL1 and hNEIL3 can excise psoralen induced ICLs in three- and four-stranded DNA structures (Martin *et al.*, 2017). FA cells are highly sensitive to ICL inducing agents, and the *FANC* genes have been shown to be involved in ICL repair (Mehta and Ebens, 2002). Therefore, the purpose of this study was to determine the role of the DNA glycosylases NEIL1 and NEIL3 in the repair of ICLs, and potentially lead the study for possible cancer therapeutics.

## 1.1. Cancer

Cancer is one of the most challenging, if not the most challenging, forms of disease known to man, with a projected rate of one in two people being diagnosed with cancer in the United Kingdom (Ahmad *et al.*, 2015). To date, it is estimated that there are over 200 different types of cancer, the most commonly diagnosed of which is breast for women, prostate for men, and lung and colon cancers (Hassanpour and Dehghani, 2017). The causes of cancers can be simple or multifactorial, as are the causes of other more common diseases such as type II diabetes, of which environmental factors (such as chemicals, radiation, and/or a deficient healthy life-style), ageing, or genetic mutations, or a combination of all these factors could lead to an increased chance of carcinogenesis (Jorde *et al.*, 2016, Chapter 11 and 12; Hassanpour and Dehghani, 2017). Initially, six accepted principles helped rationalise the complexity of cells developing into cancers, known as the hallmarks of cancer (Hanahan and Weinberg, 2011). The cancer hallmarks are replicative immortality, angiogenic induction, resistance to cell death, suspension of proliferative signalling, evasion of growth suppressors, and promoting invasion and metastasis (Hanahan and Weinberg, 2011). However, the primary basis of carcinogenesis is altered cell-regulatory genes, leading to a common phenotype of uncontrolled cell growth (Jorde *et al.*, 2016). Cancers can also occur at an increased rate when a patient is diagnosed with another disease or disorder with contributing genetic mutations (Jorde *et al.*, 2016), such as xeroderma pigmentosum (Daya-Grosjean, 2008) and Fanconi Anaemia (Cheung and Taniguchi, 2017). Whatever the cause, the greatest challenge is to administer the correct treatment suitable for the difficulties surrounding the diagnosis of the cancer. The most common treatments are surgery and a systemic form of chemotherapy, which involves the use of DNA-damaging agents and/or radiation (O'Connor, 2015). However, the treatments rely heavily on a fully-functional DNA repair pathway that could maintain DNA stability within non-cancerous cells, while targeting treatable cancerous cells.

## 1.2. DNA Stability

The DNA molecule stores the genetic information of the cell in discrete units called genes. In human cells, there are about 20,500 genes that code for proteins -- the macromolecules that are the principal molecular catalysts and one of the building blocks of cells (Clamp *et al.*, 2007; Strachan and Read, 2010). Therefore, it is essential that the DNA sequence remains unchanged from generation to generation and during cell division in a multicellular organism. Any permanent changes to the DNA sequence are known as mutations and if these are not prevented, they can lead to debilitating diseases, such as cancer (Strachan and Read, 2010; Jorde *et al.*, 2016). Unfortunately, the DNA molecule is susceptible to chemical modification, either due to spontaneous base loss or base modification and breakage of the phosphodiester bonds in one or both strands that make up the DNA molecule (single-strand and double-strand breaks) (O'Connor, 2015; Jorde *et al.*, 2016). If these modifications to the DNA molecule are not recognised and rectified, mutations will result. Therefore, all cells have evolved a number of DNA repair functions to combat the inherent instability of the DNA molecule and ensure that mutations are kept to a minimum (Pang and Andreassen, 2009; Krokan and Bjoras, 2013; O'Connor, 2015; Jorde *et al.*, 2016).

In analysing DNA lesions, they can be categorised as (i) endogenous damage resulting from internal cellular processes, and (ii) exogenous damage resulting from sources external to the cell (Strachan and Read 2010). It is estimated that DNA lesions can occur at a rate of  $10^5$  molecular lesions in a genome per day (Iyama and Wilson, 2014), but this rate may increase whenever aging and/or external sources are involved. Endogenous damage can result from oxidation, alkylation, hydrolysis and DNA replication-associated mismatched bases (Iyama and Wilson, 2014). Exogenous damage can result from exposure to natural products, externally sourced products of metabolism, ultra-violet (UV) radiation, ionising radiation, and thermal damage (Iyama and Wilson, 2014). Depending on the type of lesions, a repair process requires a specific DNA repair pathway.

### 1.2.1. DNA Oxidation

Reactive oxygen species (ROS) and oxidising agents are molecules containing an oxygen molecule (Maejima *et al.*, 2012; Cadet and Wagner, 2013). A ROS can be produced as a side-effect from the electron transport chain involved in mitochondrial respiration, an

oxidoreductase enzyme, or even metal catalysed oxidation (Bosshard *et al.*, 2012; Maejima *et al.*, 2012; Cadet and Wagner, 2013), although in small quantities and in secluded areas away from sensitive regions such as DNA can be considered harmless (Phaniendra *et al.*, 2015). The most common ROS are peroxides, such as superoxide anion ( $O_2^-$ ) and hydrogen peroxide ( $H_2O_2$ ), and hydroxyl radicals such as  $OH\cdot$  (Maejima *et al.*, 2012). Defences for such radicals exist, such as the enzyme superoxide dismutase (SOD) that can catalyse a conversion of two superoxide ions into oxygen and hydrogen peroxide, which is then converted further into water and oxygen (McCord and Fridovich, 1968; Maejima *et al.*, 2012). Oxidative lesions could also be caused by a free ‘one-electron’ that could alter a DNA base to a radical, and therefore vulnerable to any oxygen-containing molecule as the oxidising agent (Dizdaroglu and Jaruga, 2012; Cadet and Wagner, 2013). However, that concept would include simple molecules such as  $H_2O$ , which can act as a reducing agent under certain circumstances, to be the oxygen-containing molecule to an ionised DNA base as the oxidising agent (Kino *et al.*, 2017).

**Table 1.1: Radical and nonradical reactive oxygen species (ROS).**

Reactive Oxygen Species (ROS)			
<u>Radical</u>		<u>Nonradical</u>	
Superoxide Anion ( $O_2^{\cdot-}$ )	$O^{\cdot}-O^-$	Hydrogen Peroxide ( $H_2O_2$ )	$H-O-O-H$
Hydroxyl ( $OH\cdot$ )	$O^{\cdot}-H$	Organic Peroxide ( $RO_2H$ )	$R-O-O-H$
Alkoxy ( $RO\cdot$ )	$R-O^{\cdot}$	Hypochlorous Acid ( $HClO$ )	$H-O-Cl$
Peroxy ( $RO_2\cdot$ )	$R-O-O^{\cdot}$	Ozone ( $O_3$ )	$O^{\ominus}\cdots O^{\oplus}\cdots O^{\ominus}$
		Singlet Oxygen ( $^1O_2$ )	$O=O$

Adapted from Phaniendra *et al.*, 2015.

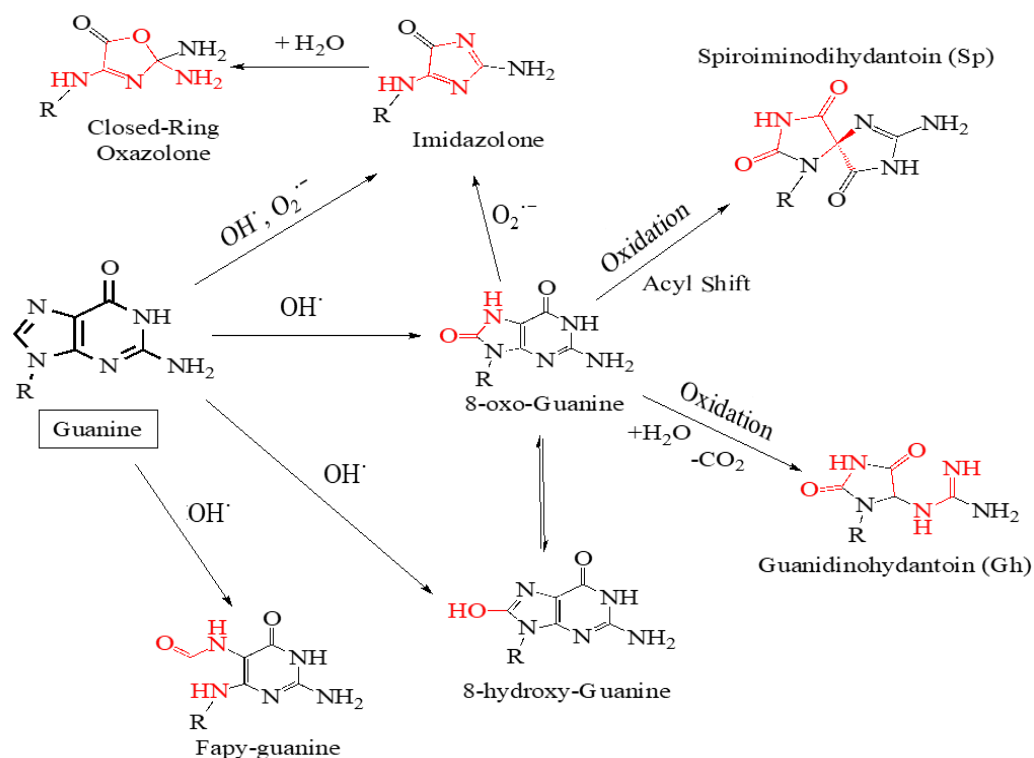


**Figure 1.1: Products of Guanine oxidation.**

Red highlights signify the alterations compared to the reference DNA base.

(Adapted and reformatted from: Tudek, 2003; White *et al.*, 2005; Lovell and Markesbery, 2007; Dizdaroglu and Jaruga, 2012; Kino *et al.*, 2017)

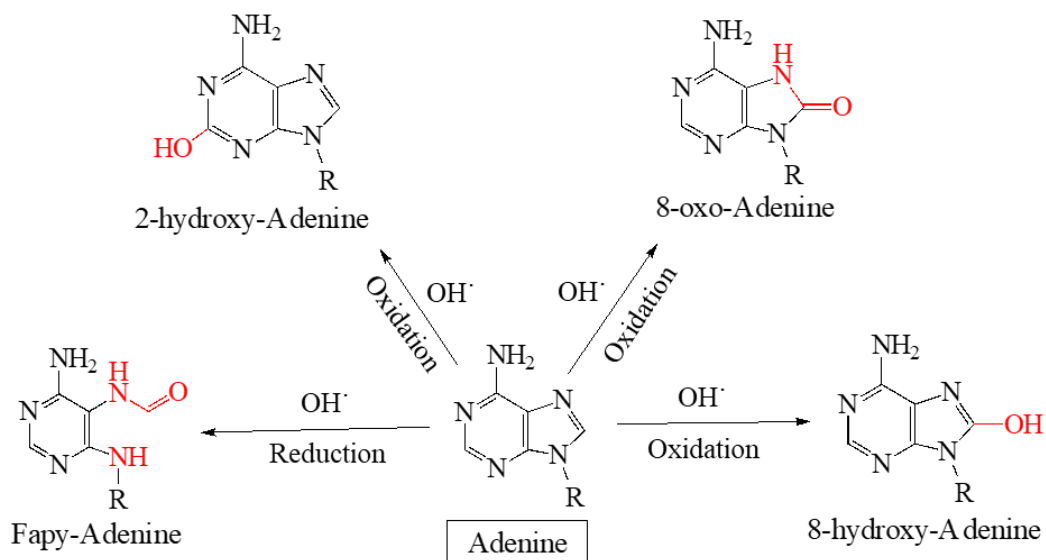


**Figure 1.2: Products of adenine oxidation.**

Red highlights signify the alterations compared to the reference DNA base.

(Adapted and reformatted from: Dizdaroglu and Jaruga, 2012; Cadet and Wagner, 2013)

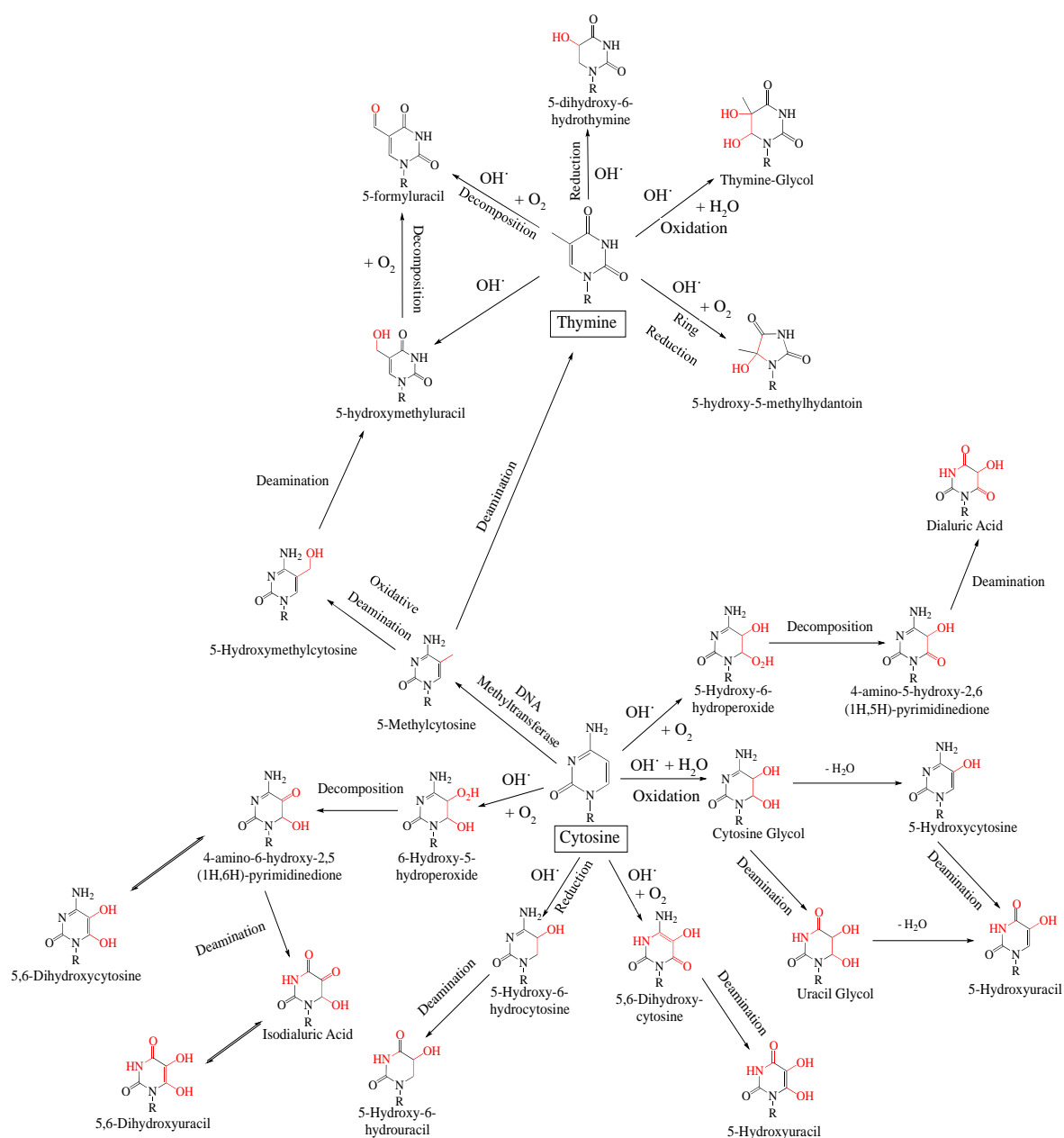


**Figure 1.3: Products of thymine and cytosine oxidation.**

Red highlights signify the alterations compared to the reference DNA base.

(Adapted and reformatted from: Tremblay and Wagner, 2007; Volk *et al.*, 2007; Evans *et al.*, 2010; Dizdaroglu and Jaruga, 2012; Smith *et al.*, 2015; Berney and McGouran, 2018)

If not removed, especially during times of oxidative stress, the chemically altered DNA bases could lead to a series of events that could trigger cellular apoptosis (Maejima *et al.*, 2012; Wallace *et al.*, 2017). As can be seen in Figures 1.1 – 1.3, and using some of the common oxidising agents listed in Table 1.1, all four DNA bases can become susceptible to chemical alterations. The literature reviews mainly use the hydroxyl radical (Table 1.1) as

the ROS agent due to its high reaction to biological molecules and rationalisation of DNA oxidation (Dizdaroglu and Jaruga, 2012). The same oxidised products may be achieved from other ROS agents displayed in Table 1.1 when interacting with the DNA bases, such as guanine with ROS agent hydrogen peroxide produces 8-oxo-7,8-dihydroguanine (8-oxoguanine, 8-oxoG) or spiroiminodihydantoin (Sp) (Chen and Lin, 2021). However, the literature reviews specifying those achievements are limited or theoretical and require further confirmation.

Most of the oxidatively-damaged DNA bases displayed in Figures 1.1 – 1.3 are pre-mutagenic, and some are considered cytotoxic. Guanine is the most frequently oxidised base and 8-oxoG is one of the most common oxidative base lesions occurring in DNA (Bosshard *et al.*, 2012; Whitaker *et al.*, 2017). This alteration is especially important to consider as 8-oxoG can base-pair with adenine, resulting in a thymine to adenine transversion mutation following DNA replication (Whitaker *et al.*, 2017). 8-oxoG is also vulnerable to further oxidation by ROS, as seen in Figure 1.1 (Dizdaroglu and Jaruga, 2012; Cadet and Wagner, 2013). The oxidised lesion from 8-oxoG, spiroiminodihydantoin, has a high preference for base-pairing with guanine over adenine, and guanidinohydantoin (Gh) has a base-pairing preference to adenine over guanine, and therefore forcing guanine to thymine or cytosine transversion mutations (Kino *et al.*, 2020). Adenine, though structurally similar to guanine, has the least oxidative lesions as seen in Figure 1.2, although it is not understood why.

Compared to the other bases subjected to oxidative damage, cytosine has the highest number of oxidative lesions, the majority of which occur after deamination and a majority of the resulting lesions are uracil based, as seen in Figure 1.3. An example is the oxidative lesion 5,6-dihydroxy-5,6-dihydrocytosine (cytosine glycol), which can further be altered by dehydration into 5-hydroxycytosine (5-OHC) or by deamination into 5,6-dihydroxy-5,6-dihydrouracil (uracil glycol), and can alter even further by dehydration into 5-hydroxyuracil (5-OHU) (Wallace, 2002; Cadet and Wagner, 2013). Alterations like these are especially important as uracil is a common base in RNA in place of thymine during transcription, and 5-hydroxymethyluracil is known to be cytotoxic and mutagenic (Whitaker *et al.*, 2017). The deaminated alteration of 5-hydroxymethyluracil and the oxidative lesioned alteration of thymine, 5-hydroxymethyluracil, is especially mutagenic and cytotoxic as the lesion can form an intrastrand crosslink and possibly an interstrand crosslink with guanine or adenine (Cadet and Wagner, 2013). Thymine is structurally similar to cytosine, however it does not

have as many oxidative lesions as cytosine. Similar to how 8-oxoG is a common oxidative lesion of guanine, *cis* and *trans* diastereomers of thymine glycol (5,6-dihydroxy-5,6-dihydrothymine, Tg) are common lesions of thymine after oxidation (Cadet and Wagner, 2013). This oxidative lesion is especially important as it can block replicative DNA polymerases, and can form DNA-protein crosslinks with the amino acid lysine (Dolinnaya *et al.*, 2013).

### 1.2.2. Interstrand Crosslinks

Interstrand crosslinks (ICLs) are highly toxic covalent bonds between two DNA bases on opposing DNA strands, preventing DNA strand separation during transcription and DNA replication, as opposed to intrastrand crosslinks which are less toxic and are formed on the same DNA strand (Wilson and Seidman, 2010; Deans and West, 2013; Lopez-Martinez *et al.*, 2016). As seen in Figure 1.4, the introduction of a crosslinking agent forms an ICL between DNA bases. There are various ICL agents, the most recognised of which is nitrogen mustard and its derivatives, because it was the first agent studied after sulphur mustard was used as a chemical weapon during World Wars One and Two (Deans and West, 2013; Lopez-Martinez *et al.*, 2016). Only later were alternative applications and other ICL agents discovered -- in the case of nitrogen mustard, the modified version melphalan -- and they are still being used as a form of treatment for cancer therapy (Wilson and Seidman, 2010; Deans and West, 2013). There were also studies of endogenous ICL agents, however they were difficult to experiment due to most of them being studied or assessed after mutagenicity (Pang and Andreassen, 2009). The only known endogenous ICL agents are reactive aldehydes, such as acetaldehyde (a derived metabolism of ethanol), malondialdehyde as a product of lipid peroxidation and nitric oxide (Pang and Andreassen, 2009; Lopez-Martinez *et al.*, 2016). However, most studies are concentrated on the more relevant exogenous ICL agents for testing and treatment, the most well-known examples displayed in Figure 1.4.

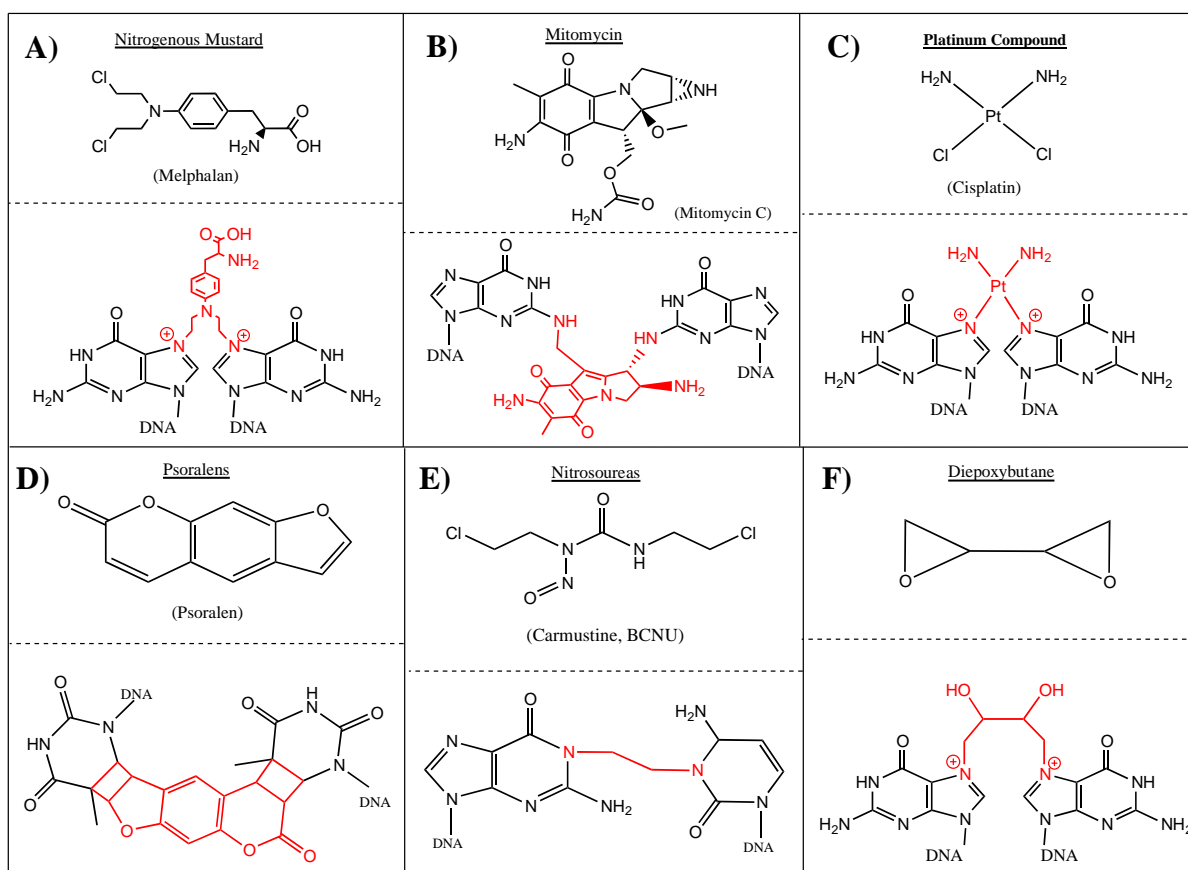


**Figure 1.4: DNA crosslinking agents and the structure of the interstrand crosslinks (ICL) produced.**

**A)** Nitrogenous mustard; **B)** mitomycin C (MMC); **C)** platinum compound; **D)** psoralens; **E)** nitrosoureas; **F)** diepoxybutane.

(Adapted and reformatted from Lopez-Martinez *et al.*, 2016).

Other ICL inducing agents include mitomycin C (MMC), a naturally occurring antibiotic compound from *Streptomyces caespitosus*; platinum compounds such as cisplatin [cis-diamminedichloroplatinum(II)]; psoralens, a natural compound produced from plants; nitrosoureas such as 1,3-bis(2-chloroethyl)-1-nitrosourea; and diepoxybutane (1,2,3,4-diepoxybutane), a bio-transformed product from the gas contaminant 1,3-butadiene (Lopez-Martinez *et al.*, 2016). Unlike nitrogen mustard, platinum compounds and diepoxybutane ICLs, MMC, psoralens or nitrosoureas do not form ICLs without first being metabolically reduced, irradiated by UV, or undergoing metabolic activation (Lopez-Martinez *et al.*, 2016).

The ICL formation and potency depend on the chemical reaction preference of the ICL agent involved, the specificity of the DNA bases and their positions along the DNA strands.

Nitrogen mustard agents are mostly used for treatment of lymphoid tumours, produce mostly monoadducts, and only 1 – 5% of lesions are ICLs that are two nucleotides apart and preferably between guanines in opposing 5'-GNC-3' sequences (Wang and Gautier, 2010; Wilson and Seidman, 2010). Platinum compound agents produce the same amount of ICLs but are one nucleotide apart and preferably between guanines in opposing 5'-GC-3' sequences, produce mostly intrastrand crosslinks, and are mostly used for ovarian, testicular and lung cancer treatments (Jung and Lippard, 2007; Wang and Gautier, 2010). Nitrosoureas agents produce mostly monoadducts and intrastrand crosslinks, but only 3 – 8% ICLs between base pairs guanine and cytosine, and are mostly used for treating glioblastoma tumours (Wang and Gautier, 2010). MMC produces only 5 – 13% ICLs that are one nucleotide apart and preferably between cytosines in opposing 5'-CG-3' sequences, but mostly produces ROSs, and is used to treat gastrointestinal, breast, lung and bladder cancers and Fanconi anaemia diagnosis (Mehta and Ebens, 2002; Wang and Gautier, 2010). Psoralen agents produce mostly monoadducts and up to 40% ICLs that are one nucleotide apart, preferably between thymines in opposing 5'-TA-3' sequences, and are mostly used for treating cutaneous T-cell lymphoma (Deans and West, 2013; Lopez-Martinez *et al.*, 2016). Diepoxybutane is known to produce monoadducts, SSBs (SSBs), DNA-protein crosslinks and ICLs, mainly between guanines in opposing 5'-GCC-3' sequences (Lopez-Martinez *et al.*, 2016). However, although the percentage of ICLs is not stated, it is most likely higher than MMC due to its use in Fanconi anaemia diagnosis (Auerbach, 2015).

As the role of chemotherapeutics is to increase DNA replication stress during the cell cycles S phase, a common issue in treating cancer through chemotherapy is drug resistance (Boulikas *et al.*, 2008; Ubhi and Brown, 2019). In metastatic pancreatic cancer treatment, MMC and cisplatin, even when combined with fluorouracil or gemcitabine, respectively, had low response rates (Wolff *et al.*, 2003). But when treating pancreatic ductal adenocarcinoma with *BRCA1/2* or *PALB2* mutations, response rates were increased when combined gemcitabine and cisplatin were administered (O'Reilly *et al.*, 2020). Increased resistance to platinum compound agents are commonly known to occur over time during treatment as they could cause cellular drug accumulation reduction, increase detoxification systems and DNA repair processes, decrease apoptosis and promote autophagy (Zhou *et al.*, 2020). Although recently a developed oxaliplatin Pt(IV) prodrug conjugated with gadolinium-texaphyrin, as an alternative platinum compound agent of oxaliplatin, promoted

expression of tumour suppressor p53 in ovarian cancer cells with cisplatin resistance (Thiabaud *et al.*, 2020).

### 1.3. DNA Repair

DNA repair is initiated after a DNA lesion is identified and repair initiated by the DNA damage response (DDR) pathway (O'Connor, 2015). For example, the highly mutagenic and cytotoxic lesion *O*<sup>6</sup>-methylguanine (*O*<sup>6</sup>-meG) caused by a methylating agent is repaired by *O*<sup>6</sup>-methylguanine-DNA-methyltransferase (MGMT) by direct repair (Iyama and Wilson, 2014; Pierce, 2014). MGMT removes the methyl (or alkyl group) from the guanine to a cysteine residue in the active site of the protein, which inactivates MGMT that is then ubiquitinated and degraded (Srivenugopal *et al.*, 1996; Iyama and Wilson, 2014). However, direct repair is rare and with the exception of double-strand breaks (DSBs), most DNA damage is repaired by excision repair processes, either nucleotide excision repair (NER) for bulky damage and intrastrand crosslinks or base excision repair (BER) for SSBs, abasic sites and chemically modified bases (Pierce, 2014; O'Connor, 2015). DSBs are repaired by one of two mechanisms, non-homologous end-joining when the cell is in the G0 and G1 phase of the cell cycle and homologous recombination (HR) when the cell is in G2 and a sister-chromatid is available for homologous repair (O'Connor, 2015).

The DDR uses the protein kinases ataxia-telangiectasia mutated (ATM) and ATM- and Rad3-related (ATR) as the main damage detectors (Liang *et al.*, 2009). ATM is responsible for detecting DNA DSBs, and ATR for DNA SSBs (Tšuiiko *et al.*, 2019). Downstream through phosphorylation, the cell-cycle regulators checkpoint kinase 1 (CHK1) and CHK2 stop the cell-cycle in G1 and activate DNA repair (Tšuiiko *et al.*, 2019). Based on the DDR and the protein kinase that detects the DNA damage, the appropriate repair pathway is activated. To date, there are six main DNA repair pathways: BER, NER, mismatch repair (MMR), homologous recombination (HR), non-homologous end joining and the FA pathway (Iyama and Wilson, 2014; Wu *et al.*, 2019). BER is responsible for repairing DNA SSBs and more specifically, chemically-altered bases, which is detailed further in Section 1.5. NER is also responsible for repairing SSBs, but more specifically modified nucleotides resulting in bulky adducts, intrastrand crosslinks such as UV-induced pyrimidine dimers (O'Connor, 2015; Fakouri *et al.*, 2019). MMR resolves mismatched base pairs and base

insertions and deletions (Iyama and Wilson, 2014; O'Connor, 2015). HR and non-homologous end-joining are responsible for repairing DNA DSBs, as described earlier (Chang *et al.*, 2017). The FA pathway, which is also regarded as the ICL repair pathway (Wu *et al.*, 2019), requires ATR activation but is categorised more as being responsible for the repair of DNA DSBs, due to the recruitment of proteins that create a DSB after incision of ICLs, which then require recruiting proteins following the HR repair mechanics, as detailed in Section 1.4.

#### 1.4. Fanconi Anaemia Pathway

Fanconi Anaemia (FA) is an inherited autosomal-recessive disorder that, due to poor development of blood cells, can lead to the phenotypes of abnormal development, bone-marrow failure, aplastic anaemia and an increased vulnerability to blood-related carcinogenesis and solid tumours (Mehta and Ebens, 2002; Garaycochea *et al.*, 2018). Rarely, FA could also be inherited as an autosomal dominant disorder through a variant of RAD51 (FANCR) or as an X-linked disorder through a variant of FANCB, but FA is mostly inherited in an autosomal-recessive pattern through variants of FANCA (Mehta and Ebens, 2002). Diagnosis of the disease is normally conducted by testing lymphocytes for increased chromosomal breakage using MMC or diepoxybutane, and by genetic testing for specific mutations in genes known to be involved in the FA pathway (Mehta and Ebens, 2002; Auerbach, 2015). The FA pathway is a DNA repair pathway that is involved in targeting and excising ICLs using the affected FA complementation group (FANC) genes during DNA replication (Cheung and Taniguchi, 2017; Garaycochea *et al.*, 2018). The FA pathway primarily operates during the S-phase of the cell-cycle and it tends to be DNA replication-dependent (Datta and Brosh Jr., 2019).

Biochemical studies on patient-derived cell lines have been carried out since the 1980's (Ishida and Buchwald, 1982), and currently there are 22 known *FANC* genes (Wu *et al.*, 2019), as seen in Table 1.2. FA diagnosed cells are deficient in a FANC or related protein (such as BRCA2, also known as FANCD1), that destabilises the necessary protein complexes (Cheung and Taniguchi, 2017), making the patient vulnerable to certain types of DNA lesions. Options for treatment are also limited, as some of the ICL-inducing agents described in Section 1.2.2. are also used for chemotherapy and therefore should be avoided for those diagnosed with FA. Interestingly, hematopoietic stem cell transplants dosed with

total body irradiation have been considered to be dosed with the alternative intrastrand crosslinking agent busulfan instead to increase engraftment and lower hepatotoxicity before treatment (Mehta *et al.*, 2019). Since Mehta *et al.* (2019) determined that patients with FA and non-FA traits had no significant differences in toxicity when treated with busulfan, the crosslinking agent has been considered as the alternative method for hematopoietic stem cell transplants and is currently being investigated as a potential chemotherapy treatment for FA cancer patients (Mehta and Ebens, 2002; Mehta *et al.*, 2019). The specific functionality and mechanics of the individual FANC proteins, and their combined involvement during the FA pathway, are still being investigated and debated, however the basic understanding of the FA pathway is currently accepted, as displayed in Figure 1.5. Prior to the understanding of the role of the FA pathway, the repair for ICLs in DNA was theorised to have been completed by, or a combination of the repair pathways NER and HR, but was not understood why or how the repair pathways were recruited together (McHugh *et al.*, 2001). That was until studies into the FA pathway had revealed that over half of the recognised FANC proteins listed in Table 1.2 were recognised as proteins involved in NER as the FA incision complex that unhooks the ICL, and HR for the DNA DSB repair. Therefore the connection between the repair pathways was established and the FA pathway was accepted as the principal ICL repair pathway.

**Table 1.2: Gene names and molecular function of the Fanconi Anaemia complementation groups (FANCs) in the Fanconi Anaemia (FA) pathway.**

Fanconi Anaemia Complementation Group ( <i>FANC</i> ) #	Recognised Gene Name	Molecular Function Within the FA Pathway
<b>A</b>	<i>FANCA</i>	FA core complex localisation and translocation
<b>B</b>	<i>FANCB</i>	FA core complex scaffold; FA ID complex ubiquitylation efficiency improvement
<b>C</b>	<i>FANCC</i>	FA core complex; stabilise FA ID complex interaction and ubiquitylation efficiency improvement
<b>D1</b>	<i>BRCA2</i>	HR; recruits RAD51
<b>D2</b>	<i>FANCD2</i>	FA ID complex, initiates unhooking of nucleases
<b>E</b>	<i>FANCE</i>	FA core complex; stabilise FA ID complex interaction and ubiquitylation efficiency improvement
<b>F</b>	<i>FANCF</i>	FA core complex, stabilise FA ID complex interaction and ubiquitylation efficiency improvement
<b>G</b>	<i>FANCG</i>	FA core complex localisation and translocation
<b>I</b>	<i>FANCI</i>	FA ID complex, initiates unhooking by nucleases
<b>J</b>	<i>BRIP1</i>	Promotes HR pathway when phosphorylated
<b>L</b>	<i>FANCL</i>	FA core complex; E3 ligase monoubiquitinates FA ID complex
<b>M</b>	<i>FANCM</i>	FANCM/MHF and FA core complexes; binds to DNA at flipped ICL site
<b>N</b>	<i>PALB2</i>	HR; mediates BRCA1/2 to DNA strand
<b>O</b>	<i>RAD51C</i>	HR; RAD51 paralog for nucleoprotein filament assembly
<b>P</b>	<i>SLX4</i>	FA incision complex; recruitment and scaffolding for first ICL incision and unhooking.
<b>Q</b>	<i>ERCC4</i>	FA incision complex; first ICL incision and unhooking
<b>R</b>	<i>RAD51</i>	HR; searches for homology template and DNA strand exchange
<b>S</b>	<i>BRCA1</i>	HR promotion; dissociates CMG helicase after ICL detected, joins BRCA2 as part of HR
<b>T</b>	<i>UBE2T</i>	FA core complex; E2 ligase monoubiquitin control from FA ID complex.
<b>U</b>	<i>XRCC2</i>	HR; RAD51 paralog for nucleoprotein filament assembly
<b>V</b>	<i>REV7</i>	Translesion synthesis; extension to polymerase $\zeta$
<b>W</b>	<i>RFWD3</i>	HR complex; mediates replication protein A (RPA) to promote HR

Adapted and reviewed from Taylor *et al.* (2020).

When an ICL is present, the DNA damage response is the RING-Type E3 ubiquitin ligase TRAIP (TRAIP), which ubiquitylates the replicative DNA helicase protein complex CMG (CDC45, MCM2 – 7 and GINS) and stalls DNA replication (Wu *et al.*, 2019). This was initially thought to be the responsibility of FANCM in the FANCM/MHF (FA-associated protein 24 [FAAP24], histone fold protein 1 [MHF1] and 2 [MHF2]) complex with breast cancer associated protein 1 (BRCA1) and BARD1 (BRCA1-associated really interesting new gene domain protein 1) after ATR DNA damage response, thus following the standard FA pathway (Ceccaldi *et al.*, 2016; Datta and Brosh Jr., 2019). Wu *et al.* (2019) had shown that FANCM was not necessary, however it may be more accurate to assume that under a specific replication model in response to a specific type of ICL, that TRAIP or FANCM/MHF is recruited to detect and respond, and requires further investigation for clarification. Following the ICL response and protein complex recruitment, the DNA is unwound and remodelled as the replication fork converged at the ICL site (Datta and Brosh Jr., 2019; Wu *et al.*, 2019). Following the standard accepted FA pathway, FANCM/MHF acts as an anchor to the ICL site and a platform for the recruitment of other proteins to form the FA core complex, which consists of FANCM/MHF complex, FANCA, -B, -C, -E, -F, -G and -L, UBE2T, FAAP100 and FAAP20 (Ceccaldi *et al.*, 2016). The FA core complex acts as the ubiquitin ligase to recruit and monoubiquitinate the individual proteins FANCD2 and FANCI of the heterodimer FA ID complex (Cheung and Taniguchi, 2017; Datta and Brosh Jr., 2019). The FA ID complex stalls the replication fork and, so long as the complex is ubiquitinated, is prevented from deubiquitylation by ubiquitin-specific protease 1 (USP1) and USP1-associated factor 1 (UAF1), therefore preventing premature FA pathway inactivation (Taylor *et al.*, 2020).

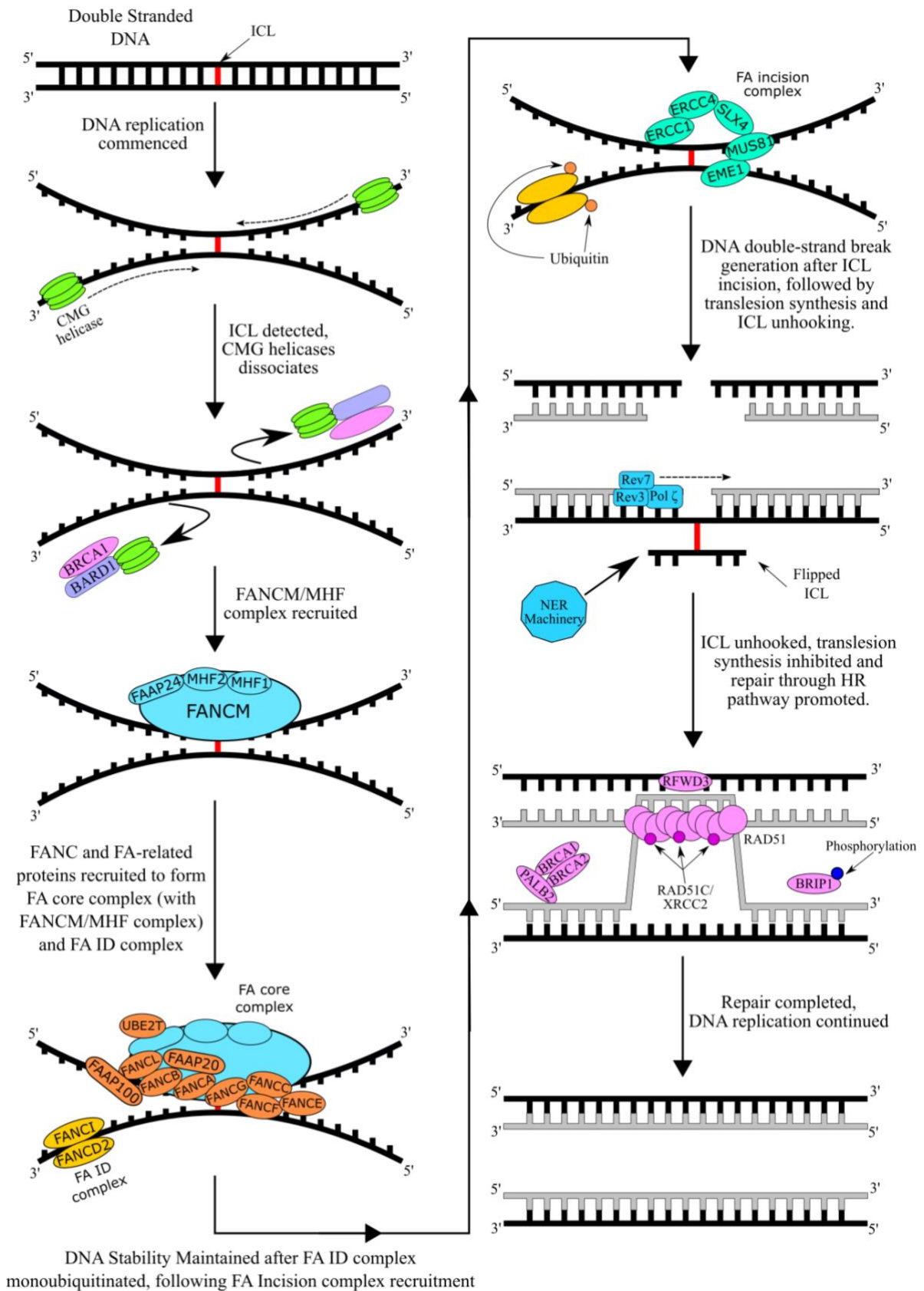


**Figure 1.5: ICL unhooking and repair through the Fanconi Anaemia pathway.**

Adapted and reformatted from Cheung and Taniguchi (2017) and Taylor *et al.* (2020).

After the FA ID complex is monoubiquitinated and stabilises as a DNA ‘clamp’ of the DNA replication fork (Alcón *et al.*, 2020), the FA incision complex, a protein scaffold involving excision repair cross complementing protein 1 (ERCC1) with ERCC4 and MUS81 with Essential Meiotic Structure-Specific Endonuclease 1 (EME1), combined with SLX4, is recruited for the incision and flipping of the ICL, resulting in a generated DNA double-stranded break (Martin *et al.*, 2017; Datta and Brosh Jr., 2019). Opposite the flipped ICL, the single-stranded DNA gap is sealed with DNA polymerases Rev1 or  $\zeta$ , which contain the subunits Rev3 and Rev7 (Datta and Brosh Jr., 2019; Taylor *et al.*, 2020). It is currently thought that the ICL is removed by NER, or more recently a theory favours BER, due to the supporting evidence of DNA glycosylases NEIL1 and NEIL3 with the aid of a third and fourth DNA strand (Martin *et al.*, 2017). After the ICL incision, the remaining single-stranded DNA gap is sealed with DNA polymerases Rev1 or  $\zeta$  again, followed by completing DNA repair after RAD51-catalysed HR using RAD51, RAD51C, BRCA1, BRCA2, PALB2, BRIP1 and BARD1 (Ceccaldi *et al.*, 2016).

The FANC genes/proteins and their ICL repair relation were studied extensively within the FA pathway, mainly in relation to the protein complexes FA core and FA ID. Specifically, the FANC genes/proteins studied the most were FANCA and FANCD2. FANCA had the highest percentage of FA-attributed gene variants and was determined by Garcia-Higuera *et al.* (1999) to bind to FANCG and FANCC in the FA core complex, which also had high percentages of gene variants (Kimble *et al.*, 2018). The absence or depletion of FANCA rendered the FA core complex non-functional, and therefore, the FA ID complex was not recruited and ubiquitinated. FANCD2 had more FA-attributed gene variants than FANCD1 in the FA ID complex, though they were both considered rare compared to other FANC genes (Kimble *et al.*, 2018). FANCD2 was extensively researched due to its association with the BRCA1 (FANCS) and BRCA2 (FANCD1) proteins involved in the HR pathway (Garcia-Higuera *et al.*, 2001; Hussain *et al.*, 2004), and the FA ID complexes monoubiquitination from the FA core complex promoting the nuclear incision protein complex recruitment (Mehta and Ebens, 2002). However, the absence/depletion of FANCD2 rendered the FA ID complex non-functional, and therefore down regulating the recruitment of protein complexes for ICL repair.

## 1.5. Base Excision Repair

Base excision repair (BER) is responsible for repairing chemically modified DNA bases and SSBs (Pierce, 2014). These DNA-base lesions are induced by oxidation, deamination, alkylation and hydrolysis (Bosshard *et al.*, 2012; Iyama and Wilson, 2014). BER follows the major steps of recognising and excising an irregular base, nicking the resulting abasic site, processing the terminal ends, replacing the excised nucleotide and sealing the nick (Pierce, 2014), as shown in Figures 1.6 and 1.7.

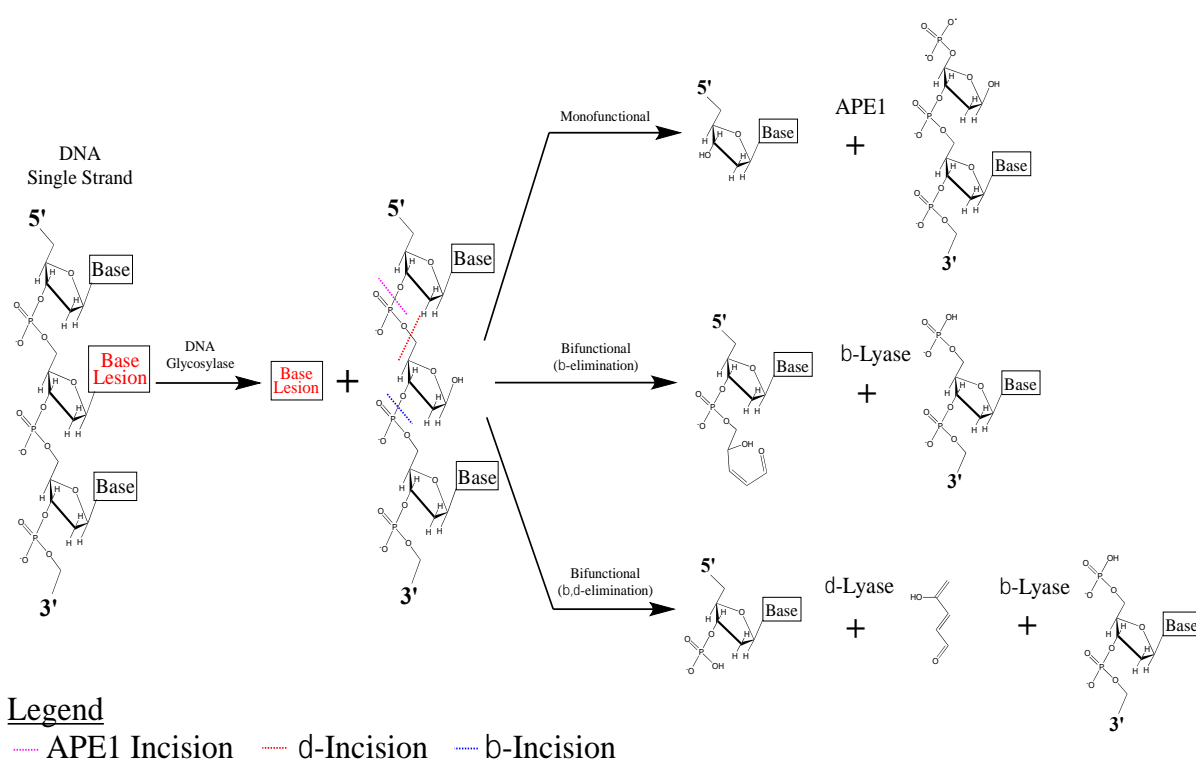


**Figure 1.6: Activity of mono- and bi-functional DNA glycosylases showing the different ends produced.**

Reviewed and reformatted from Krokan and Bjoras (2013), and Parsons and Edmonds (2016).

BER starts either when a DNA glycosylase recognises and excises a chemically-modified base, or when PARP1 is activated at the site of a SSB and recruits the necessary proteins for SSB repair (Pierce, 2014; Fakouri *et al.*, 2019). DNA glycosylases are classed as monofunctional or bifunctional (Bosshard *et al.*, 2012; Iyama and Wilson, 2014), and function as displayed in Figure 1.6. Monofunctional DNA glycosylases hydrolyse the N-

glycosylic bond, which leaves an AP (apurinic or apyrimidinic) site followed by cleavage of the DNA backbone at the 5'-side of the AP site by AP-endonuclease 1 (APE1), leaving a DNA SSB with 3'-hydroxyl (3'-OH) and 5'-deoxyribose phosphate (5'-dRP) ends (Bosshard *et al.*, 2012; Iyama and Wilson, 2014). The 5'-dRP is then removed by DNA polymerase  $\beta$  (Pol  $\beta$ ) to create a 5'-phosphate before a complementary nucleotide is added. Bifunctional DNA glycosylases follow the same principle, except they also have a 3'-AP lyase activity incising the phosphodiester backbone at the 3' side of the AP site by  $\beta$ -elimination resulting in a 5'-phosphate and a 3'-phosphoglycolate residue respectively (Bosshard *et al.*, 2012; Iyama and Wilson, 2014). Alternatively, some bifunctional DNA glycosylases, including Fpg/Nei (formamidopyrimidine DNA glycosylase [Fpg] and endonuclease VIII [Nei]) cleave by  $\beta,\delta$ -elimination, resulting in 5'- and 3'-phosphate groups with the 3'-phosphate converted to a 3'-OH group by polynucleotide kinase/phosphatase (PNKP) (Bosshard *et al.*, 2012; Krokan and Bjoras, 2013). Whichever the case, the result is the excision of the chemically modified base and a DNA SSB that is repaired by one of two methods, short-patch or long-patch BER.

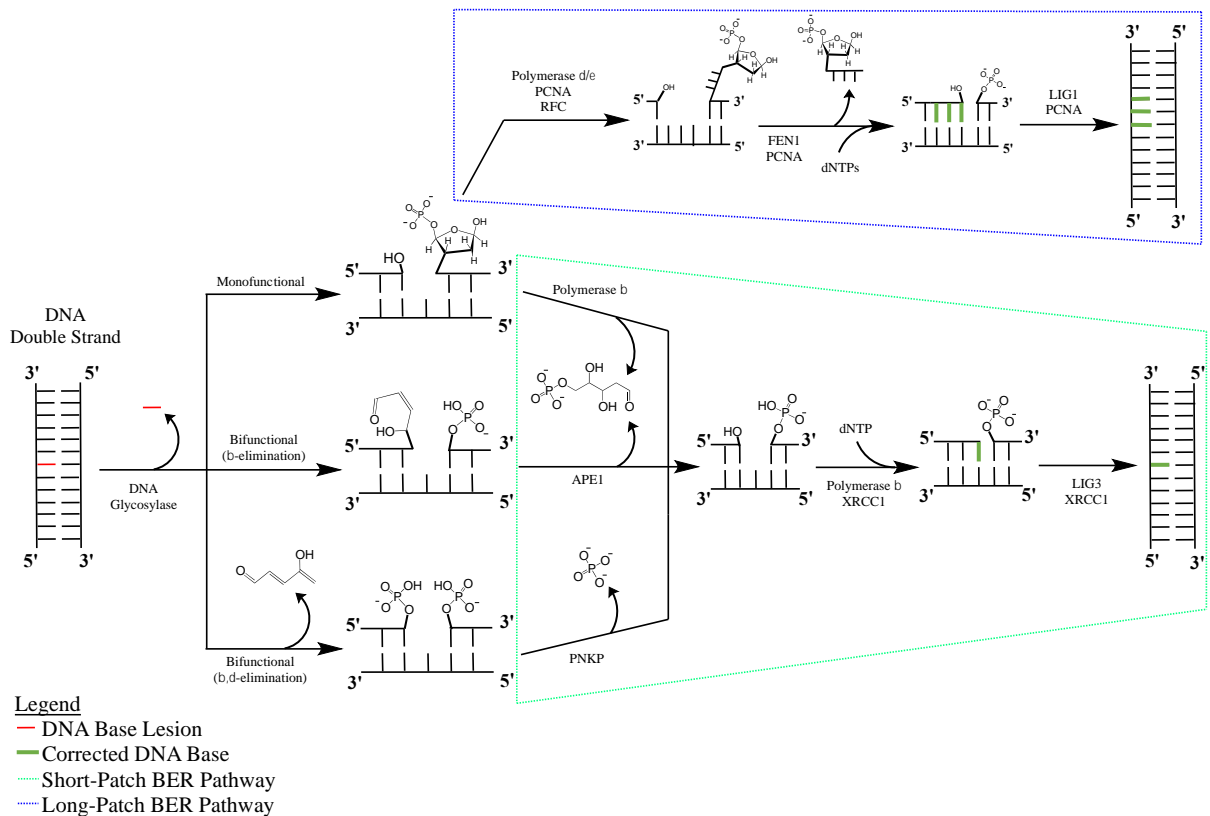


**Figure 1.7: Base excision repair.**

(Reviewed and reformatted from Krokan and Bjoras, 2013, and Parsons and Edmonds, 2016).

The different pathways of BER are summarised in Figure 1.7. Following N-glycosylic bond cleavage, short-patch BER starts with end-processing using either Pol  $\beta$  to cleave the 5'-dRP, APE1 to remove the 3' phosphoglycolate residue, or PNKP to change the 3'-phosphate group to 3'-OH. (Krokan and Bjoras, 2013; Albelazi *et al.*, 2019). This leads to repair synthesis with Pol  $\beta$ , followed by ligation of the appropriate nucleotide by XRCC1/DNA ligase III (LIG3) (Krokan and Bjoras, 2013; Iyama and Wilson, 2014).

Long-patch BER (Figure 1.7) is characterised by the excision of up to thirteen nucleotides, often involving clustered oxidative base lesions (Krokan and Bjoras, 2013; Iyama and Wilson, 2014; Whitaker *et al.*, 2017). The proteins involved in long-patch BER are expressed during S-phase and are involved in DNA replication (Zhou *et al.*, 2017). For monofunctional DNA glycosylases, after DNA backbone incision by APE1, if the 5'-dRP is not removed by Pol  $\beta$ , then the repair is continued by strand displacement (Maynard *et al.*, 2008) by DNA polymerase  $\delta$  or  $\epsilon$  (Pol  $\delta/\epsilon$ ), and proliferating cell nuclear antigen (PCNA),

with replication factor C (RFC) (Krokan and Bjoras, 2013; Iyama and Wilson, 2014). The DNA flap is then excised by flap endonuclease 1 (FEN1), allowing the ligation of the newly synthesised DNA strand by DNA ligase I (LIG1) (Krokan and Bjoras, 2013).

#### 1.5.1. DNA Glycosylases

DNA glycosylases are the proteins responsible for starting BER by excising the chemically modified DNA base (Bosshard *et al.*, 2012; Krokan and Bjoras, 2013; Iyama and Wilson, 2014). As displayed in Table 1.3, there are eleven DNA glycosylases in mammalian cells, and each one is involved in targeting a specific set of DNA base modifications (Bosshard *et al.*, 2012; Jacobs and Schär, 2012; Krokan and Bjoras, 2013).

Depending on the DNA base in question, the DNA glycosylases are further identified by their function. For example, 3-methyl-purine glycosylase (MPG), also known as alkyladenine DNA glycosylase (AAG) in humans, is the only monofunctional DNA glycosylase that specifically targets and excises alkylated bases, including 3-methyladenine, 3-methylguanine, 7-methylguanine as well as hypoxanthine and 1,N<sup>6</sup>-ethenoadenine (Jacobs and Schär, 2012; Whitaker *et al.*, 2017). However, the majority of the DNA glycosylases target uracil-related lesions or oxidative lesions.

**Table 1.3: General summary of the structural motif superfamilies, name, class and common lesions targeted by mammalian DNA glycosylases.**

<b>Structural Motif Superfamily</b>	<b>DNA Glycosylase Name</b>	<b>Monofunctional or Bifunctional</b>	<b>Common DNA Base Lesion</b>
<b>3-methyl-purine glycosylase (MPG)</b>	3-methyl-purine glycosylase (MPG)	Monofunctional	3-methyladenine; 7-methylguanine; hypoxanthine
<b>Alpha-beta fold Motif (Uracil DNA Glycosylase [UDG] Superfamily)</b>	Uracil-N glycosylase (UNG)	Monofunctional	Uracil and derivatives
	Single-strand-specific monofunctional uracil DNA glycosylase 1 (SMUG1)	Monofunctional	Uracil and derivatives
	Thymine DNA glycosylase (TDG)	Monofunctional	Thymine mismatches; Uracil and derivatives
<b>Helix 2-turn Helix (H2tH) (NEIL superfamily)</b>	Endonuclease VIII-Like 1 (NEIL1)	Bifunctional	Tg; FapyG; FapyA; 8-oxoG
	Endonuclease VIII-Like 2 (NEIL2)	Bifunctional	Tg; FapyG; FapyA; 8-oxoG
	Endonuclease VIII-Like 3 (NEIL3)	Monofunctional/Bifunctional	FapyA; FapyG; Sp; Gh
<b>Helix-hairpin-helix (HhH)</b>	Methyl-binding domain glycosylase 4 (MBD4)	Monofunctional	Thymine mismatches; Uracil and derivatives
	8-OxoG DNA glycosylase 1 (OGG1)	Bifunctional	8-oxoG; FapyA; FapyG
	MutY homolog DNA glycosylase (MUTYH)	Monofunctional	Adenine opposite 8-oxoG
	Endonuclease III-like 1 (NTHL1)	Bifunctional	Tg; FapyG

Adapted from Whitaker *et al.* (2017).

Four monofunctional DNA glycosylases specialise in excising uracil and uracil derivatives, however, three of them are differentiated by their protein structural motif, and individually are further differentiated by their lesion excision specificity. Uracil-DNA glycosylase (UNG), single-strand-specific monofunctional uracil DNA glycosylase 1 (SMUG1) and thymine DNA glycosylase (TDG) are DNA glycosylases in the uracil DNA glycosylase superfamily, containing the alpha-beta fold motif (Bosshard *et al.*, 2012). UNG targets uracil, preferably opposite to adenine, and deaminated residues of cytosine opposite to guanine alloxan, 5-hydroxyuracil and isodialuric acid (Jacobs and Schär, 2012; Krokan and Bjoras, 2013). SMUG1 also targets uracil and uracil derivatives in place of UNG in a supportive role, but specifically targets uracil and 5-hydroxymethyluracil when opposite to guanine and also in single-stranded DNA (Kavli *et al.*, 2002; Evans *et al.*, 2010). TDG specifically targets thymine based mismatches with guanine that are close to CpG islands, more than SMUG1 with uracil and 5-hydroxymethyluracil, and the oxidised 5-carboxylcytosine, before correcting to cytosine in double-stranded DNA (Tini *et al.*, 2002; He *et al.*, 2011). The methyl-binding domain glycosylase 4 (MBD4) is similar to TDG in targeting mispaired-bases and SMUG1 in targeting 5-hydroxymethyluracil in CpG island mismatches in double-stranded DNA, however, MBD4 can target in a broader range including thymine and uracil when mispaired with guanine but does not have significant activity against 5-hydroxymethyluracil (Hendrich *et al.*, 1999; Jacobs and Schär, 2012).

Four bifunctional DNA glycosylases specialise in excising oxidative lesions, however three of the four are differentiated by their protein structural motif and their bifunctional  $\beta$ - and  $\beta,\delta$ -elimination, and individually are further differentiated by their lesion excision specificity. 8-oxoG DNA glycosylase (OGG1) is a bifunctional HhH type,  $\beta$ -elimination DNA glycosylase that specifically targets 8-oxoG opposite cytosine. However, it also has activity against the oxidised purine lesions, 2,6-diamino-4-hydroxy-5-formamidopyrimidine (FapyG) when opposite cytosine, 7,8-dihydro-8-oxoadenine (8-oxoA) when not opposite thymine, and 4,6-diamino-5-formamidopyrimidine (FapyA) (Bosshard *et al.*, 2012; Wallace, 2013; Nakabeppu, 2014). The monofunctional MutY homolog DNA glycosylase (MUTYH) is the only DNA glycosylase that specifically targets a natural base opposite a chemically modified lesion, in this case adenine paired to 8-oxoG, which may occur post DNA replication (Wallace, 2013). MUTYH initiates BER with polymerase  $\lambda$  when replicative polymerases bypass 8-oxoG and the opposite paired adenine is not corrected to cytosine

(Bosshard *et al.*, 2012). After the correct cytosine is paired, OGG1 can initiate BER to excise 8-oxoG (Nakabeppu, 2014).

Endonuclease III-like 1 (NTHL1) is another HhH family member that carries out  $\beta$ -elimination, a DNA glycosylase that specifically targets ring fragmented purines and oxidised pyrimidines in double-stranded DNA, such as Tg, FapyA, FapyG, 5-hydroxycytosine and 5-hydroxyuracil (Jacobs and Schär, 2012; Wallace, 2013). The DNA glycosylases endonuclease VIII-like (NEIL)-1 (NEIL1), NEIL2 and NEIL3 are bifunctional  $\beta,\delta$ -elimination DNA glycosylases in the NEIL superfamily, containing the Helix 2-turn helix (H2tH) motif (Albelazi *et al.*, 2019). Similar to NTHL1 and OGG1, the NEIL DNA glycosylases specifically target multiple oxidative base lesions, in both single- and double-stranded DNA (Jacobs and Schär, 2012). However, cell cycle expression and substrate specificities differ for the NEIL DNA glycosylases, and these are discussed further in Sections 1.5.1.1. – 1.5.1.3. An example is NEIL1 and NEIL3 that have high activity on the further oxidation products of 8-oxoG, spiroiminodihydroantoin (Sp) and guanidinohydroantoin (Gh) (Martin *et al.*, 2017; Albelazi *et al.*, 2019).

#### 1.5.1.1. NEIL1

NEIL1 is the second largest of the NEIL DNA glycosylases, the human variant having 390 amino acids, and has an Fpg/Nei superfamily domain, helix 2-turn helix (H2tH) domain, and a NEIL1 DNA binding domain (as can be seen from Figure 1.8). The NEIL1 DNA glycosylase has been reported to initiate short-patch BER through  $\beta,\delta$ -elimination when targeting oxidised DNA bases and has been found to be cell cycle regulated, with the highest expression being during S-phase and after oxidative stress (Hegde *et al.*, 2013). The expression steadily increases with age as a mid-age threshold takes effect, reaching its peak before dropping again at an older age (Bosshard *et al.*, 2012). Albelazi *et al.* (2019) further characterised the biochemical role of NEIL1 as the primary DNA glycosylase to excise oxidative bases in double-stranded DNA before DNA replication fork unwinding and maintaining DNA replication fork stability, when compared to NEIL3 in single-stranded and double-stranded DNA. The disorders directly associated with NEIL1 are metabolic syndrome, based on NEIL1 knockout and heterozygous-mutated mouse models displaying a reduction in DNA stability and glycosylase activity (Vartanian *et al.*, 2006; Roy *et al.*,

2007). An increase in cancer development with significantly elevated somatic mutations was noted most cases with NEIL1 underexpression detected (Shinmura *et al.*, 2016). This implies the phenotypical consequences of cells deficient in NEIL1 expression to be susceptible to DNA instability, especially to oxidative stress, but there are currently no phenotypic consequences related to cells with NEIL1 overexpression.

### hNEIL1

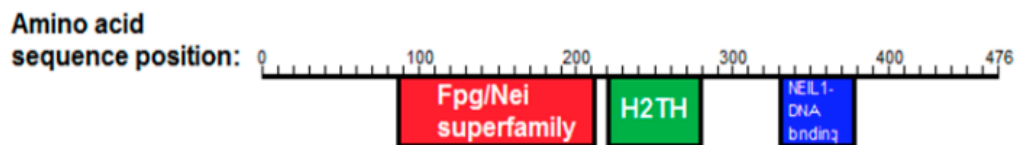


**Figure 1.8: Conserved domains of the DNA glycosylase NEIL1.**

Albelazi *et al.* (2019).

NEIL1 has been found to target oxidatively damaged bases such as Tg, FapyG, FapyA, and 8-oxoG and 5-OHU in single- and double-stranded DNA (Bosshard *et al.*, 2012). However, the DNA glycosylase has been found to prefer targeting certain oxidative lesions over others, such as Sp and Gh in double-stranded DNA and quadruplex DNA structures than with 8-oxoG, and Tg and 5-OHU in double-stranded DNA and when close to the DNA replication fork (Zhou *et al.*, 2013; Albelazi *et al.*, 2019). NEIL1 also showed evidence of unhooking ICLs, a DNA lesion usually repaired by the FA pathway. The first evidence was confirmed in three-stranded DNA structures with psoralen-induced ICLs unhooked by NEIL1 (Couvé *et al.*, 2009), which implied DNA repair from SSBs instead of DSBs. The evidence was further supported when NEIL1 aided in excising ICLs induced by psoralens in three- and four-stranded DNA compared to NEIL3, and ICLs induced by MMC in FANCA and FANCC deficient FA cells (Macé-Aimé *et al.*, 2010; Martin *et al.*, 2017). This suggested that NEIL1 could be used as a potential alternative treatment for ICL repair from FA phenotypical cells and phenotypically similar cancers. However, ICLs induced by other genotoxic agents required further confirmation.

### 1.5.1.2. NEIL2

NEIL2 is the smallest of the NEIL DNA glycosylases, with a protein amino acid length of 332 aa in human cells, and has an Fpg/Nei superfamily domain and an H2tH domain (as can be seen from Figure 1.9). Compared to the other NEIL glycosylases only NEIL2 has no DNA binding domains or zinc-finger domains at the C-terminus. Unlike the other NEIL DNA glycosylases, NEIL2 has been found to be constitutively expressed, independent of the cell cycle (Neurauter *et al.*, 2012), and regardless of age (Bosshard *et al.*, 2012). Similar to NEIL1, NEIL2 removes oxidatively damaged bases such as Tg, FapyG, FapyA, and 8-oxo-G, 5-OHU, 5-OHC, 5,6-dihydrothymine and 5,6-dihydrouracil (Bosshard *et al.*, 2012). However, NEIL2 would seem to prefer targeting cytosine-based oxidative lesions, and in single-stranded, double-stranded and bubble-structured DNA (Jacobs and Schär, 2012; Krokan and Bjoras, 2013).

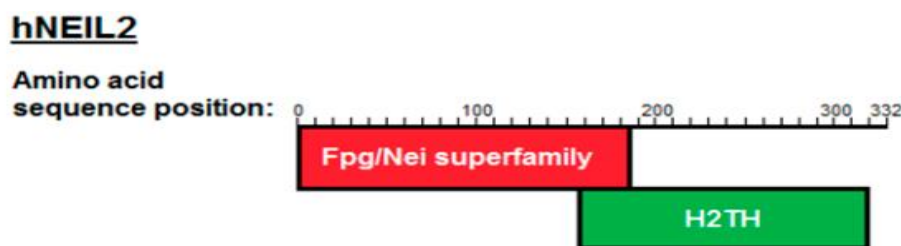


**Figure 1.9: Conserved domains of the DNA glycosylase NEIL2.**

Albelazi *et al.* (2019).

### 1.5.1.3. NEIL3

NEIL3 is the largest of the NEIL DNA glycosylases, with 605 amino acids in the human variant and has an Fpg/Nei superfamily domain, an H2tH domain, a Ran BP- zinc-finger (zf-RanBP) domain, and two zinc finger GRF (zf-GRF) domains (as can be seen from Figure 1.10). Of all the NEIL DNA glycosylases, only NEIL3 has three zinc-finger domains, including tandem GRF domains at the C-terminus. According to Wallace *et al.* (2017), the zf-GRF domain on the AP endonuclease 2 (APE2) is essential in activating the DDR following oxidative stress, because the DNA-binding regions coincide with the GRF region and zinc coordination. When compared to the NEIL3 amino acid sequence, the only common feature with APE2 is the zinc coordination, however the second zf-GRF in NEIL3 contains a lysine instead of arginine (Wallace *et al.*, 2017). Unlike NEIL1 and 2, the role of the DNA

glycosylase has been recently defined to generally initiate short-patch BER through bifunctional ( $\beta$ -elimination) when targeting oxidised DNA bases, but also could initiate long-patch BER through monofunctional DNA glycosylase activity when protecting telomeres from oxidative damage, while also maintaining DNA replication fork stability (Zhou *et al.*, 2017; Albelazi *et al.*, 2019). NEIL3 has been found to be cell-cycle regulated, the highest expression being during the S and G2 phase (Neurauter *et al.*, 2012), and highly expressed in the thymus, testes and tumour tissues, particularly metastatic tumours (Shinmura *et al.*, 2016; Klattenhoff *et al.*, 2017). It is also suggested that TRAIP is the regulator for NEIL3 under the same initial conditions as in the FA pathway when an ICL is present, however priorities are given to NEIL3 over the FA pathway based on the short and long ubiquitin chain lengths respectively (Wu *et al.*, 2019).

### **hNEIL3**

Amino acid  
sequence position:

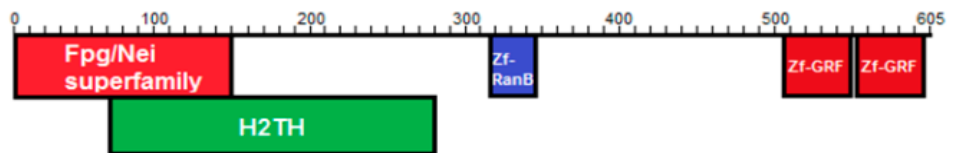


**Figure 1.10: Conserved domains of the DNA glycosylase NEIL3.**

Albelazi *et al.*, 2019.

A lack of NEIL3 has been found to increase the risk of autoimmune disorders with increased lymphocyte cell death and autoantibodies (Massaad *et al.*, 2016). Increased chromosomal damage and loss of telomeres has also been implicated with a lack of NEIL3 (Zhou *et al.*, 2017), and exhibit similarities to premature cell senescence and reduced ability of neurogenesis (Regnell *et al.*, 2012; Reis and Hermanson, 2012) when associated to NEIL3 deficiency, and an increase in cancer development and from chemotherapy resistance in cases displaying significantly elevated somatic mutations and NEIL3 overexpression (Shinmura *et al.*, 2016; Tran *et al.*, 2020). Although in mouse triple-knockouts of DNA glycosylases NEIL1, -2 and -3, accumulated spontaneous mutations were not increased, and cancers were not detected (Rolseth *et al.*, 2017). This implies the phenotypical consequences of cells deficient in NEIL3 expression to be susceptible to DNA instability, especially to oxidative stress, indicating that NEIL3 acts as cell-maintenance protein, but also NEIL3 overexpression indicates the DNA glycosylase as an aid to cancer. Therefore, NEIL3 requires strict control of expression in cells.

Normally the DNA glycosylase would target oxidatively damaged bases such as FapyA, FapyG, Sp and Gh in single-stranded DNA (Bosshard *et al.*, 2012; Klattenhoff *et al.*, 2017). However, recently through Albelazi *et al.* (2019), NEIL3 had shown a strong preference for excising 5-OHU and Tg, in single-stranded DNA and in the single DNA strand after the DNA replication fork. When compared to NEIL1, NEIL3 is categorised as the primary DNA glycosylase to excise oxidative lesions in single- and double-stranded DNA at the DNA replication fork, though it is possible that it may have a backup role when NEIL1 fails to excise an oxidative lesion in double-stranded DNA prior to the DNA replication fork (Albelazi *et al.*, 2019). Martin *et al.* (2017) had also found that NEIL3 had targeted Sp and Gh and not, as was thought, to also target 8-oxoG in three- and four-stranded DNA, in a more monofunctional manner. The same study also found psoralen-induced ICLs to be preferably unhooked by NEIL3 over NEIL1, which was thought to be the priority of the FA pathway but was first noticed by Semlow *et al.* (2016) being independent of the FA ID complex. Similar to the accumulated evidence of NEIL1 unhooking psoralen-induced ICLs (Couvé *et al.*, 2009; Macé-Aimé *et al.*, 2010; Martin *et al.*, 2017), this implied DNA repair from SSBs instead of DSBs from NEIL3. This also suggested that NEIL3 could be used as a potential alternative treatment for ICL repair from FA phenotypical and phenotypically similar cancers. However, ICLs induced by other genotoxic agents and through human cell cultures required further confirmation.

## 1.6. Hypothesis

NEIL3 knockout mouse embryonic fibroblasts (MEF) have been shown to be sensitised to cisplatin (Rolseth *et al.*, 2013), and the overexpression of *NEIL1* increased resistance to the ICL agent MMC (Macé-Aimé *et al.*, 2010). Furthermore, it has recently been shown that hNEIL1 and hNEIL3 can excise psoralen induced ICLs in three- and four-stranded DNA structures (Martin *et al.*, 2017). Fanconi anaemia cells are exquisitely sensitive to ICL inducing agents, and the *FANC* genes have been shown to be involved in ICL repair (Mehta and Ebens, 2002). Therefore, this project set out to determine if the overexpression of NEIL1 or NEIL3 in FA cells would increase their resistance to ICL inducing agents and siRNA knockdown of NEIL3 increase the sensitivity of FA cells to crosslinking agents, further indicating a role for these DNA glycosylases in the repair of ICLs in mammalian cells.

Indeed, during the duration of this project, Li *et al.* (2020) reported that NEIL3 knockout in FA generated cancer cells were sensitive to psoralen induced ICLs (Li *et al.*, 2020).

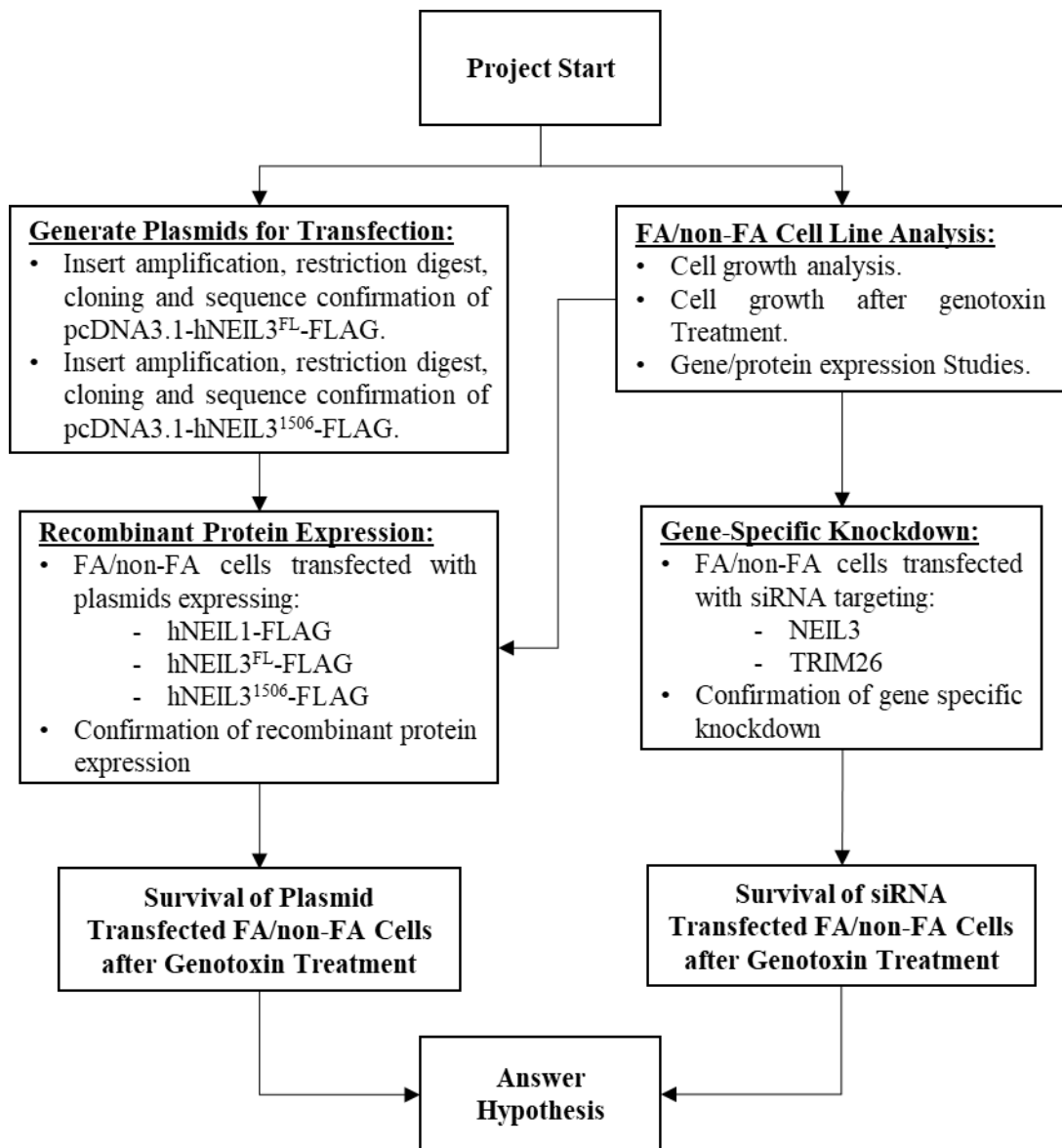


**Figure 1.11: Overall flowchart of the thesis project.**

The aims and objectives of this project was to (i) obtain background information on cell growth analysis, cell growth inhibition after ICL- and oxidative-inducing agent treatment and gene and protein expression on the FA and non-FA phenotypical cells (ii) generate an expression vector for FLAG-tagged NEIL3 full-length (hNEIL3<sup>FL</sup>) and truncated (hNEIL3<sup>1506</sup>) for recombinant expression in FA and non-FA phenotypical cells, (iii) compared to the expression vector with FLAG-tagged hNEIL1, determine the role of highly

expressed NEIL1 and NEIL3 in FA and non-FA phenotypical cells when treated with ICL- and oxidative-inducing genotoxic agents, and (iv) determine the role of NEIL1 and NEIL3 in FA and non-FA phenotypical cells with NEIL3 and NEIL1 ubiquitin-associated TRIM26 knockdown when treated with ICL- and oxidative-inducing genotoxic agents. An overall flow chart displaying how the aims and objectives were to be achieved can be observed in Figure 1.11.

## Chapter 2 Materials and Methods

### 2.1 Materials

#### 2.1.1. Cell lines

The human lymphocyte cell lines, HSC-93 (GM13072), HSC-72 (GM13022), HSC-72-Corrected, HSC-536 (GM13020) and HSC-536-Corrected, and the SV40 – immortalised human fibroblasts PD20 (GM16633) and FANCD2-3.15 (GM16634, referred to as 3.15) were kind gifts of Filippo Rosselli at the Institut Gustave Roussy, Paris, France. Subsequently, new stocks of PD20 and 3.15 were obtained from the NIGM Human Genetic Cell Repository at the Coriell Institute for Medical Research, Camden, New Jersey, USA. The FA status of all these cell lines is specified in Table 2.1 and reformatted from information displayed by the Coriell Institute database. The cancer cell lines HeLa and U2OS (WT and FANCD2 deficient) were kind gifts of Wojciech Niedzwiedz at The Institute of Cancer Research, London, UK. The cancer cell lines with the FANCD2 deficiency phenotype are referred to as HeLa-D2 and U2OS-D2, respectively, and were generated using the CRISPR/Cas9 method described in Schwab *et al.* (2015).

**Table 2.1: Fanconi anaemia cell line information.**

<b>Cell Line</b>	<b>Mutation(s) and Additional Information</b>	<b>Phenotype</b>
<b>HSC-72</b>	FA cell line, homozygous deletion of exons 18 to 28 of <i>FANCA</i> , resulting in <i>FANCA</i> deficiency and increased chromosomal breakage and ICL sensitivity (Joenje <i>et al.</i> , 2000).	<i>FANCA</i> Deficient
<b>HSC-72 Corrected</b>	Transfected with an episomal mammalian expression plasmid pCEP4 or pMEP4 with FLAG-tagged <i>FANCA</i> insert (Waisfisz <i>et al.</i> , 1999).	<i>FANCA</i> Corrected
<b>HSC-536</b>	FA cell line, T to C transition at nucleotide 1916 in exon 14 of <i>FANCC</i> , resulting in substitution of proline for leucine at codon 554. <i>FANCC</i> deficiency, increased chromosome breakage and ICL sensitivity (Coriell Institute).	<i>FANCC</i> Deficient
<b>HSC-536 Corrected</b>	Transfected with an episomal mammalian expression plasmid pMEP4 with FLAG-tagged <i>FANCC</i> insert (Waisfisz <i>et al.</i> , 1999).	<i>FANCC</i> Corrected
<b>PD20</b>	FA cell line with compound <i>FANCD2</i> heterozygosity: one allele has A to G transition at nucleotide 376, resulting in glycine substitution for serine at codon 126, and abnormal splicing and insertion of 13 bp from intron five into mRNA. Second allele has G to A transition at nucleotide 3707, resulting in histidine substitution for arginine at codon 1236. <i>FANCD2</i> deficiency, increased chromosome breakage and ICL sensitivity (Timmers <i>et al.</i> , 2001).	<i>FANCD2</i> Deficient
<b>3.15</b>	PD20 with microcell-mediated transfer of chromosome 3p, regular <i>FANCD2</i> expression (Timmers <i>et al.</i> , 2001). Also regarded as cell line <i>FANCD2</i> -3.15 (Castillo <i>et al.</i> , 2011).	<i>FANCD2</i> Corrected
<b>HeLa-D2</b>	HeLa cancer cells with 62 nucleotide deletion in exon 4 of <i>FANCD2</i> by CRISPR/Cas9. Based on the methodology from Schwab <i>et al.</i> (2015) used to generate U2OS-D2 cells.	<i>FANCD2</i> Deficient
<b>U2OS-D2</b>	U2OS cancer cells with 62 nucleotide deletion in exon 4 of <i>FANCD2</i> by CRISPR/Cas9. Based on the methodology from Schwab <i>et al.</i> (2015) and stated as <i>FANCD2</i> <sup>-/-</sup> .	<i>FANCD2</i> Deficient

### 2.1.2. Cell Culture Reagents

All cells described in Table 2.1 and their wild type counterparts (HeLa and U2OS WT) were cultured at 37°C, 5% CO<sub>2</sub> in a humidified atmosphere using complete culture medium as specified in Table 2.2, with the reagents specified in Table 2.3. Stock solutions of genotoxic agents were prepared according to the specifications listed in Table 2.4.

**Table 2.2: Cell lines and culture media.**

Cell Line	Cell Type	Culture Medium	Freezing Medium
<b>HSC-93</b>	Human lymphoblast; suspension cells	RPMI 1640 with 12% (v/v) FBS, 1% (v/v) L-glutamine and 1% (v/v) pen/strep	Culture Medium with 5% (v/v) DMSO
<b>HSC-72</b>			
<b>HSC-72 Corrected</b>			
<b>HSC-536</b>			
<b>HSC-536 Corrected</b>			
<b>PD20</b>	Human fibroblast; adherent cells	MEM with 12% (v/v) FBS, 1% (v/v) L-glutamine and 1% (v/v) pen/strep	Culture Medium with 10% (v/v) DMSO
<b>3.15</b>			
<b>U2OS</b>	Human epithelial; adherent cells	RPMI 1640 with 10% (v/v) FBS, 1% (v/v) L-glutamine and 1% (v/v) pen/strep	Culture Medium with 5% (v/v) DMSO
<b>U2OS-D2</b>			
<b>HeLa</b>	Human cervical, immortalised cancer cell line; adherent cells	DMEM with 10% (v/v) FBS, 1% (v/v) L-glutamine and 1% (v/v) pen/strep	
<b>HeLa-D2</b>			

**Table 2.3: Cell culture reagents.**

<b>Reagent</b>	<b>Specifications</b>
<b>Dimethyl Sulfoxide (DMSO)</b>	98-100% (#10213810, Fisher Chemical)
<b>Dulbecco's Modified Eagle Medium (DMEM)</b>	High glucose, sodium pyruvate, and phenol red (#21969035, Gibco)
<b>Foetal Bovine Serum (FBS)</b>	Heat-inactivated (#10500064, Gibco)
<b>G418 Solution</b>	50 mg/ml solution (#10092772, Gibco or #04727878001, Roche)
<b>L-glutamine</b>	200 mM (#25030024, Gibco)
<b>Minimal Essential Medium (MEM)</b>	Contains Earle's Balanced salt solution and phenol red (#12-125, Lonza)
<b>Opti-MEM</b>	Reduced serum medium (#31985062, Gibco)
<b>Penicillin/Streptomycin (Pen/Strep)</b>	10,000 Units/ml Penicillin, 10,000 µg/ml Streptomycin (#15140122, Gibco)
<b>Roswell Park Memorial Institute 1640 (RPMI 1640) medium</b>	Contains phenol red (#12-167, Lonza)
<b>TrypLE Express Enzyme</b>	1x working solution containing EDTA (1 mM) and phenol red (#12605028, Gibco)

**Table 2.4: Details of the genotoxic agents.**

		<b>Molecular Weight</b>	<b>Batch Stock Weight</b>	<b>Mass Required to Obtain 1 mM Stock in a Solvent</b>
<b>Genotoxic Agent</b>	<b>Mitomycin-C (MMC, Fisher BioReagents)</b>	334.33	10 mg	1 mg in 3 ml of dH <sub>2</sub> O
	<b>Cisplatin (Enzo Life Sciences)</b>	304.55	50 mg	0.9 mg in 3 ml of 0.9% saline
	<b><i>tert</i>-Butyl Hydroperoxide (TBHP, Sigma-Aldrich)</b>	90.12	70% of 0.93 g/ml	0.7 µl in 5 ml of dH <sub>2</sub> O

### 2.1.3. Microbiology and Molecular Biology Reagents

Stock solutions of microbial and molecular biology reagents were prepared as specified in Tables 2.5 and 2.6. Antibody solutions were prepared with blocking buffer, as specified in Table 2.12, with the antibodies listed in Table 2.7 at their specified dilution ratio. The prepared primary antibody solutions listed in Table 2.7 may be stocked and reused for up to ten reactions. The secondary antibody solution was prepared fresh at the time of use for one reaction.

**Table 2.5: Microbiology Reagents**

<b>Reagent</b>	<b>Specifications</b>
<b>Ampicillin</b>	100 mg/ml of ampicillin sodium salt (BP1760, Fisher BioReagents) in dH <sub>2</sub> O
<b>Kanamycin</b>	50 mg/ml of kanamycin (BP906, Fisher BioReagents) in dH <sub>2</sub> O
<b>Lysogeny Broth (LB)</b>	Luria low salt (L3397, Sigma-Aldrich)
<b>Ponceau S Solution</b>	0.1% (w/v) of electrophoresis grade Ponceau S (J60744, Alfa Aesar) in 5% (v/v) acetic acid

**Table 2.6: LB medium and LB-agar.**

<b>Component</b>	<b>LB Medium</b>	<b>LB-Agar</b>
<b>LB</b>	1.55 g	1.55 g
<b>Agar (Millipore)</b>	-	1.5 g
<b>dH<sub>2</sub>O</b>	100 ml	100 ml

Prepared LB-agar was suitable for four agar plates, approximately 25 ml per Petri dish.

**Table 2.7: Primary and secondary antibodies used for probing proteins  $\beta$ -Actin, FANCD2, FLAG-tag, GAPDH, NEIL1, NEIL3, and TRIM26.**

<b>Antibody</b>	<b>Antibody Use</b>	<b>Dilution Ratio</b>	<b>Protein of Interest</b>	<b>Expected Molecular Weight (kDa)</b>
<b>Anti-<math>\beta</math>-Actin, Mouse (sc-47778, Santa Cruz)</b>	Primary, Monoclonal	1:3000	$\beta$ -Actin	42
<b>Anti-FANCD2, Mouse (sc-20022, Santa Cruz)</b>	Primary, Monoclonal	1:1000	FANCD2	164
<b>Anti-FLAG, Mouse (F1804, Sigma-Aldrich)</b>	Primary, Monoclonal	1:1000	FLAG-tag	Protein of Interest + 1
<b>Anti-GAPDH, Mouse (CB1001, Sigma-Aldrich)</b>	Primary, Monoclonal	1:10000	GAPDH	36
<b>Anti-NEIL1, Mouse (sc-271164, Santa Cruz)</b>	Primary, Monoclonal	1:1000	NEIL1	43
<b>Anti-NEIL3, Mouse (sc-393703, Santa Cruz)</b>	Primary, Monoclonal	1:1000	NEIL3	68 (FL) 56 (1506)
<b>Anti-TRIM26, Mouse (sc-393832, Santa Cruz)</b>	Primary, Monoclonal	1:1000	TRIM26	62
<b>Anti-Mouse, Goat (A5278, Sigma-Aldrich)</b>	Secondary, Polyclonal, HRP	1:3000	Primary-antibodies grown in mouse	N/A

#### 2.1.4. Buffers

Stock solutions of 1x PBS and 1x TBE were prepared as specified in Table 2.8. The prepared lysis buffer, as detailed in Table 2.9, and 3x SDS-PAGE loading buffer, as detailed in Table 2.11, may be prepared fresh on day of use or stored at -20°C until required. The diluted 1x

stock solutions of from the 10x buffers detailed in Table 2.10 are stored at 4°C. The 1x SDS-PAGE running buffer and 1x WB transfer buffer stocks may be filtered after use and reused for up to ten reactions before fresh 1x buffer stocks were prepared.

**Table 2.8: List of pre-prepared buffers.**

<b>Buffer</b>	<b>Specifications</b>
<b>Phosphate Buffered Saline (PBS)</b>	10x solution (BP399-4, Fisher BioReagents) or 1x tablet per 100 ml solution (#12821680, Fisher BioReagents) diluted with dH <sub>2</sub> O
<b>Tris Base, Boric Acid and EDTA (TBE)</b>	10x solution (#20-6000-100, Severn Biotech Ltd.) diluted with dH <sub>2</sub> O

**Table 2.9: Lysis buffer for protein extraction.**

<b>Component</b>	<b>Final Concentration</b>
<b>Tris-HCl pH 7.5</b>	50 mM
<b>NaCl</b>	150 mM
<b>SDS</b>	0.1% (w/v)
<b>Sodium Deoxycholate</b>	0.5% (w/v)
<b>NP40</b>	1% (w/v)
<b>Halt Protease Inhibitor Cocktail (100x) (#87786, Thermo Scientific)</b>	1x

**Table 2.10: 10x SDS-PAGE running buffer and 10x western blot (WB) transfer buffer.**

<b>Component</b>	<b>10x SDS-PAGE Running Buffer</b>	<b>10x WB Transfer Buffer</b>
<b>Tris Base</b>	30 g	30 g
<b>Glycine</b>	144 g	144 g
<b>SDS</b>	10 g	-
<b>dH<sub>2</sub>O</b>	Up to 1 L	Up to 1 L

Diluted stock solutions of 1x SDS-PAGE running buffer in dH<sub>2</sub>O and 1x WB transfer buffer in dH<sub>2</sub>O with a final concentration of 20% (v/v) methanol.

**Table 2.11: 3x SDS-PAGE loading buffer.**

Component	Final Concentration
<b>Tris-HCl pH 6.8</b>	240 mM
<b>SDS</b>	6% (w/v)
<b>Glycerol</b>	30% (v/v)
<b>2-mercaptoethanol</b>	16% (v/v)
<b>Bromophenol blue</b>	0.006% (w/v)

**Table 2.12: Western blot blocking buffer and wash buffer.**

Component	Blocking Buffer	Washing Buffer
<b>Non-fat milk powder</b>	5% (w/v)	-
<b>PBS</b>	1x	1x
<b>Tween-20</b>	0.1% (v/v)	0.1% (v/v)

### 2.1.5. Plasmids

The plasmids pcDNA3.1-hNEIL1-FLAG and pETDUET2-hNEIL3 were from Elder Laboratory stocks. The pcDNA3.1 vector expresses highly stable and transient recombinant protein, aided by the human cytomegalovirus promoter, in mammalian cells, can be selected through neomycin resistance and sub-cloned through ampicillin resistance (pcDNA<sup>TM</sup>3.1(+/-) manual, Invitrogen). The pcDNA3.1-hNEIL1-FLAG plasmid was maintained as a NEIL1 expressing plasmid and the restriction double-digested vector for the ligation of the amplified NEIL3 coding sequences generated from pETDUET2-hNEIL3 and the subsequent pcDNA3.1-hNEIL3<sup>FL</sup>-FLAG plasmid throughout Section 2.2. The plasmids pcDNA3.1-hNEIL3<sup>FL</sup>-FLAG and pcDNA3.1-hNEIL3<sup>1506</sup>-FLAG the were described as ‘new’ plasmids throughout Section 3.4 were purchased through the plasmid subcloning services GeneArt (Thermo Fisher Scientific). The freshly purchased pcDNA3.1 plasmid (V79520, Invitrogen) was used for the plasmid transfection control in Sections 2.3.7. and 2.3.8. The pCR-Blunt II-TOPO plasmid was also from lab stocks as part of the ZeroBlunt PCR Cloning Kit with One Shot TOPO10 chemically competent *E. coli* cells (K2800J10, Invitrogen). The pCR-Blunt II-TOPO plasmid was used for cloning blunt-ended NEIL3 coding sequences amplified from pETDUET2-hNEIL3 and subsequent pcDNA3.1-

hNEIL3<sup>FL</sup>-FLAG before restriction double-digested with sticky ends to the restriction digested pcDNA3.1 vector.

#### 2.1.6. Nucleotide Sequences

The primer sequences for the amplification of the different *NEIL3* sequences for generating NEIL3 expressing plasmids are specified in Table 2.13, and the primer sequences for amplification of *β-Actin*, *ERCC1*, *FANCA*, *FANCD2*, *GAPDH*, *NEIL1*, *NEIL2*, and *NEIL3* are specified in Table 2.14. The siRNA's for GAPDH, NEIL3 and TRIM26 knockdown are detailed in Table 2.15

**Table 2.13: List of PCR primers for amplification of hNEIL3<sup>843</sup>, hNEIL3<sup>1506</sup> and hNEIL3<sup>FL</sup> inserts.**

<b>Primer</b>	<b>Primer Sequence (5' → 3')</b>	<b>PCR product size (bp)</b>
<b><u>XbaI</u>- hNEIL3- FLAG Fwd</b>	5'- <u>TCTAGAG</u> CCACCATGGTGGAAAGGACCAGGCTGTAC-3'	N/A
<b><u>EcoRI</u>- hNEIL3<sup>843</sup>- FLAG Rev</b>	5'-GAATTCCGGTCACTTGTCATCGTCGTCCTTGTAGT CTTTTGGACAGTGAGGACAGAAATATGTCATTC-3'	891
<b><u>EcoRI</u>- hNEIL3<sup>1506</sup>- FLAG Rev</b>	5'-GAATTCCGGTCACTTGTCATCGTCGTCCTTGTGTA GTCAGGATTTAAGGTACGAGGGCCATCTGT-3'	1554
<b><u>EcoRI</u>- hNEIL3<sup>FL</sup>- FLAG Rev</b>	5'-GAATTCCGGTCACTTGTCATCGTCGTCCTTGTGTA GTCGCATCCAGGAATAATTTTATTCTGTC-3'	1863

**Table 2.14: Primers for amplification of *β-Actin*, *ERCC1*, *FANCA*, *FANCD2*, *GAPDH*, *NEIL1*, *NEIL2*, and *NEIL3*, and their expected PCR product size.**

<b>Gene of Interest</b>	<b>Primer</b>	<b>Primer Sequence (5' → 3')</b>	<b>PCR Product Size (bp)</b>
<i>β-Actin</i>	β-ACTIN Fwd	5'-TCTGGCACCACACCTTCTAC-3'	166
	β-ACTIN Rev	5'-AGCACAGCCTGGATAGCAAC-3'	
<i>ERCC1</i>	ERCC1 Fwd	5'-CAAAACGGACAGTCAGACCCT-3'	146
	ERCC1 Rev	5'-TCAAGAAGGGCTCGTGCAG-3'	
<i>FANCA</i>	FANCA Fwd	5'-GCTCAAGGGTCAGGGCAA-3'	91
	FANCA Rev	5'-GAAGCTCTTTTTTCGGGCACC-3'	
<i>FANCD2</i>	FANCD2 Fwd	5'-GGCTTTCTGGCTGGGCAATC-3'	181
	FANCD2 Rev	5'-AATGCAACCATCAGTGCCAGAC-3'	
<i>GAPDH</i>	GAPDH Fwd	5'-GGTGGTCTCCTCTGACTTCAACA-3'	127
	GAPDH Rev	5'-GTTGCTGTAGCCAAATTCGTTGT-3'	
<i>NEIL1</i>	NEIL1 Fwd	5'-AGAAGATAAGGACCAAGCTGC-3'	212
	NEIL1 Rev	5'-GATCCCCCTGGAACCAGATG-3'	
<i>NEIL2</i>	NEIL2 Fwd	5'-GCCTTAGAAGCTCTAGGCCA-3'	145
	NEIL2 Rev	5'-GCACTCAGGACTGAACCGAG-3'	
<i>NEIL3</i>	NEIL3 Fwd	5'-CGCCTCTGCATTGTCCGAGT-3'	147
	NEIL3 Rev	5'-TGGAACGCTTGCCATGGTTG-3'	

**Table 2.15: siRNA for targeted knockdown.**

siRNA with Catalogue Number (Qiagen)	Target	siRNA Sequence (5' → 3')
<b>AllStars Negative Control siRNA (#1027280)</b>	Non-Specific (NS)	N/A
<b>Hs_GAPDH_3 (Si03571113)</b>	GAPDH	5'-AAGGUCGGAGUCAACGGAUUU-3'
<b>Hs_NEIL3_1 (Si00121205)</b>	NEIL3	5'-CAGAUGGCCCUUCGUACCUUAA-3'
<b>Hs_TRIM26_4 (Si00052129)</b>	TRIM26	5'-ACCGGAGAAUUCUCAGAUAAA-3'

All siRNA were purchased predesigned from the FlexiTube siRNA (Qiagen) service.

## 2.2. Plasmid Sub-Cloning Methods

### 2.2.1. Agarose Gel Electrophoresis

Agarose (Fisher Chemical) was weighed according to the percentage specified in later protocols and mixed with either 50 ml or 100 ml of 0.5x TBE buffer in a 250 ml Duran bottle. For a small casting tray (loading up to eight samples), 50 ml of buffer was required, and for a large casting tray (loading up to 20 samples), 100 ml of buffer was used. The agarose mixture was heated in a microwave oven at a medium-high setting until the agarose had dissolved. Then, 0.01% (v/v) of SYBR Safe gel stain concentrate (Thermo Scientific) was added, and the agarose solution was left to cool down to around 50°C before it was poured into a casting tray with a well-forming comb. Once set, the agarose gel and casting tray were transferred to an electrophoresis apparatus with the wells at the cathode end, submerged under 0.5x TBE buffer and the comb removed. Together with a DNA ladder (100 bp DNA ladder [NEB] or GeneRuler 50 bp DNA ladder [Thermo Scientific] for up to 1.5 kb DNA product; Hyperladder 1 kb [Bioline] or 1 kb DNA ladder [NEB] for up to 10 kb DNA product), samples were loaded with a pipette and electrophoresis carried out as specified in sections 2.2.2., 2.2.5., 2.2.6., 2.3.3. and 2.4.

### 2.2.2. Polymerase Chain Reaction (PCR)

For the amplification of different NEIL3 coding sequences, using the primers listed in Table 2.13, one of two proofreading DNA polymerases obtained from New England Biolabs (NEB) was used, either Phusion DNA polymerase or Q5 DNA polymerase. The reaction mixtures and reaction conditions for each are given in Tables 2.16 and 2.17.

**Table 2.16: Phusion and Q5 PCR reaction mixture.**

<b>Component</b>	<b>Phusion Reaction Mixture</b>	<b>Q5 Reaction Mixture</b>
<b>5x HF Phusion Buffer</b>	4 $\mu$ l	-
<b>5x Q5 Reaction Buffer</b>	-	5 $\mu$ l
<b>10 mM dNTPs</b>	0.4 $\mu$ l	0.5 $\mu$ l
<b>10 <math>\mu</math>M Forward Primer</b>	1.0 $\mu$ l	1.25 $\mu$ l
<b>10 <math>\mu</math>M Reverse Primer</b>	1.0 $\mu$ l	1.25 $\mu$ l
<b>Template DNA</b>	< 250 ng	< 1 $\mu$ g
<b>Phusion DNA Polymerase</b>	0.2 $\mu$ l	-
<b>Q5 High-Fidelity DNA Polymerase</b>	-	0.25 $\mu$ l
<b>Nuclease-Free Water</b>	Up to 20 $\mu$ l	Up to 25 $\mu$ l

The PCR reaction mixtures were prepared in 0.2 ml PCR tubes as detailed in Table 2.16. The samples, along with a negative control containing no DNA template, were kept in ice until ready for transfer to a thermocycler. PCR conditions are given in Table 2.17.

**Table 2.17: Thermocycling conditions for Phusion or Q5 PCR.**

Step	Temperature	Time
Hot Lid	105°C	-
Initial Denaturation	98°C	30 s
30 Cycles	98°C	10 s
	*50 – 72°C	30 s
	72°C	30 s/kb
Final Extension	72°C	10 min (Phusion)
		2 min (Q5)
Hold	4 – 10°C	∞

The annealing temperature (\*) depended on the melting temperature of the primers used in Table 2.13. Annealing temperature for NEIL3<sup>843</sup>-FLAG (Phusion) and NEIL3<sup>1506</sup>-FLAG (Q5), 72°C; NEIL3<sup>FL</sup>-FLAG (Phusion), 76°C with touchdown (-1°C per cycle).

To check that the PCR reactions had been successful, an aliquot of the PCR reaction mixture was subjected to agarose gel electrophoresis. A 1% (w/v) agarose gel was prepared as described in Section 2.2.1. Five microlitres of each PCR reaction was combined with 1 µl of 6x gel loading dye (NEB) and then were loaded onto the agarose gel. Electrophoresis was carried out at 100V for 1 h 20 min, after which the gel was transferred to a UV-transilluminator in a gel imager (G:BOX, Syngene) and the image recorded for further analysis.

### 2.2.3. ZeroBlunt Cloning

A ZeroBlunt PCR Cloning Kit with One Shot TOPO10 chemically competent *E. coli* cells (Invitrogen) was used for cloning the PCR products generated in Section 2.2.2. following the manufacturer's instructions. The PCR products were quantified using a spectrophotometer (NanoDrop 2000, Thermo Scientific) before the ligation reaction.

**Table 2.18: Ligation reaction mixture.**

Component	Reaction Mixture
PCR Product	> 5 ng
1.2 M NaCl	1 $\mu$ l
pCR-Blunt II-Topo	1 $\mu$ l
Nuclease-Free Water	Up to 6 $\mu$ l

The ligation reaction was prepared in a 0.5 ml microcentrifuge tube, as detailed in Table 2.18. The ligation mixture was mixed by pipetting and then incubated at room temperature (approx. 22.5°C) for 1 h, then immediately transferred to ice. Two microlitres of ligation mixture was then transferred to a thawed, 20  $\mu$ l aliquot of ‘One Shot chemically competent *E. coli*’ and incubated on ice for at least 5 min. The mixture was then heat-shocked in a water bath at 42°C for 30 s without shaking and immediately transferred into ice for a minimum of 2 min. Subsequently, 250  $\mu$ l of room-temperature S.O.C. (super optimal broth with catabolite repression, Invitrogen) medium was added and the tube containing the transformed *E. coli* cells was incubated horizontally for 1 h in a shaking incubator at 37°C and 200 rpm.

Aliquots of 10  $\mu$ l or 70  $\mu$ l of the transformed sample were then spread evenly on a pre-warmed LB-agar plate containing 50  $\mu$ g/ml kanamycin and then incubated overnight at 37°C. At least five colonies were picked and transferred to separate 30 ml universal tubes containing 6 ml of LB medium and 50  $\mu$ g/ml kanamycin. The transformed *E. coli* were then incubated for at least 16 h in a shaking incubator at 37°C and 250 rpm to allow cell growth.

#### 2.2.4. Plasmid Purification: Mini-Prep

An Isolate II Plasmid Mini Kit (Bioline) was used to purify plasmids following the manufacturer’s instructions and is described in brief here. Before proceeding, 850  $\mu$ l of the *E. coli* liquid culture was transferred to a 2 ml cryotube containing 150  $\mu$ l of 50% (v/v) glycerol, then frozen at -80°C. For each clone, a total of 5 ml of *E. coli* culture was transferred (three separate aliquots of approx. 1.7 ml each) into a 2 ml microcentrifuge tube and centrifuged at 11,000 X g for 30 s. The supernatant was discarded each time, and following the last aliquot 250  $\mu$ l of resuspension buffer (P1) was added and the bacterial cell pellet was resuspended by vortexing. Subsequently, 250  $\mu$ l of lysis buffer (P2) was added,

and the mixture was mixed by inverting the tube 8 times. The resulting lysate was then incubated at room temperature for 5 min. Three hundred microlitres of neutralisation buffer (P3) was then added and mixed thoroughly by inverting the tube 8 times, followed by centrifugation at 11,000 X g for 5 min.

The clarified supernatant was transferred into the spin column within a collection tube and centrifuged at 11,000 X g for 1 min. The flow-through was discarded and then 500 µl of 50°C preheated wash buffer (PW1) was added, followed by centrifugation at 11,000 X g for 1 min. This step was repeated, followed by the addition of 600 µl of room-temperature wash buffer (PW2). The spin column was then dried by centrifugation at 11,000 X g for 2 min, followed by the replacement of the collection tube with a 1.5 ml microcentrifuge tube. Finally, 30 µl of 70°C preheated elution buffer (P) was added directly onto the silica membrane in the spin column and incubated at room temperature for 1 min, then centrifuged at 11,000 X g for 1 min. A spectrophotometer (NanoDrop 2000, Thermo Scientific) was then used to quantify the DNA in the elution buffer containing the purified plasmids.

#### 2.2.5. Restriction Double-Digest

**Table 2.19: Restriction double-digest reaction mixture.**

<b>Component</b>	<b>Reaction Mixture</b>
<b>Template DNA</b>	Approx. 500 ng
<b>10x Cutsmart Buffer (NEB)</b>	2.5 µl
<b>Restriction Enzyme 1 (XbaI or EcoRI-HF, NEB)</b>	0.5 µl or 5 units
<b>Restriction Enzyme 2 (XbaI or EcoRI-HF, NEB)</b>	0.5 µl or 5 units
<b>Nuclease-Free Water</b>	Up to 25 µl

Restriction enzymes 1 and 2 are dependent on the orientation of the PCR product with restriction sites to the orientation of the restriction sites in the plasmid.

The reaction mixture was prepared in a 0.2 ml PCR tube, as detailed in Table 2.19, incubated at 37°C for 1 h, then placed in ice. For sequential double-digestion, the reaction mixture was prepared without restriction enzyme 2, which was added after an initial incubation period. Thus, following incubation at 37°C for 1 h and 65°C for 20 min to denature restriction enzyme 1, 0.5 µl of restriction enzyme 2 was added to the sample and incubation was carried out for a further 1 h at 37°C. To check that the reaction had worked, 5 µl of reaction mixture

was combined with 1 µl of 6x gel loading dye (NEB), and subjected to agarose gel electrophoresis through a 1% (w/v) agarose gel at 100V for 1 h 20 min. Following electrophoresis, the gel was transferred to a UV-transilluminator for gel imaging (G:BOX, Syngene) and the results recorded for further analysis.

#### 2.2.6. Purification of DNA Fragments

An ISOLATE II PCR and Gel Kit (Bioline) was used to purify DNA fragments obtained from PCR and restriction endonuclease digests, following the manufacturer's instructions. PCR and restriction endonuclease digests were performed as described in Sections 2.2.2. and 2.2.5. at double the volumes stated and, for restriction double-digests up to 5 µg of DNA template, to achieve a sufficient quantity of DNA. Agarose gel electrophoresis was carried out using a 2% (w/v) agarose gel, and electrophoresis was carried out at 120V for 2 h.

To extract DNA from an agarose gel, the desired DNA fragment was first excised with a sterilised scalpel over a UV-light source, and the excess agarose was removed before the gel was weighed and transferred into a 2 ml microcentrifuge tube. Subsequently, 200 µl of binding buffer (CW) was added per 100 mg of agarose gel and the sample was incubated at 50°C for 5 – 10 min, with vortexing approximately every 3 min until the gel slice was completely dissolved. If the DNA sample was directly derived from a PCR reaction, then two parts of binding buffer (CB) were added per one part of the sample (when less than 30 µl, the sample was adjusted to 50 µl by adding nuclease-free water beforehand).

The samples were then transferred into spin columns within collection tubes and centrifuged at 11,000 X g for 30 s, after which the flow-through was discarded. Next, 700 µl of wash buffer (CW) was added to the spin columns and centrifugation repeated at 11,000 X g for 30 s, discarding the flow-through afterwards. This step was repeated, and then the spin columns were dried by centrifugation at 11,000 X g for 1 min. The spin columns were then transferred to 1.5 ml microcentrifuge tubes, incubated at 70°C for 2 – 5 min, followed by the addition of 20 µl of elution buffer (C) directly onto the silica membrane in the spin column and incubated at room temperature for 1 min. Finally, the samples were centrifuged at 11,000 X g for 1 min and the DNA quantified using a spectrophotometer (NanoDrop 2000, Thermo Scientific).

### 2.2.7. T4 DNA Ligation

Ligation was performed using T4 DNA Ligase (NEB) following the manufacturer's instruction, and cloning was performed with NovaBlue *E. coli* cells (Novagen).

**Table 2.20: T4 ligation reaction mixture.**

Component	Reaction Mixture
<b>10x T4 DNA Ligase Buffer</b>	2 $\mu$ l
<b>Plasmid Product (5 Kb)</b>	50 ng
<b>PCR Product (2 Kb)</b>	60 ng
<b>T4 DNA Ligase</b>	1 $\mu$ l
<b>Nuclease-Free Water</b>	Up to 20 $\mu$ l

The molar ratio for plasmid:PCR-product was set at 1:3.

The ligation reaction was prepared as indicated in Table 2.20 in a 0.2 ml PCR tube and incubated at room temperature for 1 h followed by incubation at 65°C for 10 min, then immediately transferred to ice. Subsequently, 1 - 2  $\mu$ l of the ligation mixture was transferred to 20  $\mu$ l of competent NovaBlue *E. coli* cells in a 0.5 ml microcentrifuge tube and incubated on ice for at least 5 min. The transformation mixture was then heat-shocked in a water bath at 42°C for 30 s without shaking and then placed in ice for a minimum of 5 min. Subsequently, 80  $\mu$ l of room-temperature S.O.C. medium (Invitrogen) was added, and the tube placed horizontally for 1 h in a shaking incubator at 37°C and 250 rpm. Following this, aliquots of either 20  $\mu$ l or 80  $\mu$ l were spread on prewarmed LB-agar plates containing 100 mg/ml of ampicillin, then incubated overnight at 37°C.

At least four colonies were picked and transferred to separate 30 ml universal tubes containing 6 ml of LB medium and 100  $\mu$ g/ml ampicillin. The transformed *E. coli* were then incubated in a shaking incubator for at least 16 h at 37°C and 250 rpm. Plasmids were then obtained by plasmid purification, as detailed in Section 2.2.4., and correctly recombined plasmids confirmed through restriction endonuclease double-digestion as detailed in Section 2.2.5.

## 2.2.8. Sanger DNA Sequencing

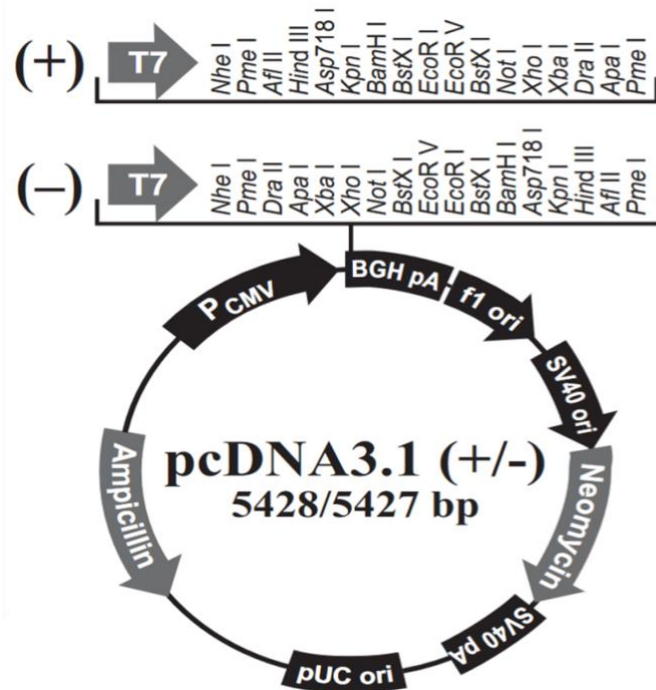


**Figure 2.1: Vector map of pcDNA3.1 with restriction digest sites in forward (+) or reverse (-).**

Derived and modified from the pcDNA<sup>TM</sup>3.1(+/-) manual (Invitrogen).

A third-party service conducted the Sanger Sequencing protocol: Source BioScience Limited, UK, with the samples prepared as per instructions provided. DNA sequencing was conducted using the primers provided by the third-party service targeting the human cytomegalovirus (CMV) promoter site (targeting P<sub>CMV</sub>, Figure 2.1) for forwarding sequencing and the bovine growth hormone (bGH) polyadenylation site (targeting BGH pA, Figure 2.1) for reverse sequencing. The sequence data was received in chromatogram ABIF file format and FASTA sequence file format. Sequence data was then compared to a reference sequence and visualised through the bioinformatics software Unipro UGENE version 39.0 (Okonechnikov *et al.*, 2012).

## 2.3. Cell Culture Methods

All work was carried out in a laminar-flow hood, and all equipment and materials were sterilised with 5% (v/v) Chemgene and 70% (v/v) ethanol before and during each protocol. Materials and conditions for cell lines are specified in Section 2.1.2. Before any experiment,

all cell cultures were prepared 24 – 48 h after sub-culturing and when the cell cultures were within the exponential growth phase.

As required, the cell culture medium was changed when adherent cells were at less than 80% confluency. At 48 – 72 h intervals, the medium was discarded and exchanged for an appropriate volume of prewarmed medium (5 ml for a T25 flask; 15 ml for a T75 flask). For splitting adherent cells to continue cell growth, the medium was discarded, cells washed with PBS, and then an appropriate volume of prewarmed TrypLE Express Enzyme (Gibco) was added to each flask (1.5 ml for a T25; 3 ml for a T75). Flasks were transferred to an incubator (37°C / 5% CO<sub>2</sub>) for 2 – 3 min, after which the flasks were removed and tapped to dislodge the cells. A volume of cell culture medium of at least twice the volume of TrypLE Express was added to deactivate enzymatic dissociation. The cell suspension was diluted 1:5 in medium and transferred to new T25 (5 ml) or T75 (15 ml) flasks before being transferred to a humidified incubator at 37°C and 5% CO<sub>2</sub>.

For suspension cells, confluency was determined through cell counting, as detailed in Section 2.3.1. The cells were transferred into a sterile 15 ml or 50 ml centrifuge tube and centrifuged at 1,500 rpm for 5 min. After centrifugation, the supernatant was discarded, and the cell pellet was resuspended in the appropriate volume of medium (10 ml for a T25 flask; 50 ml for a T75 flask). The cells were transferred to a humidified incubator at 37°C and 5% CO<sub>2</sub>.

### 2.3.1. Cell Counting

For the determination of the number of cells in culture, either 10 µl of cell culture was removed or 5 µl mixed with 5 µl of trypan blue solution (Gibco). The solution was then transferred to a Neubauer haemocytometer on top of the grid (as shown in Figure 2.2) and covered with a coverslip (unless using a disposable haemocytometer [C-Chip, NanoEntek]). Under a microscope at 10 – 40x magnification, the cells were distinguished by their viability due to the differential trypan blue staining. Blue-stained cells indicated the cells were non-viable, and clear/unstained cells indicated the cells were viable. The cell concentration was determined by counting the viable cells within the sectioned grids as shown in Figure 2.2 and then calculated using the formula(s) displayed in Figure 2.3.

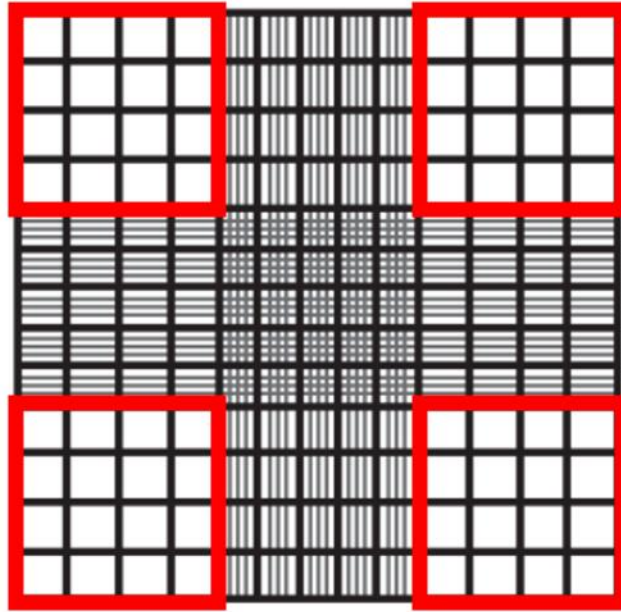


**Figure 2.2: Neubauer haemocytometer grid with grid sections highlighted in red for cell counting.**

Derived and modified from C-Chip Instructions (NanoEntek).

$$\text{Cell concentration} = \frac{\begin{array}{c} \text{(Total number of viable cells in} \\ \text{highlighted grid sections)} \end{array}}{4} \times \text{dilution factor} \times 10^4$$

(total number of grid sections)

$$\text{Cell viability} = \frac{\text{Total number of viable cells}}{\begin{array}{c} \text{Total number of cells} \\ \text{(viable + non-viable)} \end{array}} \times 100$$

**Figure 2.3: Mathematical formulas for calculating the cell concentration (cells/ml) and percentage cell viability.**

### 2.3.2. Freeze/Thaw Protocol for Cell Lines

For freezing cell lines, the concentration of cells in a given volume was determined, as described in Section 2.3.1., and cells diluted or concentrated as required to obtain the desired target of  $2 \times 10^6$  cells per ml of freezing medium (Table 2.2). The suspension cells were transferred to a 1.5 – 2 ml cryotube and incubated at room temperature for 2 min before adding and mixing the DMSO. The cells were immediately transferred to an isopropanol

chamber, then to a -80°C freezer for slow controlled freezing overnight, before being transferred to liquid-nitrogen storage. For seeding stocks, the cells remained in the -80°C freezer until needed.

For thawing cells, a vial of frozen cells was transferred to a 37°C water bath for 1 – 2 min. The thawed cell stock was gently mixed by pipetting before being transferred to a 2 ml centrifuge tube and centrifuged at 2,000 rpm for 3 min. The supernatant was discarded, and the cell pellet was resuspended in 1 ml of cell culture medium before transfer to a T25 vented cell-culture flask containing appropriate cell culture medium (5 ml for adherent cells; 10 ml for suspension cells). Finally, the cells were transferred to a humidified incubator at 37°C and 5% CO<sub>2</sub>. The cells were analysed the next day and, if appropriate, sub-cultured after 24 h of the initial incubation.

### 2.3.3. Mycoplasma Contamination Detection and Treatment

To detect mycoplasma contamination in cell cultures, a LookOut® Mycoplasma PCR Detection Kit with JumpStart *Taq* DNA Polymerase (Sigma-Aldrich) or a Mycoplasma PCR Detection Kit (ABM) was used. The cells were grown until approximately 70% confluent or higher and 24 – 72 hours after sub-culturing.

For the mycoplasma detection kit from Sigma-Aldrich, cell samples were prepared by transferring 100 µl of cell culture medium (or fresh culture medium as a control) to 0.5 ml microcentrifuge tubes, followed by incubation at 95°C for 5 min before pulse – centrifugation for approximately 5 s.

**Table 2.21: PCR reaction mixtures for mycoplasma detection (Sigma-Aldrich kit).**

<b>Component</b>	<b>Positive Control (Pink Tube)</b>	<b>Negative Control (Clear Tube)</b>	<b>Test Sample (Clear Tube)</b>
<b>DNA Polymerase/ Buffer Master Mix</b>	25 µl	23 µl	23 µl
<b>Test Sample Supernatant</b>	-	-	2 µl
<b>Nuclease-Free Water</b>	-	2 µl	-

Coloured tubes were prepared and assigned as per instructions in the protocol booklet.

For each reaction, the DNA Polymerase/Buffer master mix of 25  $\mu$ l total was prepared with 24.5  $\mu$ l of rehydration buffer mixed with 0.5  $\mu$ l of JumpStart *Taq* DNA polymerase. The reactions were prepared as shown in Table 2.21. The samples were then incubated at room temperature for 5 min, then kept in fresh ice until ready for transfer to a thermocycler. The PCR conditions are given in Table 2.22.

**Table 2.22: Thermocycling conditions for mycoplasma detection (Sigma-Aldrich kit).**

Step	Temperature	Time
<b>Heated Lid</b>	105°C	-
<b>Initial Denaturation</b>	94°C	2 min
<b>40 Cycles</b>	94°C	30 s
	55°C	30 s
	72°C	40 s
<b>Hold</b>	4 – 8°C	$\infty$

For the mycoplasma detection kit from ABM, samples were prepared by transferring 0.5 ml of cell culture medium (or fresh culture medium as a control) to 1.5 ml microcentrifuge tubes, centrifuged at 2,000 rpm for 3 min to pellet any cells. Followed by transferring 450  $\mu$ l of supernatant to another 1.5 ml microcentrifuge tube, the supernatant was centrifuged at 15,000 X g or higher for 10 min. Four hundred microlitres of supernatant was then discarded, with the residual 50  $\mu$ l supernatant used to resuspend a non-visible pellet and as the test sample. The PCR reactions were prepared as shown in Table 2.23 and were then kept in ice until ready for transfer to a thermocycler. The PCR conditions are given in Table 2.24.

**Table 2.23: PCR reaction mixtures for mycoplasma detection (ABM kit).**

Component	Positive Control	Negative Control	Test Sample
<b>2x PCR <i>Taq</i> Master Mix</b>	12.5 $\mu$ l	12.5 $\mu$ l	12.5 $\mu$ l
<b>Mycoplasma PCR Primer Mix</b>	1 $\mu$ l	1 $\mu$ l	1 $\mu$ l
<b>Mycoplasma Positive Control</b>	1 $\mu$ l	-	-
<b>Test Sample</b>	-	-	2.5 $\mu$ l
<b>Nuclease-Free Water</b>	10.5 $\mu$ l	11.5 $\mu$ l	9 $\mu$ l

**Table 2.24: Thermocycling conditions for mycoplasma detection (ABM kit).**

Step	Temperature	Time
<b>Heated Lid</b>	105°C	-
<b>Initial Denaturation</b>	95°C	5 min
<b>40 Cycles</b>	95°C	30 s
	55°C	30 s
	72°C	1 min
<b>Final Extension</b>	72°C	10 min
<b>Hold</b>	4°C	∞

The PCR reaction mixtures from either mycoplasma detection kit were subsequently subjected to agarose gel electrophoresis, with a 1.2% (w/v) agarose gel prepared as described in Section 2.2.1. Ten microlitres of the PCR reaction were loaded into the agarose gel, and electrophoresis was carried out at 100V for 30 min. The agarose gel was transferred to a UV-transilluminator in a gel imager (G:BOX, Syngene), and results were recorded for further analysis.

If mycoplasma contamination was detected, the Plasmocin™ Treatment kit (InvivoGen) was used, following the manufacturer's instructions. A fresh stock of complete medium containing 25 µg/ml of Plasmocin was prepared. Using the standard protocol of sub-culturing, cells were grown in this 'treatment medium' for at least 2 weeks. By the end of the allotted time, cells were transferred to the standard culture medium without Plasmocin, and incubation continued for 24 – 48 hours before samples were collected, as described above. If mycoplasma contamination was still detected, the Plasmocin treatment was continued for a further week. Following this, if mycoplasma was still detected, the cells were discarded.

#### 2.3.4. MTT/MTS Assay

To measure cell proliferation and growth inhibition, the MTT/MTS assay was used as a measure of cellular metabolic activity. The MTT assay was used for adherent cells in flat-bottomed 96-well plates, and the MTT solution was prepared as 3 mg/ml of thiazolyl blue tetrazolium bromide (Acros Organics) in 1x PBS solution. The MTS assay was used for

suspension cells in U-shaped bottomed 96-well plates, and the CellTiter 96<sup>®</sup> AQueous One Solution Reagent (Promega) was used as the MTS solution.

After a 96-well plate of treated cells had completed the allotted incubation time the MTT/MTS solutions were added to all wells containing cell culture medium. For adherent cells, 25 µl of MTT solution per 100 µl of cell culture medium was added, and for suspension cells, 20 µl of MTS solution per 100 µl of cell culture medium was added. The plates were incubated in the dark at 37°C with 5% CO<sub>2</sub> in a humidified environment for 3 – 4 h. For MTT assay only, following this, the MTT solution was carefully aspirated from the wells, and 100 µl of DMSO was added. Subsequently, the 96-well plates were agitated on a rocker at 930 rpm for 30 s to ensure complete solubilisation of the purple formazan crystals before the plate was placed in a plate-reader spectrophotometer (Multiskan Ascent, Thermo Scientific). The absorbance reading was taken for MTT assay at 570 nm, or an absorbance filter between 540 nm and 610 nm (CellTiter<sup>®</sup> 96 Non-radioactive Cell Proliferation Assay manual for MTT, Promega), and at 490 nm, or an absorbance filter between 450 nm and 540 nm, for MTS assay (CellTiter<sup>®</sup> 96 AQueous One Solution Cell Proliferation Assay manual for MTS, Promega). A reference wavelength at 690 nm, or an absorbance filter between 630 nm and 750 nm, is also taken to eliminate background readings contributed to nonspecific absorbance readings, debris particulates and fingerprints.

#### 2.3.5. Determination of Cell Growth Rate

Four 96-well plates were labelled with the time period of the assay conducted (24 h, 48 h, 72 h and 96 h) and by the cells to be added per triplicate wells. The cell culture(s) were first quantified, as described in Section 2.3.1., and then diluted to an appropriate cell concentration that could be aliquoted as the initial stock. As an example of aliquoting  $2 \times 10^3$ ,  $4 \times 10^3$ , and  $8 \times 10^3$  cells in triplicates the number of cells required is  $4.2 \times 10^4$  cells per cell line, or, for four plates, a total of  $1.68 \times 10^5$  cells per cell line; therefore, at least  $2 \times 10^5$  cells per cell line were needed.

Once the preparations were completed, 200 µl of 1x PBS, 100 µl of complete medium and 100 µl of diluted cell cultures were aliquoted to their assigned wells. The 1x PBS was aliquoted to the outer-most wells of the 96-well plate to form a condensation barrier in the incubator, and the complete medium as a MTT/MTS assay absorbance reading control

between complete medium with and without cells. The 96-well plates were then incubated at 37°C with 5% CO<sub>2</sub> in a humidified environment, and the time of the incubation period was noted. At 24 h, the appropriate plate was removed from the incubator and the standard MTT/MTS assay described in Section 2.3.4. was followed. The assay step was repeated for the remaining 48-, 72- and 96-h plates at their appropriate times and the data was recorded for further analysis.

### 2.3.6. The Effect of Genotoxic Agents on Cell Growth

Liquid stocks of each genotoxic agent were prepared using the parameters described in Table 2.4. Preparations were carried out within a fume-hood, and with as little light as possible, due to the light sensitivity of some of the chemicals. For long-term storage, stock solutions were stored at -80°C, unless stated otherwise from the product's safety data sheet. A 96-well plate was labelled by the components to be added per well. Based on the cell-lines growth curve results, the cell culture(s) were first quantified, as described in Section 2.3.1., and then diluted to the appropriate cell concentration. The dilutions were then taken into account when aliquoting 100 µl of the quantified cell cultures per triplicate technical repeats, per treatment concentration reaction. Once the preparations were completed, 200 µl of 1xPBS for the condensation barrier, 200 µl of complete medium for MTT/MTS assay control between mediums with and without cells, and 100 µl of diluted cell cultures were aliquoted to their assigned wells. When done, the 96-well plate(s) was then incubated at 37°C and 5% CO<sub>2</sub> in a humidified atmosphere for the appropriate incubation period.

Up to twenty-three hours after the allotted time, a duplicate 96-well plate was labelled by the components to be added mirroring the cell-culture plate. This duplicate plate was in preparation for initial serial dilution of the genotoxic-agent stocks before aliquoting to the plate of cells at a final dilution. As an example, if the aim of a final genotoxic agent dilution was 5 µM as Dilution 1 for the plate of cells (96-well plate, row A), then 10 µM was prepared in the respectable duplicate plate wells before aliquoting. Within the duplicate plate, 150 µl of complete medium was transferred to the dilution-assigned wells (96-well plate, rows B - H) apart from the Dilution 1 wells (row A). With the prepared genotoxic-agent stocks diluted at an appropriate concentration in complete medium, 300 µl was transferred to the assigned Dilution 1 wells. Initial serial dilution was commenced by transferring 150 µl from row A

to row B, mixed by pipetting, then repeated from row B onwards till row G, concluding the initial serial dilutions.

After the allotted time, 100  $\mu$ l from the duplicate plate was transferred to the assigned contents of the plate of cells respectfully. The plate of cells was then incubated for the time period dependent on the results interpreted from the growth curve, at 37°C with 5% CO<sub>2</sub> humidified environment. At the end of the desired incubated time period (usually 72 h), MTT/MTS assay was followed, as described in Section 2.3.4. Data was recorded for further analysis and optimisation to the ideal conditions of cell quantity, incubation time and genotoxic-agent dilution range before the experiment was done in triplicate scientific repeats for accurate results. If the results were considered not ideal or are incorrect based on the determined cell growth results, then the protocol can be repeated with  $5 \times 10^2$  cells per well, diluted genotoxic agent(s) aliquoted on the same day as cell seeding, and up to 168 h incubation after treatment. This is based on the standard procedure for cancer cells from The Institute of Cancer Research, London, UK.

### 2.3.7. Plasmid Transfection

The Lipofectamine® LTX & PLUS™ reagent (Invitrogen) was used for plasmid transfection to sensitive cells, following the manufacturer's instructions adjusted for reverse transfection. A 12-well plate was labelled by the components to be added per well, including a control well of non-transfected cells and empty-vector transfected cells. In preparation for plasmid transfection, 1  $\mu$ g of designated plasmid was diluted in 200  $\mu$ l of serum-free medium (Opti-MEM, Gibco) within the designated wells of the 12-well plate. Following this, 2.5  $\mu$ l of Lipofectamine LTX was added to the plasmid samples and mixed by rocking, followed by incubation at room temperature for 15 – 20 min. During the incubation of the lipofectamine-plasmid complexes, the assigned cell cultures to the plate were quantified, as described in Section 2.3.1., and then diluted to the appropriate cell concentration as initial stock. The quantification of the cell culture would have been adequate to have been 800  $\mu$ l of 70 – 80% confluent cells per well of a 12-well plate. Usually,  $3 - 4 \times 10^5$  cells seeding per well, and therefore no more than  $3 \times 10^6$  cells per cell line was needed. Within the 15 – 20 min mark, the quantified cell culture was aliquoted drop-wise to the designated wells in the 12-well plate, followed by mixing by rocking. The 12-well plate was then incubated at 37°C with

5% CO<sub>2</sub> humidified environment for 24 h, notating the incubation period. The plasmid-transfected cells were then checked before continuing further for the intended experimental protocol and transferred to a 6-well plate for continued cell growth if necessary.

For an experiment requiring more than  $3 \times 10^5$  transfected cells, the protocol was adjusted to a 6-well plate with 2.5 times the volume and concentration of the components described previously. After a further 24 h or more incubation, overexpression of desired protein was determined by protein expression and detection, as described throughout Section 2.5.

### 2.3.8. Antibiotic-Selection

Based on the cell line used and the plasmid to be transfected, the aim was to determine the optimal antibiotic-selection concentration relative to the time to render all non-transfected cells as nonviable within 72 – 96 h. The antibiotic-selection required depended on the antibiotic-selection-resistance gene in the desired plasmid for transfection. A 12-well plate was labelled by the components assigned, including a control well of non-antibiotic treated cells. The cell cultures were quantified, as described in Section 2.3.1., and then diluted to the appropriate concentration that could be aliquoted as initial stocks. The quantification of the cells would have to have had been adequate enough for seeding, and after 24 h reached approximately 80% confluency. Usually a seeding of  $1.5 - 2 \times 10^5$  cells in 1 ml per well, and therefore no more than  $2.4 \times 10^6$  cells per cell line was needed. The quantified cells were then aliquoted to their assigned wells, and the 12-well plate was then incubated at 37°C with 5% CO<sub>2</sub> humidified environment for 24 h, notating the incubation period.

After 24 h, serial-diluted antibiotic-selection stocks were prepared in 1 ml of cell-culture medium without antibiotics per assigned well. Subsequently, the cell-culture medium was removed from the cells, followed by PBS wash, before the prepared antibiotic-selection stocks were aliquoted to the designated wells. The plate was returned for incubation (37°C, 5% CO<sub>2</sub>, humidified environment) for a further 72 – 96 h. The treated cells were observed after every 24 h incubation interval until 90 – 100% treated cells were rendered as non-viable. The treated cells were then captured by a microscope tablet camera (YW5699, Android) or cell imaging system (Evos FL Auto 2, Invitrogen) for analysis to determine the optimal amount of antibiotic-selection per relative time. The antibiotic-selection procedure

could be continued or repeated in a 6-well plate, and for plasmid-transfected cells, it was repeated based on the determined antibiotic-selection result alongside non-transfected cells as control.

#### 2.3.9. Short Interfering RNA (siRNA) Transfection

The Lipofectamine<sup>®</sup> RNAiMAX reagent (Invitrogen) was used for siRNA transfection, following the manufacturer's instructions for reverse transfection and described here in brief. A 6-well plate was labelled by the components to be added per well, as listed in Table 2.15, including a control well of no siRNA transfection. In preparation for the siRNA transfection, a 60 pmol of designated siRNA was diluted in 500  $\mu$ l of serum-free medium (Opti-MEM, Gibco) within the designated well of the 6-well plate. Following this, 7.5  $\mu$ l of Lipofectamine RNAiMAX was added to the siRNA samples and mixed by rocking, followed by incubation at room temperature for 15 – 20 min. During the incubation of the lipofectamine-siRNA complexes, cells were first quantified, as described in Section 2.3.1., and then diluted to the appropriate cell concentration that could be aliquoted as initial stock. The cells were quantified with an approximate 30% cell confluency in 1.5 ml medium per well of a 6-well plate. Usually,  $2.5 - 3 \times 10^5$  cells per well, and therefore no more than a total of  $2 \times 10^6$  cells per cell line was needed per 6-well plate. Within the 15 – 20 min mark, the quantified cell culture was aliquoted drop-wise to the designated wells in the 6-well plate, followed by mixing by rocking. The plate was then incubated at 37°C with 5% CO<sub>2</sub> humidified environment for 24 h, notating the incubation period.

After 24 h, the siRNA-transfected cells were then checked under microscope for changes in cell vitality before preparing for the intended experimental protocol. The knockdown of genetic or protein expression was determined after a further 24 h incubation by gene expression, described throughout Section 2.4., and protein expression and detection, as described throughout Section 2.5.

#### 2.4. Determination of Gene Expression by Reverse Transcription PCR (RT-PCR)

RT-PCR was used to determine and confirm the expression of the genes of interest, using the primers listed in Table 2.14 in the experimental cells listed in Table 2.2. Genes include  *$\beta$ -Actin*, *ERCC1*, *FANCA*, *FANCD2*, *GAPDH*, *NEIL1*, *NEIL2*, and *NEIL3*.

#### 2.4.1. RNA Extraction

The Isolate II RNA Mini kit (Bioline) was used for RNA extraction from the different cell lines, following the manufacturer's instructions described in brief here. A stock of  $1 - 5 \times 10^6$  cells per cell line was aliquoted, pelleted, the supernatant discarded as much as possible and washed with prewarmed PBS. The cell pellet was then snap-frozen in dry ice or taken directly for RNA extraction.

The pelleted cells were resuspended in 350  $\mu$ l of lysis buffer (RLY) containing 3.5  $\mu$ l of 2-mercaptoethanol and vortexed vigorously. The filter spin column (violet) was placed in a 2 ml collection tube, and the lysate was transferred into the filter column and centrifuged at 11,000 X g for 1 min. Discarding the filter column, 350  $\mu$ l of 70% ethanol was added to the filtered lysate solution and mixed eight times by pipetting. With a prepared mini column (blue) in a 2 ml collection tube, the sample lysate was transferred into the mini column and centrifuged for 30 s at 11,000 X g. The mini column was transferred to another 2 ml collection tube and 350  $\mu$ l of membrane desalting buffer (MEM) was added into the column and centrifuged for 1 min at 11,000 X g, discarding the flow-through afterwards. With the prepared DNase I reaction mixture (for each test sample: 10  $\mu$ l DNase I with 90  $\mu$ l reaction buffer for DNase I (RDN) mixed gently by flicking and briefly centrifuged), 95  $\mu$ l was added directly onto the silica membrane in the mini column, and then incubated at room temperature for 15 min. The silica membrane was washed by adding 200  $\mu$ l of wash buffer 1 (RW1) into the mini column and then centrifuged for 30 s at 11,000 X g. After transferring the column into a new 2 ml collection tube, the wash-step was repeated again with 600  $\mu$ l of wash buffer 2 (RW2), the flow-through was discarded, and then the wash step was repeated again with 250  $\mu$ l for 2 min in the centrifuge. Finally, after transferring the column into a nuclease-free sterile 1.5 ml collection tube, 60  $\mu$ l of RNase-free water was added into the mini column and centrifuged for 1 min at 11,000 X g. This step was repeated with the same eluate sample to increase RNA yield and concentration. Quantification of the extracted RNA was determined by spectrophotometer (NanoDrop 2000, Thermo Scientific) and, if necessary, analysed by agarose gel electrophoresis (1% agarose gel, run at 100V for 1 h) described in Section 2.2.1. for RNA purification.

#### 2.4.2. Reverse Transcription and RT-PCR

The QuantiNova Reverse Transcription kit (Qiagen) and the OneTaq<sup>®</sup> Quick-Load 2X Master Mix with Standard Buffer (NEB) were used for reverse transcription and RT-PCR of the extracted RNA, respectively, following the manufacturer's instructions. For the RT-PCR, primers used were for *ERCC1*, *NEIL1*, *NEIL2*, *NEIL3*, *FANCA*, *FANCD2*, for the positive control *GAPDH* or  *$\beta$ -Actin* (see Table 2.14 for primer sequences and expected PCR product sizes).

**Table 2.25: Genomic DNA removal reaction mixture.**

Component	Reaction Mixture
<b>gDNA Removal Mix</b>	2 $\mu$ l
<b>Template RNA</b>	Up to 5 $\mu$ g
<b>RNase-Free Water</b>	Up to 15 $\mu$ l

As indicated in Table 2.25, the reaction mixtures were prepared in a 0.2 ml PCR tube on ice and mixed by pipetting. The reaction samples were incubated at 45°C for 5 min, then placed on ice. Aliquots of RT enzyme (1  $\mu$ l) and RT master mix (4  $\mu$ l) were then added and mixed by pipetting in the reaction mixtures and incubated at 25°C for 3 min. Incubation continued for 20 min at 45°C, followed by 5 min at 85°C. The RT samples were then placed in ice and cDNA quantified using a NanoDrop 2000 spectrophotometer (Thermo Scientific).

**Table 2.26: RT-PCR reaction mixture.**

Component	Reaction Mixture
<b>cDNA Template</b>	1,500 ng
<b>10 <math>\mu</math>M Forward Primer</b>	0.5 $\mu$ l
<b>10 <math>\mu</math>M Reverse Primer</b>	0.5 $\mu$ l
<b>2x OneTaq Master Mix (NEB)</b>	12.5 $\mu$ l
<b>Nuclease-Free Water</b>	Up to 25 $\mu$ l

RT-PCR reactions were prepared in a 0.2 ml PCR tube, following the RT-PCR reaction mixture displayed in Table 2.26. The number of test samples, including a positive control of *GAPDH* or  *$\beta$ -Actin* expression and negative control without primers for *GAPDH* or  *$\beta$ -Actin*

expression, were kept on ice until ready for thermocycling conditions, as shown in Table 2.27.

**Table 2.27: PCR conditions for RT-PCR.**

Step	Temperature	Time
<b>Hot Lid</b>	105°C	-
<b>Initial Denaturation</b>	94°C	1 min
<b>35 Cycles</b>	94°C	15 s
	*Up to 72°C	15 s
	68°C	15 s
<b>Final Extension</b>	68°C	5 min
<b>Hold</b>	4 – 10°C	∞

The annealing temperature (\*) depended on the melting temperature of the primers listed in Table 2.14. Annealing temperature for *NEIL1* and *TRIM26*, 52°C; *NEIL2* and *GAPDH*, 54°C; *β-Actin*, *FANCA* and *ERCC1*, 55°C; *FANCD2*, 56°C; *NEIL3*, 57°C.

To check that the RT-PCR reactions had been successful and for gene expression analysis, aliquots of the RT-PCR reaction mixtures were subjected to agarose gel electrophoresis. A 2% (w/v) agarose gel was prepared as described in Section 2.2.1. Fifteen microlitres of the RT-PCR reaction mixtures were loaded into the agarose gel, and electrophoresis was carried out at 120V for 1 h. The agarose gel was transferred to a UV-transilluminator in a gel imager (G:BOX, Syngene), and results were recorded for further analysis. Quantitative presentational analysis was conducted through Image Studio™ Lite version 5.2.5 (LI-COR) from the signal intensity emitted from the recorded images.

## 2.5. Protein Expression and Detection

Western blotting was used to detect proteins of interest expressed by the experimental cells (Table 2.2) under different conditions. Proteins included *β-Actin*, *FANCD2*, *GAPDH*, *NEIL1*, *NEIL1-FLAG*, *NEIL3*, *NEIL3<sup>FL</sup>-FLAG*, *NEIL3<sup>1506</sup>*, *NEIL3<sup>1506</sup>-FLAG*, and *TRIM26*.

### 2.5.1. Protein Extraction and Quantification

Stocks of at least  $1 \times 10^6$  cells per cell culture were counted (see Section 2.3.1.), aliquoted, and pelleted in 1.5 ml microcentrifuge tubes and washed with cold ( $4^{\circ}\text{C}$ ) PBS. Cell pellets were used immediately for protein extraction with lysis buffer, as prepared using the parameters described in Table 2.9. The cell pellet was resuspended thoroughly with 100  $\mu\text{l}$  of cold ( $4^{\circ}\text{C}$ ) lysis buffer per  $1 \times 10^6$  cells, followed by 30 min incubation in ice. Lysed cells were vortexed for 3x 15 sec after 10 – 15 min during incubation. Lysed cells were then centrifuged at 16,000 X g for 15 min, at  $4^{\circ}\text{C}$ . Without disturbing the pelleted debris, the supernatant was transferred to a 0.5 ml microcentrifuge tube before storage at  $-80^{\circ}\text{C}$ .

Once obtained, the soluble protein fraction was quantified using the Bradford assay (Bradford, 1976; He, 2011). Samples were prepared and mixed by pipetting in 1.5 ml cuvettes containing 2  $\mu\text{l}$  of extracted protein, 200  $\mu\text{l}$  of Bradford reagent (Bio-Rad) and 800  $\mu\text{l}$  of distilled water, followed by incubation in the dark at room temperature for 5 min. A blank was also prepared, with the same conditions as the samples, but without extracted protein. Once prepared, samples were read in a spectrophotometer at 595 nm against the blank. Results were collected and compared to a BSA standard-curve calculation in  $\mu\text{g}/\mu\text{l}$ .

### 2.5.2. Sodium Dodecyl Sulfate–Polyacrylamide Gel Electrophoresis (SDS-PAGE)

Two SDS-PAGE gels were prepared and cast in assembled casting plates with 10-well combs, according to the components listed in Table 2.28. Once completed, the gels were assembled in an SDS-PAGE running tank, with the appropriate amount of 1x SDS-PAGE running buffer (Table 2.10).

**Table 2.28: Components required for producing a 4% stacking gel and 12% separating gel for three 1.0 mm or two 1.5 mm SDS-PAGE Mini-gels.**

<b>Component</b>	<b>4% Stacking Gel</b>	<b>12% Resolving Gel</b>
<b>0.5 M Tris-HCl pH 6.8</b>	1.89 ml	-
<b>1.5 M Tris-HCl pH 8.8</b>	-	3.75 ml
<b>10% (w/v) SDS</b>	75 $\mu$ l	150 $\mu$ l
<b>30% (w/v) Acrylamide/Bis (37.5:1)</b>	990 $\mu$ l	6.0 ml
<b>dH<sub>2</sub>O</b>	4.5 ml	5.03 ml
<b>10% (w/v) APS</b>	37.5 $\mu$ l	75 $\mu$ l
<b>TEMED</b>	7.5 $\mu$ l	7.5 $\mu$ l

Gels were assembled as 5 – 7.5 ml of resolving gel with 1 – 2.5 ml stacking gel.

After initial preparations were completed, the protein test samples were prepared in 0.2 ml PCR tubes in duplicates containing 30  $\mu$ g of protein template and 0.5 parts of prepared 3x SDS-PAGE loading buffer (Table 2.11), followed by mixing pipetting. The test samples were then denatured by incubation at 100°C for 10 min, before the test samples and small aliquots of protein ladder (Pageruler or PageRuler Plus, Thermo Scientific) were loaded into the SDS-PAGE gels and had undergone gel electrophoresis. The gels were left to run at 100V until the loaded samples had finished running through the stacking gel, then at 130V for 1 h and 30 min.

To be sure that SDS-PAGE was successful, an SDS-PAGE gel was transferred out of the casting plates and on to a small tray for staining. The gel was carefully washed three times, 5 min each, with 50 – 100 ml of distilled water while rocking, followed by staining with 20 ml of Imperial Protein Stain (ThermoFisher) for 20 min while rocking. If proteins were not visible, staining was continued for a further 1 – 2 h or overnight until stained protein was visible. The gel was de-stained in 50 – 100 ml of distilled water for 1 h before the gel was transferred for gel imaging (G:BOX, Syngene), where results were then recorded for further analysis. The duplicate SDS-PAGE gel was preserved until determined from the staining results before continuing to western blot (Section 2.5.3.).

### 2.5.3. Western Blotting

A western blot buffer tank and its required equipment were assembled with the appropriate amount of 1x WB transfer buffer, prepared as described in Table 2.10. Two appropriately sized filter papers and foam pads were submerged in 1x WB transfer buffer, and an appropriately sized polyvinylidene difluoride (PVDF) membrane was activated by submerging in methanol. Following SDS-PAGE, the unstained duplicate gel was transferred to the western blot gel holder cassette. Without introducing air-bubbles, the gel holder cassette was assembled in the order of cathode side, foam pad, filter paper, SDS-PAGE gel, activated PVDF membrane, filter paper, foam pad, and anode side. The assembled cassette was then transferred to a western blot buffer tank, and the transfer was conducted at 400 milliamps (mA) for 1 h and 30 min in a cold room (4°C). To ensure the denatured proteins were transferred successfully, the membrane was stained with Ponceau S solution (prepared as detailed in Table 2.5) for 1 min, washed twice with distilled water, and observed for protein evidence.

The membrane was then transferred to a small closed tray, with the transferred protein side facing upward. The membrane was agitated steadily (10 rpm) on a rocker with 10 ml of blocking buffer, as prepared in detail in Table 2.12, at room temperature for 1 h. While maintaining the membrane in the tray, the blocking buffer was disposed of and replaced with 10 ml of a primary-antibody mix (blocking buffer with a primary antibody described in Table 2.7), followed by incubation with steady rocking at 4°C overnight. After collecting the primary-antibody mix, the membrane was washed by rocking rapidly (15 rpm) at room temperature, three times for 7 min each, with 10 ml of wash buffer (Table 2.12). The antibody incubation step was repeated with a freshly prepared secondary-antibody mix, prepared as described previously with Table 2.7, at room temperature for 1 h while rocking steadily (10 rpm). The secondary-antibody mix was discarded, followed by repeating the washing step as described before, and then preserved in wash buffer in the cold (4°C) until ready for chemiluminescence.

Under as little light as possible, the membrane was then dried as much as possible before transferring to a blackened or covered closed-tray, and an appropriate amount of prepared SuperSignal West Femto (Thermo Fisher Scientific) was pipetted over the membrane. The membrane was incubated for 1 min and then transferred for blot imaging (G:BOX, Syngene),

where results were then recorded for further analysis. Quantitative presentational analysis was conducted through Image Studio™ Lite version 5.2.5 (LI-COR) from the signal intensity emitted from the recorded images.

## Chapter 3 Results

The aims and objectives of the project involved generating mammalian expression plasmids based on pcDNA3.1 with the FLAG-tagged hNEIL3<sup>FL</sup> and hNEIL3<sup>1506</sup> inserts. The hNEIL3<sup>1506</sup> coding sequence was chosen as it contains the putative nuclear localization sequence but lacks the coding sequence for the two GRF zinc fingers at the C-terminus of NEIL3. Therefore, any role of these domains in the repair of ICLs could be observed and would expand the hypothesis to see if the expressed truncated-NEIL3 protein would enter the nucleus. The generated plasmids, together with pcDNA3.1-hNEIL1-FLAG for NEIL1 expression, would then be transfected in *FANC*-deficient and *FANC*-complemented cell lines used in the Macé-Aimé *et al.* (2010) studies and in FA-generated and Wild Type (WT) cancer cell lines used in the Schwab *et al.* (2015) studies to determine the role of NEIL1 and NEIL3 overexpression in ICL resistance. Furthermore, the cell lines would be transfected with siRNA for NEIL3 and TRIM26 knockdown for their ICL-induced resistance. TRIM26 had been shown to ubiquitinate both NEIL1 and NEIL3 for proteasomal degradation in cancer cells (Edmonds *et al.*, 2017; Martin, 2018), but was never tested in FA cells. Transfection reagents and methods would be conducted using Lipofectamine LTX and RNAiMAX for the plasmids and siRNA, respectively. The resistance to the ICL-inducing agents MMC and cisplatin and an oxidising agent, *tert*-butyl hydroperoxide (TBHP), as an additional control would be determined by a survival assay's half-maximal inhibitory concentration (IC<sub>50</sub>) result. Oxidative-induced ICLs were mostly studied through cancer cells (Chen *et al.*, 2014; Martin, 2018), but were rarely studied through FA primary cells, and FA cell survival from TBHP treatment had never been done before.

### 3.1. Initial Cell Culture Experiments

The aims and objectives of this work was to confirm or reconfirm an initial background confirmation of the FA phenotypical cell lines before the intended experiments with differential expressions of NEIL1 or NEIL3. Therefore, the FA phenotypical consequences of the cell lines when treated with ICL-inducing agents MMC and cisplatin and at what concentration and incubation range to work with, determining any noteworthy differences in sensitivity to the oxidative-inducing agent TBHP, and determining the expression of NEIL1 and NEIL3. Based on the literature review it was not specified if there was a

difference in sensitivity to TBHP and how expressed NEIL3 was in FA cells compared to non-FA cells. As displayed in Figure 3.1, the aims and objectives of Section 3.1 were planned according to the approach to the work displayed in the flow chart.

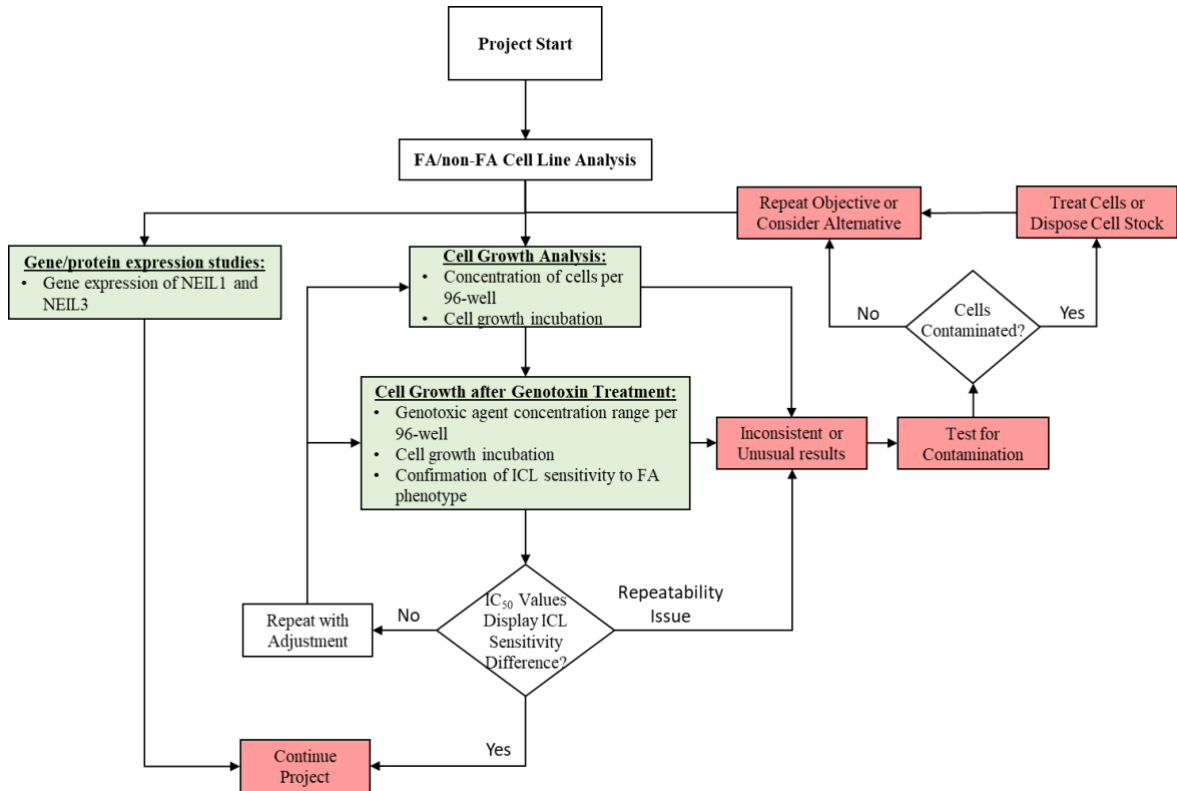


**Figure 3.1: Flowchart on the approach to cell line analysis work.**

Expanded subsection of the overall flowchart displayed in Section 1.6 (Figure 1.11). Red highlights, issues encountered; green highlights, results achieved.

The initial plan was to use the lymphoblast suspension cell lines HSC-93 (WT) as the unaltered FANCA alteration factor and the FANCA related cell lines HSC-72 (FANCA deficient) and HSC-72-Corrected as the focus. While initial experiments confirmed the expected sensitivity of the HSC-72 cells to ICL inducing agents, these results were not reproducible. When investigating potential causes, it was discovered that the cell-culture stocks were contaminated with mycoplasma, as shown in Figure 3.2.

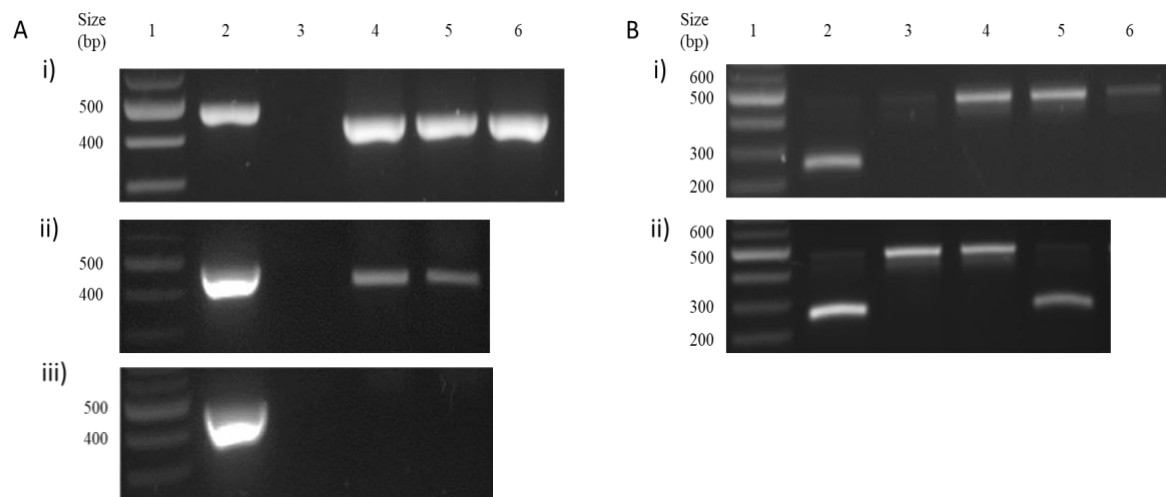


**Figure 3.2: Mycoplasma detection from cultured cells before (A) and after (B) Plasmocin (InvivoGen) treatment.**

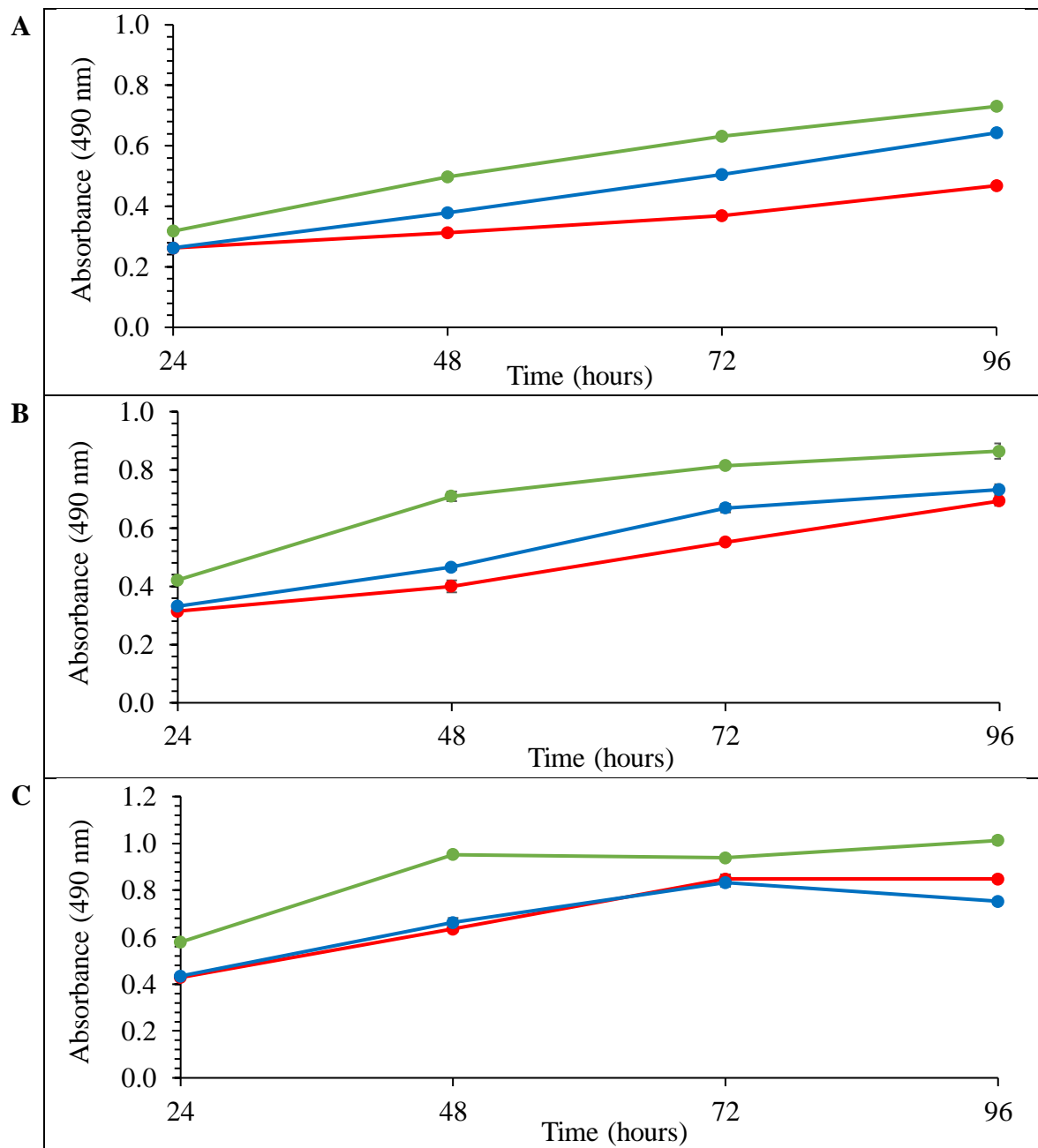
(A) ABM detection kit; (B) Sigma-Aldrich detection kit. Lane 1, DNA ladder; lane 2, positive control; lane 3, negative control; lane 4, (A[i], B[i]) HSC-93, (A[ii + iii]) HSC-536, (B[ii]) PD20; lane 5, (A[i], B[i]) HSC-72, (A[ii + iii]) HSC-536 Corrected, (B[ii]) 3.15; lane 6, (A[i], B[i]) HSC-72 Corrected.

As displayed in Figure 3.2A(i), the cell lines HSC-93 (WT), HSC-72 (FANCA deficient) and HSC-72-Corrected (lanes 4 – 6) were revealed to have been heavily contaminated with mycoplasma when compared to the positive control (lane 2). As an alternative to other lymphoblast cell lines, HSC-536 (FANCC deficient) and HSC-536-Corrected also tested positive for mycoplasma contamination (Figure 3.2A[ii], lanes 4 and 5, respectively). Based on these initial results, it was assumed that all FA cell line stocks were contaminated. However, upon further analysis, it was discovered there was a potential to rescue the contaminated cells with the Plasmocin (InvivoGen) treatment, and therefore continue with the project. FA cell lines of FANCA (HSC-72 and HSC-72-Corrected cells), FANCD2 (PD20 and 3.15 cells), and FANCC (HSC-536 and HSC-536-Corrected cells) as well as the WT cells HSC-93, were treated before continuing. Not all treatments were successful at first, such as the FANCD2 corrected cells (3.15) in lane 5 of Figure 3.2B(ii), which required either further treatment or treatment of another cell-culture stock. Described throughout Section 3.1, the experiments for the Plasmocin treated cells were repeated for FA phenotypic confirmation and expression confirmation before continuing towards the aims and objectives for the research. However, poor cell culture growth as well as other noticeable factors described throughout Section 3.1 had become evident amongst the treated cells. From Section 3.2 onwards, the experiments were repeated with fresher cell stocks and alternative FA-phenotypical cell lines to continue with the project. The results from Section 3.1 from a

WT or corrected cell-line (HSC93, HSC-72-Corrected and HSC536-Corrected) compared to a FA cell line (HSC-72 and HSC536) could be used as a confirmation or expectation for the new cell line results in Section 3.2. As displayed in Figure 3.1, some results were salvageable for the cell growth analysis (Section 3.1.1.), cell growth analysis after genotoxin treatment (Section 3.1.2.) and cell culture gene-expression studies (Section 3.1.3.), but because the cell lines tested and attempted were contaminated with mycoplasma, even after Plasmocin treatment the project could not continue and replacement cell lines had to be considered.

### 3.1.1. Cell Growth Analysis

Based on the suggestions from Filippo Rosselli at the Institut Gustave Roussy, Paris, France who gifted the FA cells and the methodology in Macé-Aimé *et al.* (2010), the cells were tested at  $1 \times 10^4$  cells per well in a 96-well plate. However, it proved more appropriate to test with  $5 \times 10^3$ ,  $1 \times 10^4$  and  $2 \times 10^4$  cells. As can be seen in Figure 3.3, the cell lines seem to have entered or were about to enter the plateau phase at 96 h for  $1 \times 10^4$  cells (Figure 3.3B) and around the 72 h (Figure 3.3A – C), though possibly a little earlier for WT cells (HSC-93), for  $2 \times 10^4$  cells (Figure 3.3C). It was also observed that the HSC-93 cells started at a higher absorbance reading than the FANCA deficient (HSC-72) and corrected (HSC-72 Corrected) cells, though both started on almost the same absorbance reading for all cell quantities. With those in mind, it had to be determined whether the results for HSC-93 were diverging prior to the 24-hour mark or perhaps there was another quantity of cells to consider between  $5 \times 10^3$  and  $1 \times 10^4$  cells, and the absorbance readings had to be reconfirmed. Therefore, before concluding which was the correct cell quantity to use for future genotoxic agent testing, it was appropriate to repeat the MTS assays again for  $5 \times 10^3$ ,  $7.5 \times 10^3$  and  $1 \times 10^4$  cells.



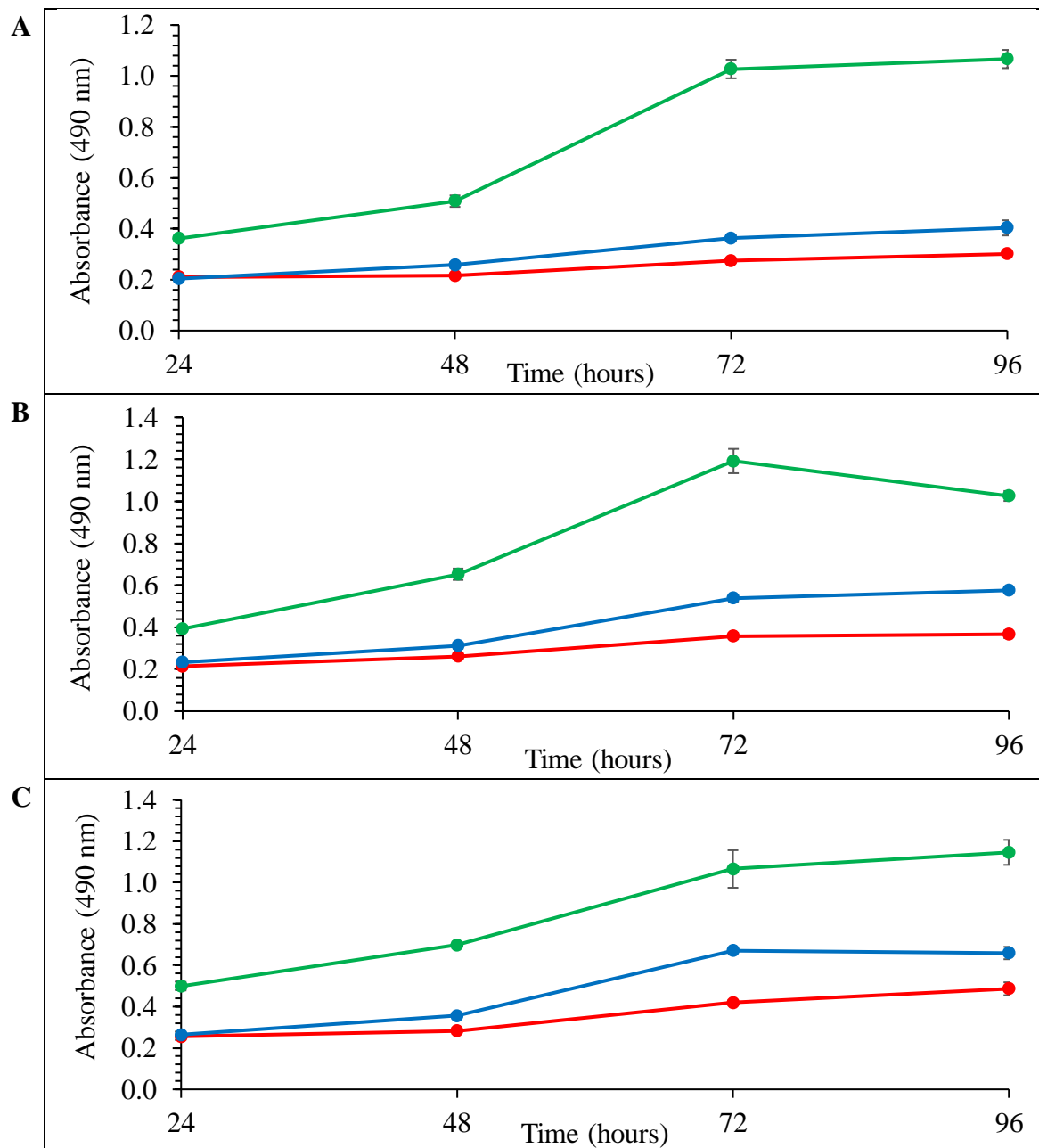
**D**

	Doubling Time			
	5 x 10 <sup>3</sup> cells	1 x 10 <sup>4</sup> cells	2 x 10 <sup>4</sup> cells	Mean ± SD
<b>HSC-93</b>	48.47 min	32.09 min	33.49 min	38.02 ± 9.08 min
<b>HSC-72 Corrected</b>	55.90 min	47.48 min	50.97 min	51.45 ± 4.23 min
<b>HSC-72</b>	87.74 min	61.89 min	48.47 min	66.03 ± 19.96 min

**Figure 3.3: Growth of HSC-93 (green), HSC-72 (red) and HSC-72-Corrected (blue), determined using MTS assay.**

(A) 5 x 10<sup>3</sup> cells, (B) 1 x 10<sup>4</sup> cells, and (C) 2 x 10<sup>4</sup> cells per well. (D) Doubling times of HSC-93, HSC-72 and HSC-72-Corrected cells from cell seedings (A-C) between 24 h and 96 h. Mean data was collected from triplicate technical repeats.

As displayed in Figure 3.4, the cell lines seem to have entered or were about to enter the plateau phase at 72 h for  $5 \times 10^3$  and  $7.5 \times 10^3$  cells (Figure 3.4A and B, respectively), and around 96 h for  $1 \times 10^4$  cells (Figure 3.4C), though possibly earlier for HSC-72-Corrected, for  $1 \times 10^4$  cells. The HSC-93 cells (WT) were still observed at a higher absorbance reading than HSC-72 and HSC-72-Corrected cells; however, this was confirmed to be a common phenotype for the WT cell line HSC-93. The FA (HSC-72) and corrected (HSC-72-Corrected) cell lines were observed to grow slower when seeded less than  $1 \times 10^4$  cells (Figure 3.4) compared to more than  $1 \times 10^4$  cells (Figure 3.3), and both cell lines were observed to grow slower than the WT cells (HSC-93). This could be due to the individual cells being too far apart, which was predictable and therefore proliferation would improve if increased cell numbers were seeded, or there were other factors not considered affecting the cells, such as the FA and FA-corrected cells from the same cell origin compared to the WT cells from a different cell origin, or the FANCA alteration factor affecting the stability of the cells. Interestingly, HSC-93 (WT) displays higher cell proliferation in Figures 3.3 and 3.4 than HSC-72-Corrected, which was described in Table 2.1 as the FANCA-deficient cell line HSC-72 with plasmid transfected FANCA expression, and both cell lines were more proliferate than HSC-72. Based on the comparison of all the results from Figures 3.3 and 3.4, it could be concluded and confirmed that all three cell lines HSC-93, HSC-72, and HSC-72-Corrected could be used at a quantity of  $1 \times 10^4$  cells per well in a 96-well plate, and could be incubated at the same time for no more than 72 h.



**D**

	Doubling Time			
	5 x 10 <sup>3</sup> cells	7.5 x 10 <sup>3</sup> cells	1 x 10 <sup>4</sup> cells	Mean ± SD
<b>HSC-93</b>	31.80 min	30.01 min	43.87 min	35.22 ± 7.54 min
<b>HSC-72 Corrected</b>	57.76 min	39.61 min	35.73 min	44.37 ± 11.76 min
<b>HSC-72</b>	100.46 min	64.78 min	71.46 min	78.90 ± 18.97 min

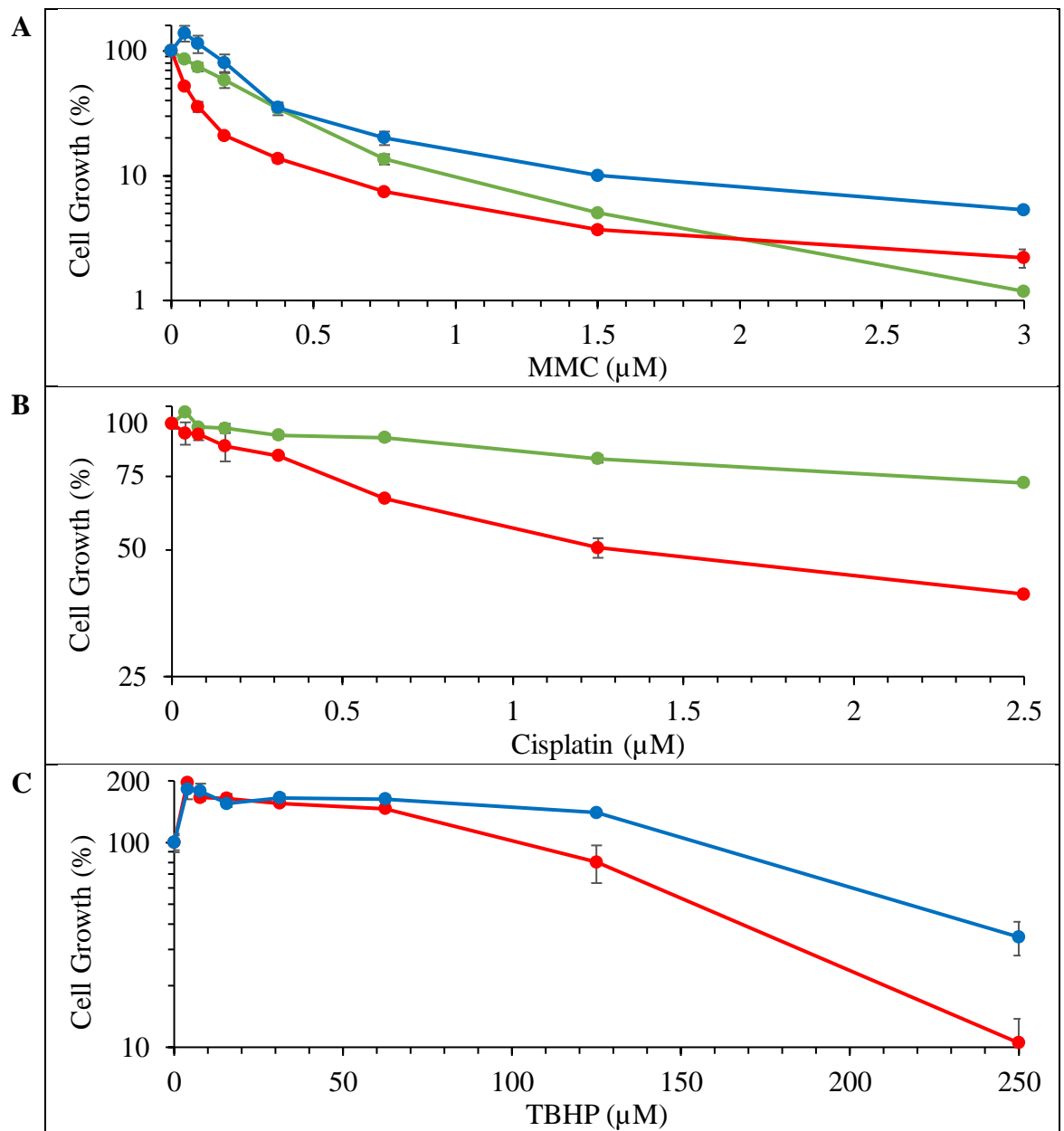
**Figure 3.4: MTS assay to determine the growth characteristics of HSC-93 (green), HSC-72 (red) and HSC-72-Corrected (blue) cells.**

(A) 5 x 10<sup>3</sup> cells, (B) 7.5 x 10<sup>3</sup> cells, and (C) 1 x 10<sup>4</sup> cells per well. (D) Doubling times of HSC-93, HSC-72 and HSC-72-Corrected cells from cell seedings (A-C) between 24 h and 96 h. Mean data was collected from triplicate technical repeats.

### 3.1.2. Cell Growth after Genotoxin Treatment

Based on the results from the growth curve, the protocol was adjusted for  $1 \times 10^4$  cells per well in a 96-well plate, incubated for 24 h before adding the genotoxic agents, followed by incubation for 72 hours. Tests were attempted to be repeated at least two times before data analysis. However, issues were becoming noticeable, possibly related to the cells being treated from mycoplasma and eventually not proliferating, or possibly the cell lines entering senescence.

The maximum concentration was 3  $\mu\text{M}$  for MMC and Cisplatin (Figure 3.5A and B, respectively), and 250  $\mu\text{M}$  for TBHP (Figure 3.5C) for the cell lines HSC-93 (WT), HSC-72 (FANCA deficient) and HSC-72-Corrected. It was expected to see non-FA and FA-corrected cells, in this case HSC-93 and HSC-72-Corrected, to display resistance to the ICL agents MMC and cisplatin, compared to FA cells such as HSC-72. Figure 3.5 shows the FANCA deficient cells (HSC-72) with the least resistance to the ICL-inducing agents MMC ( $\text{IC}_{50}$  0.05  $\mu\text{M}$ ) and cisplatin ( $\text{IC}_{50}$  1.32  $\mu\text{M}$ ), and the WT cells (HSC-93) displayed an increased resistance to MMC ( $\text{IC}_{50}$  0.24  $\mu\text{M}$ ) and cisplatin ( $\text{IC}_{50}$   $>2.5$   $\mu\text{M}$ ). Furthermore, the FANCA corrected cells (HSC-72-Corrected) display an increased resistance to MMC ( $\text{IC}_{50}$  0.05  $\mu\text{M}$  and 0.30  $\mu\text{M}$ ). Surprisingly, the HSC-72-Corrected cells displayed more resistance to MMC than HSC-93 (Figure 3.5A), though statistically HSC-93 and HSC-72-Corrected may have the same resistance based on the standard deviations (Figure 3.5D,  $0.24 \pm 0.02$   $\mu\text{M}$  and  $0.30 \pm 0.12$   $\mu\text{M}$ , respectively). This could be due to the cells transfected episomal mammalian expression plasmid as the correction, described in Figure 2.1, in the HSC-72-Corrected cells constantly expressing FANCA, compared to the HSC-93 cells being a wild-type cell line without an FA pathway alteration, and therefore increasing the resistance against ICL agents. The difference in resistance with the oxidative agent TBHP in Figure 3.5C was unexpected, with an  $\text{IC}_{50}$  of 154  $\mu\text{M}$  for HSC-72 (FANCA deficient) and 217  $\mu\text{M}$  for HSC-72-Corrected, though statistically it may be an anomaly based on one scientific replicate ( $\text{IC}_{50}$   $154 \pm 180$   $\mu\text{M}$  and  $217 \pm 75$   $\mu\text{M}$  respectively). However, this could be due to the oxidised nucleotides potentially being susceptible to forming endogenous ICLs, examples of which were mentioned in Section 1.2.1. Despite this difference in resistance not being as substantial as the differences in resistance against MMC or cisplatin, it could be a significant background result to consider or an anomaly to bear in mind. Experimental repeats were required to confirm.



**D**

	IC <sub>50</sub> ± SD Values		
	MMC	Cisplatin	TBHP
HSC-93	0.24 ± 0.02 μM	> 2.5 μM	-
HSC-72 Corrected	0.30 ± 0.12 μM	-	217 ± 75 μM
HSC-72	0.05 ± 0.00 μM	1.32 ± 0.20 μM	154 ± 180 μM

**Figure 3.5: Growth inhibition of HSC-93 (WT, green), HSC-72 (FANCA deficient, red) and HSC-72-Corrected (blue) following treatment with A) mitomycin C (MMC), B) cisplatin, and C) TBHP.**

**D)** IC<sub>50</sub> values for growth inhibition following treatment. 1 x 10<sup>4</sup> cells per 96-well, incubated for 72 h. Mean data was collected from triplicate technical repeats from two (A) and one (B – C) scientific repeats.

### 3.1.3. Gene Expression Studies

There were previous attempts through western blot in determining the expression of NEIL1 and NEIL3 in the FANCA deficient and corrected cell lines (HSC-72 and HSC-72-Corrected, respectively) as well as before and after a genotoxic agent treatment to determine the potential variety of protein expression at different concentrations and incubation time periods (Appendix Figure 1). However, NEIL1 and NEIL3 expression could not be determined at the time, therefore the alternative in expression determination through RT-PCR. As shown in Figure 3.6A, the WT (HSC-93, lanes 5 – 7), FANCA deficient (HSC-72, lanes 8 – 10) and FANCA corrected (HSC-72 Corrected, lanes 11 – 13) cells were compared with a cancer cell line U2OS (lanes 2 – 4), which was previously tested by colleagues and locally known to express *NEIL3*. All four cell lines displayed expression of *NEIL3* (lanes 4, 7, 10 and 13), though only U2OS and HSC-93 display visible expression of *NEIL1* (lanes 3 and 6, respectively). As observed from Figure 3.6B, compared to their respective *GAPDH* expression, the cells display *NEIL3* expression at a 1:0.8 ratio in U2OS cells, a 1:3 ratio in HSC-93 and HSC-72 cells, and a 1:5 ratio in HSC-72-Corrected cells. Furthermore, there is greater expression of *NEIL3* in the cancer cells (U2OS) compared to the lymphoblast cell lines at an almost 1:3 ratio (HSC-93 and HSC-72) and a 1:4 ratio (HSC-72 Corrected). However, there are no major differences in *NEIL3* expression between the FANCA deficient cells (HSC-72) and the FANCA corrected (HSC-72 Corrected) or WT (HSC-93) cells. As for the *NEIL1* expression observed in Figure 3.6B, compared to their respective *GAPDH* expression, the HSC-93 cells had the highest expression (approximately 1:10 ratio), followed by U2OS with (approximately 1:50 ratio). However, *NEIL1* expression was scarcely detectable for HSC-72 and HSC-72-Corrected. Based on these results, it was more appropriate for the cell lines HSC-72 and HSC-72-Corrected to be transfected with pcDNA3.1-hNEIL1-FLAG rather than with pcDNA3.1-hNEIL3<sup>FL</sup>-FLAG or pcDNA3.1-hNEIL3<sup>1506</sup>-FLAG, but also appropriate for NEIL3 knockdown.

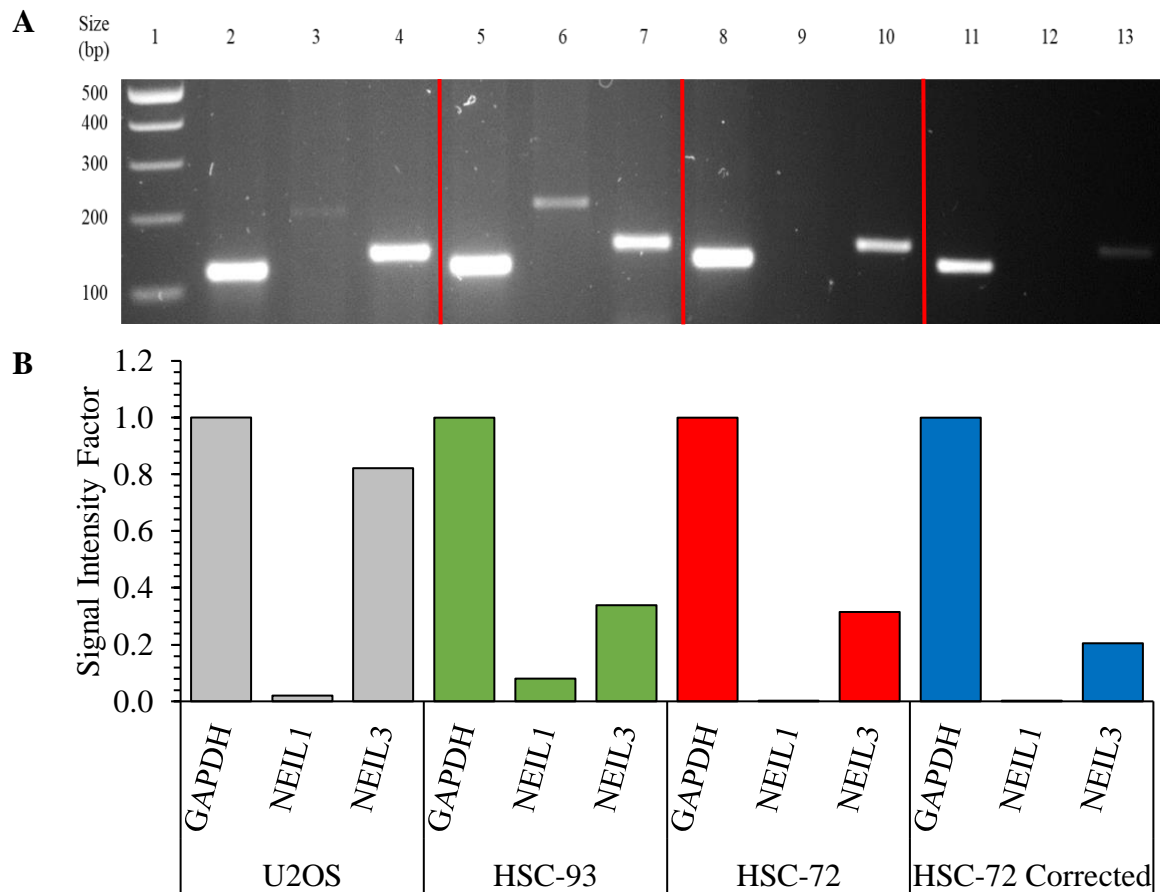


**Figure 3.6: Expression of *GAPDH*, *NEIL1* and *NEIL3* from cell lines U2OS (WT, grey), HSC-93 (WT, green), HSC-72 (FANCA deficient, red) and HSC-72-Corrected (blue) by RT-PCR.**

(A) Gel electrophoresis image with U2OS (lanes 2 – 4), HSC-93 (lanes 5 – 7), HSC-72 (lanes 8 – 10) and HSC-72-Corrected (lanes 11 – 13). Lane 1, DNA ladder; lanes 2, 5, 8, 11, *GAPDH*; lanes 3, 6, 9, 12, *NEIL1*; lanes 4, 7, 10, 13, *NEIL3*. Expected amplicon length: *GAPDH*, 127 bp; *NEIL1*, 212 bp; *NEIL3*, 147 bp. (B) Quantified signal intensity from amplicons in section A relative to *GAPDH* expression, based on one scientific replicate.

### 3.2. Cell Culture of the FANCD2-related Cell lines

Due to the issues surrounding the initial cell culture experiments described in Section 3.1 of the experimented FA cell lines detected for mycoplasma contamination, treated to save the cell lines to continue with the project, results unable to be repeated for accuracy due to continued factors related to mycoplasma after treatment and the assumption of the rest of the gifted FA cell lines being contaminated as well, the project was repeated on new and fresh cell lines with another FANCD2-related deficiency. The aims and objectives for this work were the same as attempted for Section 3.1, which was to confirm or reconfirm an initial background

confirmation of the FA phenotypical cell lines before the intended experiments with differential expressions of NEIL1 or NEIL3. As detailed in Sections 2.1.1. and 2.1.2. and Tables 2.1 and 2.2, the FANCD2 deficient cell lines PD20, HeLa-D2 and U2OS-D2 were phenotypically FA, and their counterpart cell lines 3.15 (PD20 corrected), HeLa and U2OS (WT) were non-FA with similar FANCD2 correction. All cells were fibroblast cell lines, but significant differences were that the PD20 and 3.15 cells were FA cells, and HeLa, HeLa-D2, U2OS and U2OS-D2 were cancer cells. Although the objectives were not achieved for the FANCA-related cell lines (HSC-72 and HSC-72-Corrected) in Section 3.1, the results had at least indicated what was to be expected and to bear in mind for other cell lines of similar FA and non-FA phenotypes. All FANCD2-related cell lines PD20.3.15, U2OS/-D2 and HeLa/-D2 showed no evidence of mycoplasma when tested before experimentation. As displayed in Figure 3.7, the aims and objectives of Section 3.2 were repeated from Section 3.1 (Figure 3.1), but with the testing of the new cell cultures for contamination as the first condition before continuing with the approach to the work displayed in the flow chart. The new results for the cell growth analysis (Section 3.2.1.), cell growth analysis after genotoxin treatment (Section 3.2.2.), and cell culture gene-expression studies (Section 3.3.3.) allowed the project to continue to the next stage of the project.

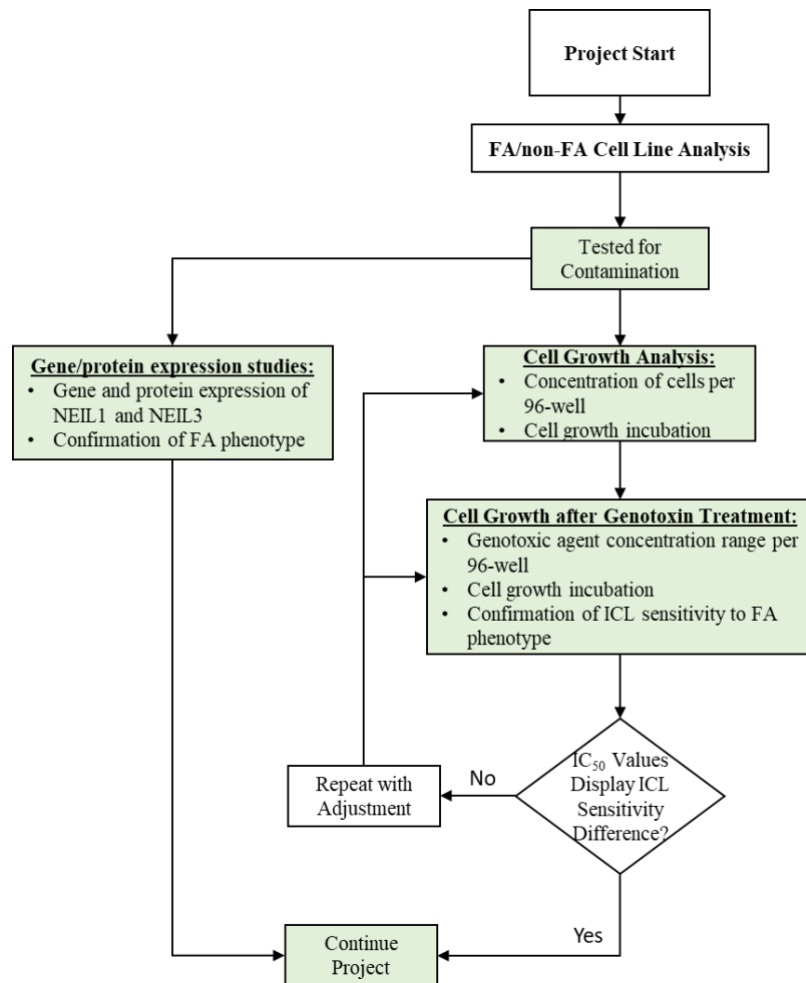


**Figure 3.7: Refined flowchart on the approach to cell line analysis work.**

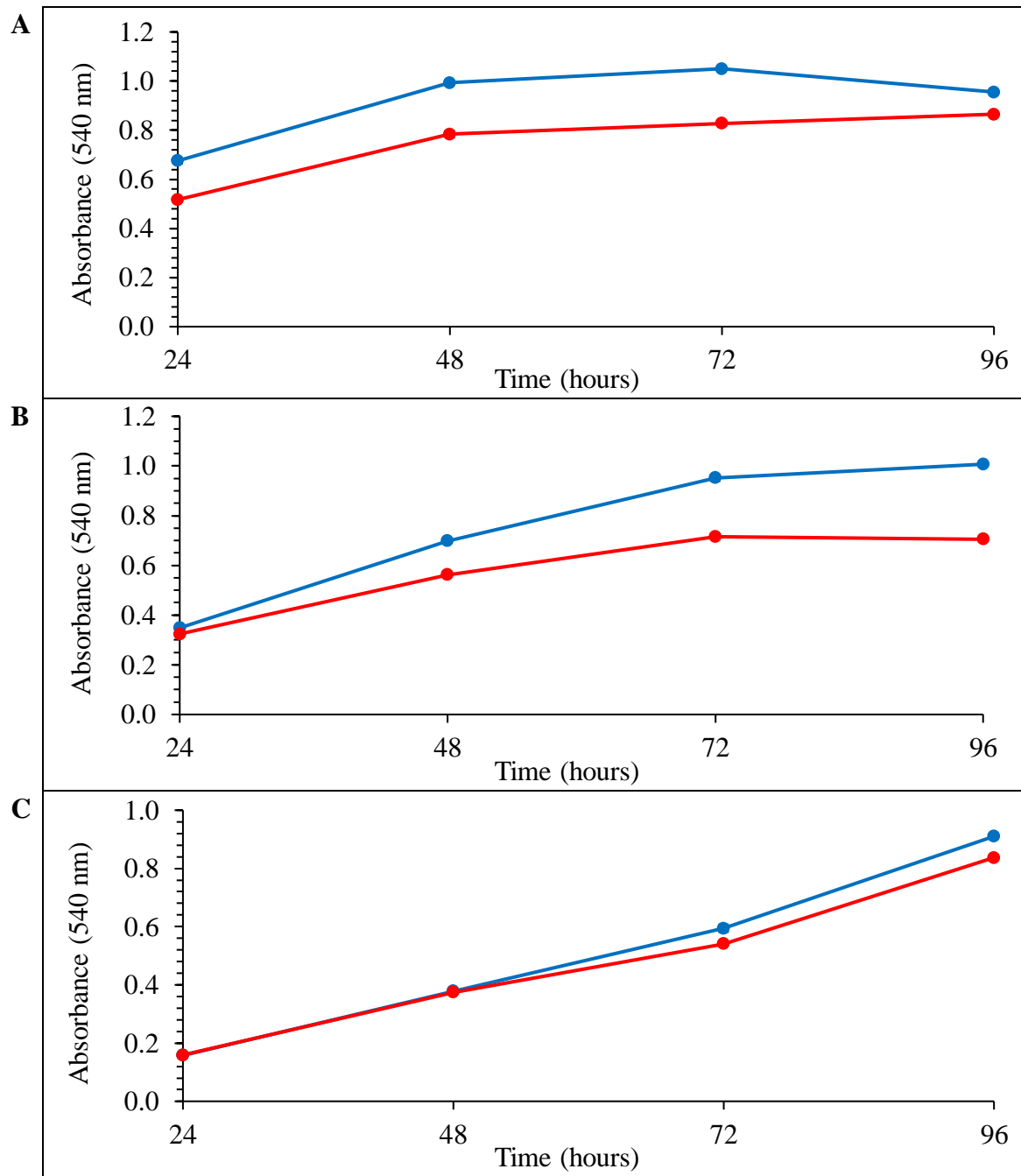
Expanded subsection of the overall flowchart displayed in Section 1.6 (Figure 1.11). Green highlights, results achieved.

### 3.2.1. Cell Growth Analysis

Due to the time being limited, the cell growth curve results analysed and displayed in Section 3.2.1. were based on one scientific repeat that was considered acceptable, as the priority of the project was shifted to the accuracy and reproducibility of the results from genotoxic studies before and after transfection of plasmids expressing NEIL1 or NEIL3 and the NEIL3 and TRIM26 knockdown studies. Based on the cell survival methodology from Wang *et al.* (2010) and the collective experience from colleagues, the cell growth of the FA cells PD20 (FANCD2 deficient) and 3.15 (FANCD2 corrected) were tested at  $2 \times 10^3$ ,  $4 \times 10^3$  and  $8 \times 10^3$  cells per well in a 96-well plate, with  $4 \times 10^3$  cells being the predicted experimental concentration. As can be seen in Figure 3.8, the cell lines seem to have entered the plateau phase at the 48 – 72 h for  $8 \times 10^4$  cells (Figure 3.8A) and were entering the plateau phase

from 72 h for  $4 \times 10^3$  cells (Figure 3.8B), but not for  $2 \times 10^3$  cells (Figure 3.8C). In Figure 3.8A the growth difference was noticeable at 24 h between the FANCD2 corrected (3.15) over FANCD2 deficient (PD20) cell lines. Possibly due to the high number of cells seeded ( $8 \times 10^3$  cells) proliferating and becoming confluent over the remaining space in the wells or possibly due to pipetting error. Since the general practice for MTT assay for the survival of cells from genotoxic agents usually required 72 h incubation after treatment, it was considered ideal to use between  $2 - 4 \times 10^3$  cells. However, compared to  $4 \times 10^3$  and  $8 \times 10^3$  cells (Figure 3.8B and A respectively), it was observed that for  $2 \times 10^3$  cells (Figure 3.8C) the difference in growth rate between the cell lines was not noticeable until the 48-hour mark, does not expand greatly and remains parallel after 72 h. It was also observed that at  $4 \times 10^3$  cells, the FANCD2 deficient cells (PD20) were declining slightly at 96 h, possibly indicating the cell line was entering the death stage. Therefore, it was considered ideal to use  $3 \times 10^3$  cells per 96-well for up to 96 h incubation for the cell growth studies.

The cell survival methodology from Schwab *et al.* (2015) did not mention how many cells per well or for how long incubation for the cancer cell lines U2OS (WT) and U2OS-D2 (FANCD2 deficient), nor on whether there were similarities for the HeLa (WT) and HeLa-D2 (FANCD2 deficient) cell lines. However, based on the collective experience from colleagues on U2OS and together with the cell growth data of the FA cells PD20 (FANCD2 deficient) and 3.15 (FANCD2 corrected) described previously, the cancer cell lines were tested at  $2 \times 10^3$ ,  $4 \times 10^3$  and  $8 \times 10^3$  cells per well in a 96-well plate, with  $4 \times 10^3$  cells theoretically being the predicted experimental concentration. Similar to the FA results in Figure 3.8, U2OS and U2OS-D2 cells growth rates were divergent from each other, with the FA generated phenotype (U2OS-D2) at a lower absorbance reading and growing at a slower rate, as was expected. However, the cell lines at a higher cell concentration eventually converged at a later period. As displayed in Figure 3.9B, at  $4 \times 10^3$  cells the U2OS-D2 cells growth rate remained divergent from the U2OS cells growth rate until 96 h. Similarly, at  $8 \times 10^3$  cells (Figure 3.9A), the same cell lines were similarly divergent until just before 72 h, but then from 72 – 96 h the U2OS-D2 cells growth rate had converged and overlapped the U2OS cells growth rate. Furthermore, the U2OS cell lines showed no indication of entering the plateau phase but possibly were about to enter it if incubated longer than 96 h for  $8 \times 10^4$  cells (Figure 3.9A) and  $4 \times 10^3$  cells (Figure 3.9B). Although unexpected, there was at least some promise for  $2 \times 10^3$  cells (Figure 3.9C), which was then considered to be the ideal cell concentration for further cell growth studies.

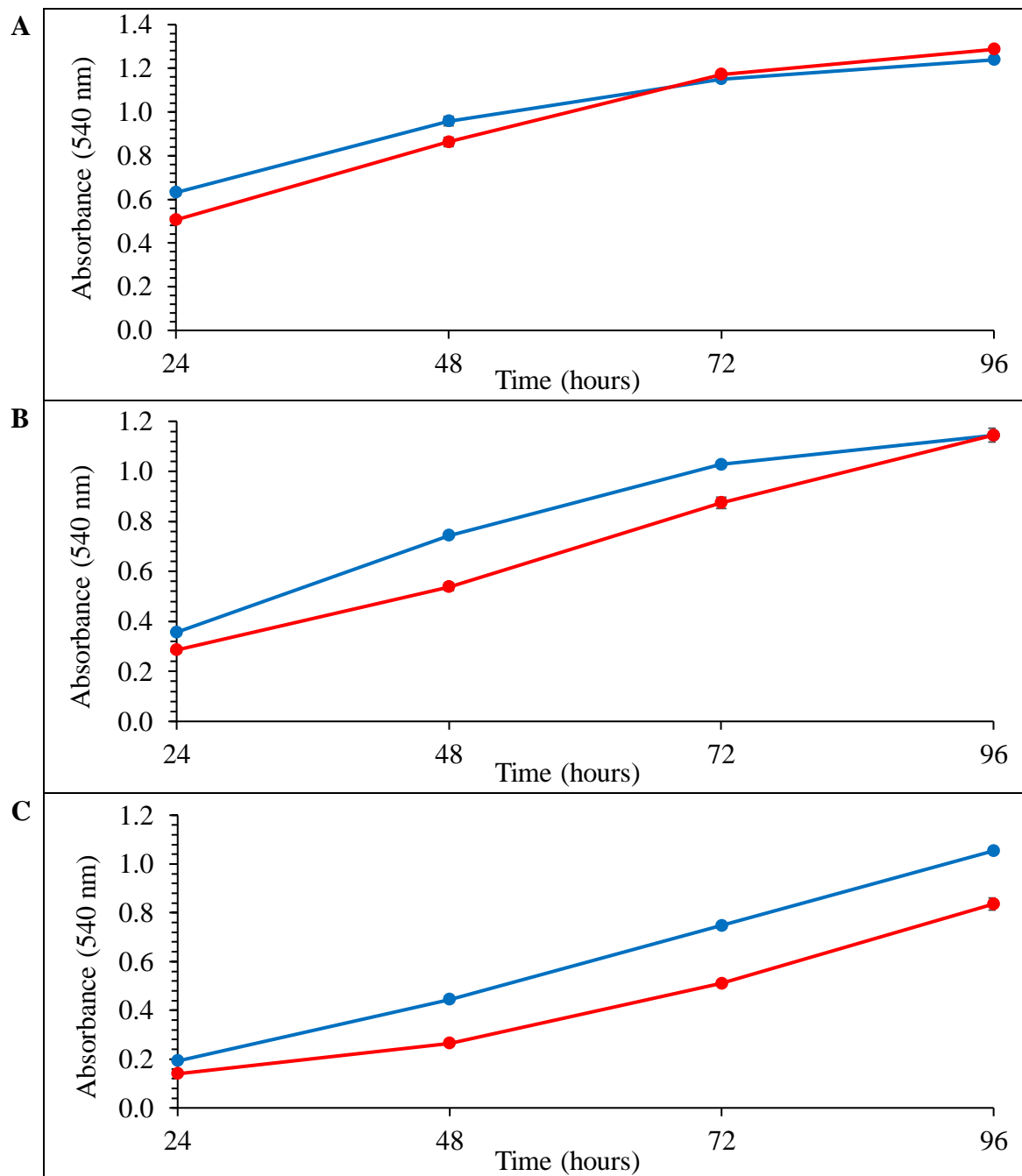


**D**

	Doubling Time			
	8 x 10 <sup>3</sup> cells	4 x 10 <sup>3</sup> cells	2 x 10 <sup>3</sup> cells	Mean ± SD
<b>3.15</b>	59.70 min	33.16 min	29.12 min	40.66 ± 16.61 min
<b>PD20</b>	40.07 min	42.01 min	31.08 min	37.72 ± 5.83 min

**Figure 3.8: Growth of PD20 (FAND2 deficient, red) and 3.15 (PD20 corrected, blue) determined using the MTT assay.**

(A) 8 x 10<sup>3</sup> cells, (B) 4 x 10<sup>3</sup> cells and (C) 2 x 10<sup>3</sup> cells per well. (D) Doubling times of PD20 and 3.15 cells from cell seedings (A-C) between 24 h and 96 h. Mean data was collected from triplicate technical repeats.

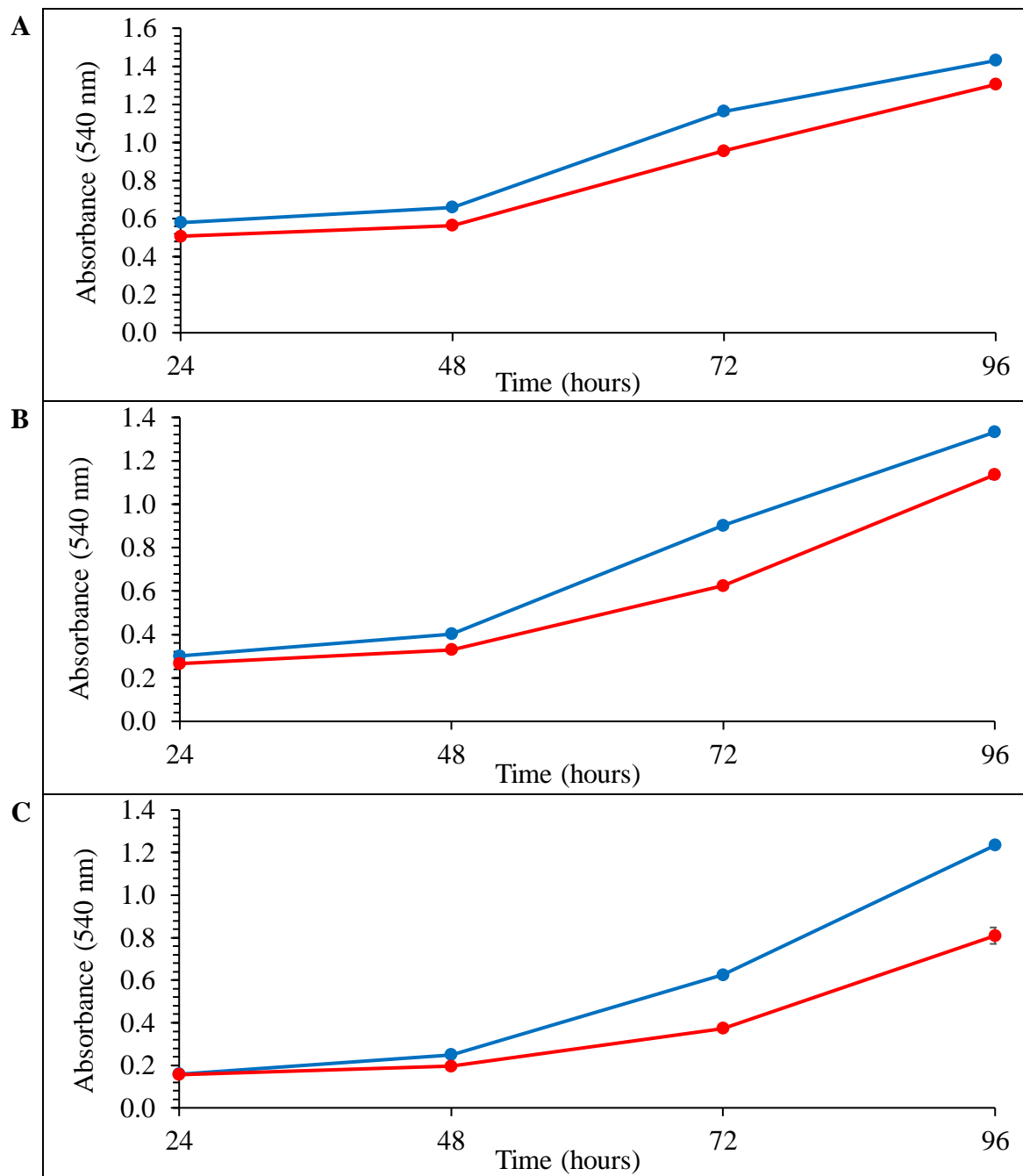


**D**

	Doubling Time			
	8 x 10 <sup>3</sup> cells	4 x 10 <sup>3</sup> cells	2 x 10 <sup>3</sup> cells	Mean ± SD
U2OS	39.84 min	31.51 min	29.62 min	33.65 ± 5.44 min
U2OS-D2	39.61 min	35.73 min	27.62 min	34.32 ± 6.12 min

**Figure 3.9: Growth of U2OS (WT, blue) and U2OS-D2 (FANCD2 deficient, red) determined using the MTT assay.**

(A) 8 x 10<sup>3</sup> cells, (B) 4 x 10<sup>3</sup> cells and (C) 2 x 10<sup>3</sup> cells per well. (D) Doubling times of U2OS and U2OS-D2 cells from cell seedings (A-C) between 24 h and 96 h. Mean data was collected from triplicate technical repeats.



**D**

	Doubling Time			
	8 x 10 <sup>3</sup> cells	4 x 10 <sup>3</sup> cells	2 x 10 <sup>3</sup> cells	Mean ± SD
<b>HeLa</b>	29.25 min	27.73 min	20.82 min	25.93 ± 4.49 min
<b>HeLa-D2</b>	39.61 min	26.87 min	23.42 min	29.96 ± 8.53 min

**Figure 3.10: Growth of HeLa (WT, blue) and HeLa-D2 (FANCD2 deficient, red) determined using the MTT assay.**

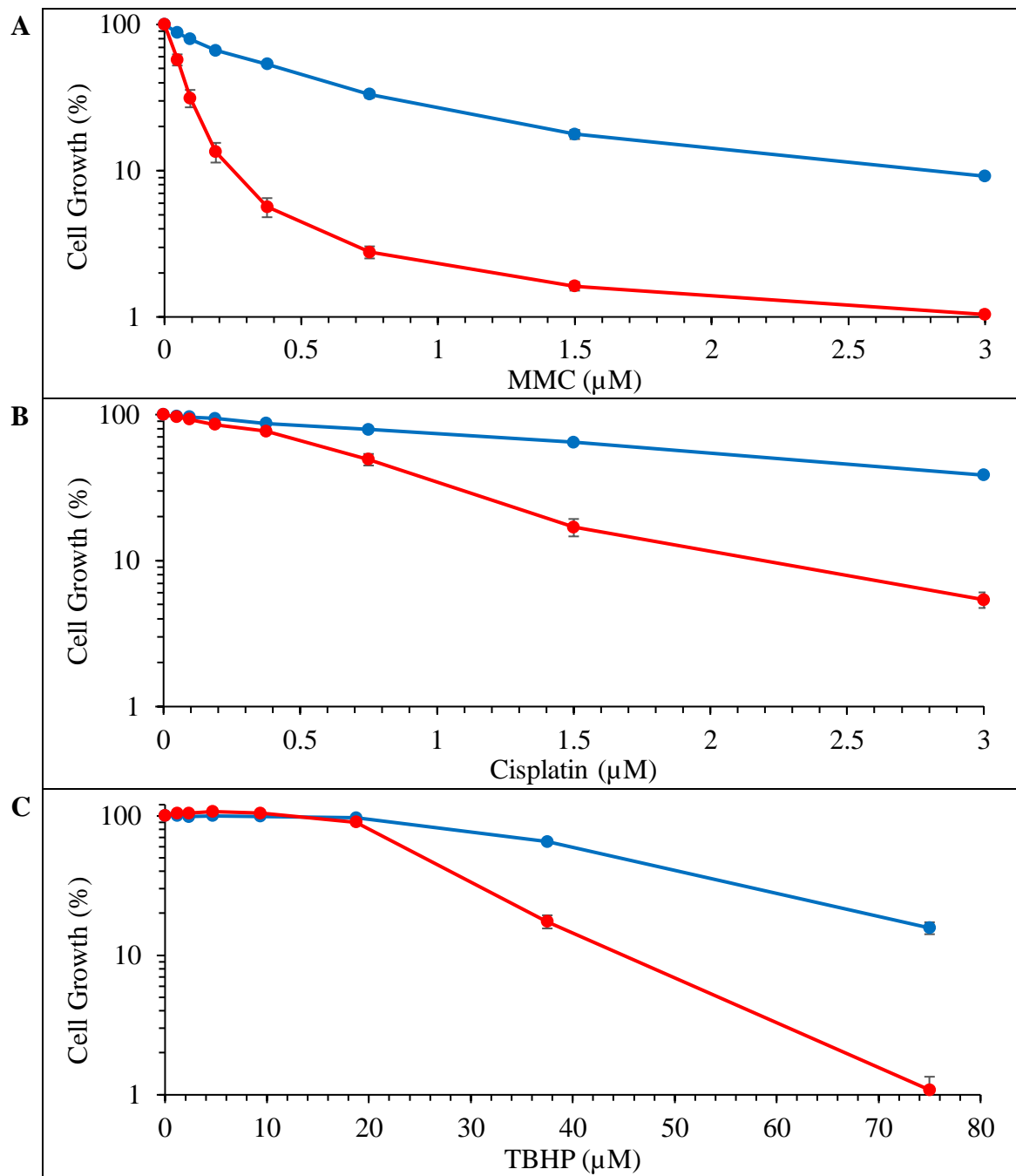
(A) 8 x 10<sup>3</sup> cells, (B) 4 x 10<sup>3</sup> cells and (C) 2 x 10<sup>3</sup> cells per well. (D) Doubling times of U2OS and U2OS-D2 cells from cell seedings (A-C) between 24 h and 96 h. Mean data was collected from triplicate technical repeats.

The HeLa (WT) and HeLa-D2 (FANCD2 deficient) growth rate results in Figure 3.10 were similar to the U2OS (WT) and U2OS-D2 (FANCD2 deficient) results displayed (Figure 3.9) and described previously. Furthermore, similar to the FA results in Figures 3.8 and 3.9, HeLa and HeLa-D2 cells growth rates were divergent from each other, with the FA generated phenotype (HeLa-D2) at a lower absorbance reading and growing at a slower rate, as was expected. As observed similarly from the U2OS/-D2 results (Figure 3.9), other than possibly for HeLa at  $8 \times 10^4$  cells if incubated longer than 96 h (Figure 3.10A), there was no indication of a plateau phase with either cell concentration in Figure 3.10. However, the possibility of the HeLa and HeLa-D2 cells growth rate converging seemed highly probable for  $8 \times 10^4$  cells (Figure 3.10A) and  $4 \times 10^4$  cells (Figure 3.10B) after 72 h, and their difference in growth rate was not as diverse as would be expected compared to previous growth curve results of other cell lines. Figure 3.10C displayed the only results that seemed more suitable for cell growth studies, and therefore similar to U2OS and U2OS-D2, seemed ideal to use  $2 \times 10^3$  cells per 96-well for up to 96 hrs. Based on the doubling times displayed in Figures 3.8 – 3.10 of the non-FA and FA phenotypical cell cultures 3.15/PD20, U2OS/-D2 and HeLa/-D2 doubling approximately every 20 min to 40 min, the cell lines may also have been suitable at less than  $2 \times 10^3$  cells seeding and a longer incubation time period for MTT assays. Although clonogenic assays may also have been a suitable method for determining cell survival after genotoxin treatment as fewer cells are required for seeding. However due to the project's limited time the priority was maintained on focusing to complete the aims and objectives with what was already experienced, and even though clonogenic assay was not considered at the time, the incubation time required would have been weeks instead of days.

### 3.2.2. Cell Growth after Genotoxin Treatment

Because Schwab *et al.* (2015) only based the FA phenotype on the difference of susceptibility to cisplatin instead of MMC as the primary ICL agent for U2OS and U2OS-D2, and therefore, in theory, the same for HeLa and HeLa-D2, then cisplatin was used to confirm the FA phenotype. However, the FA phenotype confirmation still had to be determined with MMC as the primary ICL agent. Based on the results from the growth curve, the protocol was adjusted for  $3 \times 10^3$  cells per 96-well for the FA cell lines PD20 (FANCD2 deficient) and 3.15 (FANCD corrected), incubated for 24 h before genotoxic agent treatment

and followed by 72 h incubation. Adjustments were also made for the cancer cell lines U2OS/-D2 and HeLa/-D2 (WT/ FANCD2 deficient, respectively) at  $2 \times 10^3$  cells per 96-well. However, the MTT assay results for the cancer cell lines displayed evidence that was considered incorrect compared to standard FA background research as well as Section 3.1.2. for visual comparison. The achieved results displayed either insignificant differences in genotoxic-agent resistance, expected differences in ICL-induced resistance when affected by cisplatin but not by MMC, ICL-induced resistance in the opposite expected orientation for FA and WT/corrected resistance, or non-calculable  $IC_{50}$  values in genotoxic-agent resistance between the WT and FANCD2 deficient cancer cell lines. Attempts were made at various cell concentrations and incubation times, but the protocol was adjusted based on the standard procedure from The Institute of Cancer Research, London, UK, due to the lack of time and resources. The standard procedure was seeding  $5 \times 10^2$  cells in 96-well, treated on the same day as seeding, and incubated for 168 h. Due to the incubation time being too long and with limited time remaining, adjustments to the protocol were attempted to be closer to the standard protocol used in the Elder Laboratory for faster results and analysis in case of potential issues. However the protocol was only adjusted to  $1 \times 10^3$  cells for U2OS and U2OS-D2, based on a confirmation of cell growth analysis (Appendix Figure 2), and  $5 \times 10^2$  cells for HeLa and HeLa-D2 per 96-well plate, and the genotoxic agents were added at the same day as seeding, followed by incubation for 96 h (U2OS/-D2) or 168 h (HeLa/-D2). The following results were based on the adjusted protocols.



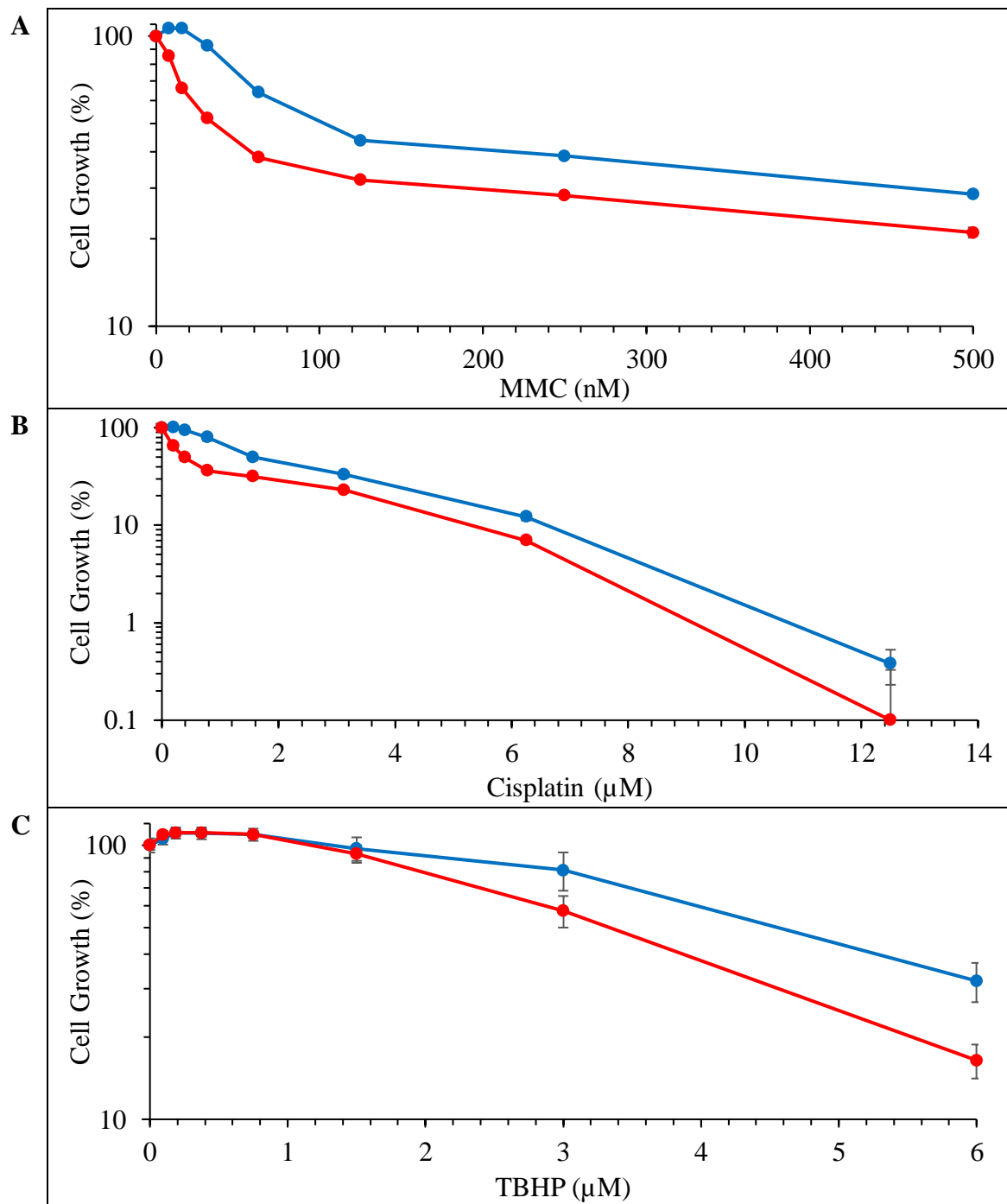
**D**

	IC <sub>50</sub> ± SD Values		
	MMC	Cisplatin	TBHP
<b>3.15</b>	0.43 ± 0.02 μM	2.24 ± 0.14 μM	49 ± 1.01 μM
<b>PD20</b>	0.06 ± 0.00 μM	0.74 ± 0.04 μM	29 ± 0.86 μM

**Figure 3.11: Growth inhibition of PD20 (FANCD2 deficient, red) and 3.15 (PD20 Corrected, blue) following treatment with A) mitomycin C (MMC), B) cisplatin, and C) TBHP.**

**D) IC<sub>50</sub> values for growth inhibition following treatment. 3 x 10<sup>3</sup> cells per 96-well, incubated for 72 h. Mean data was collected from triplicate technical and scientific repeats.**

Figure 3.11 shows the effect of MMC, cisplatin and TBHP for both PD20 (FANCD2 deficient) and 3.15 (FANCD2 corrected) cells. Similar to the results described in Section 3.1.2. when comparing FANCD2 expressed cells to FANCD2 deficient cells, the difference in resistance to the ICL and oxidative inducing agents could also be observed in the FANCD2 deficient (PD20) and FANCD2 corrected (3.15) cells in the expected orientation. As observed in Figure 3.11, compared to the  $IC_{50}$  of the PD20 cells, the 3.15 cells show a significantly increased resistance to MMC by a factor of 7.2 ( $IC_{50}$  0.06  $\mu$ M [PD20] to 0.43  $\mu$ M), cisplatin by a factor of 3 ( $IC_{50}$  0.74  $\mu$ M [PD20] to 2.24  $\mu$ M), but not for TBHP by a factor of 1.7 ( $IC_{50}$  29  $\mu$ M [PD20] to 49  $\mu$ M). Compared to the MTS assay results observed from Figure 3.5 on HSC-93 (WT), HSC-72 (FANCA deficient) and HSC-72 Corrected, the MTT assay results of FANCD2 deficient (PD20) and corrected (3.15) cells in Figure 3.11 displayed a larger difference in cell growth and genotoxic agent resistance, between 3  $\mu$ M and 0  $\mu$ M (control) for MMC (Figure 3.11A), between 3  $\mu$ M and approximately 0.4  $\mu$ M for cisplatin (Figure 3.11B), and between 75  $\mu$ M and approximately 19  $\mu$ M of TBHP (Figure 3.11C). This indicates how sensitive the FA cells PD20 are to ICL and oxidative inducing agents, from MMC to cisplatin, to TBHP. Compared to the MMC (A) and cisplatin (B) results, Figure 3.11C displays a notable plateau from the genotoxin-treated cells between 0  $\mu$ M and 18.75  $\mu$ M TBHP. This indicates that the PD20 (FANCD2 deficient) and 3.15 (PD20 corrected) cells were sensitive to TBHP from 18.75  $\mu$ M and the cells were approaching or had reached high confluency after 72 h incubation, similarly corresponding to the cell growth analysis from Figure 3.8B after 72 h to 96 h. Furthermore, it could mean the protocol could be adjusted by treating cells at the same day as seeding and possibly shorten the incubation time.



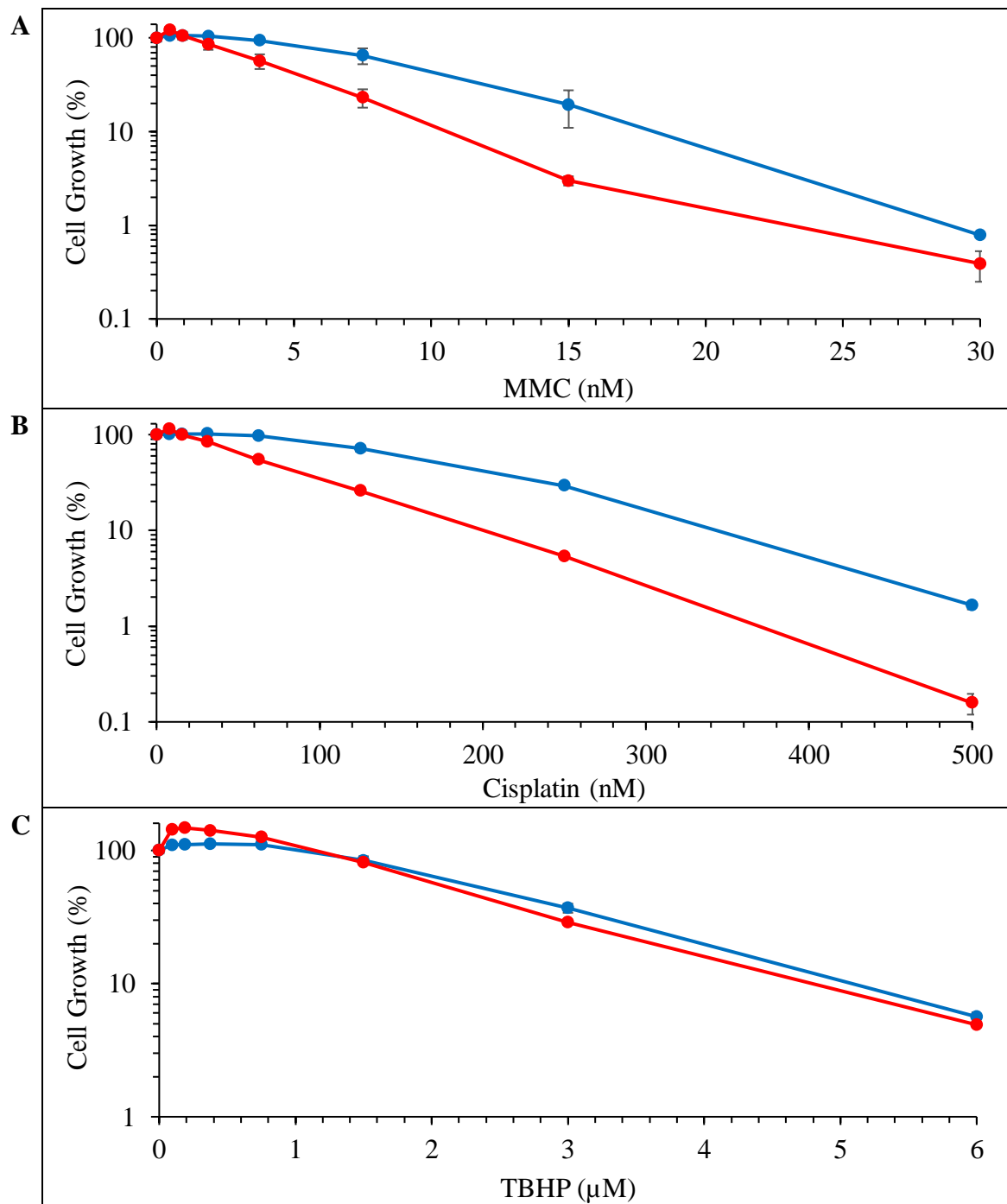
**D**

	IC <sub>50</sub> ± SD Values		
	MMC	Cisplatin	TBHP
U2OS	103 ± 16.97 nM	1.57 ± 0.27 µM	4.56 ± 1.10 µM
U2OS-D2	36 ± 5.43 nM	0.40 ± 0.13 µM	3.34 ± 0.55 µM

**Figure 3.12: Growth inhibition of U2OS (WT, blue) and U2OS-D2 (FANCD2 deficient, red) following treatment with A) mitomycin C (MMC), B) cisplatin and C) TBHP.**

**D)** IC<sub>50</sub> values for growth inhibition following treatment.  $1 \times 10^3$  cells per 96-well, incubated for 96 h. Mean data was collected from triplicate technical and scientific repeats.

A comparison of Figures 3.11 and 3.12 suggests that compared to the FA cell lines, the U2OS and U2OS-D2 cell lines are more susceptible to ICL and oxidative inducing agents than PD20 (FANCD2 deficient) and 3.15 (FANCD2 corrected) cells. As observed in Figure 3.12, compared to the  $IC_{50}$  of U2OS-D2 (FANCD2 deficient) cells, the U2OS (WT) cells show significantly increased resistance to MMC by a factor of 2.9 ( $IC_{50}$  36 nM [U2OS-D2] to 103 nM), cisplatin by a factor of 3.9 ( $IC_{50}$  0.40  $\mu$ M [U2OS-D2] to 1.57  $\mu$ M) but not for TBHP by a factor of 1.4 ( $IC_{50}$  3.34  $\mu$ M [U2OS-D2] to 4.56  $\mu$ M), as was expected for an FA phenotype. However, compared to the results shown in Figure 3.11, though the U2OS/-D2 cell growth difference was still significant, based on the  $IC_{50}$  values, it was not displayed as substantially different to each other as the PD20/3.15 difference in cell growth (Figure 3.11) for MMC (7.2 factor difference), cisplatin (3 factor difference) or TBHP (1.7 factor difference). From Figure 3.12, the differences in cell growth after genotoxin treatment between U2OS (WT) and U2OS (FANCD2 deficient) could be observed as almost parallel, from 500 nM to approximately 125 nM of MMC (Figure 3.12A) and from 12.5  $\mu$ M to approximately 1.6  $\mu$ M of cisplatin (Figure 3.12B). Furthermore, compared to the  $IC_{50}$  of TBHP treated FA cells PD20 (FANCD2 deficient) and 3.15 (PD20 corrected) in Figure 3.11D, the  $IC_{50}$  statistics of TBHP treated cancer cells U2OS (WT) and U2OS-D2 (FANCD2 deficient) may suggest either an experimental error or no real difference. Similar to the observations of Figure 3.11C, an arched plateau was noticed in Figure 3.12C the genotoxin treated U2OS and U2OS-D2 cells between 0  $\mu$ M and approximately 1  $\mu$ M TBHP. Other than indicating the WT (U2OS) and FANCD2 deficient (U2OS-D2) cells were sensitive to TBHP from approximately 1  $\mu$ M, the cells had reached high confluency after 96 h incubation, similarly corresponding to the cell growth analysis from Figure 3.9A and B after 96 h but not for  $1 \times 10^3$  cells (Appendix Figure 2B). This could mean the protocol could be adjusted by treating the U2OS/-D2 cells at  $5 \times 10^2$  seeding or possibly shorten the incubation time.



**D**

	IC <sub>50</sub> ± SD Values		
	MMC	Cisplatin	TBHP
HeLa	9.1 ± 0.81 nM	176 ± 5.83 nM	2.44 ± 0.19 μM
HeLa-D2	4.3 ± 1.51 nM	70 ± 4.88 nM	2.20 ± 0.51 μM

**Figure 3.13: Growth inhibition of HeLa (WT, blue) and HeLa-D2 (FANCD2 deficient, red) following treatment with A) mitomycin C (MMC), B) cisplatin and C) TBHP.**

**D)** IC<sub>50</sub> values for growth inhibition following treatment. 5 x 10<sup>2</sup> cells per 96-well, incubated for 168 h. Mean data was collected from triplicate technical and scientific repeats.

These data are in agreement with the U2OS/-D2 results described in Figure 3.12, where susceptibility to the genotoxic agents suggests that compared to the FA cell lines, the cancer cell lines U2OS (WT) and U2OS-D2 (FANCD2 deficient), as well as the HeLa/-D2 cells, are more susceptible to the ICL and oxidative inducing agents than previous FA original cell lines. Interestingly, the HeLa/-D2 cells are more sensitive than U2OS/-D2 cells to MMC and cisplatin but equally responsive to TBHP. This would signify that, compared to U2OS/-D2, the HeLa/-D2 cells are more susceptible to ICL-inducing agents than the oxidative-inducing agent. As observed in Figure 3.13, compared to the IC<sub>50</sub> of HeLa-D2 (FANCD2 deficient) cells, the HeLa (WT) cells show a significantly increased resistance to MMC by a factor of 2.1 (IC<sub>50</sub> 4.3 nM [HeLa-D2] to 9.1 nM) and cisplatin by a factor of 2.5 (IC<sub>50</sub> 70 nM [HeLa-D2] to 176 nM), as it was again expected for an FA phenotype, but barely a difference in resistance to TBHP (IC<sub>50</sub> 2.20 μM [HeLa-D2] to 2.44 μM). Though HeLa/-D2 showed statistically equal sensitivity to TBHP, it was not uncommon for similar results to appear from previous cell lines attempted when treated with TBHP (Appendix Figure 3). It may be due to experimental error or is more likely that the cancer cell lines U2OS/-D2 and HeLa/-D2 (WT/FANCD2 deficient) are not as susceptible to oxidative damage, and therefore no real difference, as the FA cell lines PD20/3.15 (FANCD2 deficient/corrected) with a noticeable difference. Similar to the observations of Figure 3.11C, an arched plateau was noticed in Figure 3.12C the genotoxin treated U2OS and U2OS-D2 cells between 0 μM and approximately 1 μM TBHP. Other than indicating the WT (U2OS) and FANCD2 deficient (U2OS-D2) cells were sensitive to TBHP from approximately 1 μM, the cells had reached high confluency after 96 h incubation and were still growing from, similarly corresponding to the cell growth analysis from Figure 3.9A and B after 96 h but not for 1 x 10<sup>3</sup> cells (Appendix Figure 2B). This could mean the protocol could be adjusted by treating the cells at 5 x 10<sup>2</sup> seeding or possibly shorten the incubation time. Compared to the PD20/3.15 results and U2OS/-D2 results displayed in Figures 3.11 and 3.12, respectively, though the HeLa/-D2 cell growth difference was still notable, it was not as greatly significant or greater than PD20/3.15, nor similar to U2OS/-D2 as it might have been expected.

### 3.2.3. Gene and Protein Expression Studies

Due to the difficulty of detecting NEIL1 and mainly NEIL3 by western blot methods, examples of which can be seen in Appendix Figures 1 and 4, qRT-PCR was attempted. Although the data was initially encouraging, reproducibility was poor and not improved by

modification of methods and use of new reagents (example displayed in Appendix Figure 5). Western blotting was again attempted using alternative methodologies as the standard protocol (Section 2.5) but were again unsuccessful. Time constraints meant that RT-PCR was adopted with PCR amplicons quantified by their captured images through Image Studio Lite (LI-COR), and therefore based on one scientific replicant.

Compared to the results observed in Section 3.1.3., it could be expected that the RT-PCR expression results for the PD20 (FANCD2 deficient) and 3.15 (FANCD2 corrected) cells would be similar to the HSC-72 (FANCA deficient) and HSC-72 Corrected cells (lanes 8 – 13, Figure 3.6). As it could be seen from Figure 3.14A, both the 3.15 cells (i) and PD20 (ii) cells displayed noticeable expression of *NEIL2* and *NEIL3* (lanes 5 and 6, respectively), but not visibly for *NEIL1* (lane 4). Compared to the cell's respective *GAPDH* expression in Figure 3.14B, *NEIL2* and *NEIL3* were expressed at an approximate ratio of 1:14 and 1:2 in the FANCD2 corrected cells (3.15), respectively, and at an approximate ratio of 1:10 and 1:1 in the FANCD2 deficient cells (PD20). Between the PD20 and 3.15 cell lines there is no significant difference in *NEIL1* and *NEIL2*, though based on the literature review these cell lines were not profiled before for *NEIL1* and *NEIL2* expression but have for *NEIL1* underexpression in the PD20 cells. However, it has been known for underexpressed *NEIL1* to upregulate *NEIL3* expression (Li *et al.*, 2020), and as displayed in Figure 3.14 it may be the case for the FA cell lines PD20 (FANCD2 deficient) and 3.15 (PD20 corrected) observed to have a significantly increased expression of *NEIL3* in relation to *NEIL1*. Interestingly, compared to the expression of *NEIL3* in the 3.15 cells, a significant difference of approximately 1:2 ratio of expression of *NEIL3* could be observed in the PD20 cells, which was similarly seen in Figure 3.6 with *NEIL3* expression in favour of HSC-72 (FANCA deficient) over HSC-72 Corrected, but not as substantial. This may signify that in response to the FA phenotype, the PD20 cells may be expressing *NEIL3* as the substitute to the cells FANCD2 deficiency.

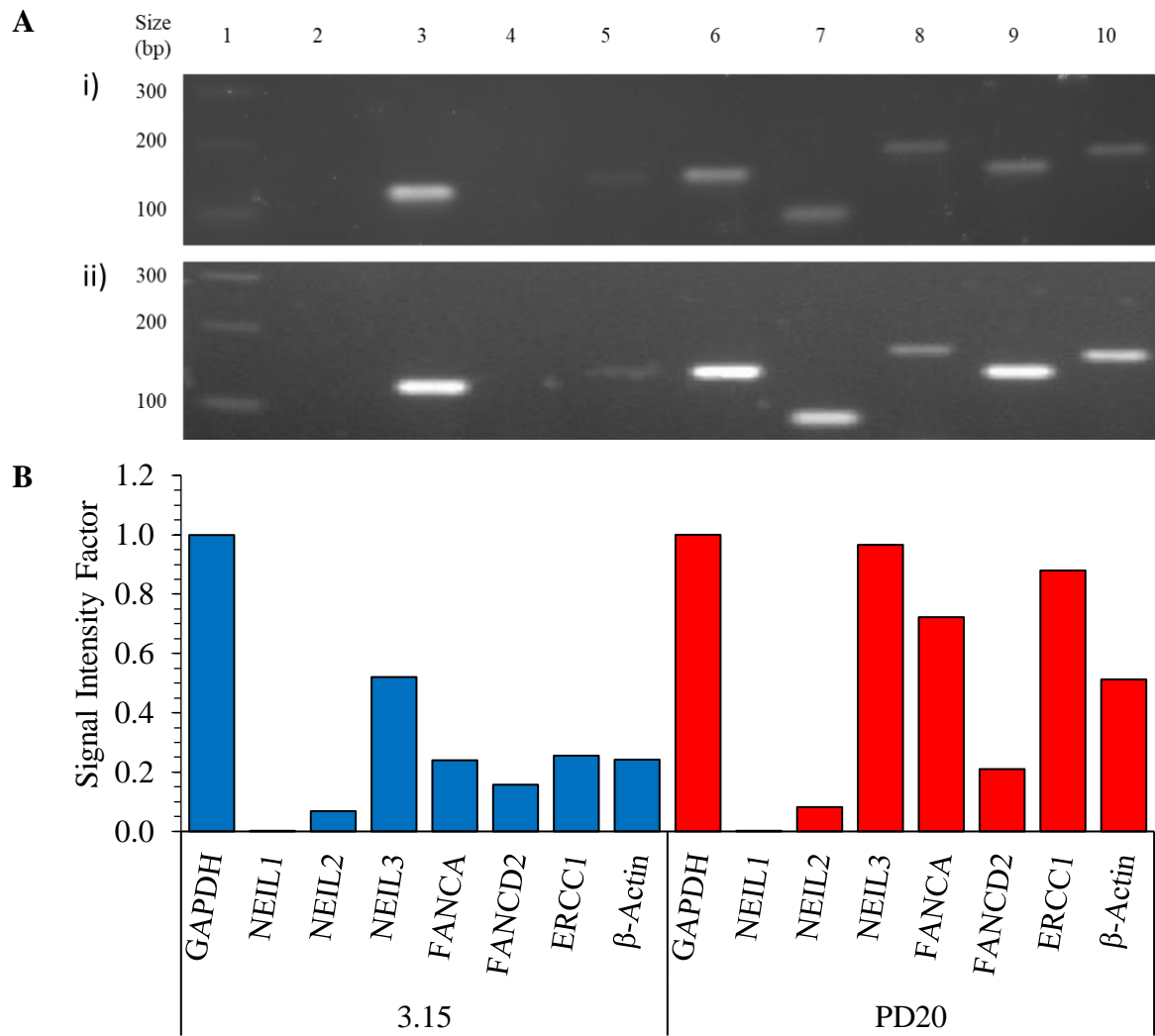


**Figure 3.14: Expression of *GAPDH*, *NEIL1*, *NEIL2*, *NEIL3*, *FANCA*, *FANCD2*, *ERCC1*, and  $\beta$ -Actin from cell lines A(i) 3.15 (PD20 corrected) and A(ii) PD20 (FANCD2 deficient), by RT-PCR.**

(A) Separate gel electrophoresis images. Lane 1, DNA ladder; lane 2, negative control; lane 3, *GAPDH*; lane 4, *NEIL1*; lane 5, *NEIL2*; lane 6, *NEIL3*; lane 7, *FANCA*; lane 8, *FANCD2*; lane 9, *ERCC1*; lane 10,  $\beta$ -Actin. Expected amplicon length: *GAPDH*, 127 bp; *NEIL1*, 212 bp; *NEIL2*, 145 bp; *NEIL3*, 147 bp; *FANCA*, 91 bp; *FANCD2*, 181 bp; *ERCC1*, 146 bp;  $\beta$ -Actin, 166 bp. (B) Quantified signal intensity from amplicons in section A relative to the cell's *GAPDH* expression, based on one scientific replicate.

Expressions for *FANCA*, *FANCD2*, *ERCC1* and  $\beta$ -Actin were also observed for background confirmation and for potential uses in relation to the project. It was not expected for there to be a difference in expression of *FANCA* compared to *FANCD2*, but it was interesting to know that *FANCA* was more expressed than *FANCD2* by an approximate ratio of 1:3 in FANCD2 deficient cells (PD20) and 1:2 in FANCD2 corrected cells (3.15, Figure 3.14B). As described in Table 2.1 and through the literature review for the FA cell lines PD20 and

3.15, the *FANCD2* mutations could only be detected with specific primers, and expression could be quantified and compared only by protein expression through western blot. Furthermore, the 3.15 cell line was described as PD20 cells corrected with microcell-mediated transfer of chromosome 3p, allowing regular expression of *FANCD2*. Therefore, it was not expected for there to be a significant difference in expression through RT-PCR expression since the *FANCD2* primers used (Table 2.14) were not mutation-specific and compared to their respective *GAPDH* expression, both PD20 and 3.15 have an approximate 1:5 *FANCD2*-expression ratio (Figure 3.14B). *FANCD2* expression was later determined for FA phenotype validation through western blot. *ERCC1* expression was considered a possible relation to *NEIL3* protein expression when *NEIL3* not being visualised on a western blot was being investigated. However, it was later considered insignificant concerning the project, although interestingly the PD20 cells had a *NEIL3:ERCC1* expression ratio of almost 1:1, but 1:2 in the 3.15 cells (Figure 3.14B). *β-Actin* expression was only considered an alternative for expression control for *GAPDH*, and therefore, nothing significant was researched further.

Similar to the PD20/3.15 cell extracts for RT-PCR amplification in Figure 3.14, as it could be seen from Figure 3.15A, both the U2OS (WT, [i]) and U2OS-D2 (*FANCD2* deficient, [ii]) cells displayed expression of *NEIL2* and *NEIL3* (Figure 3.15A[i], lanes 4 and 5, respectively; Figure 3.15A[ii], lanes 5 and 6, respectively), but not visibly for *NEIL1* (Figure 3.15A[i], lane 3; Figure 3.15A[ii], lane 4). Interestingly, *NEIL2* expression was more noticeable in the U2OS/-D2 cells than in PD20/3.15 cells (Figure 3.14) or in the HeLa/-D2 cells (Figure 3.16). Compared to the cell's respective *GAPDH* expression in Figure 3.15B, *NEIL2* and *NEIL3* were expressed at an approximate ratio of 1:5 and 1:3, respectively, in both the U2OS (WT) and U2OS-D2 (*FANCD2* deficient) cells, but no significant differences when compared to each other. Notably, there was a difference in *FANCA* expression by an approximate 1:3 ratio in favour of the U2OS cells, which was observed in the opposite orientation when comparing the *FANCD2* corrected cells (3.15) to the *FANCD2* deficient cells (PD20, Figure 3.14). Although there was no substantial difference in expression of *FANCA* compared to *FANCD2*, for the *FANCD2* deficient cells (U2OS-D2), *FANCD2* expression was unexpectedly present (lane 7, Figure 3.15A[ii]). Compared to their respective *GAPDH* expression in Figure 3.15B, *FANCD2* was expressed at an approximate 1:3 ratio in U2OS cells and an approximate 1:5 ratio in U2OS-D2 cells, but the WT (U2OS) cells *FANCD2* amplification appeared to be twofold higher than the *FANCD2* deficient (U2OS-

D2) cells *FANCD2* amplification. Protein expression was later determined for FA-generated phenotype validation.

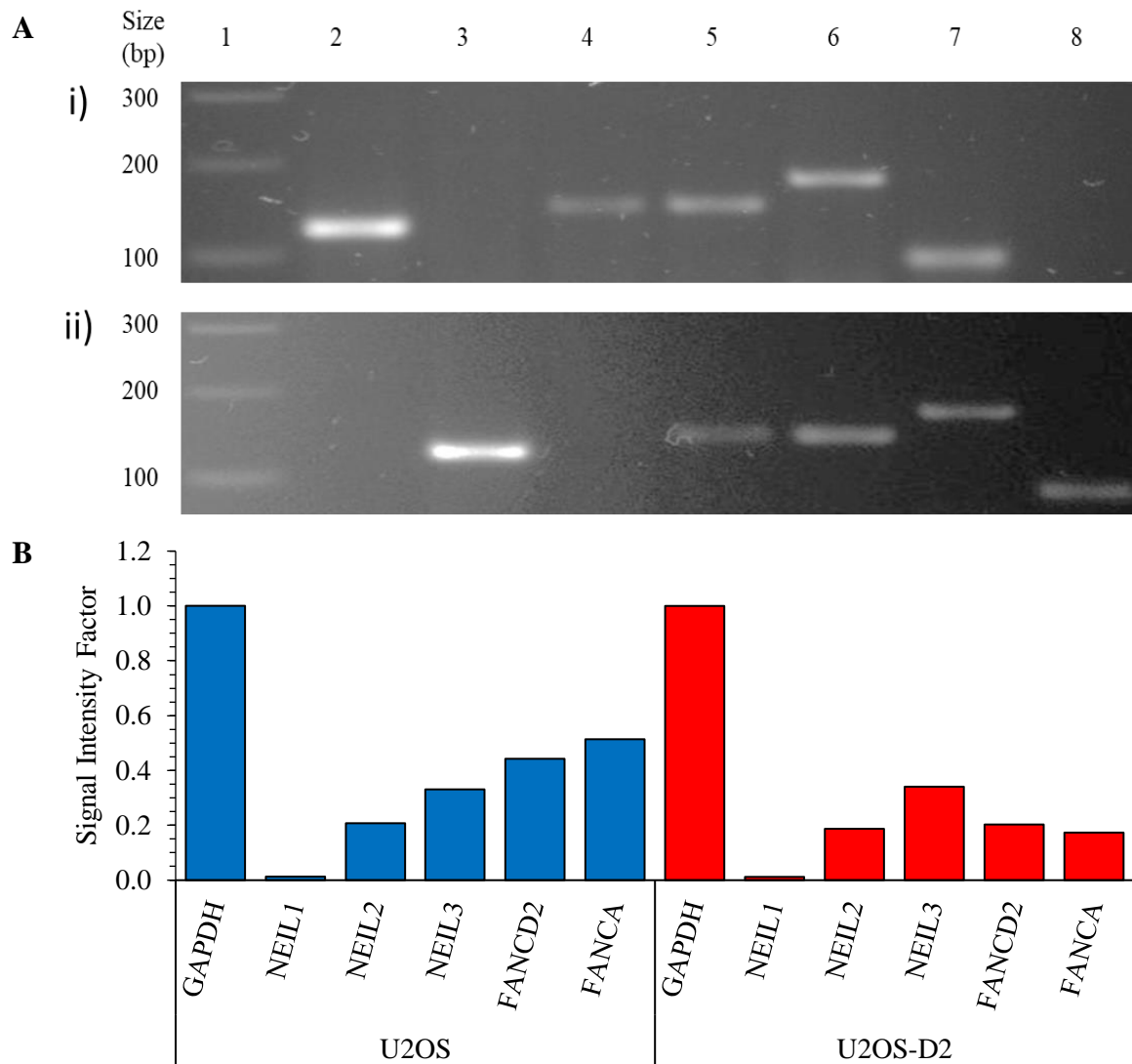


**Figure 3.15: Expression of GAPDH, NEIL1, NEIL2, NEIL3, FANCD2 and FANCA from cell-lines A(i) U2OS (WT) and A(ii) U2OS-D2 (FANCD2 deficient), by RT-PCR.**

(A) Gel electrophoresis image sectioned in two parts. A(i) Lane 1, DNA ladder; lane 2, GAPDH; lane 3, NEIL1; lane 4, NEIL2; lane 5, NEIL3; lane 6, FANCD2; lane 7, FANCA; lane 8, negative control. A(ii) Lane 1, DNA ladder; lane 2, negative control; lane 3, GAPDH; lane 4, NEIL1; lane 5, NEIL2; lane 6, NEIL3; lane 7, FANCD2; lane 8, FANCA. Expected amplicon length: GAPDH, 127 bp; NEIL1, 212 bp; NEIL2, 145 bp; NEIL3, 147 bp; FANCD2, 181 bp; FANCA, 91 bp. (B) Quantified signal intensity from amplicons in section A relative to the cell's *GAPDH* expression, based on one scientific replicate.

Similar to the U2OS/-D2 results in Figure 3.15, as observed in Figure 3.16A, both the HeLa (WT, [i]) and HeLa-D2 (FANCD2 deficient, [ii]) displayed expressions for *NEIL1* – *NEIL3* (lanes 4 – 6, respectively), with *NEIL3* significantly expressed compared to the barely visible

*NEIL1* and *NEIL2* (lanes 4 and 5, respectively) by an approximate 1:10 ratio or greater (Figure 3.16B). Compared to the cell's respective *GAPDH* expression in Figure 3.16B, *NEIL1* and *NEIL2* were barely expressed at an approximate 1:100 ratio in both the HeLa and HeLa-D2, but *NEIL3* was expressed at an approximate ratio of 1:5 and 1:8 in HeLa and HeLa-D2 respectively. Compared to the WT cells (HeLa), the FANCD2 deficient cells (HeLa-D2) had a twofold higher expression in *NEIL3*, which was the opposite of the RT-PCR results observed from the FANCD2 deficient/corrected cell line (PD20/3.15, respectively) extracts in Figure 3.14, and neither observed from the U2OS/-D2 cell (WT/FANCD2 deficient, respectively) extracts in Figure 3.15. Furthermore, similar to the results observed of the 3.15 and PD20 cell extracts (Figure 3.14), the HeLa and HeLa-D2 cells displayed a threefold and fivefold, respectively, increase in expression of *FANCA* compared to *FANCD2*. Similar to the U2OS-D2 cells RT-PCR results (Figure 3.15), *FANCD2* expression was also unexpectedly, though faintly, present in the HeLa-D2 cells RT-PCR results (Figure 3.16A[ii], lane 7). As observed in Figure 3.16B, compared to their respective *GAPDH* expression, *FANCD2* was expressed at an approximate 1:5 ratio in HeLa cells, and an approximate 1:100 ratio in HeLa-D2 cells, but the WT (HeLa) cells *FANCD2* expression appeared to be approximately five times higher than the FANCD2 deficient (HeLa-D2) cells *FANCD2* expression. Similarly to the U2OS/-D2 cells RT-PCR results (Figure 3.15), protein expression from HeLa/-D2 cell extracts were also later determined for FA-generated phenotype validation.

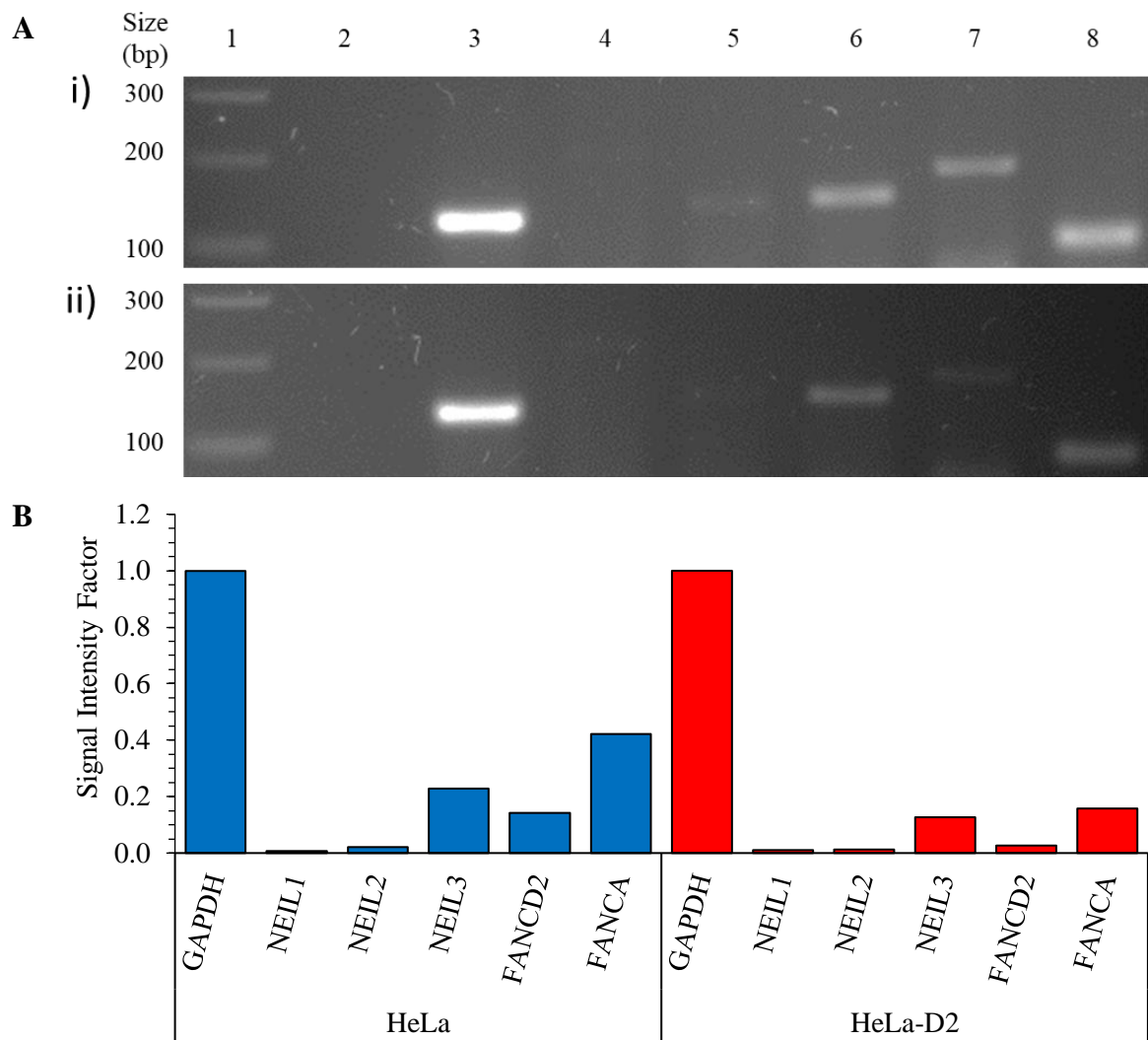


**Figure 3.16: Expression of *GAPDH*, *NEIL1*, *NEIL2*, *NEIL3*, *FANCD2* and *FANCA* from cell-lines A(i) HeLa (WT) and A(ii) HeLa-D2 (*FANCD2* deficient), by RT-PCR.**

(A) Gel electrophoresis image sectioned in two parts. Lane 1, DNA ladder; lanes 2, negative control; lane 3, *GAPDH*; lane 4, *NEIL1*; lane 5, *NEIL2*; lane 6, *NEIL3*; lane 7, *FANCD2*; lane 8, *FANCA*. Expected amplicon length: *GAPDH*, 127 bp; *NEIL1*, 212 bp; *NEIL2*, 145 bp; *NEIL3*, 147 bp; *FANCD2*, 181 bp; *FANCA*, 91 bp. (B) Quantified signal intensity from amplicons in section A relative to the cell's *GAPDH* expression, based on one scientific replicate.

Following RT-PCR, protein expression from the cell extracts of FA and WT/corrected cells were analysed after western blot, as displayed in Figure 3.17. As it could be seen in Figure 3.17A(i), the *FANCD2* deficient (PD20) cell extract displayed no protein expression of *FANCD2*, as was expected of a *FANCD2*-related FA cell line, whereas the *FANCD2* corrected (3.15) cell extract displayed *FANCD2* protein expression, as was also expected. Similarly, in Figure 3.17A(ii), the WT cancer cells U2OS (lane 2) and HeLa (lane 4) extracts were also observed expressing *FANCD2* protein, as was expected, though their FA-

generated cell counterparts U2OS-D2 (lane 3) and HeLa-D2 (lane 5) extracts were barely expressing FANCD2 protein, which was unexpected. From the RT-PCR results observed previously, the unexpected U2OS-D2 (Figure 3.15A[ii]) and HeLa-D2 (Figure 3.16A[ii]) *FANCD2* expression results suggested potential FANCD2 expression, which contradicted the generated *FANCD2*<sup>-/-</sup> phenotype of the cells described in Table 2.1 and Schwab *et al.* (2015). However, based on the observed protein expression results in Figure 3.17A(ii), and compared to the MTT assay results after MMC, cisplatin and TBHP treatment cell survival (Figures 3.12 and 3.13), the FA-generated cancer cells U2OS-D2 and HeLa-D2 were considered as FANCD2 deficient or depleted cells.

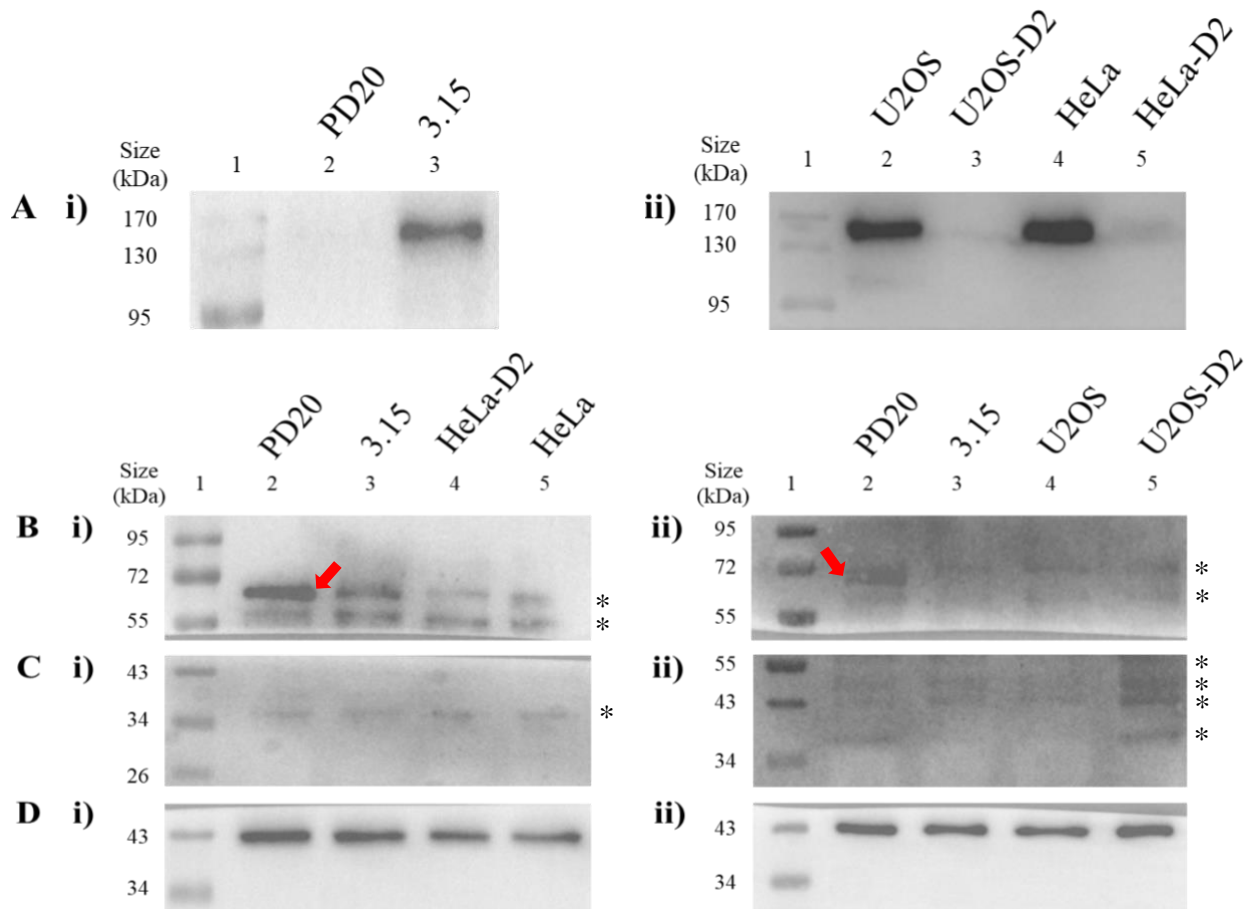


**Figure 3.17: Western blots of PD20 (FANCD2 Deficient), 3.15 (PD20 corrected), HeLa (WT), HeLa-D2 (FANCD2 deficient), U2OS (WT) and U2OS-D2 (FANCD2 deficient) cell extracts. (A) FANCD2, (B) NEIL3, (C) NEIL1, and (D)  $\beta$ -Actin.**

**A(i)** Lane 1, protein ladder; lane 2, PD20; lane 3, 3.15. **A(ii)** Lane 1, protein ladder; lane 2, U2OS; lane 3, U2OS-D2; lane 4, HeLa; lane 5, HeLa-D2. **(B[i], C[i], D[i])** Lane 1, protein ladder; lane 2, PD20; lane 3, 3.15; lane 4, HeLa-D2; lane 5, HeLa. **(B[ii], C[ii], D[ii])** Lane 1, protein ladder; lane 2, PD20; lane 3, 3.15; lane 4, U2OS; lane 5, U2OS-D2. Expected molecular weight: FANCD2, 164 kDa; NEIL3, 68 kDa; NEIL1, 43 kDa;  $\beta$ -Actin, 42 kDa. (\*) Non-specific binding. Red arrow, NEIL3 expression detected.

As displayed in Figure 3.17B, the FANCD2 deficient cells PD20 (lane 2) displayed expression of NEIL3 protein, whereas the FANCD2 correct cells 3.15 (lane 3) did not. Furthermore, the cancer cells HeLa-D2 and HeLa (lanes 4 and 5, respectively, [i]), and U2OS and U2OS-D2 (lanes 4 and 5, respectively, [ii]) in Figure 3.17B also did not display NEIL3 protein expression. NEIL1 protein expression was not observed in any of the cell extracts, as displayed in Figure 3.17C, and as expected in Figure 3.17D,  $\beta$ -Actin protein expression was observed from all cell extracts and with no suggestion of sample loading differences. Compared to the RT-PCR results (Figures 3.14 – 3.16), only the FANCD2 deficient cells PD20 showed the highest *NEIL3* expression (Figure 3.14A[ii]), which corresponded with the NEIL3 protein expression in the western blot results only visible from PD20 cell extract (lane 2, Figure 3.17B). Furthermore, all cell lines showed barely visible *NEIL1* expression in the RT-PCR results, which also corresponded with the NEIL1 protein expression observed in the western blot results (Figure 3.17C), suggesting the NEIL1 protein expression was too low to be detected.

Based on the combined background results, it was more appropriate for all six FANCD2-related cell lines to be transfected with pcDNA3.1-hNEIL1-FLAG for NEIL1 recombinant expression, and all apart from the FANCD2 deficient cells PD20 to be transfected with pcDNA3.1-hNEIL3<sup>FL</sup>-FLAG and pcDNA3.1-hNEIL3<sup>1506</sup>-FLAG. The results also suggested it was appropriate for the six-cell lines to be transfected for NEIL3 siRNA for NEIL3 knockdown. However, due to the incubation time period of siRNA knockdown generally lasting between 120 h and 168 h depending on the cell type and siRNA concentration, and the limited resources the siRNA transfection was reserved for FANCD2 deficient/corrected cells PD20/3.15, and possibly the WT and FANCD2 deficient cancer cells U2OS/-D2.

### 3.3. Generating pcDNA3.1-hNEIL3<sup>FL</sup>-FLAG and pcDNA3.1-hNEIL3<sup>1506</sup>-FLAG

The aim and objective was to generate the plasmids pcDNA3.1-hNEIL3<sup>FL</sup>-FLAG and pcDNA3.1-hNEIL3<sup>1506</sup>-FLAG from pcDNA3.1-hNEIL1-FLAG for the empty vector and pETDUET2-hNEIL3 for NEIL3 reference, before transfection of the desired plasmids to the experimented cell lines later in the project. The plan intended to use PCR to amplify the XbaI-hNEIL3<sup>FL</sup>-FLAG-EcoRI (hNEIL3<sup>FL</sup>-FLAG) and XbaI-hNEIL3<sup>1506</sup>-FLAG-EcoRI (hNEIL3<sup>1506</sup>-FLAG) inserts, digest the XbaI and EcoRI digest sites from the inserts and the

pcDNA3.1 empty vector for open sticky-ends, and then ligate the inserts to the empty vector followed by cloning and confirmation. Due to the hNEIL3<sup>FL</sup>-FLAG and hNEIL3<sup>1506</sup>-FLAG amplicons not having at least 1 – 3 nucleotides adjacent to the desired restrictive-digestion sites, instead of redesigning the predesigned primers in Table 2.13 (Section 2.1.6.), the additional cloning step of ZeroBlunt cloning (Section 2.2.3.) was used for the additional nucleotides necessary for insert preparation as well as further amplification of the desired inserts.

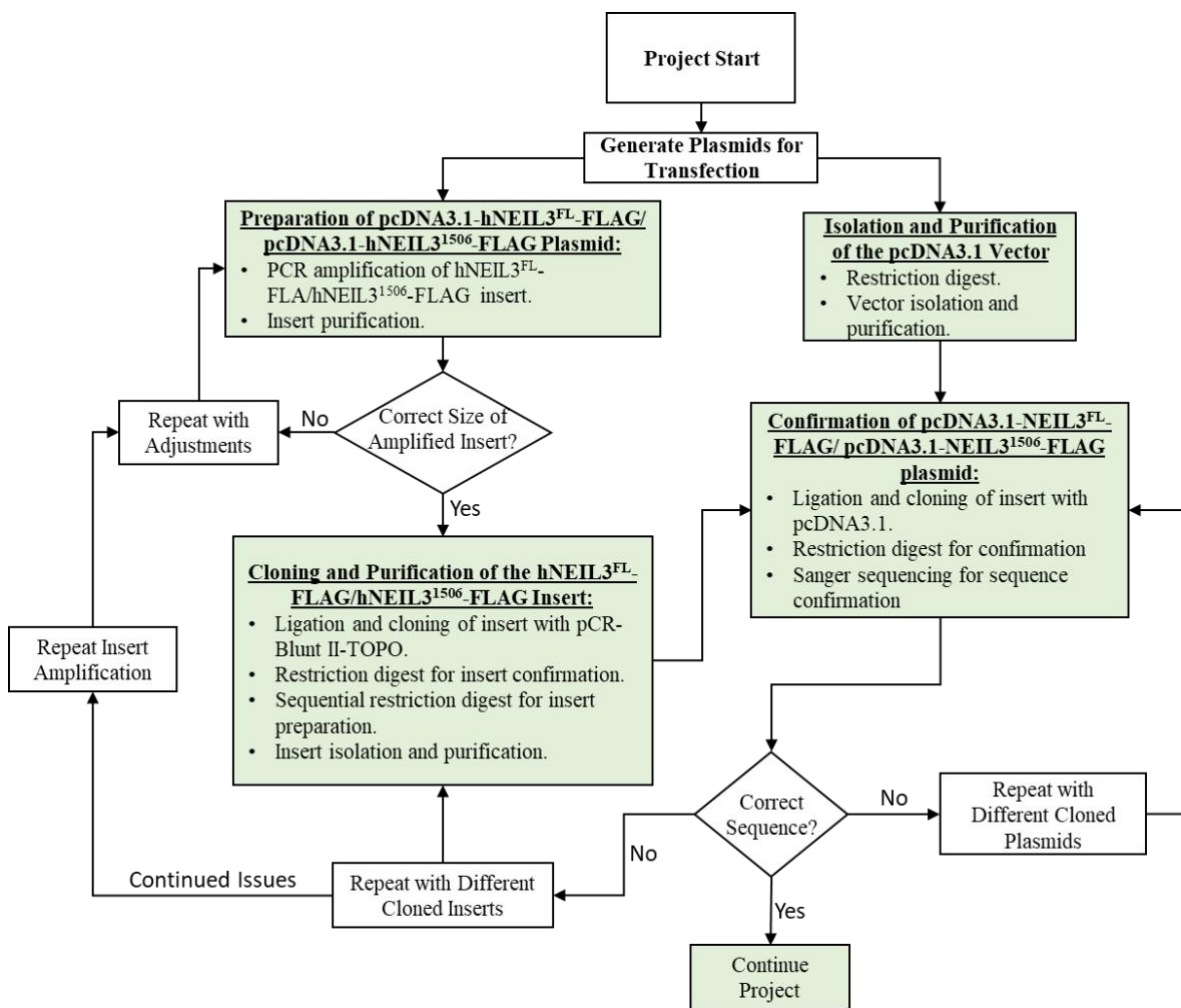


**Figure 3.18: Flowchart on the approach to plasmid generation work.**

Expanded subsection of the overall flowchart displayed in Section 1.6 (Figure 1.11). Green highlights, results achieved.

Displayed in Figure 3.18 were the aims and objectives of Section 3.3 planned according to the approach to the work displayed in the flow chart. The results for the hNEIL3<sup>FL</sup>-FLAG and hNEIL3<sup>1506</sup>-FLAG insert amplification (Sections 3.3.1. and 3.3.5.), cloning, purification and isolation of the amplified inserts (Sections 3.3.2. and 3.3.5.), isolation and purification

of the pcDNA3.1 vector (Section 3.3.3.), and cloning followed by confirmation of pcDNA3.1-hNEIL3<sup>FL</sup>-FLAG and pcDNA3.1-hNEIL3<sup>1506</sup>-FLAG plasmids (Sections 3.3.4. and 3.3.5.) allowed the project to continue to the next stage of the project.

### 3.3.1. Preparation of pcDNA3.1-hNEIL3<sup>FL</sup>-FLAG Plasmid

Initially, the protocol intended was PCR with Phusion DNA polymerase. Due to the nature of the primers used, the melting temperatures of the primers were equivalent to or greater than the extension temperature of 72°C (which would convert 3-step PCR into 2-step PCR). As displayed in Figure 3.19, results were achieved for the positive control of the hNEIL3<sup>843</sup>-FLAG fragment of 891bp-long hNEIL3 (Figure 3.19, lane 4). However, the goal was to amplify the hNEIL3<sup>FL</sup>-FLAG insert (lane 3 of Figure 3.19).

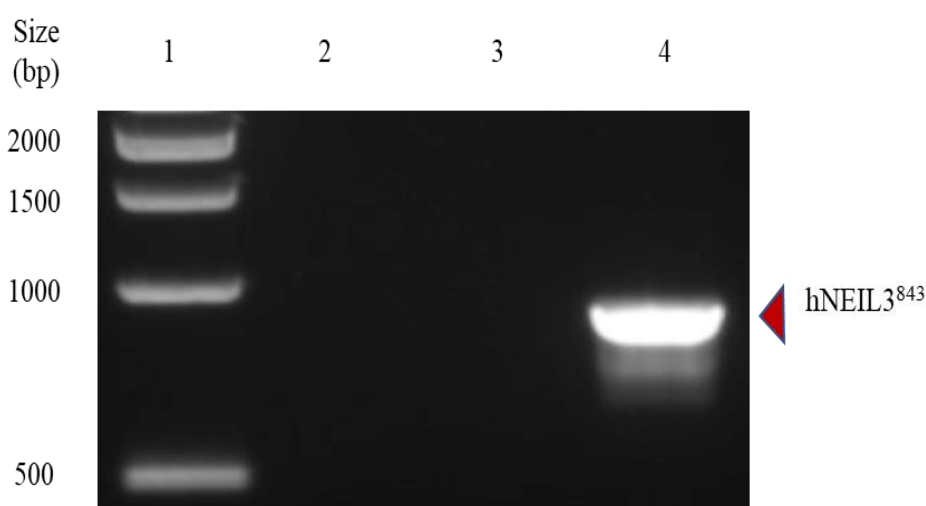


**Figure 3.19: Amplification of hNEIL3<sup>FL</sup>-FLAG and hNEIL3<sup>843</sup>-FLAG from pETDUET2-hNEIL3.**

Lane 1, DNA ladder; lane 2, negative control; lane 3, hNEIL3<sup>FL</sup>; lane 4, hNEIL3<sup>843</sup>. Expected amplicon length: hNEIL3<sup>FL</sup>-FLAG, 1864 bp; hNEIL3<sup>843</sup>-FLAG, 891 bp. Two-step PCR with Phusion DNA polymerase (72°C annealing temperature).

The experiment was repeated multiple times, independently and together, under different conditions. Following the PCR protocol (Section 2.2.2.) the range of conditions attempted included using the Phusion DNA polymerase under the two-step thermocycling condition with annealing/extension step at 1.24 min, denaturing at 95°C and annealing/extension at 1.30 min, double volume of reaction mixture with 200ng template DNA (plasmid), annealing at 67°C, repeated with Q5 DNA polymerase with or without a GC enhancer (NEB) or 5%

DMSO, repeated with OneTaq DNA polymerase (NEB), and gradient PCR to determine the optimal annealing temperature between 67°C and 81°C and 80 s extension step. Until tested with a *Taq* polymerase from MyTaq (Bioline), it did not produce the intended insert.

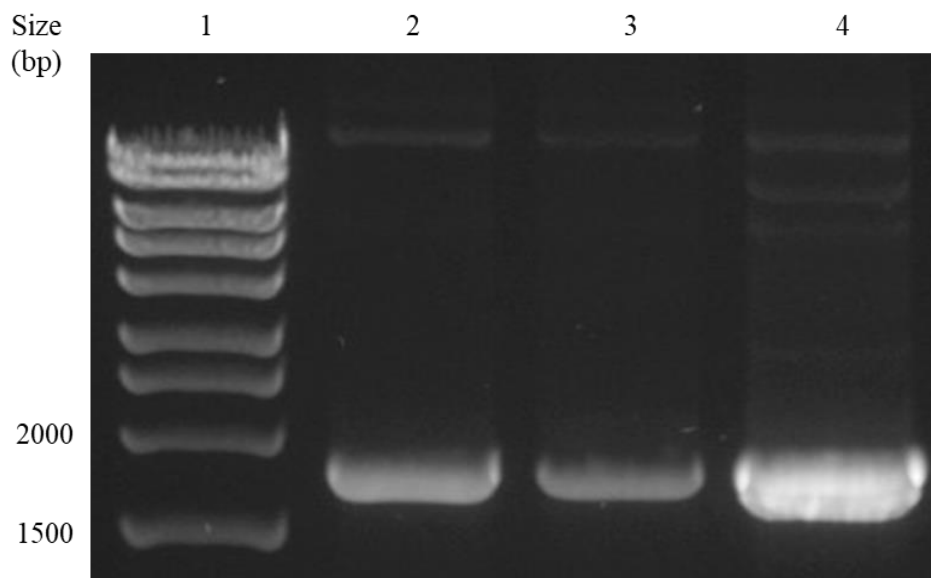


**Figure 3.20: Amplification of hNEIL3<sup>FL</sup>-FLAG from pETDUET2-hNEIL3.**

Lane 1, DNA ladder; lane 2, Phusion; lane 3, Phusion with MgCl<sub>2</sub> (4 mM); lane 4, Phusion with DMSO (3%). Expected amplicon length: hNEIL3<sup>FL</sup>-FLAG, 1864 bp. Phusion DNA polymerase and Touchdown (76°C annealing temperature -1°C per cycle).

A colleague of the Elder Laboratory attempted to amplify hNEIL3<sup>FL</sup>-FLAG using Phusion PCR with 4 mM MgCl<sub>2</sub> and a thermocycling Touchdown PCR programme (a cycling programme in which the annealing temperature gradually reduces after each cycle), and this was successful. The resulting PCR was repeated with Phusion DNA polymerase and is shown in Figure 3.20, with a Touchdown programme of 76°C annealing temperature with a reduction of 1°C per cycle. Additionally, the effect of the addition of MgCl<sub>2</sub> or DMSO is also shown in Figure 3.20 (lanes 3 and 4, respectively). However, as displayed in Figure 3.20, the critical optimisation step required was the Touchdown programme, regardless of the addition of MgCl<sub>2</sub> or DMSO to the reaction mixture, as previous attempts with altered conditions mentioned resulted in no observable band similar to what was observed in Figure 3.19 lane 3.

### 3.3.2. Cloning and Purification of the hNEIL3<sup>FL</sup>-FLAG Insert

After successfully isolating and purifying the hNEIL3<sup>FL</sup>-FLAG amplicon, it was then ligated into the pCR-Blunt II-TOPO plasmid to enable cloning into the destination vector (Section 2.2.3.). After subsequent cloning and extraction, the pCR-Blunt II-TOPO-hNEIL3<sup>FL</sup>-FLAG plasmid was tested for the presence and orientation of the insert by restriction endonuclease digest (Figure 3.21). The results indicated that the insert was present in the colonies picked, based on the EcoRI restriction digest (Figure 3.21A) and in the reverse orientation based on the XbaI restriction digest (Figure 3.21B), when compared to the vectors restriction-digest sites displayed in Figure 3.21C. The combined plasmid + insert displayed in Figure 3.21B was larger than the expected approximate size of 5400 bp, possibly due to well formation from bent comb teeth or loading error, but it was more important to discern the insert orientation by restriction digest, and the correct sizes for the pCR-Blunt II-TOPO plasmid (3500 bp) and hNEIL3<sup>FL</sup>-FLAG insert (1863 bp) were confirmed in Figure 3.21A. Using the primer specifications in Table 2.13, the amplified NEIL3<sup>FL</sup>-FLAG insert was to have the restriction digest site XbaI at the 5'-end and EcoRI at the 3'-end, therefore forward orientation sequence XbaI-NEIL3<sup>FL</sup>-FLAG-EcoRI. If the XbaI-NEIL3<sup>FL</sup>-FLAG-EcoRI sequence was inserted in the blunt product end of the pCR-Blunt II-TOPO plasmid map (Figure 3.21C) in the forward orientation, a XbaI restriction digest would result two digest products similarly displayed in Figure 3.21A, but with 49 bp added from the plasmid to the insert (3'-end of Blunt PCR Product to encircled XbaI site in Figure 3.21C). If in reverse orientation (EcoRI-FLAG-NEIL3<sup>FL</sup>-XbaI) the insert and plasmid would appear as a linearised plasmid, similarly to Figure 3.21B, but with an approximate size of 5400 bp and a digested band of approximately 50 bp (3'-end of Blunt PCR Product with XbaI site to encircled XbaI site in Figure 3.21C).

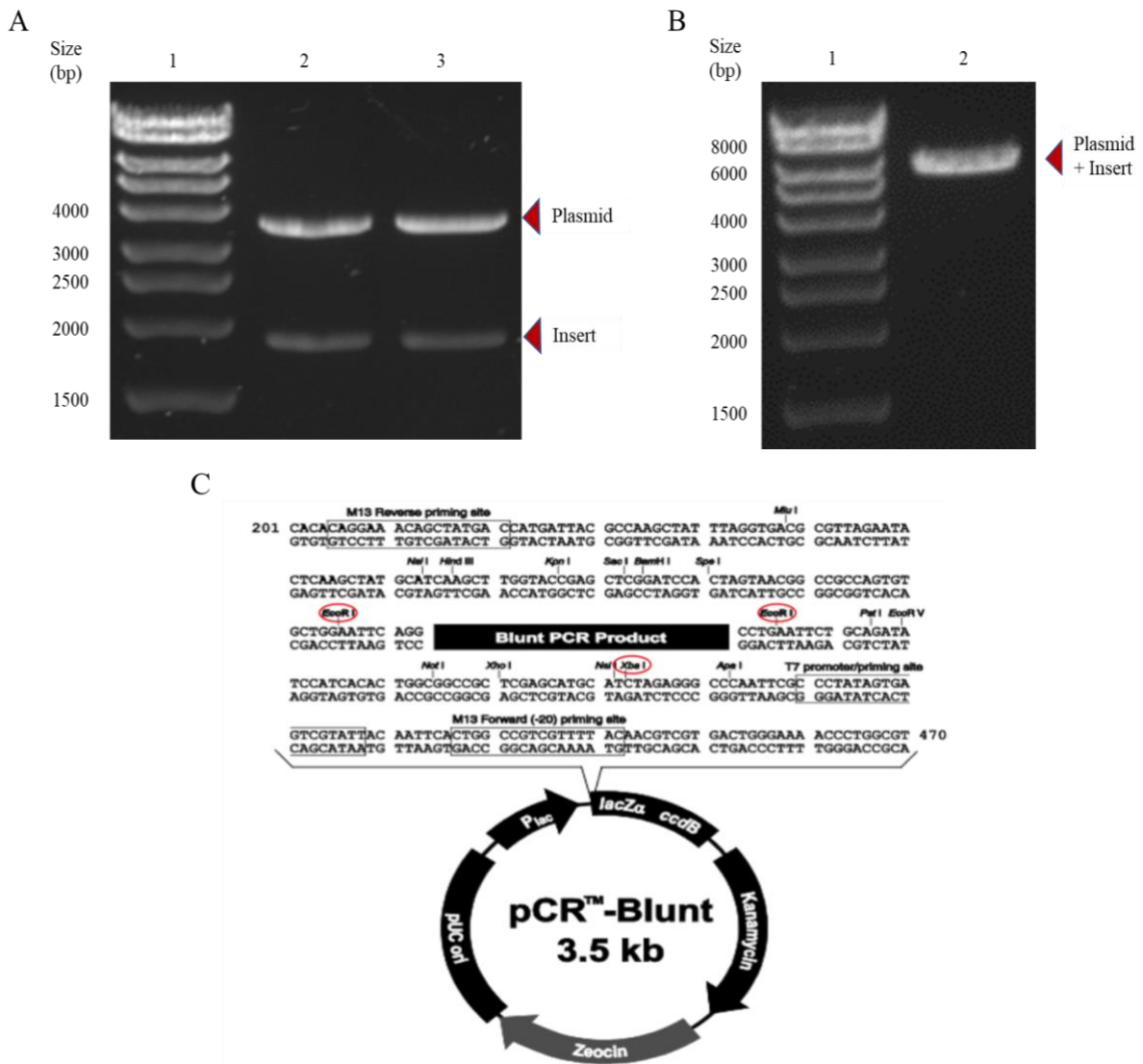


**Figure 3.21: Analysis of hNEIL3FL-FLAG insert in pCR-Blunt II-TOPO-hNEIL3FL-FLAG, using EcoRI or XbaI.**

(A) Lane 1, DNA ladder; lane 2, clone 1 with EcoRI; lane 3, clone 2 with EcoRI. (B) Lane 1, DNA ladder; lane 2, clone 2 with XbaI. Expected restriction-digested band length: linearised pCR-Blunt II-TOPO-hNEIL3FL-FLAG from XbaI, approximately 5400 bp; pCR-Blunt II-TOPO plasmid and hNEIL3<sup>FL</sup>-FLAG insert from EcoRI, approximately 3500 bp and 1900 bp, respectively. (C) Derived and modified pCR-Blunt II-TOPO plasmid map with restriction digest sites EcoRI and XbaI encircled (red) from Zero Blunt PCR cloning kit protocol guide (Invitrogen).

It was also possible that through an incomplete restriction double-digest of pCR-Blunt II-TOPO-hNEIL3<sup>FL</sup>-FLAG with XbaI and EcoRI, the sticky-ended digested hNEIL3<sup>FL</sup>-FLAG insert would have 4 bp to 57 bp additional base pairs as well as double ended XbaI or EcoRI sites, increasing the insert up to 1920 bp long, if not restriction double-digested completely.

Therefore, a sequential restriction double-digest was used to ensure complete digestion by each enzyme and to prepare a sufficient quantity of the insert DNA.

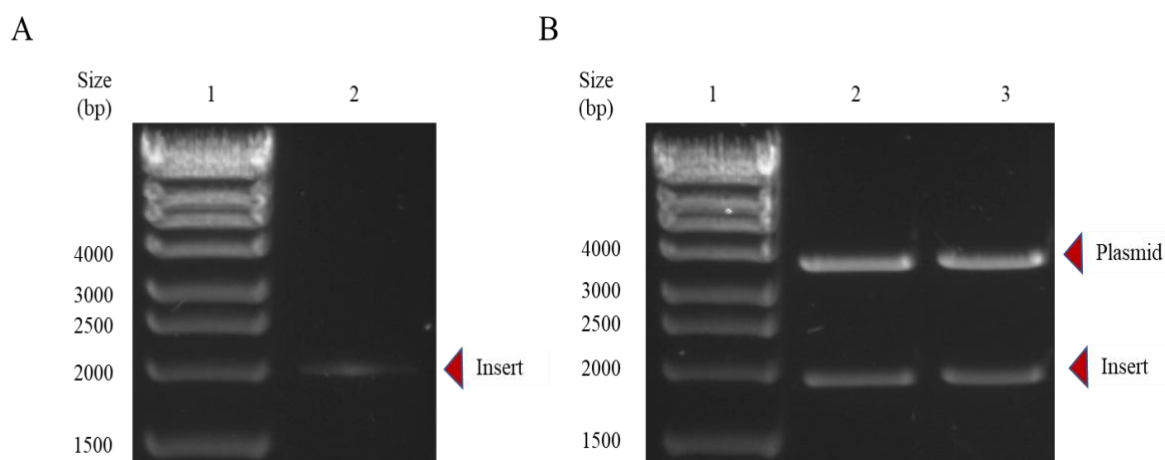


**Figure 3.22: Sequential digestion of pCR-Blunt II-TOPO-hNEIL3<sup>FL</sup>-FLAG using restriction enzymes EcoRI and XbaI.**

(A) Lane 1, DNA ladder; lane 2, clone 2 with sequential digestion and purification (XbaI followed by EcoRI). (B) Lane 1, DNA ladder; lane 2 and 3, clone 1 and 2, respectively, with sequential double-digestion (XbaI followed by EcoRI). Expected restriction-digested band length: pCR-Blunt II-TOPO plasmid, approximately 3500 bp; hNEIL3<sup>FL</sup>-FLAG insert, 1863 bp.

Initially, the experiment was carried out with restriction enzyme XbaI, followed by purification, and the restriction digest was repeated with EcoRI-HF followed by purification. However, substantial quantities were lost after each purification, and the final result appeared longer than expected (Figure 3.22A, lane 2; approximately 2,000 bp). The experiment was attempted again using a sequential double-digest method without the necessity of mid purification, and this time it was successful, as can be seen in Figure 3.22B, lanes 2 and 3. When compared to the initial attempt (Figure 3.22A), the final products appeared to be closer to the correct size (approximately 1,900 bp for the hNEIL3<sup>FL</sup>-FLAG insert and approximately 3,500 bp for the pCR-Blunt plasmid) and with minimal loss prior to purification. The inserts were then purified after gel excision and were then ready for ligation into the destination vector, pcDNA3.1.

### 3.3.3. Isolation and Purification of the pcDNA3.1 Vector

The procedure for the preparation of the pcDNA3.1 plasmid was less complex. As expected, the undigested plasmid in lane 2 Figure 3.23 displayed multiple bands above the 6000 bp ladder mark, indicating circular and nicked circular plasmids, and linearised plasmids after single restriction digest XbaI (lane 3) and EcoRI (lane 4) with no secondary band less than the 600 bp ladder mark. As can be seen in Figure 3.23, lane 5, a simple restriction double-digest was all that was required to excise the hNEIL1-FLAG insert (approximately 1,400 bp) from the pcDNA3.1 plasmid (approximately 6,000 bp). The plasmid was then purified after gel excision.

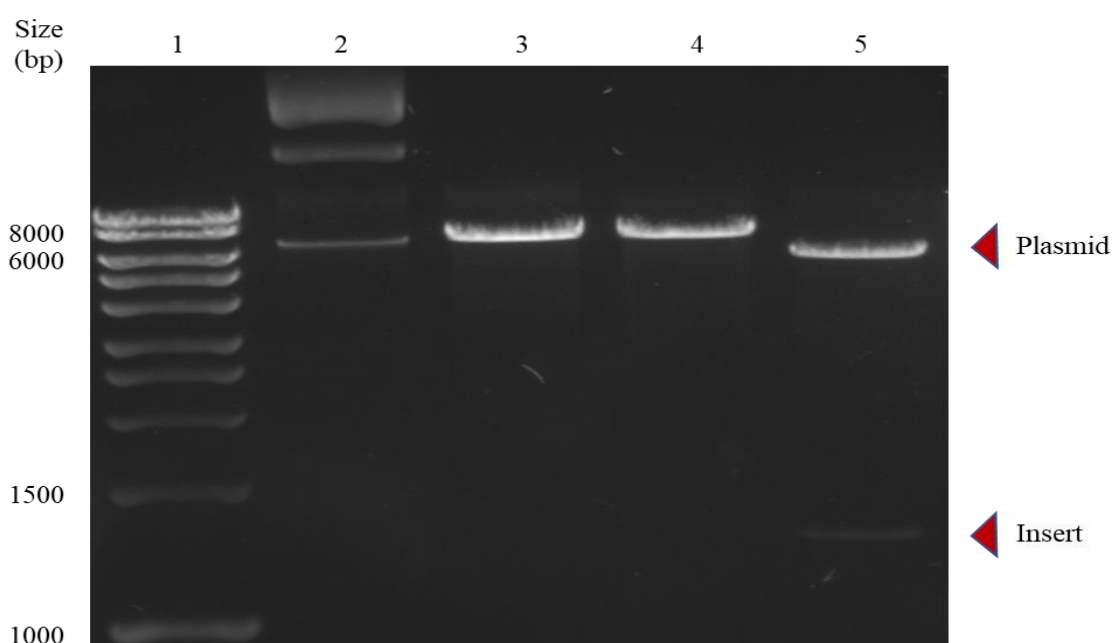


**Figure 3.23: Digestion of pcDNA3.1-hNEIL1-FLAG using XbaI and EcoRI.**

Lane 1, DNA ladder; lane 2, undigested plasmid; lane 3, XbaI digest; lane 4, EcoRI digest; lane 5, XbaI and EcoRI double-digest. Expected restriction-digested band length: undigested pcDNA3.1-hNEIL1-FLAG,  $\geq 6800$  bp; single-digested pcDNA3.1-hNEIL1-FLAG, approximately 6800 bp; double-digested pcDNA3.1 plasmid, approximately 5400 bp; double-digested hNEIL1-FLAG insert, approximately 1400 bp.

### 3.3.4. Confirmation of pcDNA3.1-NEIL3<sup>FL</sup>-FLAG plasmid

With the purified hNEIL3<sup>FL</sup>-FLAG insert and pcDNA3.1 plasmid prepared, the following step was ligation followed by an analysis of the clones through double-digestion. As can be seen in Figure 3.24, in lanes 2 to 6, five transformed colonies were selected for analysis and

four of the clones produced a band of the expected size (lanes 3 – 6). The plasmid in lane 2 of Figure 3.24 unexpectedly contained an insert similar to the hNEIL1-FLAG insert (approximately 1,400 bp) and similar to the restriction double-digest in Figure 3.23, lane 5. This may be due to an undigested plasmid not visible from the excised agarose gel for DNA fragment purification (Section 2.2.6.) was part of the DNA ligation and cloning mixture, and of the transformed *E. coli*, some colonies contained the pcDNA3.1-hNEIL1-FLAG plasmid instead of the pcDNA3.1-hNEIL3<sup>FL</sup>-FLAG plasmid.

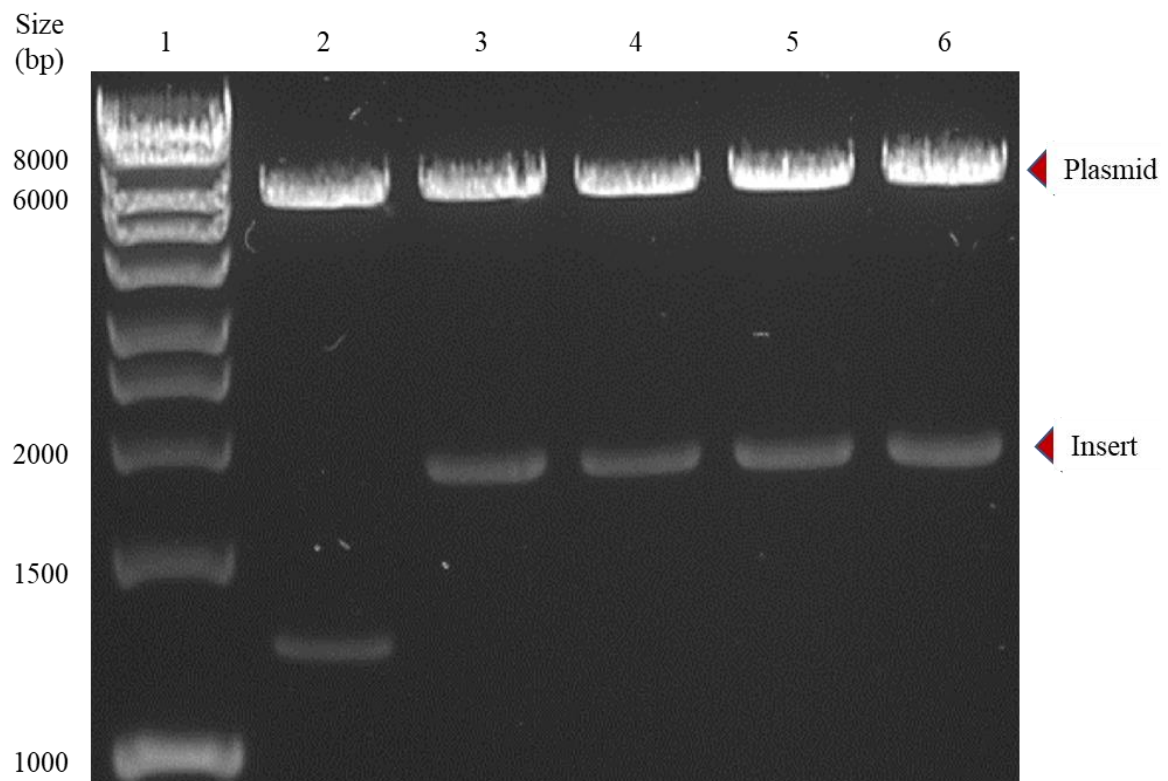


**Figure 3.24: Confirmation of hNEIL3<sup>FL</sup>-FLAG insert in pcDNA3.1-hNEIL3<sup>FL</sup>-FLAG, using XbaI and EcoRI.**

Lane 1, DNA ladder; lane 2 - 6, clones 1 – 5, respectively. Expected restriction-digested band length: pcDNA3.1 plasmid, approximately 5400 bp; hNEIL3<sup>FL</sup>-FLAG insert, 1863 bp.

**A** hNEIL3<sup>FL</sup>-FLAG Forward Sanger-Sequence Result (From CMV\_fwd\_primer)  
 >461159601\_pcDNA31\_NEIL3FL\_CMVF\_pCDNA3  
 AATGGCGGTAGGCGGTGACGGTGGGAGGTCATATAAGCAGAGCTCTCTGGCTAAC TAGAGAACCCTACTGCTTACTGGCTTATCGAAAT **TAATACGACT**  
**CACTAAGC** GAGACCCAAAGCTGGCTAGCGTTAAACGGGCC **CTAGAGCCACC** ATGGTGAAGGACCAGGCTGTACTCTGAATGGAGAGAAGATTCCG  
 AGCGCGGTGCTCCCGGCCAGGCGGTGACCGCGTGGCGGGAAGCGCTCTGCGGAGTCTGCAGGGCCGCGCCTTGC GGCTCGCAGCCTCCACGGTT  
 GTGGTCTCCCGCAGGCTGCTGCACTGAATAATGATCCAGCCAGAATGCTTTGAGCCTGTTAATGGATATGTTTACAGTGGCGTGGAACCTTTGGGGA  
 AGGAGCTCTTATGACTTTGGACAAAAGCTTACGGATTCAATTCCGGAATGAAAGGCTTCATCATGATTAATCCACTTGAGTATAAATAAAAAATGGA  
 GCTTCTCTGTTTGGAAAGTGCAGCTCACCAGATTGATTGTTTCTTTGACTCATCAGTAGAACTCAGAACTCAATGAAAAGCCAACAGAGAATA  
 AGAATGATGAAAGAATTAGATGATGTTACCTGAAATTTAGTTTCTTGAGAGCAGAAAAGTGAAGTTAAAAAACAGAAAGCCGGATGCTAGGTGATGTG  
 CTAATGGATCAGAAGCTATGCTGGAGTAGGGAACATCATCAAAAATGAAGCTCTCTTGACAGTGGTCTCCACCAGCTGTTAAAGTTTGCAATTA  
 CAGATGAACAGATCCATCACCTCATGAAAATGATACGTGATTTACGACTTCTTTTACAGGTGCCGTAAGCAGGACTTGCTCTCTAAACACTATAAG  
 GTTACAAAGCTCCCAATTTGGTTCAGTGCCTGCAAGAATACTGTGTCGCTTTGGGACAATAACAGAATGACATATTTCTGTCTCACTGTCAAAA  
 AAGAAAATCCTCAACATGTTGACATATGCAAGCTACCGACTAGAAATACATAATCAGTTGGACATCTAGCAGGGTGGATCATGTTAGGACTCCGTGGC  
 TCGGAAGTCGGAAGAGCACTGGACCTGTGTGGTGTGACTTAAATCAATAAGCCCTCTTAAAGGCATGTGATGCTTGTGACCTAAGGCCATTTGAT  
 TCAGTGCCTAAGAGTGAAGAAAATCTACTGTCTTAGCCACTAATGAAGTACCCGCTGTAATACTTTGGAAAACCTCATACAGAAGTCAAGATCAACA  
 GGAAAAGTCAATTGGAACATACTTGTCTTGACTGATTTAGCAATAAATCCAGTACTTTGGAAAAGAAAACAAAGCAAAC

**B** hNEIL3<sup>FL</sup>-FLAG Reverse Sanger-Sequence Result (From bGH\_rev\_primer)  
 >461159601\_pcDNA31\_NEIL3FL\_bGHR  
 TTTACAGGTGCCGTAAAGCAGGACTTGCTCTCTTAAACTATAAGGTTTACAAGCGTCCCAATTGTGGTCAAGTGCCTACTGCAGAATAACTGTGTGCC  
 GCTTTGGGGACAATAACAGAATGACATATTTCTGTCTCACTGTCAAAAAGAAAATCCTCAACATGTTGACATATGCAAGCTACCGACTAGAACTACT  
 AATATGTTGGACATCTAGCAGGGTGGATCATGTTATGGACTCCGTGGCTCGGAAGTCGGAAGGACTGGACCTGTGTGGTGTGACTTTAATCAATA  
 GCCCTCTTCAAGGCATGTGATGCTTGTCTGACTCAAGGCCATTTGATTCAGTCTCAAGAGTGAAGAAAATTTACTGTCTTTAGCCACTTAATGAAG  
 TACCCGTGTAATACTTTGGAAAACCTCATACAGAAGTCAAGATCAACAGGAAAAGTGCATTTGGAAGTCAACTGCTTGTCTGTGACTGATTTAGCAATA  
 AATCCAGTCTTTGGAAAAGAAAACAAAGCAAAACAGATACATGATGAGGAGTTTCAAAAAGTCTCTCTGTGATGTTGATGATATACAGC  
 ACCCTCCAAAGACAACAAACGATATAACTCAACCATCCAGCAAAAGTAAACATATCACCTACAATCAGTTCAGAATCTAAATATTTAGTCCAGCACA  
 TAAAAACCGAAAACAGCCAAATCTATCACAGAGCTTAAAAGCTCAACCTTGGATATTTAACAGTGAATTCAAATTAATATGACAGATGGCC  
 TCGTACCTAAATCCTGACAGCCCTCGCTGCAGTAAACCAACAGCCCTCACTTCCGATTTCCGAGTTGTGAGGAAGGATGGGAAAACAAAGCCAGTCA  
 TTTATGCTGTCTCTACCTAGAGAAGCAATGTGGATTTTGAATGGGCAGATTTGCTCTCCATTCTGCAACCATGGCAAGCGTTCACCACATGAA  
 AACAGTATTGAAGATTGGACCTAACATGAAAAGAAATTTTTGTGTGCTCTTTGGGAAGGAAAACAAATGCAATTTTTCCAGTGGGCAGAAAATGG  
 GCCAGGAATAAAAATTTCTGGATGC **GACTACAAGGACGACGATGACAAGTGA** **CCGGAATTCC** ACCACACTGGACTAGTGGATCCGAGCTC

**C** hNEIL3<sup>FL</sup>-FLAG Overlapping Sanger-Sequence Result  
 AATGGCGGTAGGCGGTGACGGTGGGAGGTCATATAAGCAGAGCTCTCTGGCTAAC TAGAGAACCCTACTGCTTACTGGCTTATCGAAAT **TAATACGACT**  
**CACTAAGC** GAGACCCAAAGCTGGCTAGCGTTAAACGGGCC **CTAGAGCCACC** ATGGTGAAGGACCAGGCTGTACTCTGAATGGAGAGAAGATTCCG  
 AGCGCGGTGCTCCCGGCCAGGCGGTGACCGCGTGGCGGGAAGCGCTCTGCGGAGTCTGCAGGGCCGCGCCTTGC GGCTCGCAGCCTCCACGGTT  
 GTGGTCTCCCGCAGGCTGCTGCACTGAATAATGATCCAGCCAGAATGCTTTGAGCCTGTTAATGGATATGTTTACAGTGGCGTGGAACCTTTGGGGA  
 AGGAGCTCTTATGACTTTGGACAAAAGCTTACGGATTCAATTCGGAATGAAAAGGCTTCATCATGATTAATCCACTTGAGTATAAATAAAAAATGGA  
 GCTTCTCTGTTTGGAAAGTGCAGCTCACCAGATTGATTGTTTCTTTGACTCATCAGTAGAACTCAGAACTCAATGAAAAGCCAACAGAGAATA  
 AGAATGATGAAAGAATTAGATGATGTTACCTGAAATTTAGTTTCTTGAGAGCAGAAAAGTGAAGTTAAAAAACAGAAAGCCGGATGCTAGGTGATGTG  
 CTAATGGATCAGAACGTAATGCTGGAGTAGGGAACATCAATAAATGAAGCTCTCTTTGACAGTGGTCTCCACCAGCTGTTAAAGTTTGTCAATTA  
 CAGATGAACAGATCCATCACCTCATGAAAATGATACGTGATTTACGACTTCTTTTACAGGTGCCGTAAGCAGGACTTGCTCTCTCAACACTATAA  
**GGTTACAAGCGTCCCAATTGTGGTCAAGTGCCTGCAAGAATACTGTGTGCCGCTTTGGGACAATAACAGAATGACATATTTCTGTCTTCACTGTCA**  
**AAAAGAAAATCCTCAACATGTTGACATATGCAAGCTACCGACTAGAAATACTATAATCAGTTGGACATCTAGCAGGGTGGATCATGTTATGGACTCCGTG**  
**GCTCGGAAGTCGGAAGAGCACTGGACCTGTGTGGTGTGACTTAAATCAATAAGCCCTCTTCTAAGGCATGTGATGCTTGTGACTCAAGGCCATT**  
**GATTCAGTCTCAAGAGTGAAGAAAATCTACTGTCTTAGCCACTAATGAAGTACCCGCTGTAATACTTTGGAAAACCTCATACAGAAGTCAAGATCA**  
**ACAGGAAAAGTGCATTTGGAACATACTTGTCTTGACTGATTTAGCAATAAATCCAGTACTTTGGAAAAGAAAACAAAGCAAACAGATACTAG**  
 ATGAGGAGTTTCAAACTCTCTCTGCTAGTGTGTTGAATGATATACAGCACCCTCCAAGAAGACAACAAACGATATAACTCAACATCCAGCA  
 AAGTAAACATATCACCTCAATCAGTTCAGAATCAAAATTTAGTCCAGCATAAAAAACGAAAACAGCCCAATCTATCACAGAGCTTAAAAAG  
 CTGCAACCCTGGATATCTAACAGTGAATCAAAATTAATGACAGATGGCCCTCGTACCTTAAATCCTGACAGCCCTCGCTGCAAAACACAACCCG  
 CTCTGCATTTCCGAGTTGTGAGGAAGGATGGGAAAACAAGGCGAGGTTTATGCCTGCTCTACCTAGAGAAGCACAATGAGGATTTTTGAA  
 TGGCAGATTTGCTCTTCCCATCTGCAACCATGGCAAGCGTTCCACATGAAGCAAGTATGAAGATTGGACCTAACAAATGGAAAAGAAATTTTTGTG  
 GTCTCTTTGGGAAGGAAAACAAATGCAATTTTTCCAGTGGGCAGAAAATGGCCAGGAATAAAAATTTCTGGATGC **GACTACAAGGACGACGAT**  
**GACAAGTGA** **CCGGAATTCC** ACCACACTGGACTAGTGGATCCGAGCTC

**Figure 3.25: Confirmation of pcDNA3.1-hNEIL3<sup>FL</sup>-FLAG through Sanger-sequencing.**

(A) Sequencing result with CMV forward primer; (B) sequencing result with bGH reverse primer; (C) overlap of sections A and B for the final sequenced result. Red highlight, T7 promoter sequence; green highlight, XbaI restriction digest site; grey highlight, Kozak consensus fragment; blue highlight, FLAG-tag; yellow highlight, EcoRI restriction digest site; red letters, sequence overlap.

The extracted plasmids from clones resulted in lanes 3 – 6 (Figure 3.24) were sent for Sanger-sequencing for final confirmation. All four cloned plasmids displayed results similar to each other, as shown in Figure 3.25. No mutations were noticed within the insert, between the XbaI and EcoRI digest sites in Figure 3.25 (highlighted in green and yellow, respectively), and the insert was in the correct orientation when compared to the pcDNA3.1

vector map (Figure 2.1). Based on these interpreted results, the pcDNA3.1-hNEIL3<sup>FL</sup>-FLAG plasmid was prepared for the cell culture transfection experiments.

### 3.3.5. Isolation, Cloning and Purification of the hNEIL3<sup>1506</sup>-FLAG Insert

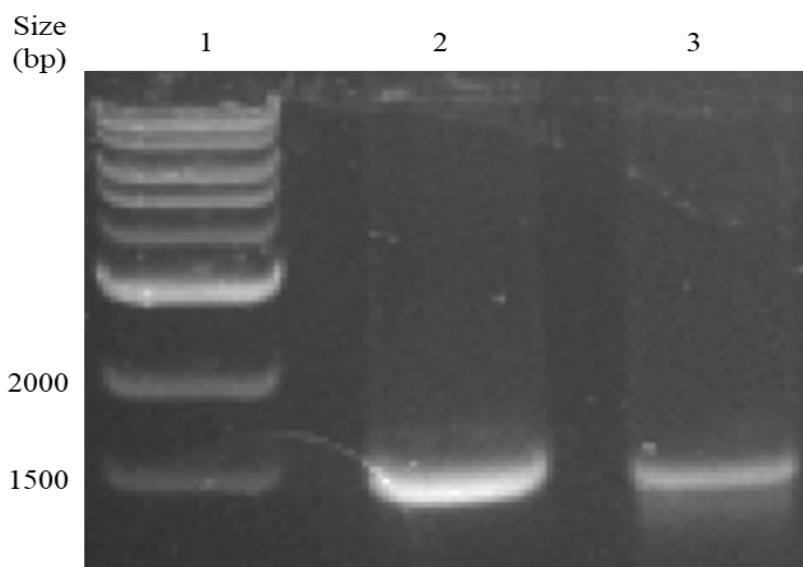


**Figure 3.26: Amplification of the hNEIL3<sup>1506</sup>-FLAG insert from pcDNA3.1-hNEIL3<sup>FL</sup>-FLAG.**

Lane 1, DNA ladder; lane 2, Q5 DNA polymerase; lane 3, Phusion DNA Polymerase. Annealing temperature at 72°C (Q5) or 82°C (Phusion). Expected amplified band length for hNEIL3<sup>1506</sup>-FLAG insert, 1554 bp.

Due to the previous experiments with the challenges and optimisations considered for preparing and completing the pcDNA3.1-hNEIL3<sup>FL</sup>-FLAG plasmid, the experiments were repeated to amplify the hNEIL3<sup>1506</sup>-FLAG insert, using pcDNA3.1-hNEIL3<sup>FL</sup>-FLAG as the template. The amplification was first considered if necessary to optimise the PCR protocol with the Touchdown programme step. Fortunately, as displayed in Figure 3.26, the optimisation was not necessary for either the Q5 PCR protocol (lane 2) or the Phusion PCR protocol (lane 3) due to the presence of the expected size for the hNEIL3<sup>1506</sup>-FLAG insert (1,554 bp). This was possibly due to a smaller sized PCR product being produced, similar to how during the initial amplification of hNEIL3<sup>FL</sup>-FLAG, only the 843bp-long hNEIL3 product had resulted (Figure 3.19, lane 4). Both amplified hNEIL3<sup>1506</sup>-FLAG insert products were purified after gel excision, followed by ligation to the pCR-Blunt II-TOPO plasmid for cloning.

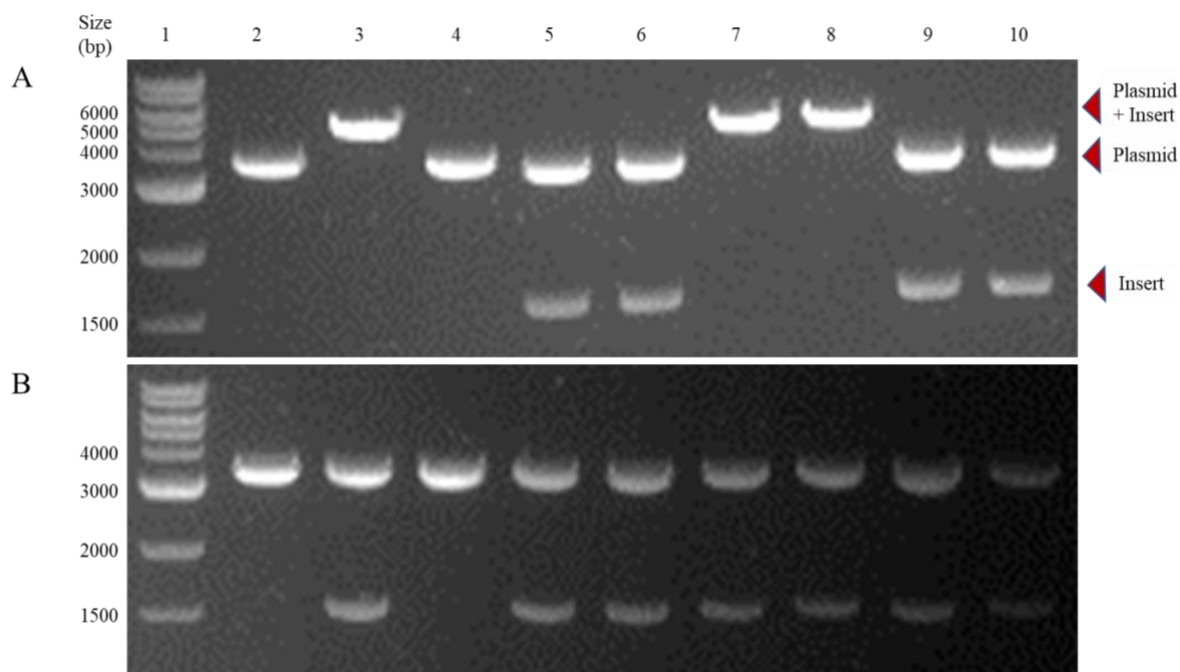


**Figure 3.27: Analysis of hNEIL3<sup>1506</sup>-FLAG insert from pCR-Blunt II-TOPO-hNEIL3<sup>1506</sup>-FLAG, with XbaI (A) followed by EcoRI (B).**

Lane 1, DNA ladder; lanes 2 – 5, Phusion-based clones 1 – 4 respectively; lanes 6 – 10, Q5-based clones 1 – 5 respectively. Expected restriction-digested band length: linearised pCR-Blunt II-TOPO-hNEIL3<sup>1506</sup>-FLAG, approximately 5054bp; pCR-Blunt II-TOPO plasmid, approximately 3500 bp; hNEIL3<sup>1506</sup>-FLAG insert, approximately 1554 bp.

After successful cloning and extraction, the pCR-Blunt II-TOPO-hNEIL3<sup>1506</sup>-FLAG insert (XbaI-hNEIL3<sup>1506</sup>-FLAG-EcoRI insert) was tested for insert presence and orientation by sequential restriction double-digest. As the results can be seen through Figure 3.27, the hNEIL3<sup>1506</sup>-FLAG insert of 1554 bp long was present in all colonies, apart from Phusion-based transformed colonies 1 and 3 (lanes 2 and 4, respectively), based on the sequential EcoRI restriction digest (Figure 3.27B) after the initial XbaI restriction digest (Figure 3.27A) from the pCR-Blunt II-TOPO plasmid (approximately 3,500 bp). Based on the lack of insert present for the Phusion-based transformed colonies 1 and 3 (lanes 2 and 4, respectively), the results may be due to self-ligated pCR-Blunt II-TOPO plasmids due to the plasmid having blunt ends. The hNEIL3<sup>1506</sup>-FLAG inserts appear in the forward orientation (XbaI-hNEIL3<sup>1506</sup>-FLAG-EcoRI) for lanes 3, 7 and 8 in Figure 3.27, but in reverse orientation (EcoRI-FLAG-hNEIL3<sup>1506</sup>-XbaI) for lanes 5, 6, 9 and 10, based on the XbaI restriction digest (Figure 3.27A) when compared to the pCR-Blunt II-TOPO plasmid map (Figure 3.21C). Therefore, the forward-oriented inserts would be sequentially digested with EcoRI then XbaI, and the reverse-oriented inserts would be sequentially digested with XbaI then EcoRI. The sequentially digested hNEIL3<sup>1506</sup>-FLAG inserts were purified after gel excision.

### 3.3.6. Confirmation of pcDNA3.1-hNEIL3<sup>1506</sup>-FLAG plasmid

With the purified hNEIL3<sup>1506</sup>-FLAG insert and pcDNA3.1 plasmid prepared, the experiments continued for the T4 DNA ligation, followed by initial confirmation through double-digestion. As can be seen in Figure 3.28, three transformed colonies were selected for initial confirmation. There were intended to be more colonies tested, however very few colonies survived from the antibiotic-selection. None survived for the Phusion-based hNEIL3<sup>1506</sup>-FLAG inserts derived from Figure 3.27 (lanes 3 and 5), leaving only the Q5-based hNEIL3<sup>1506</sup>-FLAG inserts (Figure 3.27, lanes 6 – 10) to continue testing. Of the three transformed colonies picked and displayed in Figure 3.28, only two of the transformed colonies displayed results of a plasmid containing an insert. The extracted plasmid from lane 2 in Figure 3.28 may have been a rogue stock-plasmid, though it was uncertain how it was possible as the pcDNA3.1 plasmid (approximately 6,000 bp) could not self-ligate with distinct sticky-ends. The extracted plasmids from lanes 3 and 4 in Figure 3.28 showed promising confirmation of the completed plasmid pcDNA3.1-hNEIL3<sup>1506</sup>-FLAG, based on the presence of the pcDNA3.1 plasmid and the hNEIL3<sup>1506</sup>-FLAG insert present at the expected size (1554 bp).

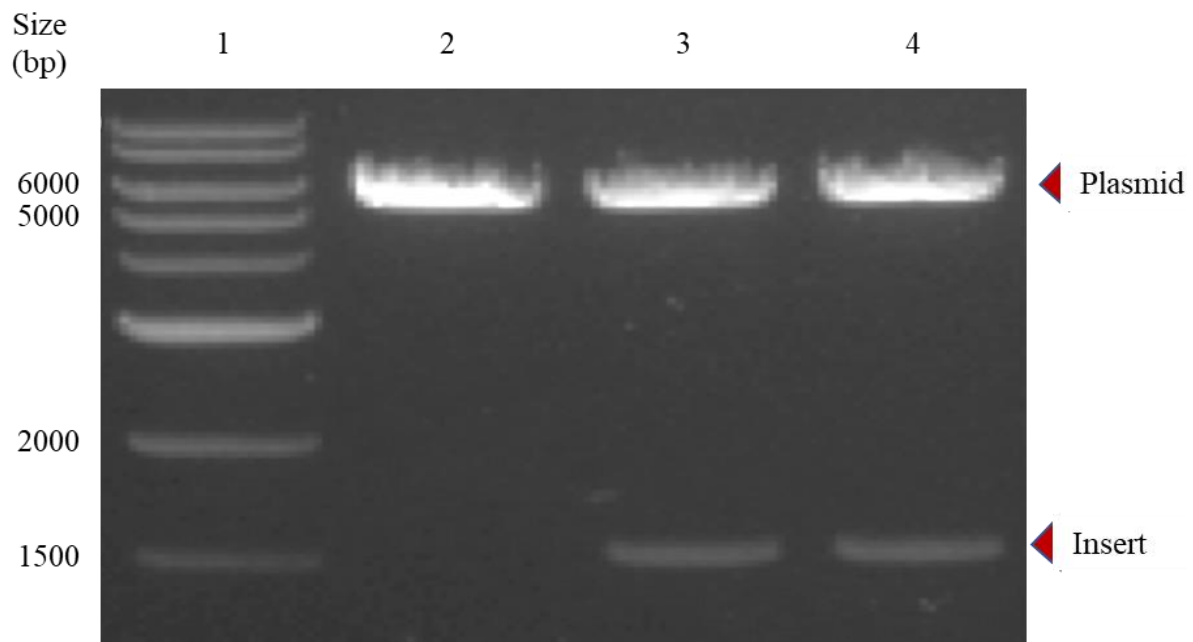


**Figure 3.28: Confirmation of the hNEIL3<sup>1506</sup>-FLAG insert in pcDNA3.1-hNEIL3<sup>1506</sup>-FLAG, using XbaI and EcoRI.**

Lane 1, DNA ladder; lanes 2 – 4, clones 1 – 3. Expected restriction-digested band length: pcDNA3.1 plasmid, approximately 5400 bp; hNEIL3<sup>1506</sup>-FLAG insert, 1554 bp.

**A** hNEIL3<sup>1506</sup>-FLAG Forward Sanger-Sequence Result (From CMV\_fwd\_primer)  
 >461159601\_pcDNA31\_NEIL3T\_CMVF\_pCDNA3  
 ATGGGCGGTAGGCGTGTACGGTGGGAGGCTATATAAGCAGAGCTCTCTGGCTAAGTAGAGAACCCTGCTTACTGGCTTATCGAAAT **TAATA**  
**CGACTCACATAGG**GAGACCCAAGCTGGCTAGCGTTTAAACGGGGCC**CTAGAGCCACC**ATGGTGGAAGGACCAGGCTGTACTCTGAATGGA  
 GAGAAGATTCCAGCGCGGGTGC TCCCGGGCCAGGCGGTGACCGCGTGC GGGAAGCGCTCTGCGGAGTCTG CAGGGCCCGCCTTGC GGCC  
 TCGCAGCCTCCACGGTGTGGTCTCCCGCAGGCTGCTGCACTGAATAATGATCCAGCCAGAATGCTTGTAGCCTGTTAATGGATATGTTA  
 CAGTGGCGTGGAAACTTTGGGAAGGAGCTCTTATGTACTTTGGACCAAAAGCTTTACGGATTCAITTCGGAATGAAAAGGCTTCATCATGAT  
 TAATCCACTTGAGTATAAATAAAAAATGGAGCTTCTCCTGTTTGGAAAGTGCAGCTACCCAAAGATTGATTTGTTTCTTTGACTCATCAGTAG  
 AACTCAGAACTC AATGGAAAGCCAACAGAGAATAAGAATGATGAAAGAATTAGATGATGTTACCTGAATTTAGTTTCTTGAGAGCAGAA  
 AGTGAAGTAAAAACAGAAAGGCCGGATGCTAGGTGATGTGCTAATGGATCAGAACGATTCCTGGAGTAGGGAACATCATCAAAAATGA  
 AGCTCTCTTTGACAGTGGTCTCCACCCAGCTGTAAAGTTTGTCAATTAACAGATGAACAGATCCATCACCTCATGAAAATGATACGTGATTT  
 AGCATCTCTTTACAGGTGCCGTAAGCAGGACTTGCTCTCTAAACACTATAAGGTTTACAAGCGTCCCAATGTGGTCAAGTCCAGAAATAACT  
 AGCAATCTCTTTACAGGTGCCGTAAGCAGGACTTGCTCTCTAAACACTATAAGGTTTACAAGCGTCCCAATGTGGTCAAGTCCAGAAATAACT  
 GAAATACTGTGTGCCGCTTTGGGGACAATAACAGAATGACATATTTCTGTCTCACTGTC AAAAAGAAAATCCTCAACATGTTGACATATGCAA  
 GCTACCCGACTAGAAATACTATAATCAGTTGGACATCTAGCAGGGTGGATCATGTTAGGACTCCGTGGCTCGGAAGTCCGAAGAGCACTGGCA  
 CTGTGTGGTGTACTTTAATCAATAAGCCCTCTTCTAAGGCATGTGATGCTTGCTTGACCTCAAGGCCTATTGATTCAGTGTCTCAAGAGTGAA  
 GAAAATCTACTGTCTTTAGCCACTTAATGAAGTACCCG

**B** hNEIL3<sup>1506</sup>-FLAG Reverse Sanger-Sequence Result (From bGH\_rev\_primer)  
 >461159601\_pcDNA31\_NEIL3T\_bGHR  
 TCCTGTTTGGAAAGTGCAGCTACCCAAAGATTGATTGTTTCTTTGACTCATCAGTAGAACTCAGAAACTCAATGGAAAGCCACAGAGAA  
 TAAGAATGATGAAAAGATTAGATGATGTTTACCTGAATTTAGTTTCTTGAGAGCAGAAAAGTGAAGTTAAAAAACAGAAAAGGCCGGATGCTA  
 GGTGATGTGCTAATGGATCAGAACGATTCCTGGAGTAGGGAACATCATCAAAAATGAAGCTCTCTTTGACAGTGGTCTCCACCCAGCTGTT  
 AAAGTTTGTCAATTAACAGATGAACAGATCCATCACCTCATGAAAATGATACGTGATTTACAGATTTCTTTACAGGTGCCGTAAGCAGGA  
 CTGTCTCTCTTAAACACTATAAGGTTTACAAGCGTCCCAATGTGGTCAAGTCCAGAAATAACTGTGTGCCGCTTTGGGGACAATAAC  
 AGAATGACATATTTCTGTCTCACTGTCAAAAAGAAAATCCTCAACATGTTGACATATGCAAGCTACCGACTAGAAAATACTATAATCAGTTGGA  
 CATCTAGCAGGGTGGATCATGTTAAGGACTCCGTGGCTCGGAAGTCCGGAAGAGCAGTGGACCTGTGTGGTGTGACTTTAATCAATAAGCCCT  
 CTCTAAGGCATGTGATGCTTGACCTCAAGGCCTATTGATTCAGTGTCAAGAGTGAAGAAAATCTACTGTCTTTAGCCACTAATGAA  
 GTACCCGTGTAATAC TTTGGAAAACCTCATA CAGAAGTCAAGATCAACAGGAAAACCTGCATTTGGA ACTACAACCTTGTCTTGACTGATTT  
 TAGCAATAAATCCAGTACTTTGGAAAAGAAAACAAAGCAAAACAGATAC TAGATGAGGAGTTTCAAAAAC TCTCTCTGCTAGTGTGTGTT  
 TGAATGATATACAGCACCCCTCCAAGAAGACAACAAACGATATAACTCAACCATCCAGCAAAAGTAAACATATCACCTACAATCAGTTCAAGAT  
 CTAATATTATTAGTCCAGCACATAAAAACCGAAAACAGCCCAATACTCATCACCAGAGCTTAAAAGCTGCAACCTGGATATTCTAACAGTG  
 AACTTCAAAATTAATATGACAGATGGCCCTCGTACCTTAAATCT**GACTACAAGGACGACGATGACAAGTGA**CCG**GAAATC**CACCACACTGGAC  
 TAGTGGATCCGAGCT

**C** hNEIL3<sup>1506</sup>-FLAG Overlapping Sanger-Sequence Result  
 ATGGGCGGTAGGCGTGTACGGTGGGAGGCTATATAAGCAGAGCTCTCTGGCTAAGTAGAGAACCCTGCTTACTGGCTTATCGAAAT **TAATA**  
**CGACTCACATAGG**GAGACCCAAGCTGGCTAGCGTTTAAACGGGGCC**CTAGAGCCACC**ATGGTGGAAGGACCAGGCTGTACTCTGAATGGA  
 GAGAAGATTCCAGCGCGGGTGC TCCCGGGCCAGGCGGTGACCGCGTGC GGGAAGCGCTCTGCGGAGTCTG CAGGGCCCGCCTTGC GGCC  
 TCGCAGCCTCCACGGTGTGGTCTCCCGCAGGCTGCTGCACTGAATAATGATCCAGCCAGAATGCTTGTAGCCTGTTAATGGATATGTTA  
 CAGTGGCGTGGAAACTTTGGGAAGGAGCTCTTATGTACTTTGGACCAAAAGCTTTACGGATTCAITTCGGAATGAAAAGGCTTCATCATGAT  
 TAATCCACTTGAGTATAAATAAAAAATGGAGCTTCT**CTGTGTTTGGAAAGTGCAGCTCACCAAAGATTGATTTGTTCTTTGACTCATCAGTAG**  
**AACTCAGAACTCAATGGAAAGCCAACAGAGAATAAGAATGATGAAAGAATTAGATGATGTTACCTGAATTTAGTTTCTTGAGAGCAGAA**  
**AGTGAAGTAAAAACAGAAAGGCCGGATGCTAGGTGATGTGCTAATGGATCAGAACGATTCCTGGAGTAGGGAACATCATCAAAAATGA**  
**AGCTCTCTTTGACAGTGGTCTCCACCCAGCTGTAAAGTTTGTCAATTAACAGATGAACAGATCCATCACCTCATGAAAATGATACGTGATTT**  
**AGCATCTCTTTACAGGTGCCGTAAGCAGGACTTGCTCTCTAAACACTATAAGGTTTACAAGCGTCCCAATGTGGTCAAGTCCAGTCC**  
**GAATAACTGTGTGCCGCTTTGGGGACAATAACAGAATGACATATTTCTGTCTCACTGTC AAAAAGAAAATCCTCAACATGTTGACATATGCAA**  
**GCTACCCGACTAGAAATACTATAATCAGTTGGACATCTAGCAGGGTGGATCATGTTAGGACTCCGTGGCTCGGAAGTCCGAAGAGCACTGGAC**  
**CTGTGTGGTGTACTTTAATCAATAAGCCCTCTTCTAAGGCATGTGATGCTTGCTTGACCTCAAGGCCTATTGATTCAGTGTCTCAAGAGTGAA**  
**GAAAATCTACTGTCTTTAGCCACTTAATGAAGTACCCG**TGAATACTTTTGGAAAACCTCATA CAGAAGTCAAGATCAACAGGAAAACCTGCA  
 TTTGGA ACTACAACCTTTGCTTGACTGATTTAGCAATAAATCCAGTACTTTGGAAGAAAACAAAGCAAAACAGATACTAGATGAGGAG  
 TTTCAAAAACCTCTCCTCTGCTAGTGTGTGTTGAATGATATACAGCACCCTCCAAGAAGACAACAAACGATATAACTCAACATCCAGCAAA  
 GTAAACATATCACCTACAATCAGTTTCAAGATCTAAATATTATTAGTCCAGCACATAAAAAACCGAAAACAGCCCAATACTCATCACCAGAGCTTA  
 AAAGTGC AACCTGGATATTCTAACAGTGA ACTTCAATTAATATGACAGATGGCCCTCGTACCTTAAATCT**GACTACAAGGACGACGATGA**  
**CAAGTGA**CCG**GAAATC**CACCACACTGGACTAGTGGATCCGAGCT

**Figure 3.29: Confirmation of pcDNA3.1-hNEIL3<sup>1506</sup>-FLAG through Sanger-sequencing.**

(A) Sequencing result with CMV forward primer; (B) sequencing result with bGH reverse primer; (C) overlap of sections A and B for the final sequenced result. Red highlight, T7 promoter sequence; green highlight, XbaI restriction digest site; grey highlight, Kozak consensus fragment; blue highlight, FLAG-tag; yellow highlight, EcoRI restriction digest site; red letters, sequence overlap.

The plasmid clones 2 and 3 from Figure 3.28 (lanes 3 and 4 respectively) were sent for Sanger-sequencing for final confirmation, and similar results are displayed in Figure 3.29. Both cloned plasmids displayed similar results, with no mutations noticed within the insert between the XbaI and EcoRI digest sites (green and yellow highlights, respectively, Figure

3.29), and compared to the pcDNA3.1 vector map (Figure 2.1) the insert was in the correct orientation. Based on these interpreted results, the pcDNA3.1-hNEIL3<sup>1506</sup>-FLAG plasmid and the previously confirmed pcDNA3.1-hNEIL3FL-FLAG plasmid were prepared for the cell culture transfection experiments.

#### 3.4. Survival of FANCD2-Related Cells when Expressing Recombinant Proteins

Based on the results concluded from Section 3.2 covering the cell culture background, the FANCD2 deficient and corrected/WT cell lines were prepared for the main experiments involving transfecting the prepared plasmids from Section 3.3. The aims and objectives for this work was to transfect the non-FA phenotypical and FA phenotypical cell lines PD20/3.15, U2OS/-D2 and HeLa/-D2, respectively, with the prepared pcDNA3.1-hNEIL1-FLAG, pcDNA3.1-hNEIL3<sup>FL</sup>-FLAG or pcDNA3.1-hNEIL3<sup>1506</sup>-FLAG plasmid, confirm expression of recombinant NEIL1 and NEIL3, and determine the role of NEIL1 and NEIL3 expression under genotoxin treatment. To maintain experimental reproducibility for each experiment involving a plasmid transfected cell line, the scientific replicate of the main experiment was based on the scientific replicate of the cell line transfected with the desired plasmid. Any additional attempts, repeats or additional scientific replicates of the main experiment were based on a separate scientific replicate of plasmid-transfected cell lines, unless stated otherwise. This research attempted transfecting the overexpressing plasmids to the FANCA-related cell lines HSC-72 (FANCA deficient) and HSC-72-Corrected and confirming the recombinant protein expression was done prior to repeating the project with the new and fresher FANCD2 related cell lines PD20/3.15 (FANCD2 deficient and corrected, respectively), U2OS/-D2 (WT/FANCD2 deficient) and HeLa/-D2(WT/FANCD2 deficient). However, issues involving NEIL1 or NEIL3 protein expression in western blot had failed to confirm protein expression, and recombinant protein expression was detected only for the FANCA correction by the FLAG-tag antibody in HSC-72-Corrected (example in Appendix Figure 6).

The project continued with the FANCD2 corrected/WT and deficient cell lines 3.15/PD20, U2OS/-D2 and HeLa/-D2, respectively, and the transfection attempts were repeated with more modified protocols. Furthermore, the confirmation of recombinant proteins and subsequent growth inhibition experiments with the prepared plasmids pcDNA3.1-



As displayed in Figure 3.30, the aims and objectives of Section 3.4 are planned according to the approach to the work displayed in the flow chart. During the remainder of the time and resources available, the results for the plasmid transfected cells were displayed in Section 3.4.1. for recombinant-protein expression confirmation, Section 3.4.2. for the survival of plasmid transfected cells after genotoxin treatment, and the repeats after antibiotic selection (Sections 3.4.3. and 3.4.4.). The unexpected results allowed the project to interpret the results to answer the hypothesis.

#### 3.4.1. Evidence of Recombinant Protein Expression

The FANCD2 deficient cells PD20 were the first cell line transfected with the prepared plasmids from Section 3.3. As it could be seen in Figure 3.31A(i) and in relation to Figure 3.31C, NEIL3 protein expression was observed in the non-transfected and transfected controls (lanes 2 – 4), as was expected when compared to the background western blot results (Figure 3.18), as well as the transfected cells (lanes 5 – 7). Compared to their respective  $\beta$ -Actin protein expression (Figure 3.31C), a noticeable increase in NEIL3 protein expression could be observed from the non-transfected control (lane 2) to the transfection-reagent only control (Lipofectamine LTX, lane 3) and the empty-vector (pcDNA3.1) transfected control (lane 4). This may be due to quantified signal intensity error on the PD20 controls' NEIL3 expression (lane 2) based on the image obtained (Figure 3.31A[i]), or a reaction to the Lipofectamine LTX reagent with or without a vector (lanes 3 and 4) when compared to the control. Furthermore, compared to non-transfected and transfected controls, NEIL3 protein expression was observed to be substantially expressed in the plasmid-transfected cells, from the pcDNA3.1-hNEIL1-FLAG (lane 5) to the pcDNA3.1-hNEIL3<sup>1506</sup>-FLAG (lane 7), to the pcDNA3.1-hNEIL3<sup>FL</sup>-FLAG transfected PD20 cells (lane 6, Figure 3.31A[i]) with the highest protein expression (Figure 3.31C). Though it was expected for NEIL3 protein expression to increase from plasmid-transfected cells with the hNEIL3<sup>FL</sup>-FLAG and hNEIL3<sup>1506</sup>-FLAG inserts, it was not expected for the pcDNA3.1-hNEIL1-FLAG transfected cells as well. As observed in Figure 3.31A(ii), endogenous NEIL1 protein expression was not observed in any of the non-transfect and transfected PD20 controls (lanes 2 – 4), as was expected when compared to the background western blot results (Figure 3.18), but unexpectedly neither was the recombinant protein observed in the pcDNA3.1-hNEIL1-FLAG transfected PD20 cells (lane 5). Furthermore, as it can be seen in Figure 3.31A(iii),

no visible band of a FLAG-tagged NEIL1 (lane 5), NEIL3<sup>FL</sup> (lane 6) or NEIL3<sup>1506</sup> (lane 7) was observed from the plasmid-transfected FANCD2 deficient (PD20) cells. In addition to the truncated NEIL3 protein (NEIL3<sup>1506</sup>) not being observed at the theoretical molecular weight (55 kDa) compared to the full-length NEIL3 protein molecular weight (68 kDa) in lane 7 of Figure 3.31A(i), the western blot results of the plasmid-transfected PD20 extracts would suggest the substantially expressed NEIL3 proteins observed were non-recombinant.

The transfection experiment and western blot confirmation was repeated for the FANCD2 deficient cell line (PD20), with the prepared and subsequently new pcDNA3.1-hNEIL3<sup>FL</sup>-FLAG and pcDNA3.1-hNEIL3<sup>1506</sup>-FLAG plasmids. However, confirmation for the recombinant proteins NEIL1 and NEIL3, through protein-specific or FLAG-tag antibodies, were not observed for the PD20 cell line. This was unexpected as, although pcDNA3.1-hNEIL1-FLAG was used as a NEIL1 expressing plasmid it was also used as a control for FLAG-tag expression, which was unintentionally confirmed with the FLAG-tagged FANCA correction in HSC-72-Corrected cells during previous transfection attempts (Appendix Figure 6). As can be seen in Figure 3.31B(i) for the FANCD2 corrected (3.15) cell extracts, no endogenous NEIL3 protein expression was observed in the non-transfected and transfected controls (lanes 2 – 3), as was expected when compared to the background western blot results (Figure 3.18). However, recombinant NEIL3 protein expression was also not observed in the transfected cells (lanes 4 – 6), especially for the pcDNA3.1-hNEIL3<sup>FL</sup>-FLAG (lane 5) and pcDNA3.1-hNEIL3<sup>1506</sup>-FLAG (lane 6) transfected cell extracts. Similarly observed in Figure 3.31B(ii), NEIL1 protein expression was not observed in the non-transfected and transfected controls, as was expected. However, of all the plasmid transfected 3.15 cells, only the pcDNA3.1-hNEIL1-FLAG transfected 3.15 cell extract (lane 4) in Figure 3.31B(ii) displayed NEIL1 expression, and based on the FLAG-tagged observed results (Figure 3.31B[iii]), the only expressed protein is the recombinant hNEIL1-FLAG.

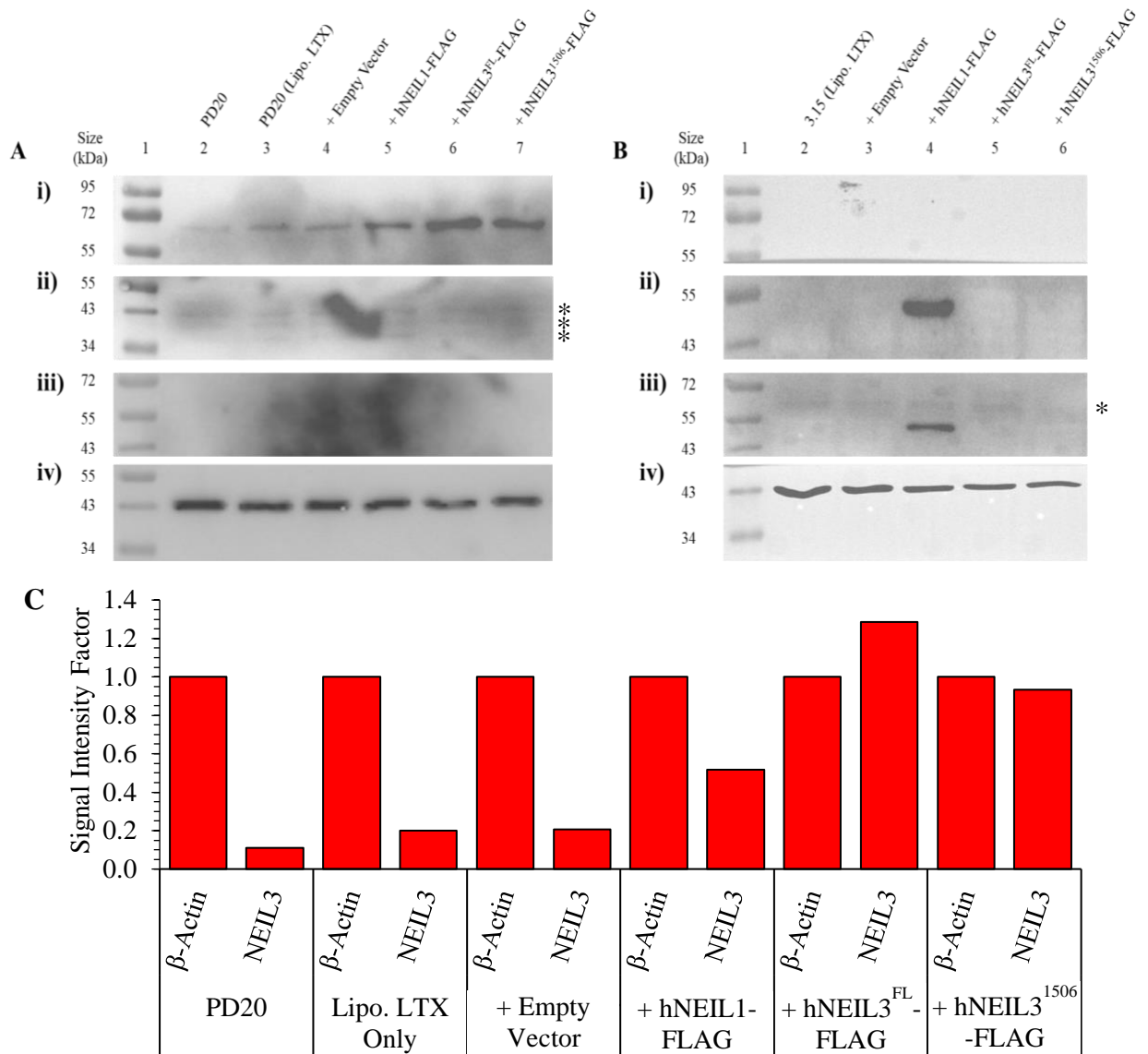


**Figure 3.31: Western blots of PD20 (FANCD2 Deficient, A[i – iv]) and 3.15 (PD20 corrected, B[i – iv]) cell extracts following transfection with different plasmids. (A, B) i) NEIL3, ii) NEIL1, iii) FLAG-tag, and iv)  $\beta$ -Actin.**

(A) Lane 1, protein ladder; lane 2, control; lane 3, control (Lipofectamine LTX only); lane 4, empty vector; lane 5, pcDNA3.1-hNEIL1-FLAG; lane 6, pcDNA3.1-hNEIL3<sup>FL</sup>-FLAG; lane 7, pcDNA3.1-hNEIL3<sup>1506</sup>-FLAG. (B) Lane 1, protein ladder; lane 2, control; lane 3, empty vector; lane 4, pcDNA3.1-hNEIL1-FLAG; lane 5, pcDNA3.1-hNEIL3<sup>FL</sup>-FLAG; lane 6, pcDNA3.1-hNEIL3<sup>1506</sup>-FLAG. Expected molecular weight: NEIL3, 68 kDa; hNEIL3<sup>FL</sup>-FLAG, 69 kDa; hNEIL3<sup>1506</sup>-FLAG, 56 kDa; NEIL1, 43 kDa; hNEIL1-FLAG, 44 kDa;  $\beta$ -Actin, 42 kDa. (\*) Non-specific binding. (C) Quantified signal intensity from chemiluminescence in section A(i) relative to the cell's  $\beta$ -Actin expression, based on one technical and scientific replicate.

Interestingly, the observed NEIL1 protein appeared at a higher kDa value than expected (Table 2.7), by approximately 8 kDa, which could suggest this visible NEIL1 is ubiquitinated

(Edmonds *et al.*, 2017). Compared to the western blot results observed of the plasmid-transfected PD20 cell extracts in Figure 3.31A, the observed results suggest both the FANCD2 deficient (PD20) and corrected (3.15) cells were plasmid-transfected successfully. However, only the pcDNA3.1-hNEIL1-FLAG transfected 3.15 cell extract displayed successful recombinant protein expression, which suggested a potential issue with the prepared plasmids pcDNA3.1-hNEIL3<sup>FL</sup>-FLAG and pcDNA3.1-hNEIL3<sup>1506</sup>-FLAG from Section 3.3. The transfection and confirmation experiments with the FANCD2 corrected cell line (3.15) were repeated with the new pcDNA3.1-hNEIL3<sup>FL</sup>-FLAG and pcDNA3.1-hNEIL3<sup>1506</sup>-FLAG plasmids, as described previously in Section 3.4. However, the results remained unchanged and the NEIL3 expression-confirmation through western blotting was beginning to become an issue again in determining the repeatability and reliability of NEIL3 expression throughout the remainder of the project.

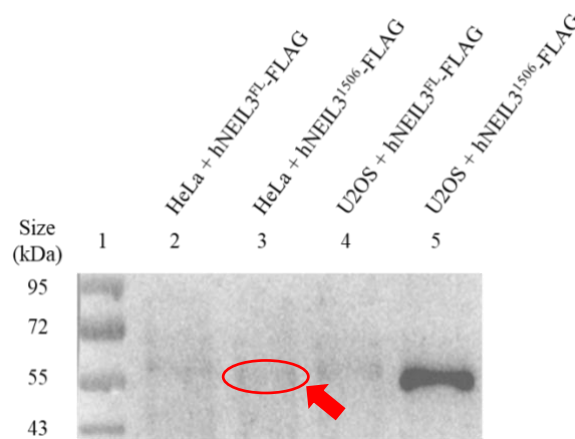


**Figure 3.32: Western blots of plasmid-transfected HeLa (WT) and U2OS (WT) cell extracts for FLAG-tag.**

Lane 1, protein ladder; lane 2, HeLa with pcDNA3.1-hNEIL3<sup>FL</sup>-FLAG; lane 3, HeLa with pcDNA3.1-hNEIL3<sup>1506</sup>-FLAG; lane 4, U2OS with pcDNA3.1-hNEIL3<sup>FL</sup>-FLAG; lane 5, U2OS with pcDNA3.1-hNEIL3<sup>1506</sup>-FLAG. Expected molecular weight: hNEIL3<sup>FL</sup>-FLAG, 69 kDa; hNEIL3<sup>1506</sup>-FLAG, 56 kDa. Red arrow and encircled, hNEIL3<sup>1506</sup>-FLAG detected.

In saving time and resources, only the WT cancer cells HeLa and U2OS were initially transfected with the new pcDNA3.1-hNEIL3<sup>FL</sup>-FLAG and pcDNA3.1-hNEIL3<sup>1506</sup>-FLAG plasmids and immunoblotted with anti-FLAG antibody before comparing and confirming with their FA phenotype counterparts. As displayed in Figure 3.32, an expressed protein could be barely observed from the pcDNA3.1-hNEIL3<sup>1506</sup>-FLAG transfected HeLa cell extract (lane 3) and was evidently visible from the pcDNA3.1-hNEIL3<sup>1506</sup>-FLAG

transfected U2OS cell extract (lane 5). Based on the approximate 55 kDa molecular protein weight and only observed in the pcDNA3.1-hNEIL3<sup>1506</sup>-FLAG transfected cell extracts, the results would suggest a successful transfection of the new plasmid, especially for the U2OS cells, and the cells were expressing the recombinant hNEIL3<sup>1506</sup>-FLAG protein, which only the anti-FLAG-tagged antibody explicitly recognised. Other noticeable protein bands were observed from the other transfected HeLa and U2OS cell extracts (lanes 2 and 4, respectively), at around 70 kDa. However, the bands are only barely noticeable, and the bands appearing across the membrane at around 60 kDa and 70 kDa may be non-specific binding.

As it could be seen in Figure 3.33, the WT/FANCD2 deficient cells HeLa/-D2 and U2OS/-D2 (sections A – D, respectively) displayed no NEIL3 protein expression in the non-transfected and transfected controls (lanes 2 – 4), as was expected and observed from the western blot background results (Figure 3.17). Similar to the plasmid-transfected FANCD2 corrected (3.15) cell extract results from Figure 3.31, only the pcDNA3.1-hNEIL1-FLAG transfected cancer cell extracts from HeLa/-D2 and U2OS/-D2 (lane 5, Figure 3.33A – D[ii], respectively) displayed expression for NEIL1 protein, and at a higher kDa than expected. This suggests the molecular weight for NEIL1 would be expectedly expressed at the molecular weight of approximately 52 kDa (with FLAG-tag, 53 kDa) instead of what was previously expected (43 kDa, Table 2.7). Furthermore, based on the antibody specificity for the FLAG-tagged protein in Figure 3.33A – D[iii], the results displayed were equivalent to the same expressed NEIL1 protein, suggesting the FLAG-tagged protein being the expressed hNEIL1-FLAG recombinant protein, as was previously observed and expected based on the pcDNA3.1-hNEIL1-FLAG transfected FANCD2-corrected cell extract results (Figure 3.31B[ii – iii]). Although it was previously confirmed in Figure 3.32 that NEIL3<sup>1506</sup>-FLAG protein expression was confirmed for the WT cancer cells U2OS and possibly HeLa, in Figure 3.33A (HeLa) and C (U2OS), the same results were not as noticeable (lane 7, Figure 3.33A[iii] and C[iii]). Furthermore, there was no evidence of NEIL3 or FLAG-tagged NEIL3 protein expression from any pcDNA3.1-hNEIL3<sup>FL</sup>-FLAG transfected (lane 6) or pcDNA3.1-hNEIL3<sup>F1506</sup>-FLAG transfected (lane 7) FANCD2 deficient cancer cells HeLa-D2 and U2OS-D2 cells (Figure 3.33B[ii – iii] and D[ii – iii], respectively). The combined results may suggest the WT cancer cells U2OS showed preferable transfection-confirmation results due to the cell line being well known for ease of transfection. Surprisingly, however, only the recombinant protein hNEIL3<sup>1506</sup>-FLAG was noticeably expressed from the

pcDNA3.1-hNEIL3<sup>1506</sup>-FLAG transfected U2OS cell extract (lane 7) when compared to the recombinant protein hNEIL1-FLAG expressed from the pcDNA3.1-hNEIL1-FLAG transfected U2OS cell extract (lane 5, Figure 3.33C[iii]), and not expressed from the equivalent U2OS-D2 cell extract (lane 7, Figure 3.33D[iii]).

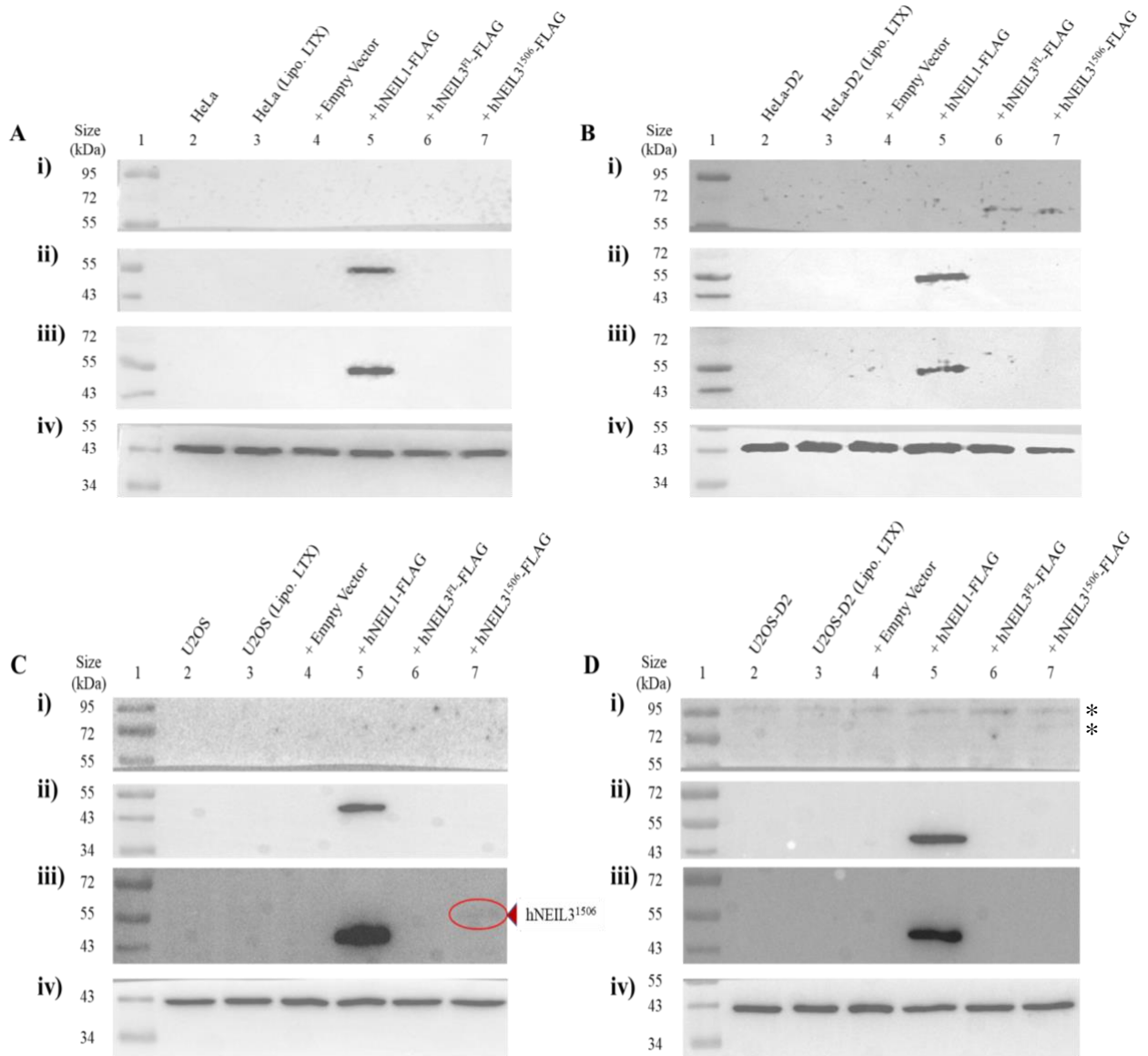


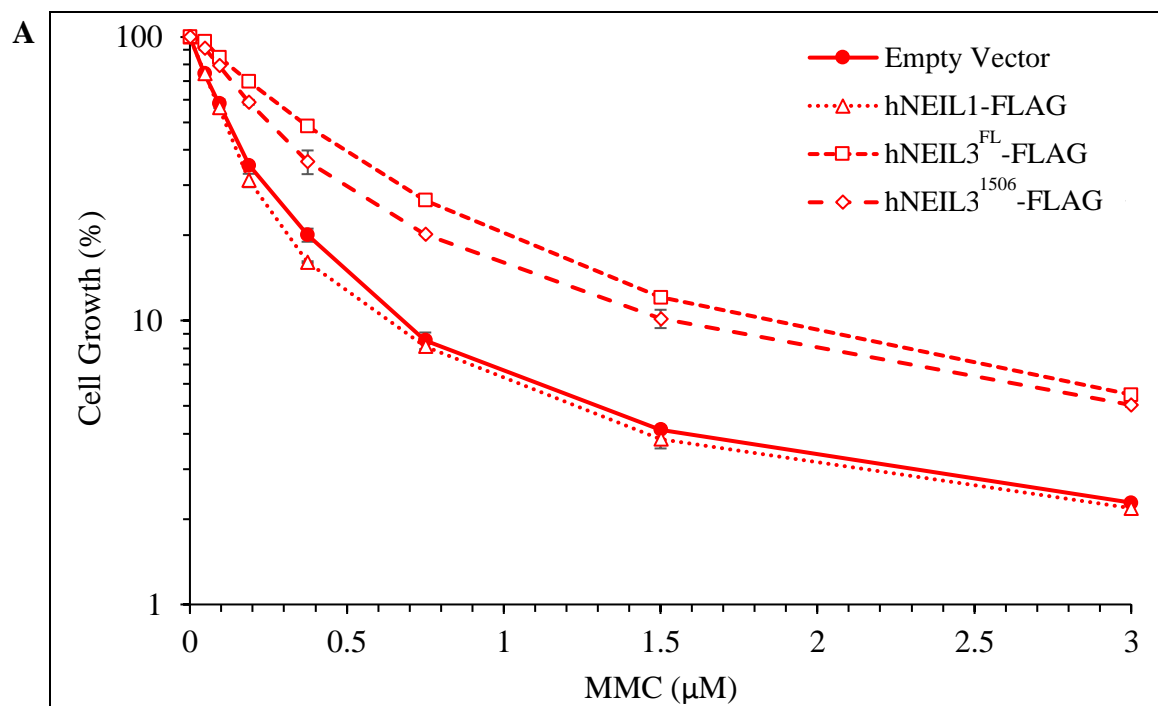
**Figure 3.33: Western blots of plasmid-transfected HeLa (WT, A[i – iv]), HeLa-D2 (FANCD2 deficient, B[i – iv]), U2OS (WT, C[i – iv]) and U2OS-D2 (FANCD2 deficient, D[i – iv]) cell extracts. (A – D) i) NEIL3, ii) NEIL1, iii) FLAG-tag, and iv) β-Actin.**

(A – D) Lane 1, protein ladder; lane 2, control; lane 3, control (Lipofectamine LTX only); lane 4, empty vector; lane 5, pcDNA3.1-hNEIL1-FLAG; lane 6, pcDNA3.1-hNEIL3<sup>FL</sup>-FLAG; lane 7, pcDNA3.1-hNEIL3<sup>1506</sup>-FLAG. Expected molecular weight: NEIL3, 68 kDa; hNEIL3<sup>FL</sup>-FLAG, 69 kDa; hNEIL3<sup>1506</sup>-FLAG, 56 kDa; NEIL1, 43 kDa; hNEIL1-FLAG, 44 kDa; β-Actin, 42 kDa. (\*) Non-specific binding.

Based on the accumulated plasmid-transfection confirmation results, the pcDNA3.1-hNEIL1-FLAG transfected cells displayed consistently successful hNEIL1-FLAG expression to all cell lines of FANCD2 deficiency and correction/WT, apart from PD20 (FANCD2 deficient cell line). The results were consistent primarily in the expression of the recombinant protein hNEIL1-FLAG, based on the anti-NEIL1 specific and anti-FLAG tag specific immunoblotting results from the FANCD2 corrected cells 3.15, and the WT/FANCD2 deficient cancer cells U2OS/-D2 and HeLa/-D2. However, confirmation of the recombinant proteins hNEIL3<sup>FL</sup>-FLAG and hNEIL3<sup>1506</sup>-FLAG from the pcDNA3.1-hNEIL3<sup>FL</sup>-FLAG and pcDNA3.1-hNEIL3<sup>1506</sup>-FLAG transfected cell extracts were not as consistent. Out of the six cell lines transfected, only the WT cancer cells U2OS and possibly HeLa displayed evidence of hNEIL3<sup>1506</sup>-FLAG recombinant protein, based on the FLAG-tagged immunoblotting results only. This may suggest the transfection of plasmids with NEIL3 inserts, full length or truncated, were not as simple as transfecting the plasmid. Transfection and expression confirmation attempts were repeated, but only the recombinant hNEIL1-FLAG protein results were confirmed, and the western blot was becoming less reliable as time passed for the NEIL3 protein confirmation.

#### 3.4.2. Survival of Plasmid-Transfected Cells

Based on the accumulated results of the plasmid transfected cell lines described previously in Section 3.4.1., and due to the lack of time and resources, specific transfections with which cell line groups had to be prioritised. The FANCD2 deficient cells PD20 and FANCD2 corrected cells 3.15 were prioritised for siRNA transfection (Section 3.5), and the WT/FANCD2 deficient cancer cells U2OS/-D2 and HeLa/-D2 were prioritised for plasmid transfection. Before the prioritisation, plasmid transfection to the PD20 and 3.15 cells were attempted based on the initial results described from Figure 3.31, with the prepared plasmids from Section 3.3. To save time and resources, the plasmid-transfected PD20 cells were initially tested for cell survival after genotoxin treatment before subsequently reattempting and comparing with the plasmid-transfected 3.15 cells with the new pcDNA3.1-hNEIL3<sup>FL</sup>-FLAG and pcDNA3.1-hNEIL3<sup>1506</sup>-FLAG plasmids.



**B**

		IC <sub>50</sub> ± SD Values
<b>PD20</b>	+ Empty Vector	0.12 ± 0.01 µM
	+ hNEIL1-FLAG	0.11 ± 0.00 µM
	+ hNEIL3 <sup>FL</sup> -FLAG	0.36 ± 0.01 µM
	+ hNEIL3 <sup>1506</sup> -FLAG	0.25 ± 0.01 µM

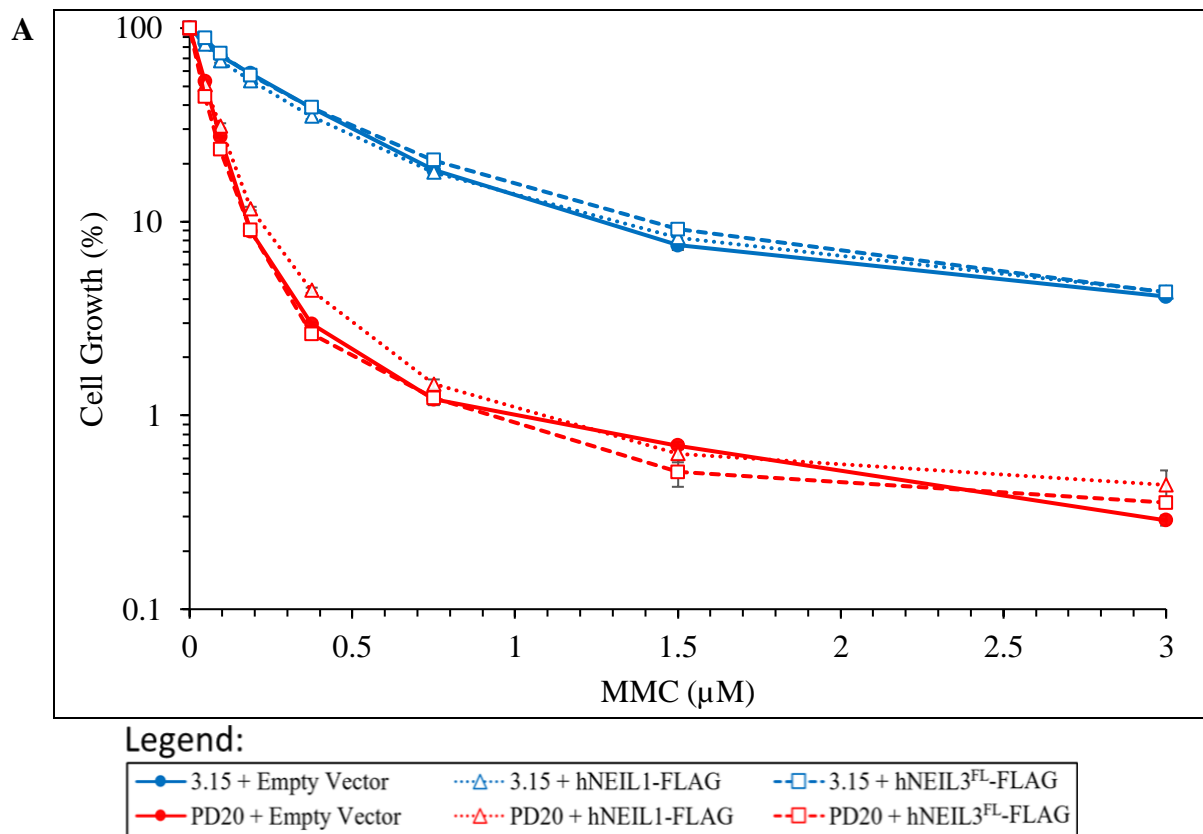
**Figure 3.34: Growth inhibition of plasmid transfected A) PD20 (FANCD2 deficient) following mitomycin C (MMC) treatment based on initial western blot confirmation.**

**B)** IC<sub>50</sub> values for growth inhibition following treatment. Cells were transfected with empty vector, pcDNA3.1-hNEIL1-FLAG, pcDNA3.1-hNEIL3<sup>FL</sup>-FLAG or pcDNA3.1-hNEIL3<sup>1506</sup>-FLAG. 3 x 10<sup>3</sup> cells per well, incubated for 72 h. Mean data was collected from triplicate technical repeats.

As displayed in Figure 3.34, the empty-vector transfected PD20 cells (FANCD2 deficient) was observed to be highly susceptible to MMC, based on the IC<sub>50</sub> displayed in Figure 3.34B being the most sensitive compared to the plasmid-transfect PD20 cells and closely equivalent to the IC<sub>50</sub> observed in non-transfected PD20 cells and within observed MMC diluted ranges in Figure 3.11D. Therefore, PD20 was highly susceptible to MMC, as was expected. Furthermore, compared to the IC<sub>50</sub> of the empty-vector transfected cells, the FANCD2 deficient cells (PD20) showed a significantly increased resistance to MMC when expressing hNEIL3<sup>1506</sup>-FLAG by a factor of 2.1 (IC<sub>50</sub> 0.12 µM [+ Empty Vector] to 0.25 µM), and also

when expressing hNEIL3<sup>FL</sup>-FLAG by a factor of 3 (IC<sub>50</sub> 0.36 μM). However, based on the observed NEIL3 protein expression results from PD20 cell extracts described in Section 3.4.1., the plasmid-transfected cells were considered expressing increased non-recombinant NEIL3 protein. Furthermore, compared to the IC<sub>50</sub> of empty-vector control, the pcDNA3.1-hNEIL1-FLAG transfected PD20 cells results displayed a barely notable resistance to MMC, which based on the literature review was expected to result in a significant increase in ICL resistance. Based on this initial attempt and the FANCD2 corrected (3.15) cells recombinant protein confirmation results described in Section 3.4.1., cell growth after genotoxin treatment was reattempted using only the pcDNA3.1-hNEIL1-FLAG and new pcDNA3.1-hNEIL3<sup>FL</sup>-FLAG plasmids.

In Figures 3.35 – 3.36 it was observed that the PD20 (FANCD2 deficient cells) empty-vector transfected controls were more susceptible to MMC (Figure 3.35) and cisplatin (Figure 3.36) than the 3.15 (FANCD2 corrected cells) empty-vector transfected controls, as was expected and previously observed in Figure 3.11. The differences in resistance between the PD20 and 3.15 cell controls were barely notable when treated by the oxidative agent TBHP (Figure 3.37). However, similar results were observed from the cancer cells HeLa (WT) and HeLa-D2 (FANCD2 deficient) when treated by the same oxidative agent (Figure 3.13C), and from previous attempts observed (Appendix Figure 2), which suggested the differences in resistance to oxidative damage was not always consistent. As it could be seen from Figures 3.36 – 3.37, compared to the empty-vector transfected cells, the FANCD2 deficient cells (PD20) showed no increased resistance to MMC (Figure 3.35) cisplatin (Figure 3.36) or TBHP (Figure 3.37) when expressing hNEIL1-FLAG or hNEIL3<sup>FL</sup>-FLAG. Similarly, it was also observed for the FANCD2 corrected cells (3.15) for MMC and cisplatin when plasmid-transfected, but for TBHP the difference in resistance was notable. In Figure 3.37, compared to the IC<sub>50</sub> of the vector-transfected cells, the 3.15 cells showed a notably increased resistance to TBHP when expressing hNEIL1-FLAG (IC<sub>50</sub> 19.4 μM [+ Empty vector] to 24.8 μM) and an increased but expected resistance when expressing hNEIL3<sup>FL</sup>-FLAG by a factor of 1.8 (IC<sub>50</sub> 19.4 μM [+ Empty vector] to 34.1 μM). Based on the accumulated MTT assay results of the plasmid transfected FANCD2-deficient (PD20) and corrected (3.15) cells survival after genotoxin treatment, the PD20 cells with NEIL3 expressions displayed a significant increase in resistance to MMC but were not repeatable, and the 3.15 cells with NEIL3 expression only displayed a significant increase in resistance to TBHP.

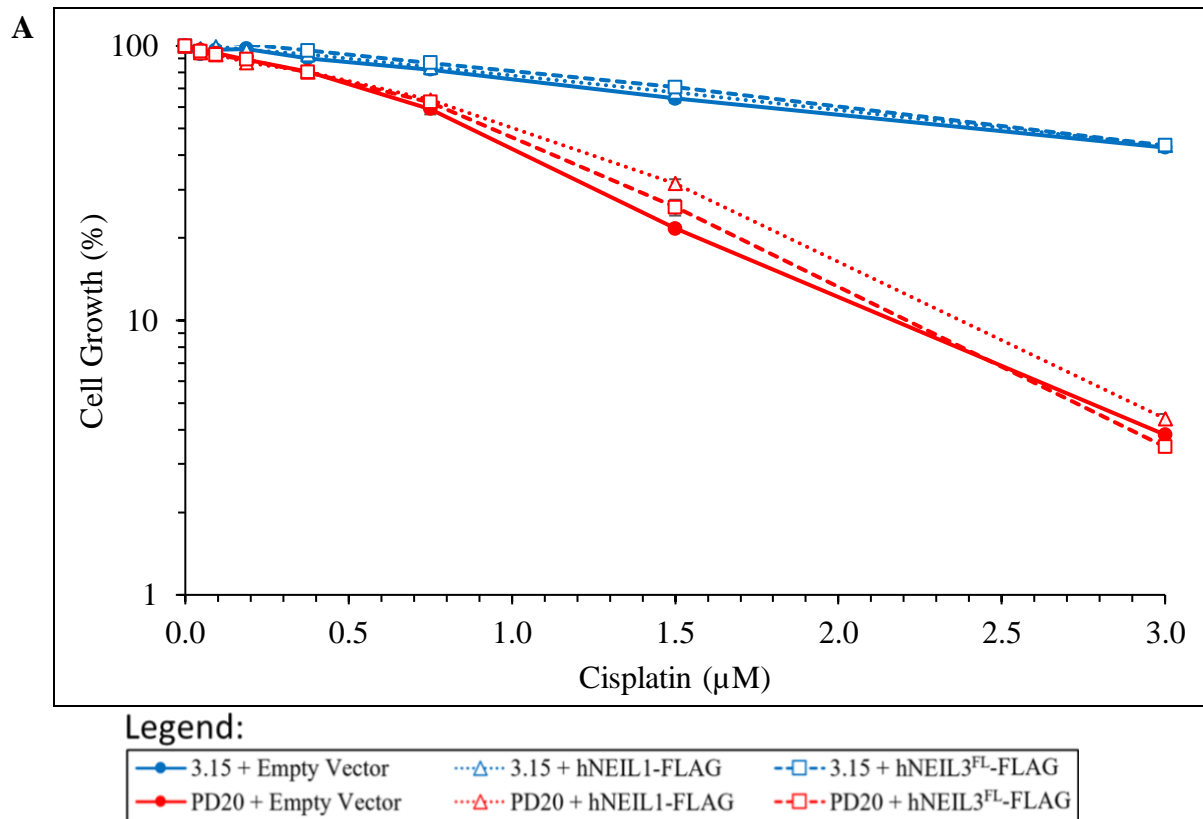


**B**

		IC <sub>50</sub> ± SD Values
3.15	+ Empty Vector	0.26 ± 0.01 µM
	+ hNEIL1-FLAG	0.25 ± 0.01 µM
	+ hNEIL3 <sup>FL</sup> -FLAG	0.22 ± 0.01 µM
PD20	+ Empty Vector	0.05 ± 0.00 µM
	+ hNEIL1-FLAG	0.05 ± 0.00 µM
	+ hNEIL3 <sup>FL</sup> -FLAG	0.04 ± 0.00 µM

**Figure 3.35: Growth inhibition comparison of plasmid transfected A) 3.15 (PD20 Corrected, blue) and PD20 (FANCD2 deficient, red), following treatment with mitomycin C (MMC).**

**B) IC<sub>50</sub> values for growth inhibition following treatment.** Cells were transfected with empty vector, pcDNA3.1-hNEIL1-FLAG or pcDNA3.1-hNEIL3<sup>FL</sup>-FLAG. 3 x 10<sup>3</sup> cells per well, incubated for 72 h. Mean data was collected from triplicate technical repeats.

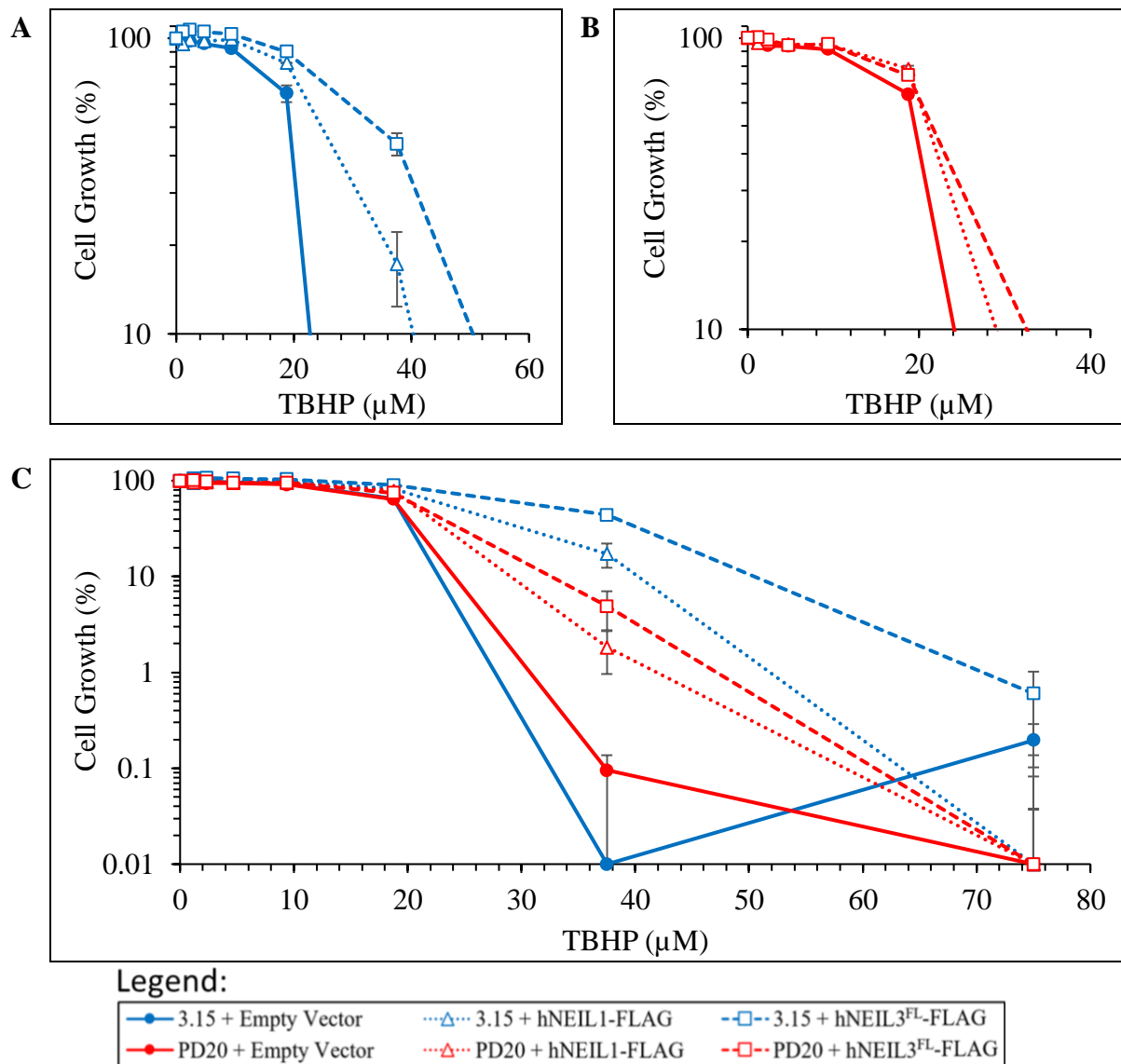


**B**

		IC <sub>50</sub> ± SD Values
3.15	+ Empty Vector	2.42 ± 0.16 µM
	+ hNEIL1-FLAG	2.53 ± 0.09 µM
	+ hNEIL3 <sup>FL</sup> -FLAG	2.57 ± 0.09 µM
PD20	+ Empty Vector	0.87 ± 0.03 µM
	+ hNEIL1-FLAG	1.01 ± 0.04 µM
	+ hNEIL3 <sup>FL</sup> -FLAG	0.94 ± 0.04 µM

**Figure 3.36: Growth inhibition comparison of plasmid transfected A) 3.15 (PD20 Corrected, blue) and PD20 (FANCD2 deficient, red), following treatment with cisplatin.**

**B)** IC<sub>50</sub> values for growth inhibition following treatment. Cells were transfected with empty vector, pcDNA3.1-hNEIL1-FLAG or pcDNA3.1-hNEIL3<sup>FL</sup>-FLAG. 3 x 10<sup>3</sup> cells per well, incubated for 72 h. Mean data was collected from triplicate technical repeats.



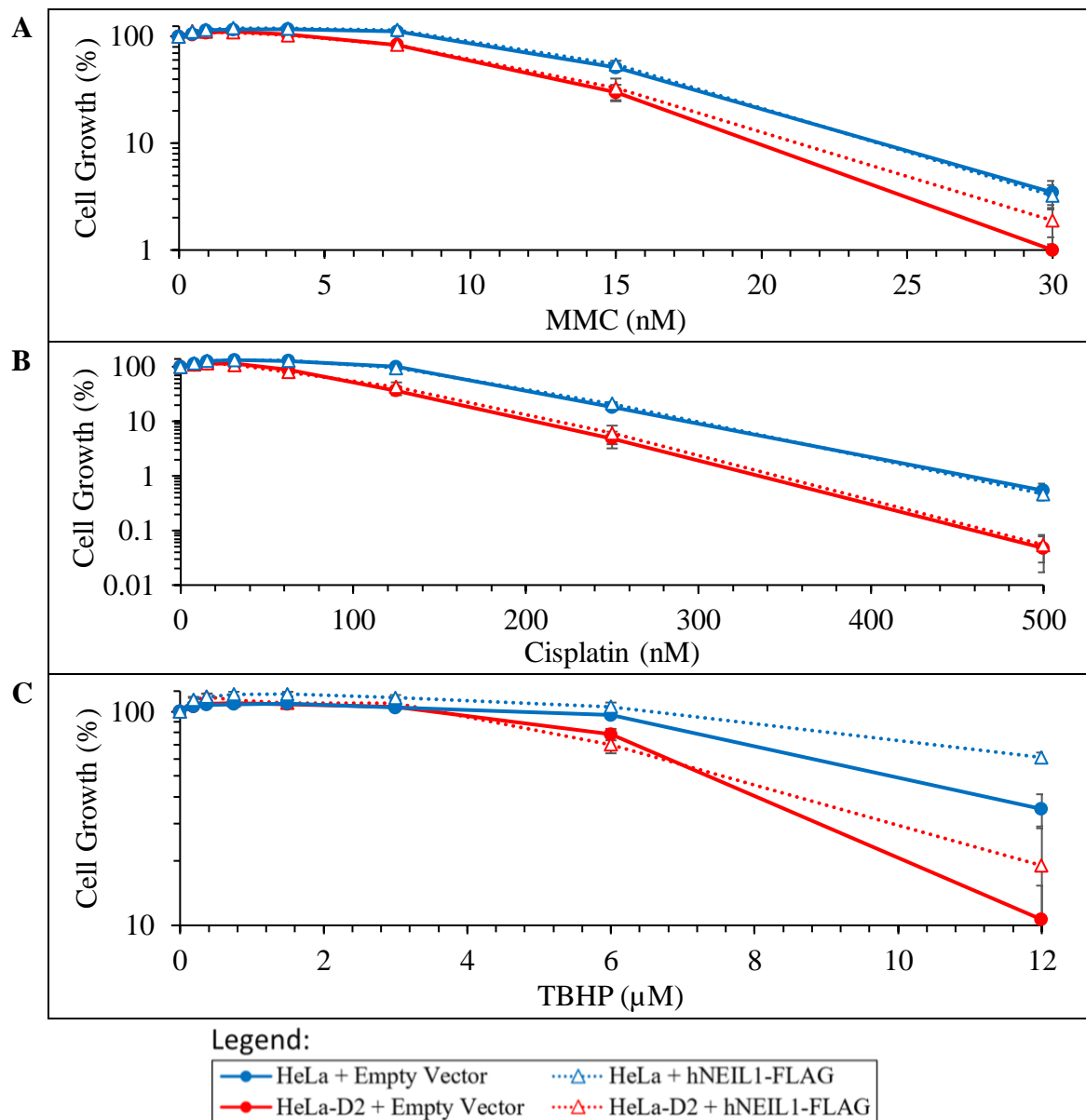
**D**

		IC <sub>50</sub> ± SD Values
3.15	+ Empty Vector	19.4 ± 0.51 μM
	+ hNEIL1-FLAG	24.8 ± 0.59 μM
	+ hNEIL3 <sup>FL</sup> -FLAG	34.1 ± 1.09 μM
PD20	+ Empty Vector	19.5 ± 0.50 μM
	+ hNEIL1-FLAG	21.0 ± 0.61 μM
	+ hNEIL3 <sup>FL</sup> -FLAG	21.5 ± 0.49 μM

**Figure 3.37: Growth inhibition of plasmid transfected (A) 3.15 (PD20 Corrected, blue) and (B) PD20 (FANCD2 deficient, red), and their comparison (C), following treatment with TBHP.**

**D)** IC<sub>50</sub> values for growth inhibition following treatment. Cells were transfected with empty vector, pcDNA3.1-hNEIL1-FLAG, or pcDNA3.1-hNEIL3<sup>FL</sup>-FLAG. 3 × 10<sup>3</sup> cells per well, incubated for 72 h. Mean data was collected from triplicate technical repeats.

For the genotoxin treatment survival studies after plasmid transfection the cancer cell lines HeLa (WT) and HeLa-D2 (FANCD2 deficient) were only transfected with pcDNA3.1-hNEIL1-FLAG, based on the expression results confirming the recombinant protein hNEIL1-FLAG after transfection confirmation (Figure 3.33). In Figure 3.38 it was observed that the empty-vector transfected HeLa (WT) cells were more resistant to MMC (A), cisplatin (B) and TBHP (C) than the empty-vector transfected HeLa-D2 (FANCD2 deficient) cells, as was expected and previously observed in untransfected cells (Figure 3.14). However, similarly to the MTT assay results displayed previously for FANCD2 deficient and corrected cells PD20 and 3.15, respectively, compared to the empty-vector transfected cells in Figure 3.38, the FANCD2 deficient cells (HeLa-D2) showed no increased resistance to MMC (A), cisplatin (B) or TBHP (C) when expressing hNEIL1-FLAG. Furthermore, it was also observed for the WT cells (HeLa) for MMC and cisplatin when expressing hNEIL1-FLAG, but for TBHP the difference in resistance was notable. In Figure 3.38C, compared to the IC<sub>50</sub> of the vector-transfected cells, the HeLa cells showed a notably increased resistance to TBHP when expressing hNEIL1-FLAG (IC<sub>50</sub> 9.90 μM and >12 μM) but difficult to determine its significance beyond the concentration range of the genotoxic agent. Compared to the FA cells (PD20/3.15) results displayed in Figures 3.35 – 3.37, NEIL1 overexpression still contradicted with the notion of decreasing susceptibility against ICL-inducing agents MMC and cisplatin. Though not substantially, the results still supported the notion of increasing resistance against an oxidative-damaging agent.



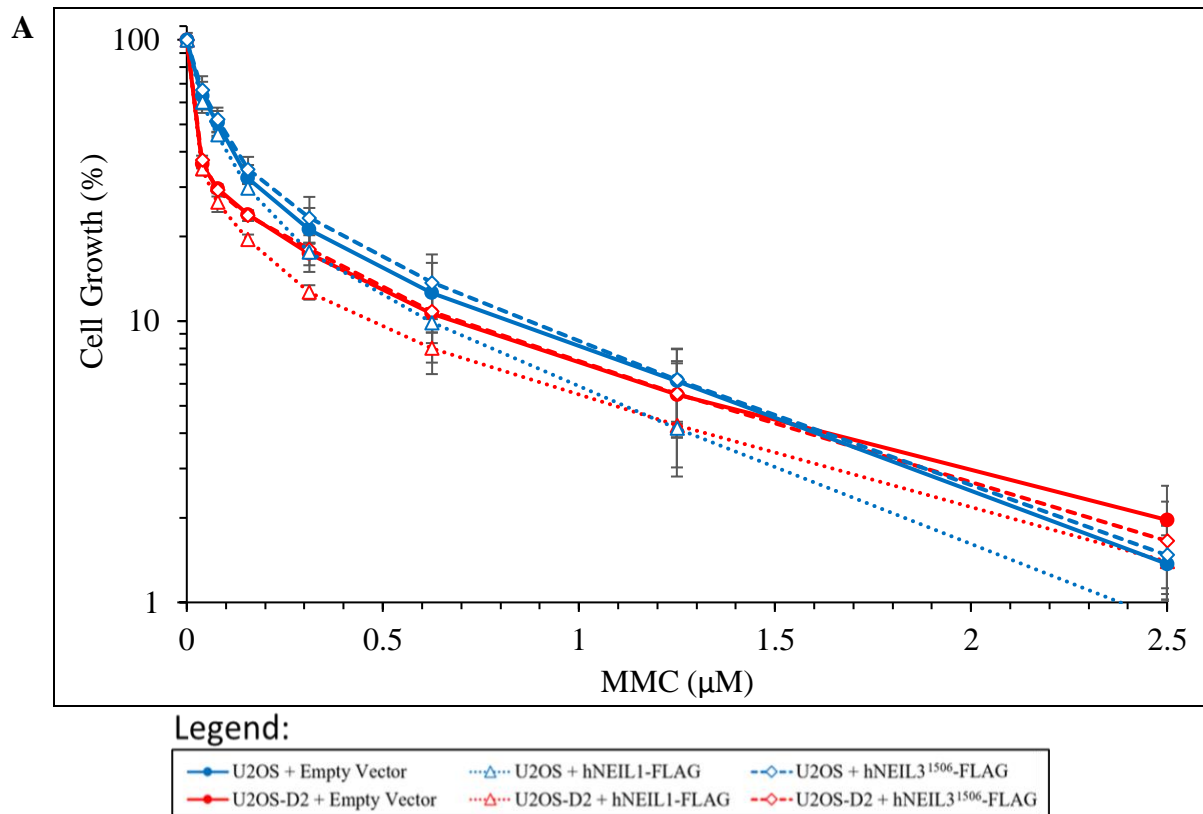
**D**

		IC <sub>50</sub> ± SD Values		
		MMC	Cisplatin	TBHP
HeLa	+ Empty Vector	15.2 ± 0.65 nM	176 ± 13.87 nM	9.90 ± 0.47 $\mu$ M
	+ hNEIL1-FLAG	15.5 ± 0.77 nM	178 ± 14.12 nM	>12.00 $\mu$ M
HeLa-D2	+ Empty Vector	11.2 ± 0.69 nM	103 ± 8.04 nM	7.35 ± 0.50 $\mu$ M
	+ hNEIL1-FLAG	11.6 ± 1.09 nM	109 ± 14.50 nM	7.56 ± 0.97 $\mu$ M

**Figure 3.38: Growth inhibition of plasmid transfected HeLa (WT, blue) and HeLa-D2 (FANCD2 deficient, red), following treatment with mitomycin C (MMC, A), cisplatin (B), and TBHP (C).**

**D)** IC<sub>50</sub> values for growth inhibition following treatment. Cells were transfected with empty vector or pcDNA3.1-hNEIL1-FLAG. 5 x 10<sup>2</sup> cells per well, incubated for 168 h. Mean data was collected from triplicate technical and scientific repeats.

In Figures 3.39 – 3.41, the cancer cells U2OS (WT) and U2OS-D2 (FANCD2 deficient) were only transfected with pcDNA3.1-hNEIL1-FLAG and pcDNA3.1-hNEIL3<sup>1506</sup>-FLAG, based on the transfection results confirming overexpression of their recombinant proteins (Figures 3.32 and 3.33). Similar to the PD20/3.15 MTT assay results from Figures 3.35 – 3.37, as displayed, the empty-vector transfected U2OS (WT) cells were more resistant to MMC (Figure 3.39) and cisplatin (Figure 3.40) than the empty-vector transfected U2OS-D2 (FANCD2 deficient) cells, as was expected and previously observed in Figure 3.13. However, the differences in resistance between the U2OS and U2OS-D2 cell controls were barely notable in an unexpectedly reverse orientation when treated by the oxidative agent TBHP (Figure 3.41). Though similar to the observed results displayed in the HeLa/-D2 growth inhibition after TBHP treatment (Figure 3.14C, Section 3.2.2.), it may be possible that the indifference in TBHP resistance is the real difference and an external factor was not considered. As observed in Figures 3.39 – 3.41, compared to the empty-vector transfected cells, the FANCD2 deficient cells (U2OS-D2) showed no notable difference in resistance to MMC (Figure 3.39), but notably decreased resistance in cisplatin (Figure 3.40) and TBHP (Figure 3.41), when expressing hNEIL1-FLAG. Furthermore, it was also notably observed that the U2OS-D2 cells increased resistance to cisplatin and TBHP, when expressing hNEIL3<sup>1506</sup>-FLAG (Figures 3.40 and 3.41, respectively). Compared to the empty-vector transfected WT cancer cells (U2OS), no notable difference in resistance was observed to MMC (Figure 3.39), decreased resistance to cisplatin and TBHP when expressing hNEIL1-FLAG (Figures 3.40 and 3.41, respectively), but increased resistance to TBHP when expressing hNEIL3<sup>1506</sup>-FLAG (IC<sub>50</sub> 1.45  $\mu$ M and 2.25  $\mu$ M). Statistically, no significant difference was observed when expressing hNEIL1-FLAG or hNEIL3<sup>1506</sup>-FLAG.

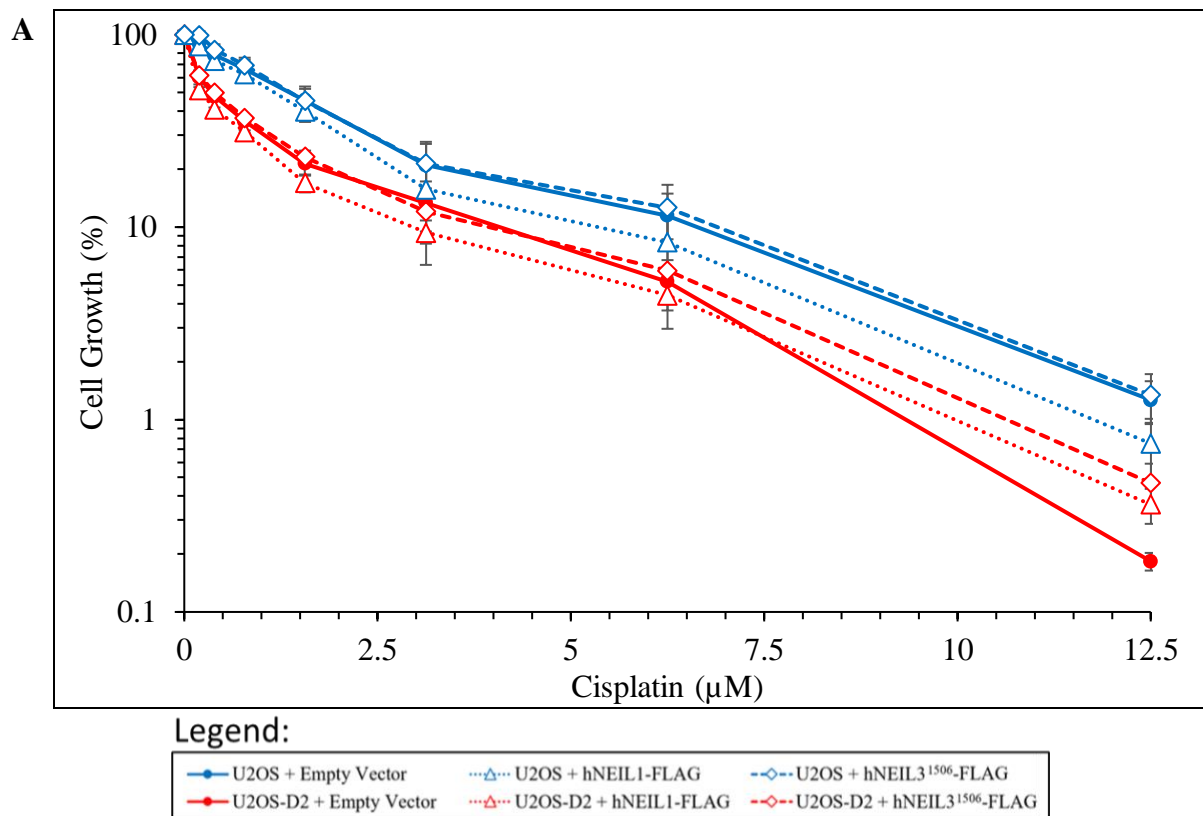


**B**

		IC <sub>50</sub> ± SD Values
U2OS	+ Empty Vector	0.08 ± 0.02 µM
	+ hNEIL1-FLAG	0.07 ± 0.01 µM
	+ hNEIL3 <sup>1506</sup> -FLAG	0.08 ± 0.02 µM
U2OS-D2	+ Empty Vector	0.03 ± 0.00 µM
	+ hNEIL1-FLAG	0.03 ± 0.01 µM
	+ hNEIL3 <sup>1506</sup> -FLAG	0.03 ± 0.00 µM

**Figure 3.39: Growth inhibition of plasmid transfected A) U2OS (WT, blue) and U2OS-D2 (FANCD2 deficient, red), following treatment with mitomycin C.**

**B)** IC<sub>50</sub> values for growth inhibition following treatment. Cells were transfected with empty vector, pcDNA3.1-hNEIL1-FLAG or pcDNA3.1-hNEIL3<sup>1506</sup>-FLAG. 1 x 10<sup>3</sup> cells per well, incubated for 96 h. Mean data was collected from triplicate technical repeats within two scientific repeats.

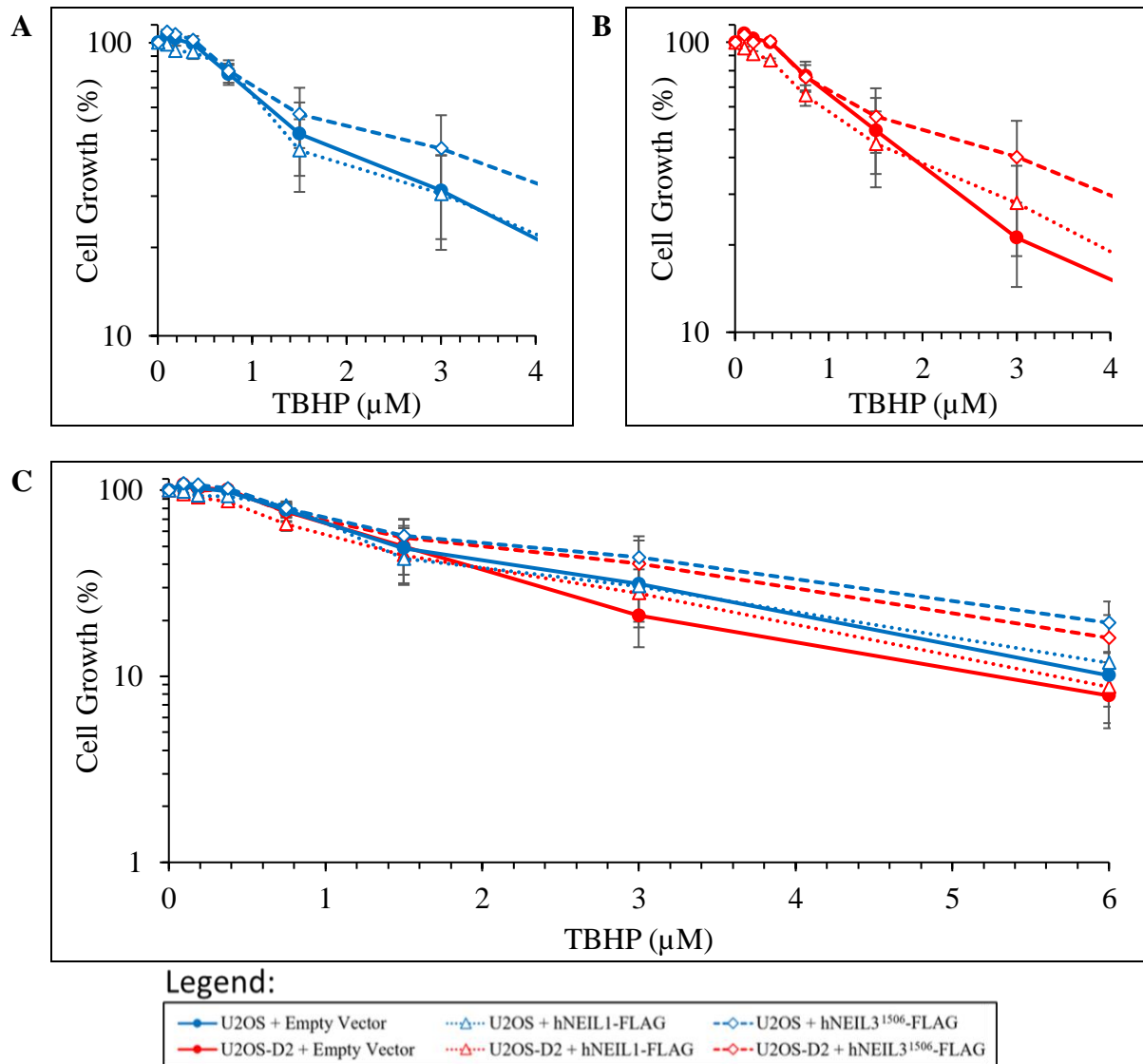


**B**

		IC <sub>50</sub> ± SD Values
U2OS	+ Empty Vector	1.30 ± 0.32 $\mu\text{M}$
	+ hNEIL1-FLAG	1.07 ± 0.15 $\mu\text{M}$
	+ hNEIL3 <sup>1506</sup> -FLAG	1.38 ± 0.31 $\mu\text{M}$
U2OS-D2	+ Empty Vector	0.35 ± 0.08 $\mu\text{M}$
	+ hNEIL1-FLAG	0.22 ± 0.04 $\mu\text{M}$
	+ hNEIL3 <sup>1506</sup> -FLAG	0.39 ± 0.06 $\mu\text{M}$

**Figure 3.40: Growth inhibition of plasmid transfected A) U2OS (WT, blue) and U2OS-D2 (FANCD2 deficient, red), following treatment with cisplatin.**

**B)** IC<sub>50</sub> values for growth inhibition following treatment. Cells were transfected with empty vector, pcDNA3.1-hNEIL1-FLAG or pcDNA3.1-hNEIL3<sup>1506</sup>-FLAG. 1 x 10<sup>3</sup> cells per well, incubated for 96 h. Mean data was collected from triplicate technical repeats within two scientific repeats.



**D**

		IC <sub>50</sub> ± SD Values
U2OS	+ Empty Vector	1.45 ± 0.43 μM
	+ hNEIL1-FLAG	1.35 ± 0.38 μM
	+ hNEIL3 <sup>1506</sup> -FLAG	2.25 ± 0.08 μM
U2OS-D2	+ Empty Vector	1.50 ± 0.38 μM
	+ hNEIL1-FLAG	1.30 ± 0.34 μM
	+ hNEIL3 <sup>1506</sup> -FLAG	2.00 ± 0.68 μM

**Figure 3.41: Growth inhibition of plasmid transfected (A) U2OS (WT, blue) and (B) U2OS-D2 (FANCD2 deficient, red), and their comparison (C), following treatment with TBHP.**

**D)** IC<sub>50</sub> values for growth inhibition following treatment. Cells were transfected with empty vector, pcDNA3.1-hNEIL1-FLAG or pcDNA3.1-hNEIL3<sup>1506</sup>-FLAG. 1 x 10<sup>3</sup> cells per well, incubated for 96 h. Mean data was collected from triplicate technical repeats within two scientific repeats.

In comparison of the FA FANCD2 deficient and corrected cells (PD20/3.15, Figures 3.36 – 3.38) and the cancer WT/FANCD2 deficient cells HeLa/-D2 (Figure 3.38) and U2OS/-D2 (Figures 3.39 – 3.41) MTT assay results, NEIL1 overexpression displayed no significant difference in increasing resistance against ICL-inducing agents MMC and cisplatin, nor to the oxidative inducing agent TBHP. Based on the literature review this was unexpected, as the accepted knowledge was a highly expressed DNA glycosylase NEIL1 would repair oxidative induced lesions in DNA, and more recent literature reviews had stated NEIL1 also repaired MMC induced ICLs. However, NEIL3 overexpression had been observed to decrease susceptibility to oxidative damage causing agents, which was expected, and the NEIL3 full length (NEIL3<sup>FL</sup>) and truncated (NEIL3<sup>1506</sup>) expressed PD20 cells were observed to significantly decrease susceptibility to MMC once. Based on these results, the project was considered to be repeated for the plasmid transfection and confirmation steps after antibiotic selection, followed by cell growth after genotoxin treatment.

#### 3.4.3. Evidence of Recombinant Protein Expression after Antibiotic-selection

Due to the results discussed in Section 3.4.2. displaying unexpected results that questioned the methodology and possibly the result repeatability from the literature review, and due to the lack of time and resources to investigate under the conditions discussed further for legitimacy, the project was repeated with the additional antibiotic step for the selection of the plasmid transfected cells to ensure the results achieved were reproducible and significant if the error in methodology could be determined. Based on the results from the FA-generated cancer cells U2OS (WT) and U2OS-D2 (FANCD2 deficient), the same cell lines were the first to be repeated. Due to the pcDNA3.1 vector containing a neomycin resistance gene (as seen in Figure 2.1), the antibiotic-selection solution used was the geneticin solution G418. Based on previous attempts with the WT/FANCD2 deficient cancer cells HeLa and HeLa-D2 (respectively, Appendix Figure 7), and local protocol recommendations for using G418 solution (Gibco) as well as based on the latest example at the time (Clément *et al.*, 2016), U2OS and U2OS-D2 were subjected to the plasmid transfection protocol followed by the antibiotic-selection protocol (Section 2.3.8.).

Following transfection of the U2OS/-D2 cells, the plasmid transfected cells were antibiotic-selected with 0.4 mg/ml G418 for one week. Within 96 h the non-transfected control cells

were observed to be no longer viable, while the transfected cells mainly were viable, and therefore, were considered only plasmid-transfected cells. After a further 48 h of recovery with standard culture medium containing pen/strep antibiotics for competitively inhibiting the G418, the experiment continued with the survival of the cells while treated with genotoxic agents. The MTT assay results displayed in Figures 3.45 – 3.47 prompted the confirmation of transfected cells after antibiotic selection as well as reconfirmation of recombinant proteins. Following discussions in the lab, the experiments were repeated with the additional cell line HEK293T (kindly gifted from Camillo Sargiacomo, University of Salford) as an antibiotic titration control and well known for its ease of transfection. The WT human embryonic kidney cells (HEK293T) were cultured under the same conditions and reagents as the HeLa (WT) cells, but without the need for suspending the cells with TrypLE Express.

The antibiotic titration was first attempted and prioritised for the FANCD2-deficient cancer cells U2OS-D2, alongside HEK293T (WT), and due to the lack of resources, a G418 solution (Roche) was gifted and was used at 0.2 – 0.8 mg/ml. It was observed under microscope every 24 h for 96 h and was concluded that 0.8 mg/ml was more suitable for U2OS-D2 at 72 h, but was not noticeable until 96 h, and HEK293T required more than 0.8 mg/ml at 96 h. This may have suggested that the Roche G418 stock solution was possibly more diluted than expected, but also that the FANCD2-deficient cancer cells were more sensitive than the WT cells (HEK293T). However, based on these results, the experiment was repeated for the other cancer cells HeLa (WT) and HeLa-D2 (FANCD2 deficient), for their intended cell survival experiments after antibiotic selection at higher G418 concentrations.

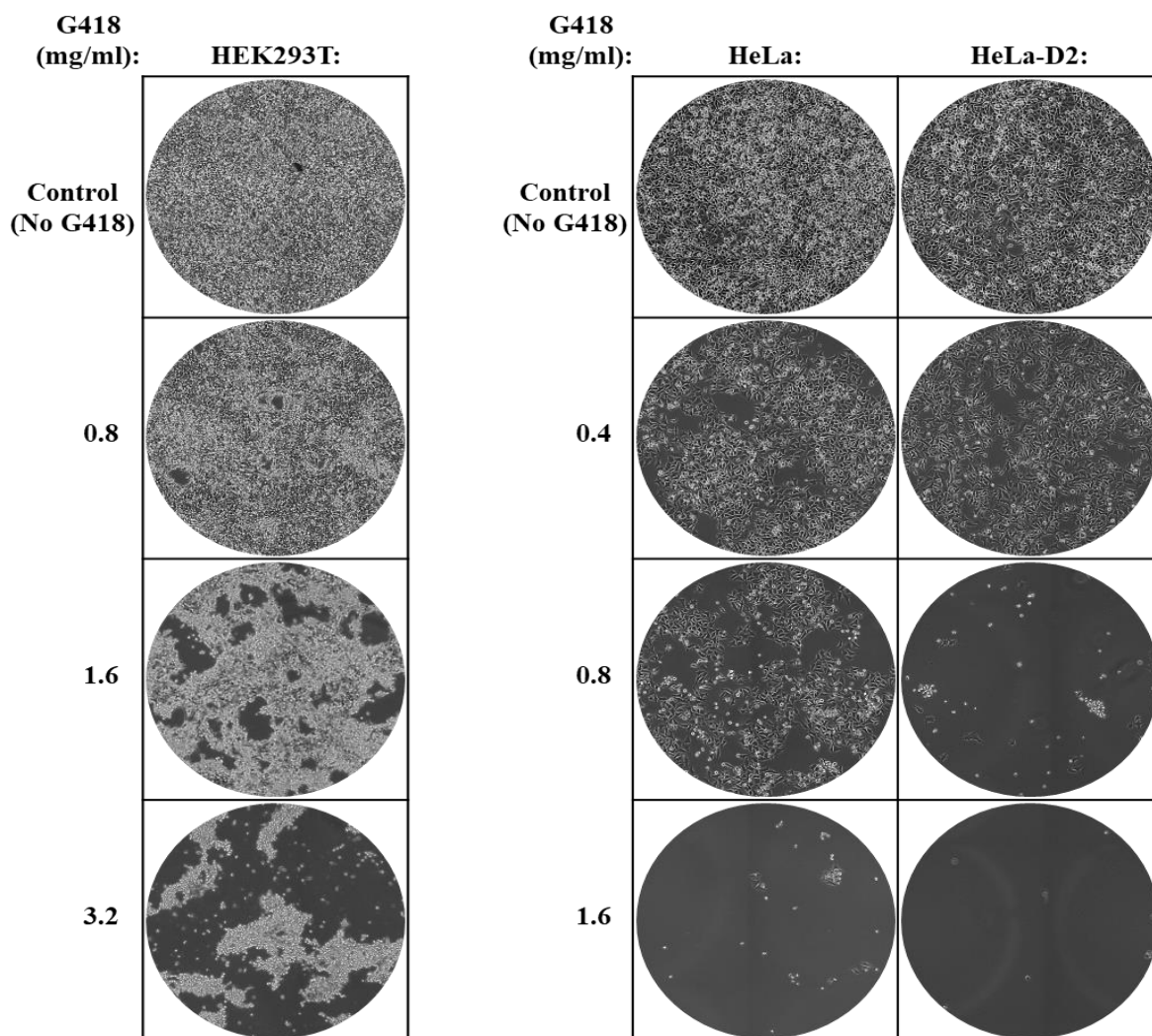


**Figure 3.42: Antibiotic titration of HEK293T (WT), HeLa (WT) and HeLa-D2 (FANCD2 deficient) with antibiotic selector G418.**

Seventy-two-hour incubation with G418 (Roche). Results captured through Evos FL Auto 2 cell imaging system (Invitrogen).

The HEK293T (WT) cells' antibiotic titration was reattempted at a higher G418 concentration range from 3.2 mg/ml, and the HeLa/-D2 (WT/FANCD2 deficient) cells were attempted at a concentration range from 1.6 mg/ml. As displayed in Figure 3.42, all three cell lines were highly confluent in the non-antibiotic selected controls, as was expected, and were progressively less viable as the G418 concentration increased. Due to the phenotypical clumping nature of the HEK293T cells and how delicate the cells were to pipetting, it was difficult to discern the viable from the nonviable cells, even when attempted to wash away the nonviable cells without suspending the viable cells. However, based on these observed results, 3.2 mg/ml G418 for 72 – 96 h seemed appropriate for antibiotic selection of the HEK293T cells. As for the WT and FANCD2 deficient cancer cells HeLa and HeLa-D2

(respectively), similar to the U2OS-D2 antibiotic titration results described previously, the HeLa/-D2 cells also seemed appropriate for antibiotic selection at 0.8 mg/ml G418 for 72 – 96 h. However, in Figure 3.42, it was notable that at 0.4 mg/ml G418 there were more viable HeLa cells than there were HeLa-D2 cells, and at 0.8 mg/ml the difference was more significant. This suggested that the FA-generated cancer cells U2OS-D2 and HeLa-D2 were more sensitive to antibiotic selection than their WT counterparts. Therefore, the HeLa and HeLa-D2 cells as a whole seemed more appropriate for antibiotic selection when using 1.6 mg/ml G418 for 72 h incubation.

Based on the antibiotic titration results observed in Figure 3.42, the three cell lines HEK293T (WT), HeLa (WT) and HeLa-D2 (FANCD2 deficient) were then subjected to plasmid transfection followed by antibiotic selection. The HeLa and HeLa-D2 cells were prioritised for cell growth after being treated with genotoxic agents, and to not lose an opportunity, the HeLa/-D2 cells were transfected with the pcDNA3.1-hNEIL1-FLAG, pcDNA3.1-hNEIL3<sup>FL</sup>-FLAG and pcDNA3.1-hNEIL3<sup>1506</sup>-FLAG plasmids, regardless of recombinant-protein confirmation results. As displayed in Figure 3.43A, all transfected HeLa/-D2 cells were observed after 72 h of antibiotic selection at 1.6 mg/ml G418. The non-transfected cancer cells were primarily non-viable and the transfected cells were primarily viable after antibiotic selection, as was expected. Of the viable transfected cells observed in Figure 3.43A, the cells displayed increased growth from the pcDNA3.1-hNEIL3<sup>FL</sup>-FLAG transfected cells, to the cells transfected with pcDNA3.1-hNEIL3<sup>1506</sup>-FLAG, almost equally with pcDNA3.1-hNEIL1-FLAG transfected cells, to the empty-vector transfected cells as mainly viable. This was similarly noticed between the empty vector and pcDNA3.1-hNEIL1-FLAG transfected HeLa/HeLa-D2 cells during an attempt at establishing an antibiotic selection kill-curve (Appendix Figure 7). This suggested that the pcDNA3.1-hNEIL3<sup>FL</sup>-FLAG plasmid was more difficult to transfect, or possibly the hNEIL3<sup>FL</sup>-FLAG protein was difficult to express or possibly caused stress or cytotoxicity to the cells. Interestingly, the HeLa/-D2 cells transfected with the truncated version of NEIL3 (hNEIL3<sup>1506</sup>-FLAG) were observed to have had fewer complications than the full-length NEIL3 (hNEIL3<sup>FL</sup>-FLAG) transfected cells, which could possibly indicate a more acceptable version of the DNA glycosylase. Regardless, the transfected and antibiotic-selected HeLa/-D2 (WT/FANCD2 deficient) cells were subsequently continued for recombinant-protein confirmation through western blot, as displayed in Figure 3.43B, and

cell growth after genotoxin treatment, results displayed in Figures 3.48 – 3.50 (Section 3.4.4.).

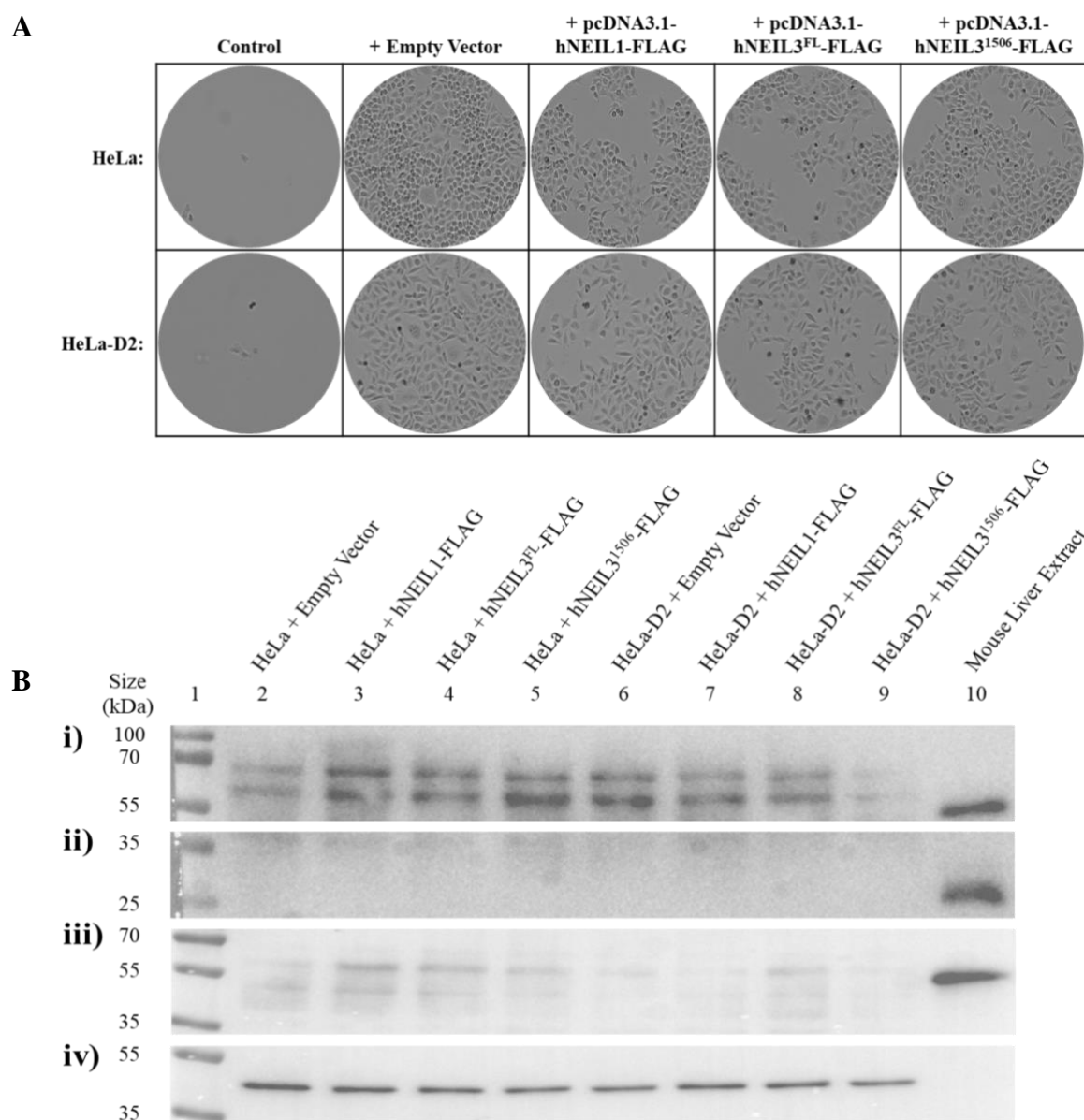


**Figure 3.43: Antibiotic-selection (A) and western blots on cell extracts (B) of plasmid-transfected HeLa (WT) and HeLa-D2 (FANCD2 deficient). (B) i) NEIL3, ii) NEIL1, iii) FLAG-tag, and iv)  $\beta$ -Actin.**

Seventy-two-hour incubation with 1.6 mg/ml of G418 (Roche). (A) Results captured through microscope tablet camera (Android). (B) Membrane 1 immunoblotted for NEIL3 (i), followed by reblotting for NEIL1 (ii); membrane 2 immunoblotted for FLAG-tag (iii), followed by reblotting for  $\beta$ -Actin (iv). Lane 1, protein ladder; lanes 2, 6, empty vector; lanes 3, 7, pcDNA3.1-hNEIL1-FLAG; lanes 4, 8, pcDNA3.1-hNEIL3<sup>FL</sup>-FLAG; lanes 5, 9, pcDNA3.1-hNEIL3<sup>1506</sup>-FLAG; lane 10, mouse liver extract. Expected molecular weight for human-specific proteins: NEIL3, 68 kDa; hNEIL3<sup>FL</sup>-FLAG, 69 kDa; hNEIL3<sup>1506</sup>-FLAG, 56 kDa; NEIL1, 52 kDa; hNEIL1-FLAG, 53 kDa;  $\beta$ -Actin, 42 kDa.

The antibiotic-selected HeLa (WT) and HeLa-D2 (FANCD2 deficient) plasmid-transfected cells were extracted following the protocols stated in Section 2.5.1., with the adjustments of using the RIPA lysis solution (Thermo Scientific), similar to the lysis buffer solution (Table 2.9), and quantified using the Pierce BCA protein assay kit (Thermo Scientific), similar to the methodology and concept of the Bradford assay. This was to verify that western blot complications were not due to the protein extraction and quantification. Also, while taking the opportunity of investigating the issue of NEIL3 immunoblotting from western blots, a control sample of mouse liver extract (Enzo Life Sciences; lane 10, Figure 3.43B) was also compared with the HeLa/-D2 transfected cell extracts. No significant differences were observed when comparing Pierce BCA protein assay with Bradford assay quantified extracts, and as it could be seen from the  $\beta$ -Actin results in Figure 3.43B(iv), there was no sample loading issue, as was expected. Unexpectedly, in Figure 3.43B(i – iii), no recombinant proteins were notably expressed in the intended transfected cells after antibiotic selection (lanes 3 – 5 and 7 – 9), either by NEIL3 or NEIL1 specific or FLAG-tagged antibodies (B[i – iii], respectively). What was mainly observed was non-specific antibiotic binding in Figure 3.43B(i) and (iii) (lanes 2 – 9) and no binding (B[ii]) in the expected kDa values of expressed recombinant proteins, based on the results viewed previously in Section 3.4.1. It may be possible for the more visible band at approximately 60 kDa to potentially be the recombinant NEIL3<sup>1506</sup>-FLAG in lanes 5 (Figure 3.43B[i]), but it is unlikely as it was not detected as extensively for the cell line counterpart (HeLa-D2) in lane 9 or by the FLAG-tag antibody (Figure 3.43B[iii]), and the same band size appears in lanes 2 – 9. Furthermore, of the immunoblotted proteins observed, only human  $\beta$ -Actin (Figure 3.43B(iv)) was visible from the transfected human cell extracts (lanes 2 – 9), and only NEIL3, NEIL1 at unexpectedly less than 44 kDa, and unexpectedly a FLAG-tagged protein, could be seen from the mouse liver extract control sample (Figure 3.43B[i – iii], respectively). This suggested the NEIL1, NEIL3 and FLAG antibodies were multispecies specific but preferred binding to mouse-specific protein. However, this also suggested that when compared to the results viewed and described in Section 3.4.1., the recombinant proteins were less visible when extracted more than 48 h after transfection.

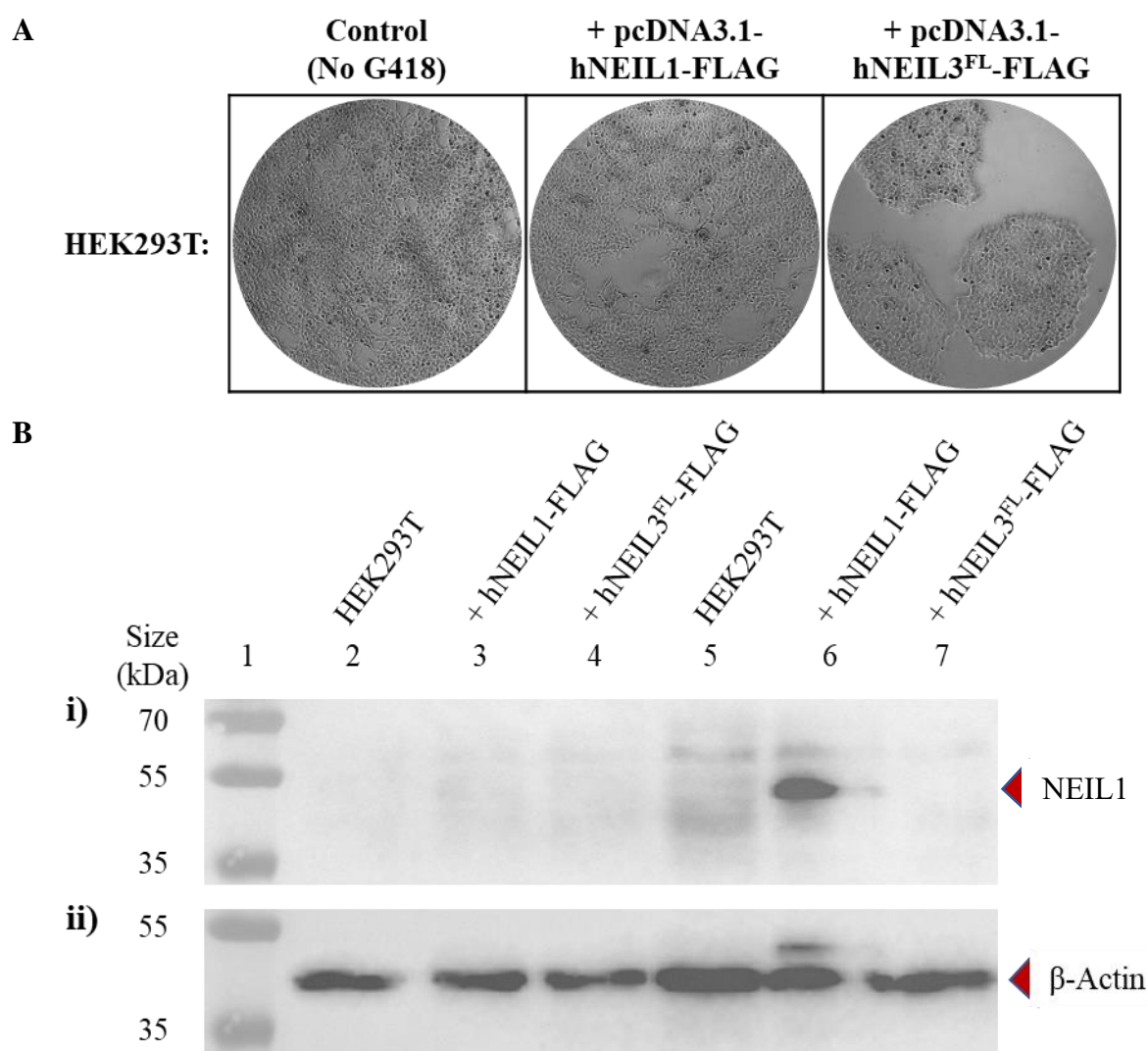


**Figure 3.44: Antibiotic-selection (A) and western blots on cell extracts (B) of plasmid-transfected HEK293T (WT). (B) i) FLAG-tag, and ii)  $\beta$ -Actin.**

Seventy-two-hour incubation with G418 (Roche) at 3.2 mg/ml, followed by recovery for 288 h (A) for cell extracts. (A) Results captured through microscope tablet camera (Android). (B) Membrane immunoblotted for FLAG-tag (i), followed by reblotting for  $\beta$ -Actin (ii). Samples of soluble protein were loaded at 30  $\mu$ g (lanes 2 – 4) and 20  $\mu$ l (lanes 5 – 7). Lane 1, protein ladder; lanes 2, 5, control; lanes 3, 6, pcDNA3.1-hNEIL1-FLAG; lanes 4, 7, pcDNA3.1-hNEIL3<sup>FL</sup>-FLAG. Expected molecular weight: hNEIL3<sup>FL</sup>-FLAG, 69 kDa; hNEIL1-FLAG, 53 kDa;  $\beta$ -Actin, 42 kDa.

Due to the lack of resources and time and the remaining empty vector (pcDNA3.1) stock prioritised for the FA-related cell lines cell-growth analysis after genotoxin treatment, the WT human embryonic kidney cells (HEK293T) were transfected only with the pcDNA3.1-hNEIL1-FLAG or pcDNA3.1-hNEIL3<sup>FL</sup>-FLAG plasmids. The antibiotic selected HEK293T cells transfected with pcDNA3.1-hNEIL1-FLAG were notably observed to have had a more prolonged recovery rate than the previously observed U2OS/-D2 and HeLa/-D2 plasmid-

transfected cells at approximately 92 h. Surprisingly, the pcDNA3.1-hNEIL3<sup>FL</sup>-FLAG transfected HEK293T cells had a significantly longer recovery time of 288 h to achieve at least  $1 \times 10^6$  cells for protein extraction. Due to the pcDNA3.1-hNEIL3<sup>FL</sup>-FLAG transfected HEK293T cells recovery time, antibiotic selection was repeated to ensure plasmid-transfection certainty. As displayed in Figure 3.44A, compared to the non-antibiotic selected control, the plasmid-transfected HEK293T cells were still viable after 72 h with 3.2 mg/ml G418 antibiotic selection and up to 288 h recovery. Furthermore, compared to the non-transfected cells, the survived pcDNA3.1-hNEIL1-FLAG transfected HEK293T cells appeared more abundant than the cells transfected with pcDNA3.1-hNEIL3<sup>FL</sup>-FLAG, as similarly observed and described previously from the plasmid-transfected and antibiotic-selected WT/FANCD2 deficient cancer cells (HeLa/-D2). This further suggested the potential complications of the pcDNA3.1-hNEIL3<sup>FL</sup>-FLAG plasmid transfection or hNEIL3<sup>FL</sup>-FLAG protein expression as observed previously, though not as drastically as displayed in the antibiotic selected and plasmid-transfected HeLa/-D2 cells (Figure 3.43A). Although the extended recovery time decreased the stability of the plasmids in the cells, the experiment continued for the recombinant-protein confirmation.

Following the cell extraction protocols described previously for the plasmid-transfected and antibiotic-selected HeLa/-D2 cells, compared to the standard loading of samples with a fixed quantified-protein concentration (30  $\mu$ g, lanes 2 – 4), an additional step of aliquoting a fixed volume of the protein-extract samples (lanes 5 – 7) was administered when considering potential sample loading issues, as displayed in Figure 3.44B. Based on the results observed from Figure 3.43B, only the immunoblotting with the FLAG-tag antibody (i) was used to target the expected recombinant proteins. Similar to the results observed from the plasmid transfected and antibiotic-selected HeLa (WT) and HeLa-D2 (FANCD2 deficient) cells described previously from Figure 3.43, the plasmid-transfected and antibiotic-selected HEK293T cells displayed no significant differences in protein quantification between the BCA protein assay kit and Bradford assay, as was expected. Furthermore, as it could be seen from the  $\beta$ -Actin results in Figure 3.44B(ii), no sample loading issues were observed in respect of their quantified sample loading (lanes 2 – 4 and 5 – 7, respectively), as was also expected. In Figure 3.44B(i), no recombinant proteins were notably expressed in the intended transfected cells after antibiotic selection from the 30  $\mu$ g loaded samples (lanes 2 and 3). However, recombinant protein expression was observed only from the pcDNA3.1-hNEIL1-FLAG transfected HEK293T cells from the 20  $\mu$ l of cell extract loaded (lane 6,

Figure 3.44B[i]), which contained approximately 120  $\mu$ g of cell extract. This suggested that after a prolonged recovery time after plasmid-transfection, the plasmid-transfect cells increasingly became difficult to observe for recombinant protein confirmation and, therefore, required more cell extract loaded or concentrated, or perhaps the recombinant protein expression was being suppressed as more time passed after transfection. Based on these observed results, the western blot was repeated for the transfected and antibiotic-selected WT (HeLa) and FANCD2 deficient (HeLa-D2) cancer cell extracts from Figure 3.43A with a fixed volume equating between approximately 75 – 120  $\mu$ g total quantified cell extract. However, the sample loading alteration displayed no substantial difference.

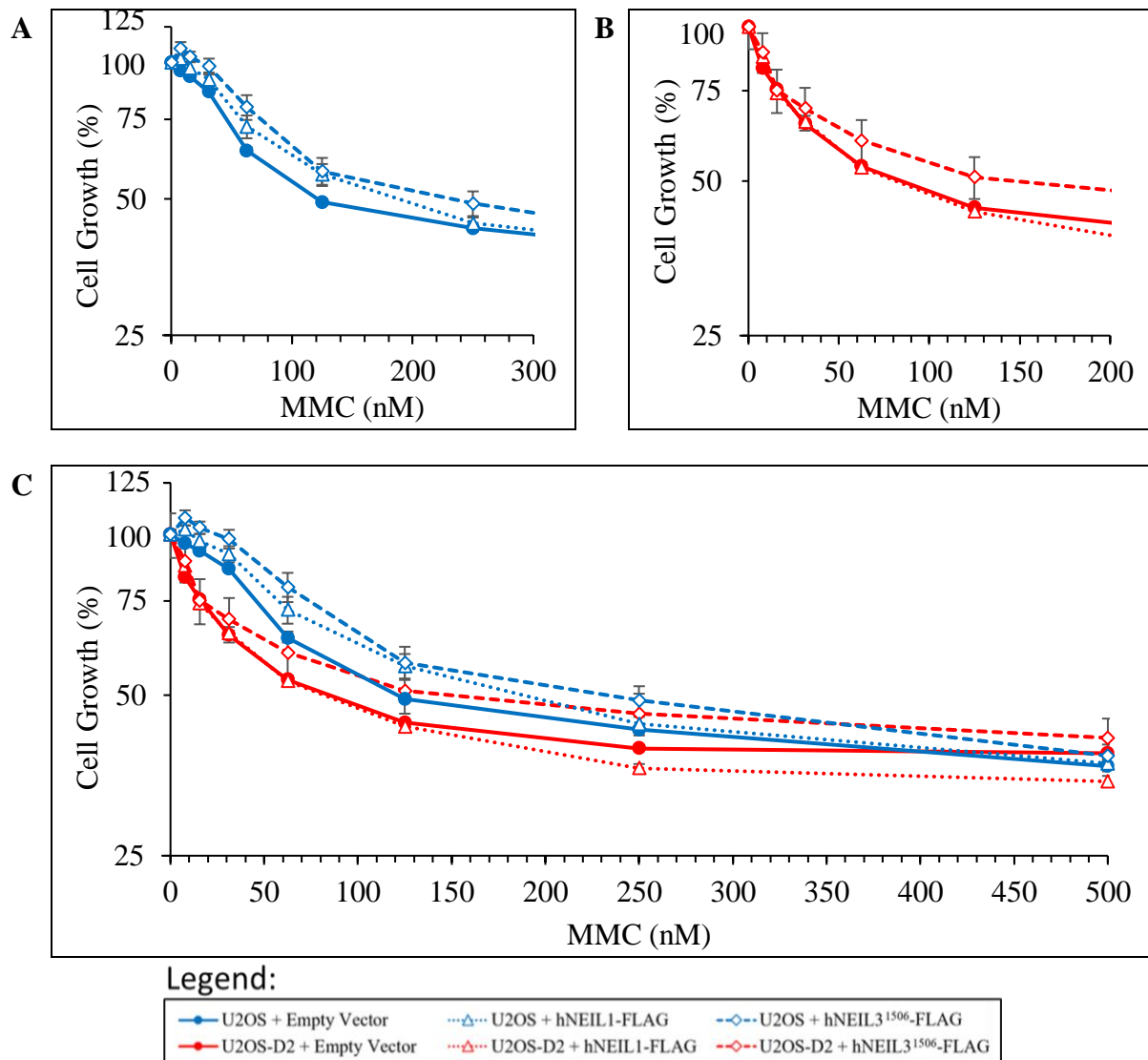
#### 3.4.4. Survival of Plasmid-Transfected Cells after Antibiotic-selection.

The plasmid-transfected and antibiotic-selected WT (U2OS and HeLa) and FANCD2 deficient (U2OS-D2 and HeLa-D2) cancer cells prepared from Section 3.4.3. were tested for survival after treatment with the ICL- and oxidative-inducing agents. Compared to the MTT assay results displayed in Figure 3.39 of the initial plasmid-transfected cell survival, the plasmid-transfected U2OS and U2OS-D2 cells after antibiotic selection were observed at a lower MMC concentration dilution range (from 2.5  $\mu$ M to 500 nM) for easier observation of difference in resistance and IC<sub>50</sub>, as displayed in Figure 3.45. As it was observed from the MTT assays of the non-transfected cells (Figure 3.12A) and empty-vector transfected cells (Figure 3.39), the empty-vector transfected and antibiotic selected U2OS-D2 cells still displayed susceptibility to MMC compared to the empty-vector transfected and antibiotic selected U2OS cells, as it was expected and displayed in Figure 3.45. However, unlike the MTT assay results displayed in Figures 3.25 and 3.39, the difference in MMC resistance observed between the transfected controls in Figure 3.45 was not as substantial as expected, based on their IC<sub>50</sub>. This suggested that the vector had affected the cells post-transfection, and therefore may have affected the growth curve of the cell lines to either require altering the cell count or incubation period before testing for cell growth.

The differences in resistance after plasmid transfection and antibiotic selection were significantly different in Figure 3.45 than observed from the plasmid transfected cells displayed in Figure 3.39. This suggested that all the plasmid-transfected cells prepared in Section 3.4.3. were guaranteed as transfected after antibiotic selection, and although recombinant protein expression was not confirmed, it was evident that an effect was

observed. Compared to the IC<sub>50</sub> of the empty-vector transfected control in Figure 3.45, the U2OS-D2 (FANCD2 deficient) cells displayed no significant difference in susceptibility to MMC when transfected with pcDNA3.1-hNEIL1-FLAG (IC<sub>50</sub> 95 nM and 89 nM). When transfected with the pcDNA3.1-hNEIL3<sup>1506</sup>-FLAG plasmid, a substantial increase in resistance was observed from the U2OS-D2 cells (IC<sub>50</sub> 136 nM), though statistically difficult to accept the significance as the standard deviation implies the imprecision to be too great. The U2OS (WT) cells displayed increased resistance to MMC from empty-vector transfection to pcDNA3.1-hNEIL1-FLAG plasmid transfection (IC<sub>50</sub> 163 nM and 209 nM), which substantially increased in resistance when transfected with the pcDNA3.1-hNEIL3<sup>1506</sup>-FLAG plasmid (IC<sub>50</sub> 255 nM). Interestingly, the pcDNA3.1-hNEIL3<sup>1506</sup>-FLAG transfected U2OS-D2 cells displayed almost the same resistance to MMC as the empty-vector transfected U2OS cells.

Similar to the MMC resistance observed in Figure 3.45, there was a significant increase in resistance to cisplatin observed in Figure 3.45 for the plasmid-transfected WT/FANCD2 deficient (U2OS/-D2) cancer cells after antibiotic selection when compared to the plasmid-transfected cells observed in Figure 3.40. As it was observed from the MTT assays of the non-transfected cells (Figure 3.13B) and empty-vector transfected cells (Figure 3.40), the antibiotic selected and empty-vector transfected U2OS-D2 cells displayed in Figure 3.46 still displayed susceptibility to cisplatin compared to the empty-vector transfected and antibiotic selected U2OS cells, as it was expected. In Figure 3.46, compared to the empty-vector transfected U2OS cells IC<sub>50</sub>, an increase in resistance to cisplatin was observed when plasmid-transfected with pcDNA3.1-hNEIL3<sup>1506</sup>-FLAG (IC<sub>50</sub> 1.44 μM and 1.95 μM) or pcDNA3.1-hNEIL1-FLAG (IC<sub>50</sub> 1.88 μM). Similarly to the plasmid-transfected U2OS-D2 cells displayed in Figure 3.45, the FANCD2 deficient (U2OS-D2) cells in Figure 3.46 displayed little difference in susceptibility to cisplatin when transfected with pcDNA3.1-hNEIL1-FLAG (IC<sub>50</sub> 0.91 μM and 0.92 μM), but a substantial increase in resistance when transfected with pcDNA3.1-hNEIL3<sup>1506</sup>-FLAG (IC<sub>50</sub> 1.77 μM). Interestingly, compared to the rest of the transfected cells observed in Figure 3.46, the pcDNA3.1-hNEIL3<sup>1506</sup>-FLAG transfected U2OS-D2 cells displayed the highest resistance to cisplatin.

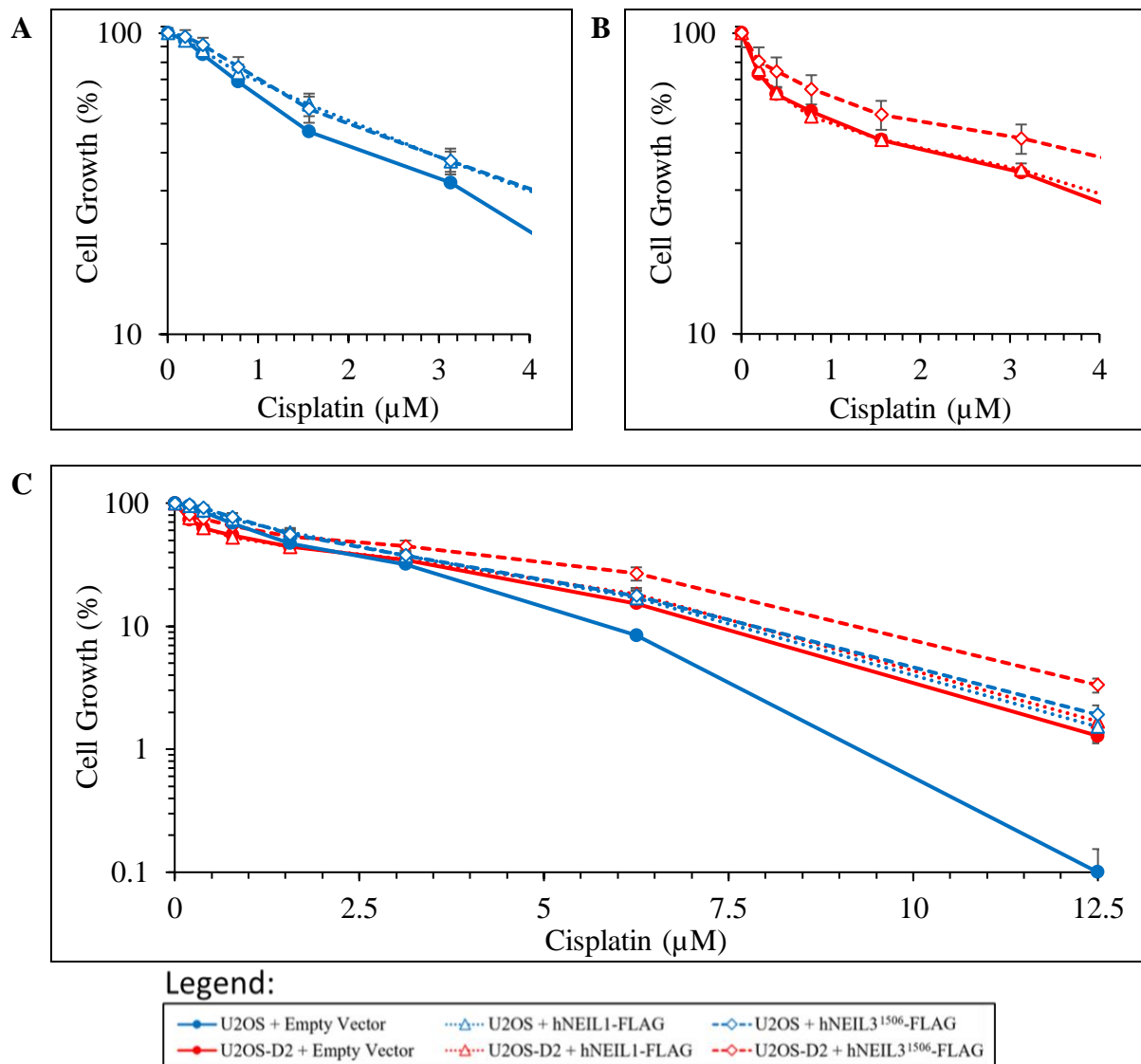


**D**

		IC <sub>50</sub> ± SD Values
U2OS	+ Empty Vector	163 ± 20.24 nM
	+ hNEIL1-FLAG	209 ± 44.14 nM
	+ hNEIL3 <sup>1506</sup> -FLAG	255 ± 74.67 nM
U2OS-D2	+ Empty Vector	95 ± 17.97 nM
	+ hNEIL1-FLAG	89 ± 17.58 nM
	+ hNEIL3 <sup>1506</sup> -FLAG	136 ± 93.97 nM

**Figure 3.45: Growth inhibition of antibiotic selected (A) U2OS (WT, blue) and (B) U2OS-D2 (FANCD2 deficient, red), and their comparison (C), following treatment with mitomycin C.**

**D)** IC<sub>50</sub> values for growth inhibition following treatment. Cells were transfected with empty vector, pcDNA3.1-hNEIL1-FLAG or pcDNA3.1-hNEIL3<sup>1506</sup>-FLAG, followed by antibiotic-selection (G418, Gibco) for 96 h. 1 × 10<sup>3</sup> cells per well, incubated for 96 h. Mean data was collected from triplicate technical repeats within two scientific repeats.



**D**

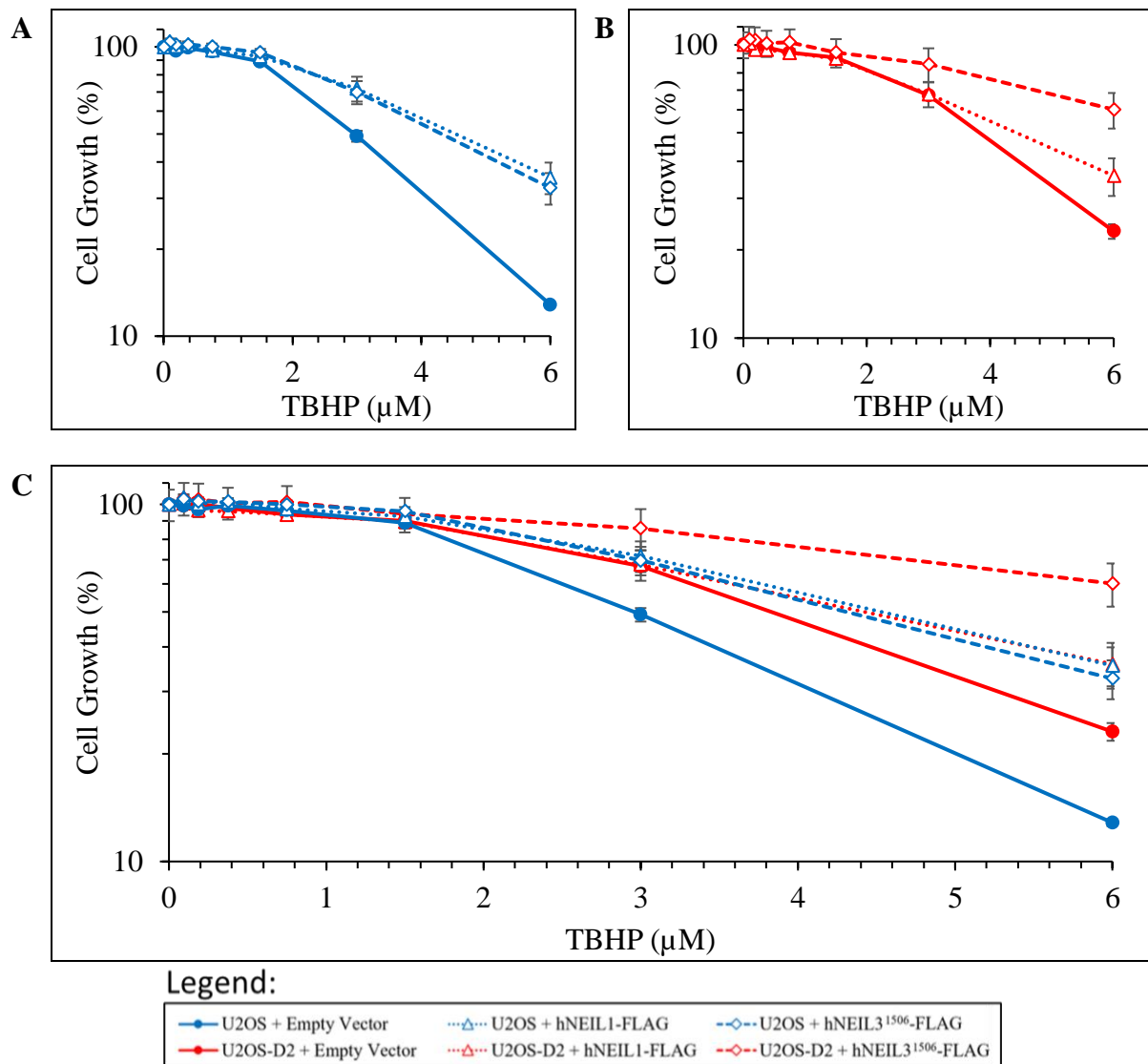
		IC <sub>50</sub> ±SD Values
U2OS	+ Empty Vector	1.44 ± 0.09 μM
	+ hNEIL1-FLAG	1.88 ± 0.37 μM
	+ hNEIL3 <sup>1506</sup> -FLAG	1.95 ± 0.47 μM
U2OS-D2	+ Empty Vector	0.91 ± 0.11 μM
	+ hNEIL1-FLAG	0.92 ± 0.20 μM
	+ hNEIL3 <sup>1506</sup> -FLAG	1.77 ± 1.39 μM

**Figure 3.46: Growth inhibition of antibiotic selected (A) U2OS (WT, blue) and (B) U2OS-D2 (FANCD2 deficient, red), and their comparison (C), following treatment with cisplatin.**

**D)** IC<sub>50</sub> values for growth inhibition following treatment. Cells were transfected with empty vector, pcDNA3.1-hNEIL1-FLAG or pcDNA3.1-hNEIL3<sup>1506</sup>-FLAG, followed by antibiotic-selection (G418, Gibco) for 96 h. 1 x 10<sup>3</sup> cells per well, incubated for 96 h. Mean data was collected from triplicate technical repeats within two scientific repeats.

Similarly to the MMC and cisplatin resistances observed in Figures 3.45 and 3.46, respectively, there was a significant increase in resistance to TBHP for the plasmid-transfected U2OS (WT) and U2OS-D2 (FANCD2 deficient) cancer cells after antibiotic selection, as it could be seen in Figure 3.47 compared to the plasmid-transfected cells observed in Figure 3.41. Contrary to Figure 3.41, Figure 3.47 unexpectedly showed that the empty-vector transfected U2OS cells were more susceptible to the oxidative inducing agent TBHP than the equally transfected U2OS-D2 cells. However, as it was observed in the MMC resistance comparison of the MTT assays in Figure 3.45 with Figures 3.25 and 3.39, the transfected vector may have affected the cells post-transfection, and therefore the reaction may have affected the growth curve of the cell lines to either suggest altering the cell count or incubation period before testing for cell growth. Therefore, it was considered more appropriate to observe the differences in TBHP susceptibility/resistance in Figure 3.47 based on the transfected-plasmid than based on the FA phenotype as a whole.

Compared to the  $IC_{50}$  of the empty-vector transfected control in Figure 3.47, the U2OS (WT) cells displayed an increase in resistance to the oxidative inducing agent TBHP when transfected with the pcDNA3.1-hNEIL3<sup>1506</sup>-FLAG ( $IC_{50}$  2.96  $\mu$ M and 4.31  $\mu$ M) or the pcDNA3.1-hNEIL1-FLAG plasmid ( $IC_{50}$  4.55  $\mu$ M). The U2OS-D2 (FANCD2 deficient) cells displayed increased resistance to TBHP from the transfected empty-vector control to the pcDNA3.1-hNEIL1-FLAG transfected cells ( $IC_{50}$  3.84  $\mu$ M and 4.50  $\mu$ M), which substantially increased in resistance when transfected with the pcDNA3.1-hNEIL3<sup>1506</sup>-FLAG plasmid ( $IC_{50}$  >6.00  $\mu$ M). Despite the contradiction in TBHP resistance and susceptibility orientation between the U2OS and U2OS-D2 cell lines, similar to what was observed from the increased resistance to MMC (Figure 3.45) and cisplatin (Figure 3.46), the pcDNA3.1-hNEIL3<sup>1506</sup>-FLAG transfected U2OS-D2 cells in Figure 3.47 displayed more resistance to TBHP than the empty-vector transfected U2OS cells.



**D**

		IC <sub>50</sub> ±SD Values
U2OS	+ Empty Vector	2.96 ± 0.14 μM
	+ hNEIL1-FLAG	4.55 ± 0.89 μM
	+ hNEIL3 <sup>1506</sup> -FLAG	4.31 ± 0.66 μM
U2OS-D2	+ Empty Vector	3.84 ± 0.24 μM
	+ hNEIL1-FLAG	4.50 ± 1.21 μM
	+ hNEIL3 <sup>1506</sup> -FLAG	>6.00 μM

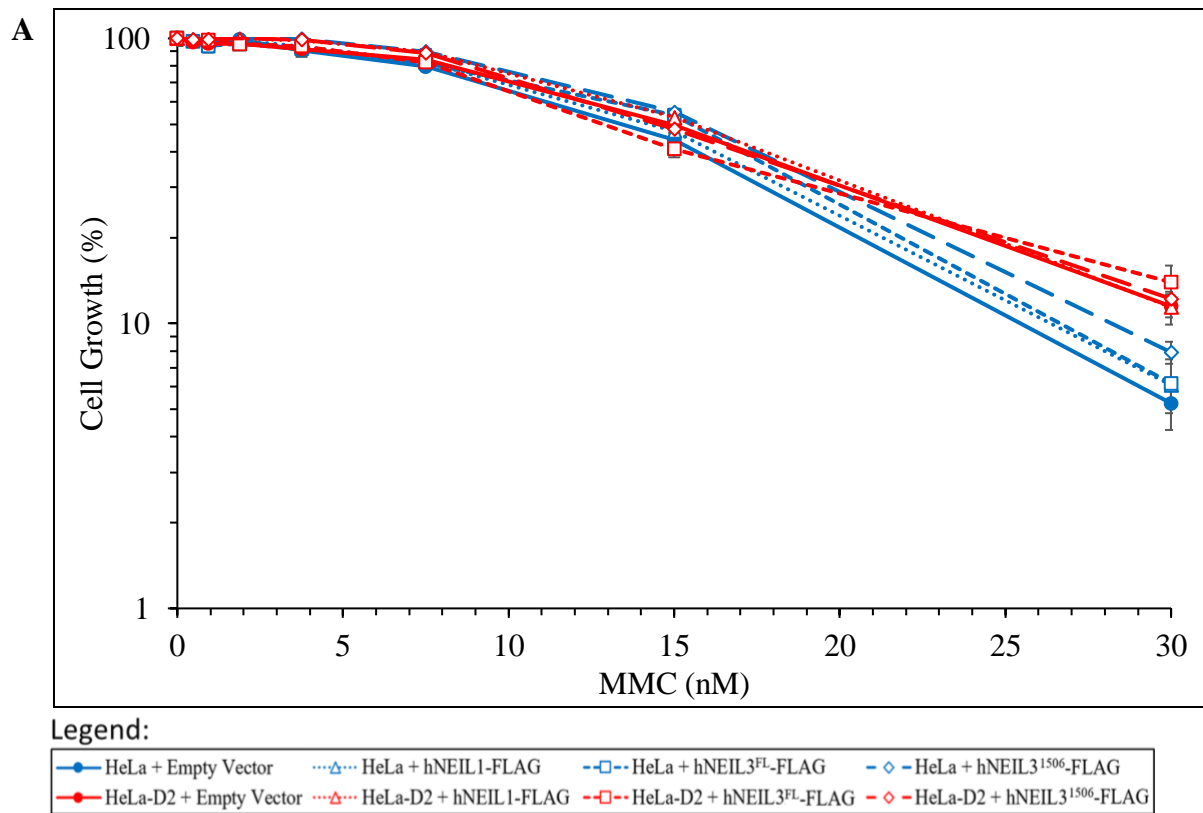
**Figure 3.47: Growth inhibition of antibiotic selected (A) U2OS (WT, blue) and (B) U2OS-D2 (FANCD2 deficient, red), and their comparison (C), following treatment with TBHP.**

**D)** IC<sub>50</sub> values for growth inhibition following treatment. Cells were transfected with empty vector, pcDNA3.1-hNEIL1-FLAG or pcDNA3.1-hNEIL3<sup>1506</sup>-FLAG, followed by antibiotic-selection (G418, Gibco) for 96 h. 1 × 10<sup>3</sup> cells per well, incubated for 96 h. Mean data was collected from triplicate technical repeats within two scientific repeats.

Considering the results observed from the U2OS (WT) and U2OS-D2 (FANCD2 deficient) cells in Figures 3.45 – 3.47 were based from two scientific repeats, the third scientific repeat was prioritised for the cancer cells HeLa (WT) and HeLa-D2 (FANCD2 deficient) in order to maintain a diverse observation of results for comparison. Unexpectedly, the plasmid transfected and antibiotic selected HeLa and HeLa-D2 cells displayed in Figures 3.48 – 3.50 displayed their resistance and susceptibility to MMC (Figure 3.48), cisplatin (Figure 3.49) and TBHP (Figure 3.50) in the reverse orientation of the genotoxic agent sensitivity expectedly observed in Figures 3.14 and 3.38. However, similar to what was observed in Figure 3.47, the transfected vector may suggest the expression reaction had affected the growth curve of the cell lines, and therefore may have required altering the incubation period before testing for cell growth. Therefore, it was considered more appropriate to observe the differences in ICL- and oxidative-induced susceptibility/resistance in Figures 3.48 – 3.50 based on the transfected-plasmids than based on the FA phenotype as a whole. Compared to the MTT assay results displayed in Figure 3.38 of the initial plasmid-transfected cell growth, the plasmid-transfected HeLa and HeLa-D2 cells after antibiotic selection were observed to have had more notable differences in resistance, but not as substantial as the observed differences described previously between former and post-antibiotic selected U2OS/-D2 cells after plasmid transfection (Figures 3.35 – 3.37 and 3.41 – 3.43, respectively).

As it could be seen in Figure 3.48, compared to the  $IC_{50}$  of the empty-vector transfected HeLa (WT) cells, a notable difference of resistance to MMC was observed when transfected with the pcDNA3.1-hNEIL1-FLAG ( $IC_{50}$  13.4 nM and 14.3 nM), pcDNA3.1-hNEIL3<sup>FL</sup>-FLAG ( $IC_{50}$  15.5 nM), or pcDNA3.1-hNEIL3<sup>1506</sup>-FLAG ( $IC_{50}$  15.8 nM) plasmid. Similarly, the FANCD2 deficient (HeLa-D2) cells displayed a notable difference in resistance to MMC when transfected with the pcDNA3.1-hNEIL1-FLAG plasmid ( $IC_{50}$  14.9 nM and 15.6 nM). However, a notable difference in susceptibility to MMC was observed from the pcDNA3.1-hNEIL3<sup>1506</sup>-FLAG ( $IC_{50}$  14.5 nM) and pcDNA3.1-hNEIL3<sup>FL</sup>-FLAG ( $IC_{50}$  12.9 nM) transfected HeLa-D2 cells. Comparing the WT and FANCD2 deficient cells observed in Figures 3.45 (U2OS and U2OS-D2, respectively) and 3.48 (HeLa and HeLa-D2, respectively), the WT cells displayed increased resistance to MMC when expressing hNEIL1-FLAG or more when expressing hNEIL3<sup>FL</sup>-FLAG or hNEIL3<sup>1506</sup>-FLAG, but FANCD2 deficient cells displayed resistance to MMC inconsistently when expressing hNEIL1-FLAG (Figure 3.48) or hNEIL3<sup>1506</sup>-FLAG (Figure 3.45). In summary of the results

analysed from Figure 3.48, no significant difference was observed from the plasmid transfected and antibiotic selected HeLa and HeLa-D2 cells.



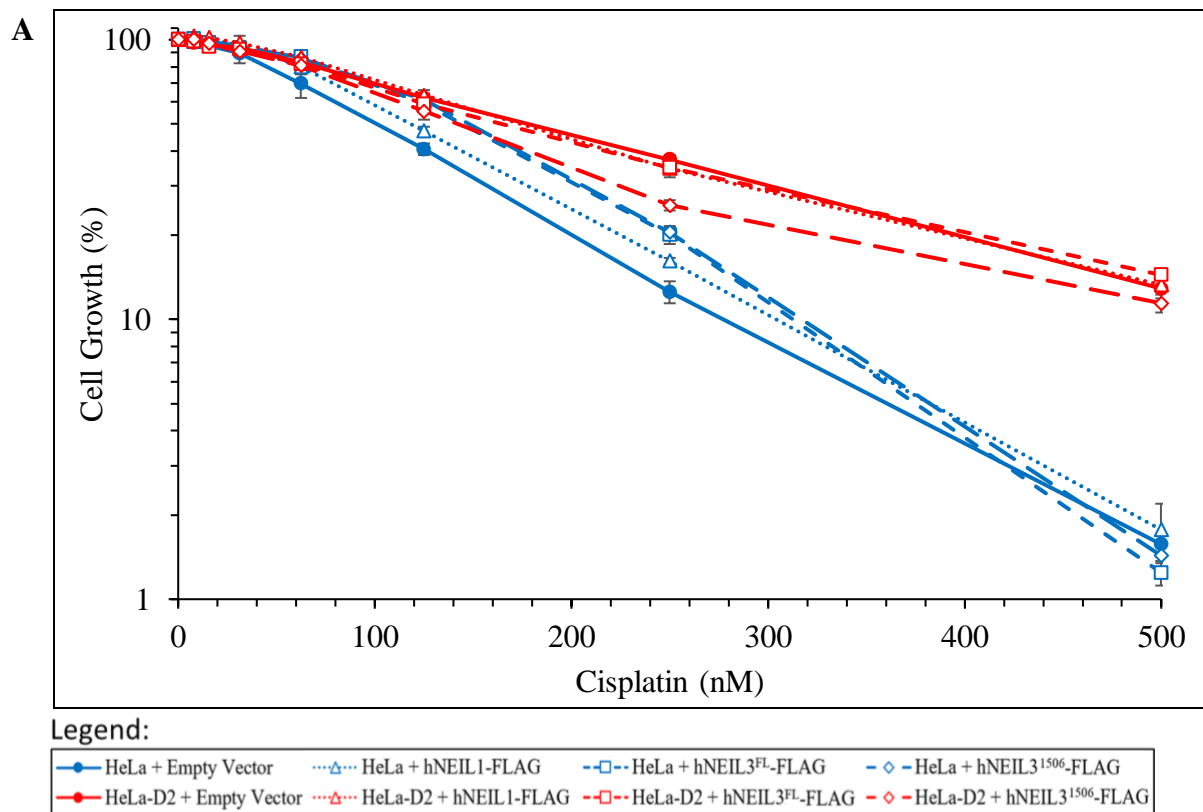
**B**

		IC <sub>50</sub> ±SD Values
HeLa	+ Empty Vector	13.4 ± 1.06 nM
	+ hNEIL1-FLAG	14.3 ± 0.81 nM
	+ hNEIL3 <sup>FL</sup> -FLAG	15.5 ± 1.06 nM
	+ hNEIL3 <sup>1506</sup> -FLAG	15.8 ± 0.57 nM
HeLa-D2	+ Empty Vector	14.9 ± 0.84 nM
	+ hNEIL1-FLAG	15.6 ± 0.61 nM
	+ hNEIL3 <sup>FL</sup> -FLAG	12.9 ± 0.70 nM
	+ hNEIL3 <sup>1506</sup> -FLAG	14.5 ± 0.57 nM

**Figure 3.48: Growth inhibition of antibiotic selected HeLa (WT, blue) and HeLa-D2 (FANCD2 deficient, red), following treatment with mitomycin C.**

**B)** IC<sub>50</sub> values for growth inhibition following treatment. Cells were transfected with empty vector, pcDNA3.1-hNEIL1-FLAG, pcDNA3.1-hNEIL3<sup>FL</sup>-FLAG or pcDNA3.1-hNEIL3<sup>1506</sup>-FLAG, followed by antibiotic-selection (G418, Roche) for 72 h. 5 × 10<sup>2</sup> cells per well, incubated for 168 h. Mean data was collected from triplicate technical repeats.

Similar to the MMC results observed in Figure 3.48, compared to the IC<sub>50</sub> of the empty-vector transfected HeLa (WT) cells in Figure 3.49, a notable progressive difference of resistance to cisplatin was observed when transfected with the pcDNA3.1-hNEIL1-FLAG (IC<sub>50</sub> 97 nM and 118 nM), pcDNA3.1-hNEIL3<sup>FL</sup>-FLAG (IC<sub>50</sub> 144 nM), or pcDNA3.1-hNEIL3<sup>1506</sup>-FLAG (IC<sub>50</sub> 148 nM) plasmid. However, contrary to the plasmid-transfected WT cells, the FANCD2 deficient cells (HeLa-D2) displayed notable differences in susceptibility to cisplatin when transfected with the pcDNA3.1-hNEIL1-FLAG (IC<sub>50</sub> 170 nM and 174 nM), pcDNA3.1-hNEIL3<sup>1506</sup>-FLAG (IC<sub>50</sub> 165 nM) or pcDNA3.1-hNEIL3<sup>FL</sup>-FLAG (IC<sub>50</sub> 139 nM) plasmid. Compared to the WT and FANCD2 deficient cells observed in Figure 3.46 (U2OS and U2OS-D2, respectively), the WT cells displayed increased resistance to cisplatin when expressing hNEIL1-FLAG, hNEIL3<sup>FL</sup>-FLAG or hNEIL3<sup>1506</sup>-FLAG. However, the FANCD2 deficient cells displayed resistance to cisplatin inconsistently when expressing hNEIL1-FLAG (Figure 3.46), or contradictory to what was theorised, regardless of the recombinant protein expressed (Figure 3.49). Similar to the observations of the growth inhibition MTT assays with MMC (Figure 3.48), the results analysed from Figure 3.49 displayed no significant difference in resistance or susceptibility to cisplatin when HeLa and HeLa-D2 cells were plasmid transfected and antibiotic selected.

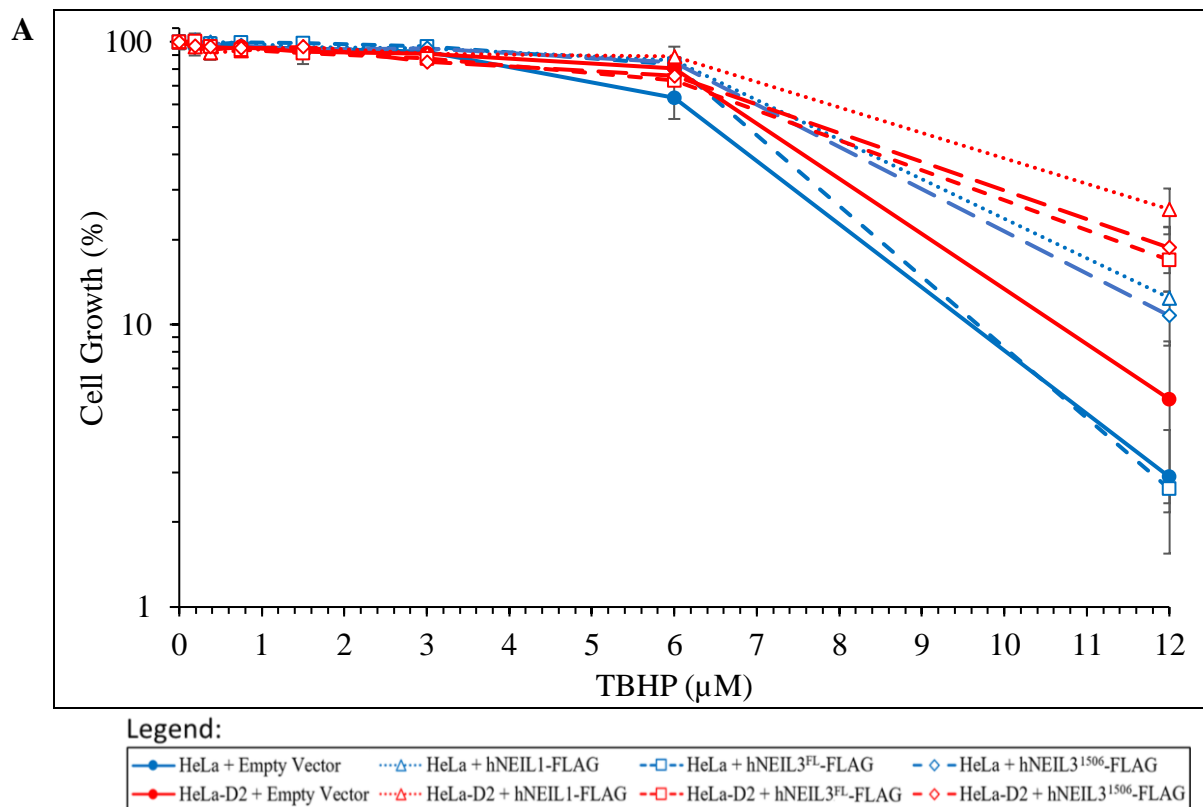


**B**

		IC <sub>50</sub> ±SD Values
HeLa	+ Empty Vector	97 ± 7.49 nM
	+ hNEIL1-FLAG	118 ± 7.16 nM
	+ hNEIL3 <sup>FL</sup> -FLAG	144 ± 7.38 nM
	+ hNEIL3 <sup>1506</sup> -FLAG	148 ± 6.72 nM
HeLa-D2	+ Empty Vector	170 ± 8.53 nM
	+ hNEIL1-FLAG	174 ± 8.53 nM
	+ hNEIL3 <sup>FL</sup> -FLAG	165 ± 8.44 nM
	+ hNEIL3 <sup>1506</sup> -FLAG	139 ± 9.37 nM

**Figure 3.49: Growth inhibition of antibiotic selected HeLa (WT, blue) and HeLa-D2 (FANCD2 deficient, red), following treatment with cisplatin.**

**B)** IC<sub>50</sub> values for growth inhibition following treatment. Cells were transfected with empty vector, pcDNA3.1-hNEIL1-FLAG, pcDNA3.1-hNEIL3<sup>FL</sup>-FLAG or pcDNA3.1-hNEIL3<sup>1506</sup>-FLAG, followed by antibiotic-selection (G418, Roche) for 72 h. 5 × 10<sup>2</sup> cells per well, incubated for 168 h. Mean data was collected from triplicate technical repeats.



**B**

		IC <sub>50</sub> ± SD Values
HeLa	+ Empty Vector	6.46 ± 0.41 µM
	+ hNEIL1-FLAG	8.38 ± 0.41 µM
	+ hNEIL3 <sup>FL</sup> -FLAG	7.40 ± 0.32 µM
	+ hNEIL3 <sup>1506</sup> -FLAG	8.15 ± 0.35 µM
HeLa-D2	+ Empty Vector	7.59 ± 1.66 µM
	+ hNEIL1-FLAG	9.49 ± 0.04 µM
	+ hNEIL3 <sup>FL</sup> -FLAG	7.74 ± 0.84 µM
	+ hNEIL3 <sup>1506</sup> -FLAG	7.99 ± 0.57 µM

**Figure 3.50: Growth inhibition of antibiotic selected HeLa (WT, blue) and HeLa-D2 (FANCD2 deficient, red), following treatment with TBHP.**

**B)** IC<sub>50</sub> values for growth inhibition following treatment. Cells were transfected with empty vector, pcDNA3.1-hNEIL1-FLAG, pcDNA3.1-hNEIL3<sup>FL</sup>-FLAG or pcDNA3.1-hNEIL3<sup>1506</sup>-FLAG, followed by antibiotic selection (G418, Roche) for 72 h.  $5 \times 10^2$  cells per well, incubated for 168 h. Mean data was collected from triplicate technical repeats.

In figure 3.50, the MTT assay results of the antibiotic selected and plasmid-transfected WT and FANCD2 deficient cells (HeLa and HeLa-D2, respectively) were observed as similar to the plasmid-transfected cells results prior to antibiotic selection (Figure 3.38C). Similar to the MTT assay results after cisplatin treatment (Figure 3.49), compared to the IC<sub>50</sub> of the

empty-vector transfected HeLa cells in Figure 3.50, a notable increase in resistance to TBHP was observed when transfected with the pcDNA3.1-hNEIL3<sup>FL</sup>-FLAG (IC<sub>50</sub> 6.46 μM and 7.40 μM), pcDNA3.1-hNEIL1-FLAG (IC<sub>50</sub> 8.38 μM), or pcDNA3.1-hNEIL3<sup>1506</sup>-FLAG (IC<sub>50</sub> 8.15 μM) plasmid. Correspondingly, the HeLa-D2 cells (FANCD2 deficient) also displayed notable differences in resistance to TBHP when transfected with the pcDNA3.1-hNEIL3<sup>FL</sup>-FLAG (IC<sub>50</sub> 7.59 μM and 7.74 μM), pcDNA3.1-hNEIL3<sup>1506</sup>-FLAG (IC<sub>50</sub> 7.99 μM) or pcDNA3.1-hNEIL1-FLAG (IC<sub>50</sub> 9.49 μM) plasmid. However, compared to the growth inhibition MTT assays observed with MMC (Figure 3.48) and cisplatin (Figure 3.49), the cancer cell lines HeLa and HeLa-D2 were observed to have had no significant difference in TBHP resistance (Figure 3.50) when plasmid transfected and antibiotic selected. Contrary to what was observed and described previously, when comparing the HeLa/-D2 cells (Figure 3.50) to the U2OS and U2OS-D2 cells (WT and FANCD2 deficient, respectively) observed in Figure 3.47, both the WT and FANCD2 deficient cells displayed increased resistance to TBHP when expressing hNEIL1-FLAG, hNEIL3<sup>FL</sup>-FLAG or hNEIL3<sup>1506</sup>-FLAG protein. This suggested that the overexpression of the DNA glycosylases NEIL1 and NEIL3 were consistent with the repair to oxidative damage, as was expected, and therefore the recombinant proteins must have been expressed in the plasmid transfected cells.

### 3.5. Survival of PD20 and 3.15 Cells after Gene-Specific Knockdown

Based on the gene and protein expression studies and plasmid transfection results observed in Sections 3.2.3. (Figures 3.14 and 3.17) and 3.4.1. (Figures 3.31 and 3.34 – 3.37), the FA cell lines PD20 and 3.15 were prioritised for siRNA transfection studies and their survival after genotoxin treatment. The aims and objectives for this work was to transfect the FA and FA corrected cell lines PD20 and 3.15, respectively, with siRNA to knockdown NEIL3 and TRIM26, confirm the reduced expression, and determine the potential roles of NEIL3 and TRIM26 underexpression under genotoxin treatment. It was also to determine if by the diminished expression of the proteins related to the FA and BER pathways, the cells would enter synthetic lethality, a combination of mutated partner genes with a synthetic lethal interaction stressing cells to death (O’Neil, Bailey and Hieter, 2017). Due to the lack of time and resources and the previously described qRT-PCR and western blot issues, the siRNA studies were confirmed through western blot and image analysis of the RT-PCR results, during and after the completion of the siRNA transfected cell survival after genotoxin

treatments. Due to further complications of analysing all expressions of interest from western blots as well as RT-PCR, TRIM26 and GAPDH knockdown was confirmed through western blot, and NEIL3 knockdown and alterations to NEIL1 and NEIL3 expression were prioritised and confirmed through RT-PCR.

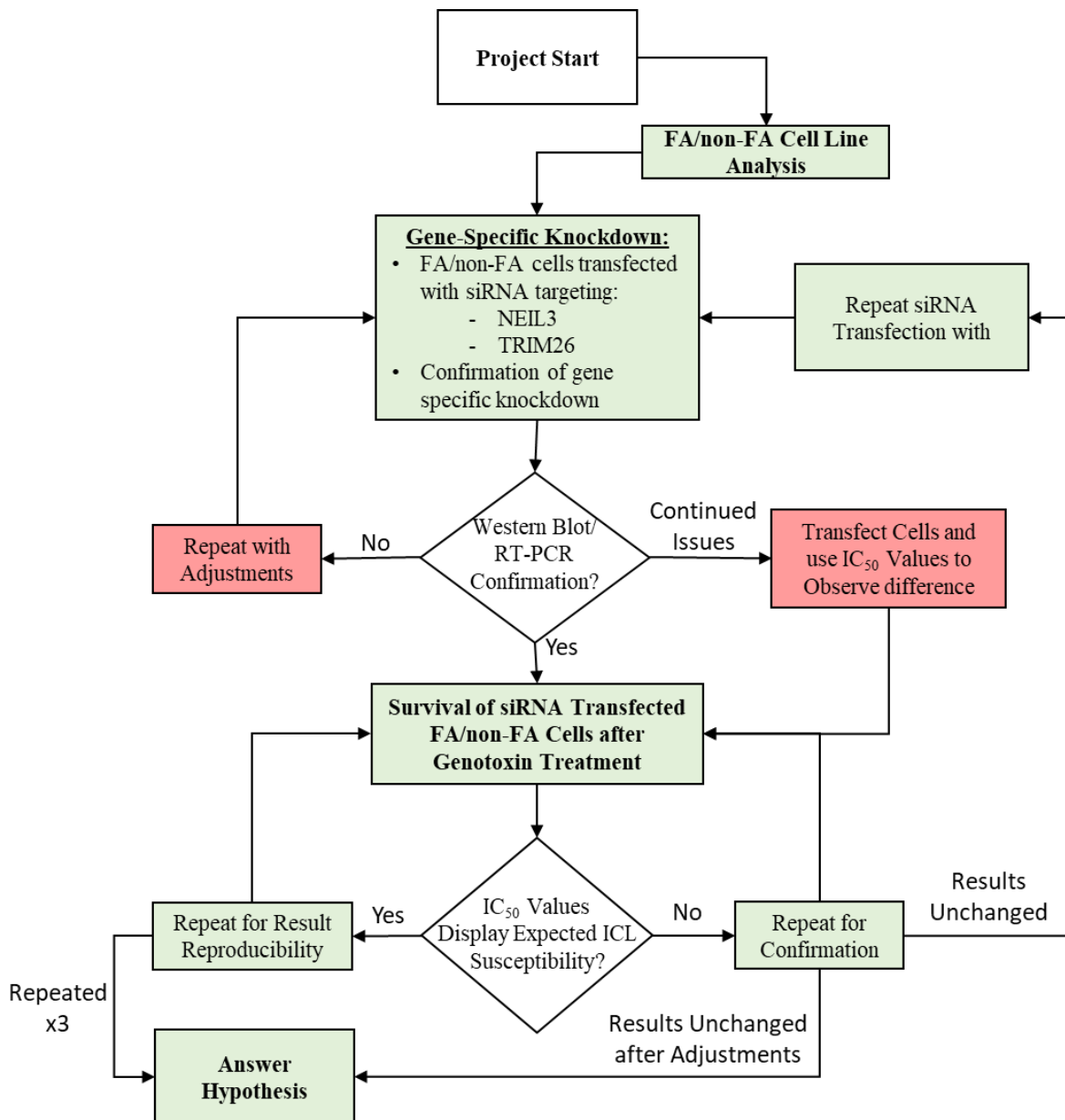


**Figure 3.51: Flowchart on the approach to siRNA transfection and cell survivability work.**

Expanded subsection of the overall flowchart displayed in Section 1.6 (Figure 1.11). Red highlights, issues encountered; green highlights, results achieved.

As displayed in Figure 3.51, similar to the approach displayed in Figure 3.30, the aims and objectives of Section 3.5 are planned according to the approach to the work displayed in the

flow chart. During the remainder of the time and resources available, the results for the siRNA transfected cells were displayed in Section 3.5.1. for NEIL3 and TRIM26 expression knockdown confirmation, and Section 3.5.2. for the survival of siRNA transfected cells after genotoxin treatment. The unexpected but intriguing results allowed the project to interpret the results to answer the hypothesis.

### 3.5.1. Evidence of NEIL3 and TRIM26 Protein and mRNA Knockdown

Compared to the non-transfected (lane 2) and non-specific (NS, lane 3) siRNA transfected controls in Figure 3.52A and B, a reduction in expression was observed from the knockdown of GAPDH control (lane 4, [ii]) and TRIM26 (lane 6, [i]), as expected, for both the FANCD2 deficient (PD20, A) and corrected (3.15, B) cells. Although a noticeable band could be observed at approximately 30 kDa across all samples in Figure 3.52A(ii), it was most likely degraded GAPDH as the same additional band could not be observed in the GAPDH knockdown sample (lane 4). Based on the image analysis of Figure 3.52A and B, and their signal intensity factors displayed in Figure 3.52C and D, respectively, compared to their respective protein expressed in the NS siRNA transfected controls, the PD20 cells (Figure 3.52C) displayed an approximate 40% knockdown in GAPDH when transfected with GAPDH siRNA, and an approximate 90% knockdown in TRIM26 when transfected with TRIM26 siRNA. Similarly, compared to their respective protein expressed in the NS siRNA transfected controls, the 3.15 cells (FANCD2 corrected, Figure 3.52D) were observed to have had an approximate 50% knockdown in GAPDH when transfected with GAPDH siRNA, and an approximate 70% knockdown in TRIM26 when transfected with TRIM26 siRNA.

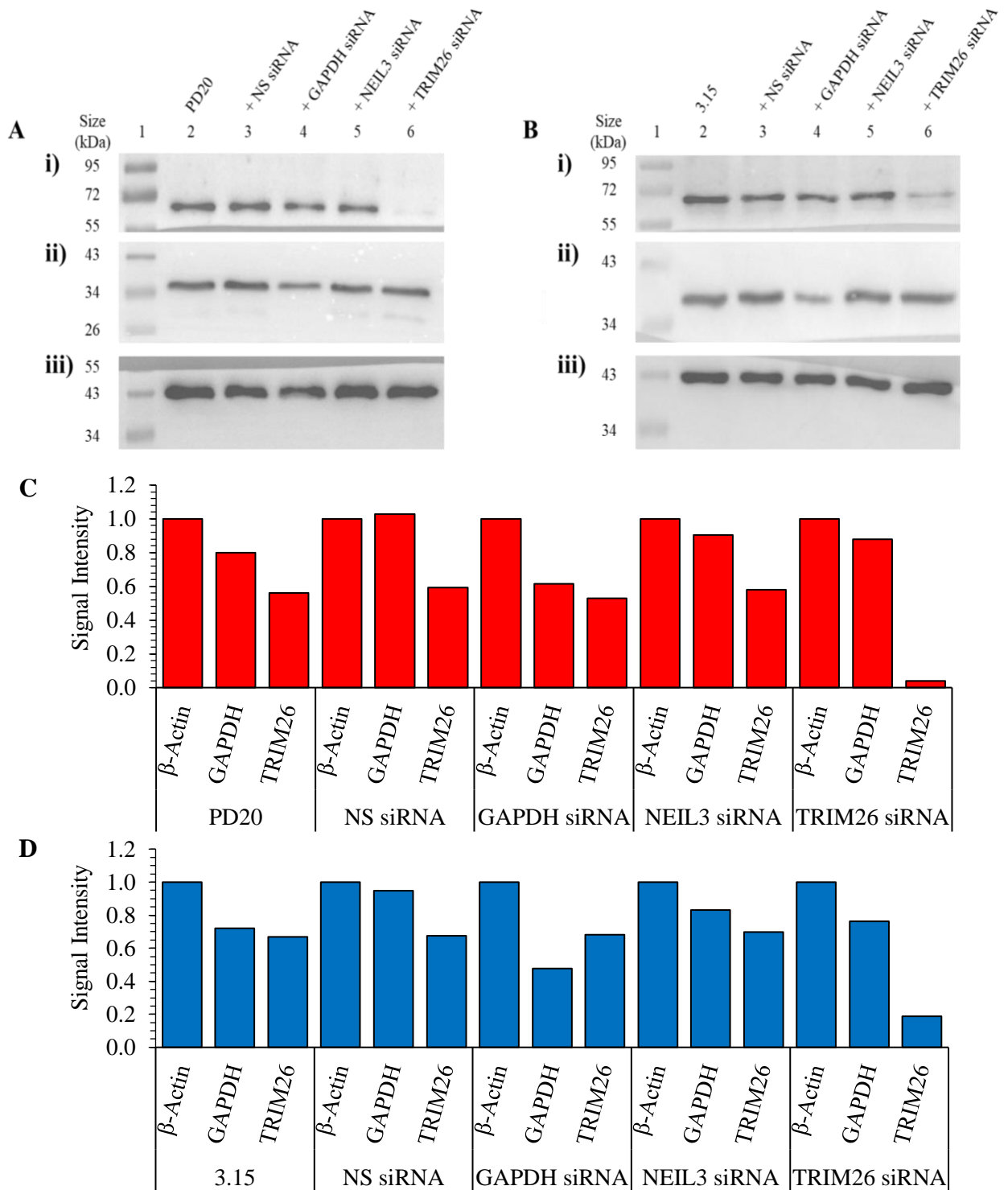


**Figure 3.52: Western blots of siRNA-transfected A) PD20 (FANCD2 Deficient) and B) 3.15 (PD20 corrected) cell extracts. (A, B) (i) TRIM26, (ii) GAPDH, and (iii)  $\beta$ -Actin.**

(A, B) Lane 1, protein ladder; lane 2, control; lane 3, non-specific (NS) siRNA; lane 4, GAPDH siRNA; lane 5, NEIL3 siRNA; lane 6, TRIM26 siRNA. Expected molecular weight: TRIM26, 62 kDa; GAPDH, 36 kDa;  $\beta$ -Actin, 42 kDa. (C, D) Quantified signal intensity from chemiluminescence in sections A and B (respectively) relative to the cells'  $\beta$ -Actin expression, based on one technical and scientific replicate.

The DNA glycosylases NEIL1 and NEIL3 protein expressions were not visible through western blot, and therefore mRNA expression was analysed through RT-PCR. Due to the lack of time and resources and based on the results described previously, RT-PCR was prioritised on the analysis of *NEIL1* and *NEIL3* expression only. As it could be observed from Figures 3.56A and 3.53A the expected amplicon sizes appear larger than expected for *β-Actin* (166 bp), *NEIL1* (212 bp) and *NEIL3* (147 bp) in all sample lanes 2 – 13. This was most likely due to excessive RT-PCR sample loading to the agarose gels, which resulted in the amplicons migrating slower and appearing larger than expected. However, compared to the previous observations of gene expression in Sections 3.1.3. (Figure 3.6) and 3.2.3. (Figure 3.14), Figures 3.52A and 3.53A display the largest and less expressed amplicon as *NEIL1* (lanes 3, 6, 9 and 12), the most expressed amplicon for expression control reference was *β-Actin* (Lanes 2, 5, 8 and 11), and the smallest amplicon who's expression was tested for siRNA knockdown was *NEIL3* (lanes 4, 7, 10 and 13).

Observed from the analysis of siRNA transfected PD20 cells (FANCD2 deficient), as displayed in Figure 3.53A, compared to the non-transfected (lanes 2 – 4) and NS siRNA transfected controls (lanes 5 – 7), knockdown of NEIL3 was observed from the NEIL3 siRNA transfected cells (lanes 8 – 10) in lane 10. Unexpectedly, in the TRIM26 knockdown sample (TRIM26 siRNA transfected PD20 cells, lanes 11 – 13), compared to the NS siRNA transfected cells, *NEIL3* amplicon were observed to have reduced in expression. Based on the image analysis of Figure 3.53A and the signal intensity factors displayed in Figure 3.53B, compared to their respective amplicons expressed in the NS siRNA transfected controls, the PD20 cells displayed an approximate 65% knockdown of *NEIL3* when transfected with NEIL3 siRNA, and an unexpected reduction in *NEIL3* expression was observed by approximately 86% when transfected with TRIM26 siRNA. Also observed from Figure 3.53 were the barely-visible amplifications of *NEIL1* from the PD20 cells, and compared to the respective *NEIL1* amplification in the NS siRNA transfected controls, *NEIL1* expression was reduced by approximately 40% in the NEIL3 siRNA transfected cells, and more than 70% reduction in the TRIM26 siRNA transfected cells. However, *NEIL1* could only barely be visible in Figure 3.53A in the controls (lanes 3 and 6) compared to the NEIL3 and TRIM26 siRNA samples (lanes 9 and 12, respectively), and therefore difficult to discern if the difference in expression could be considered significant or not.

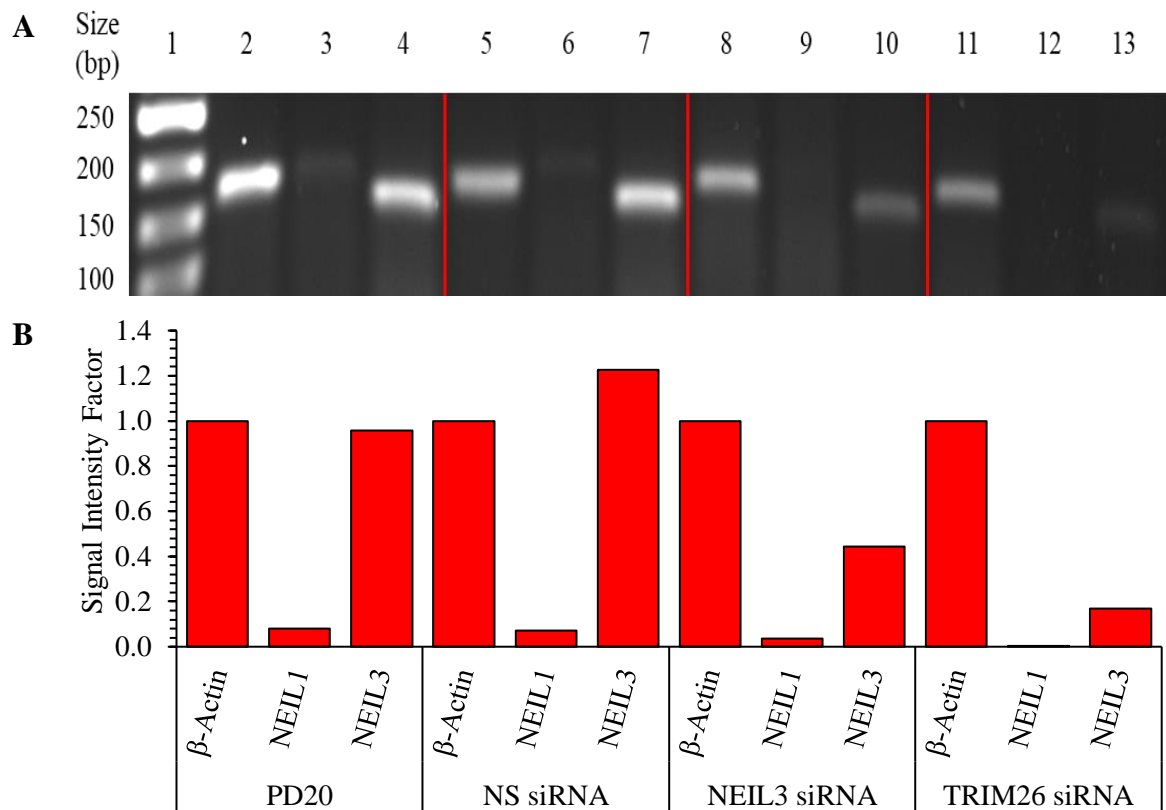


**Figure 3.53: RT-PCR of siRNA reverse-transfected PD20 (FANCD2 deficient). Expression of  $\beta$ -Actin, NEIL1 and NEIL3 after siRNA transfection targeting A) control (no transfection, lanes 2 – 4), control (non-specific siRNA, lanes 5 – 7), NEIL3 (NEIL3 siRNA, lanes 8 – 10), and TRIM26 (TRIM26 siRNA, lanes 11 – 13).**

(A) Lane 1, DNA ladder; lanes 2, 5, 8 and 11,  $\beta$ -Actin; lanes 3, 6, 9 and 12, NEIL1; lanes 4, 7, 10 and 13, NEIL3. Expected amplicon length:  $\beta$ -Actin, 166 bp; NEIL1, 212 bp; NEIL3, 147 bp. (B) Quantified signal intensity from amplicons in section A relative to the cell's  $\beta$ -Actin expression, based on one technical and scientific replicate.

As it could be seen from the analysis of siRNA transfected 3.15 cells (FANCD2 corrected), as displayed in Figure 3.54A, compared to the non-transfected (lanes 2 – 4) and NS siRNA transfected controls (lanes 5 – 7), knockdown of NEIL3 was unexpectedly not observed from the NEIL3 siRNA transfected cells (lanes 8 – 10) in lane 10. However, similarly to the results observed in Figure 3.53, the TRIM26 knockdown sample (TRIM26 siRNA transfected 3.15 cells, lanes 11 – 13) displayed reduced NEIL3 expression. Based on the image analysis of Figure 3.54A and the signal intensity factors displayed in Figure 3.54B, compared to their respective amplicons expressed in the NS siRNA transfected controls, the 3.15 cells displayed an approximate 50% increase in NEIL3 expression when transfected with NEIL3 siRNA, but unexpectedly a reduction in NEIL3 expression by approximately 45% when transfected with TRIM26 siRNA. This may suggest that, compared to the FANCD2 deficient

cells (PD20) results in Figure 3.53, the FANCD2 corrected cells (3.15) were not as susceptible to siRNA transfection as the FA cell line. *NEIL1* amplification was not visible from the 3.15 cells in Figure 3.54 (lanes 3, 6, 9 and 12), as was expectedly and observed from the background results (Figure 3.14).

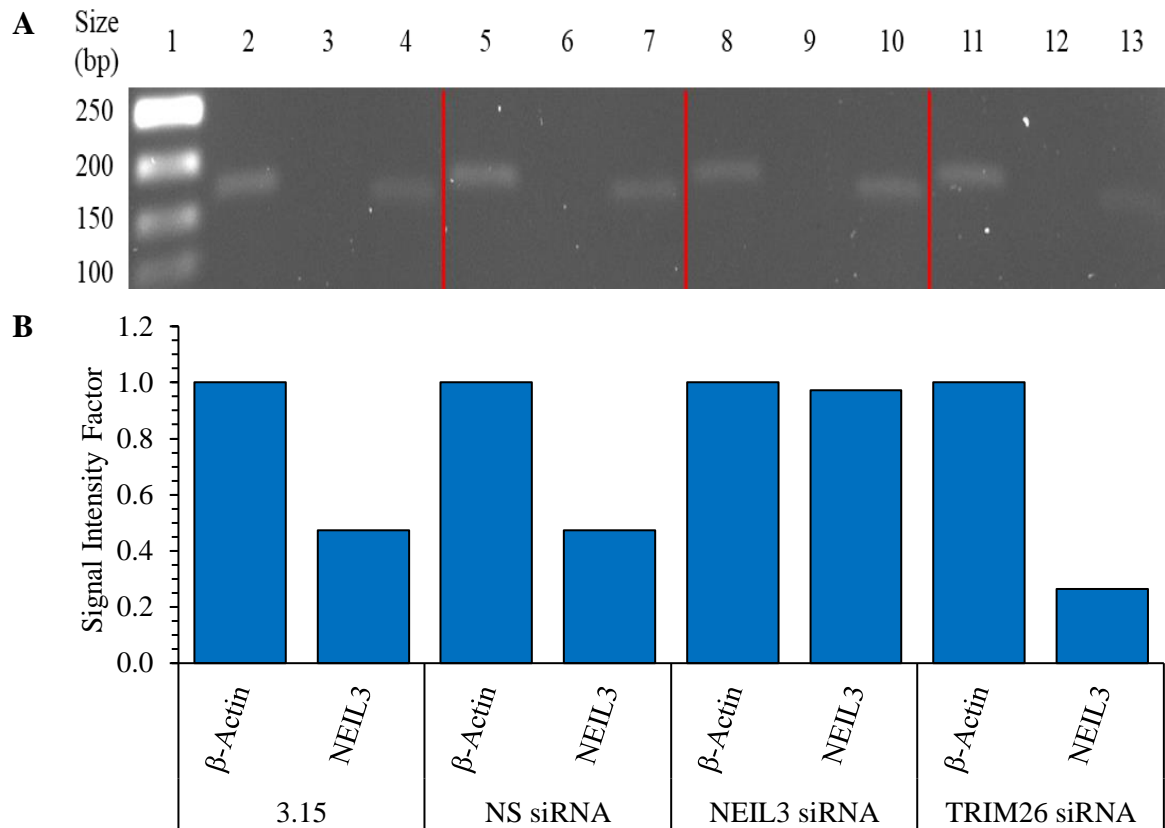


**Figure 3.54: RT-PCR of siRNA reverse-transfected 3.15 (PD20 corrected). Amplification of  $\beta$ -Actin, NEIL1 and NEIL3 after siRNA transfection targeting control (no transfection, lanes 2 – 4), control (non-specific siRNA, lanes 5 – 7), NEIL3 (NEIL3 siRNA, lanes 8 – 10), and TRIM26 (TRIM26 siRNA, lanes 11 – 13).**

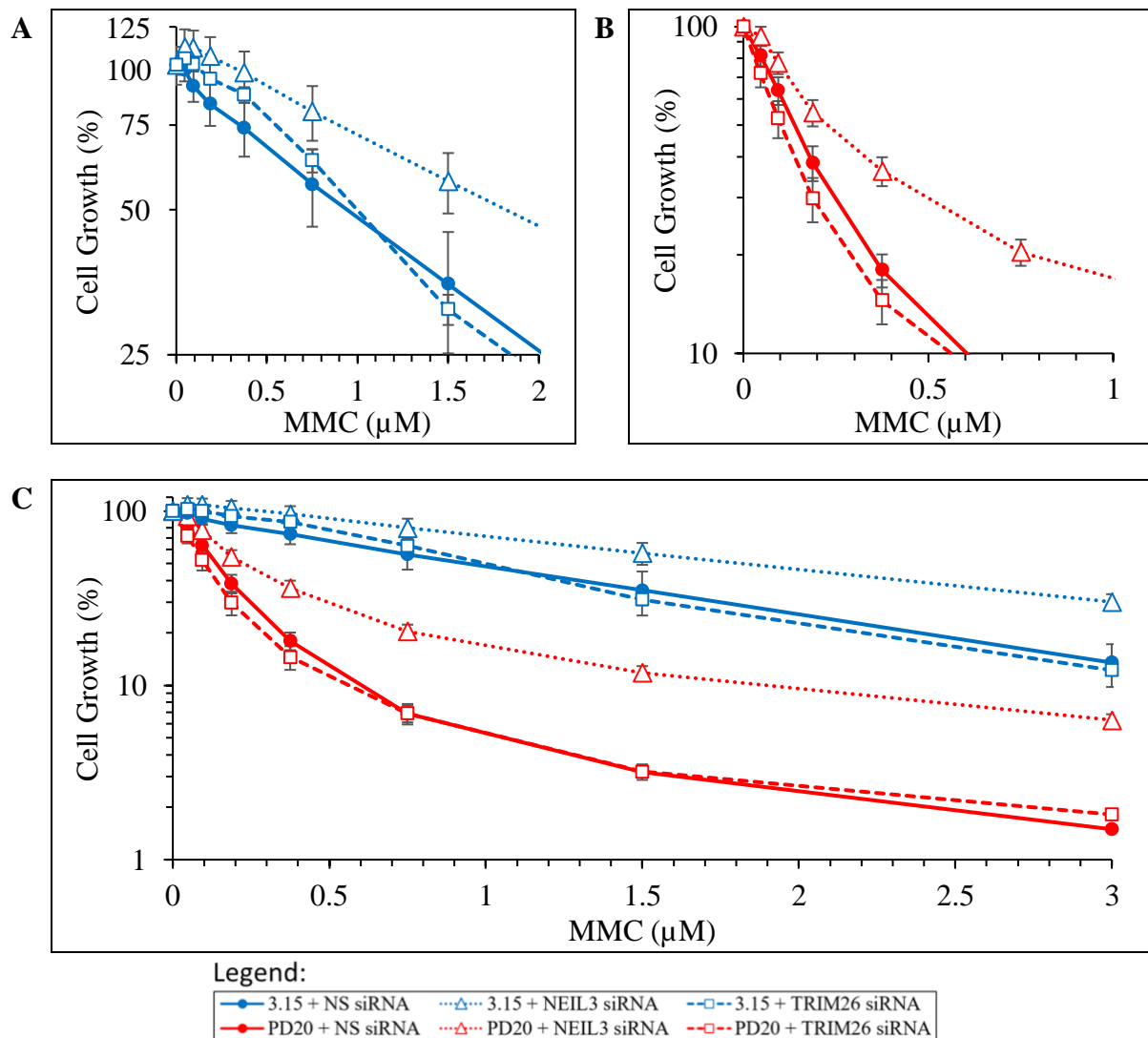
(A) Lane 1, DNA ladder; lanes 2, 5, 8 and 11,  $\beta$ -Actin; lanes 3, 6, 9 and 12, NEIL1; lanes 4, 7, 10 and 13, NEIL3. Expected amplicon length:  $\beta$ -Actin, 166 bp; NEIL3, 147 bp. (B) Quantified signal intensity from amplicons in section A relative to the cell's  $\beta$ -Actin expression, based on one technical and scientific replicate.

### 3.5.2. Survival of siRNA-Transfected Cells Following Treatment with Genotoxic Agents.

Based on the gene and protein expression studies after siRNA transfection, described previously in Section 3.5.1., the FA cell lines PD20 (FANCD2 deficient) and 3.15 (FANCD2 corrected) were siRNA transfected and tested for survival after genotoxin treatments. Due

to the lack of time and resources, the survival assays could not wait until satisfactory knockdown confirmation was concluded. The results collected were based on the initial knockdown confirmation from the PD20 transfected cells.

As displayed in Figure 3.55, the FANCD2 deficient cells (PD20) were observed as highly sensitive to the ICL-inducing agent MMC compared to the FANCD2 corrected cells (3.15), as was expected and observed from Figure 3.11. Compared to the IC<sub>50</sub> of the non-specific (NS) siRNA transfected cells, the NEIL3 siRNA transfected cells were unexpectedly observed to have had a significant twofold increase in resistance in both the PD20 cells (IC<sub>50</sub> 0.12 μM and 0.24 μM) and 3.15 cells (IC<sub>50</sub> 0.86 μM and 1.81 μM). Although statistically, the standard deviation of the NEIL3 siRNA transfected 3.15 cells (FANCD2 corrected) IC<sub>50</sub> result could imply the significance to be difficult to accept (IC<sub>50</sub> 1.81 ± 0.63 μM). Furthermore, the TRIM26 siRNA transfected cells were barely notable resistant to MMC, with PD20 transfected cells notably less resistant (IC<sub>50</sub> 0.10 μM) and 3.15 transfected cells notably more resistant (IC<sub>50</sub> 1.00 μM). The results were consistent, regardless of the FA phenotype. These contradictions in the FA and FA-corrected cells suggest that the knockdown of TRIM26 did not increase protein levels of NEIL1 or NEIL3, and therefore increased resistance to ICLs as theorised, and NEIL3 may not have been required for excising MMC-induced ICLs after knockdown. Furthermore, this could suggest that other processes may be dysfunctional in the FA original cell lines.

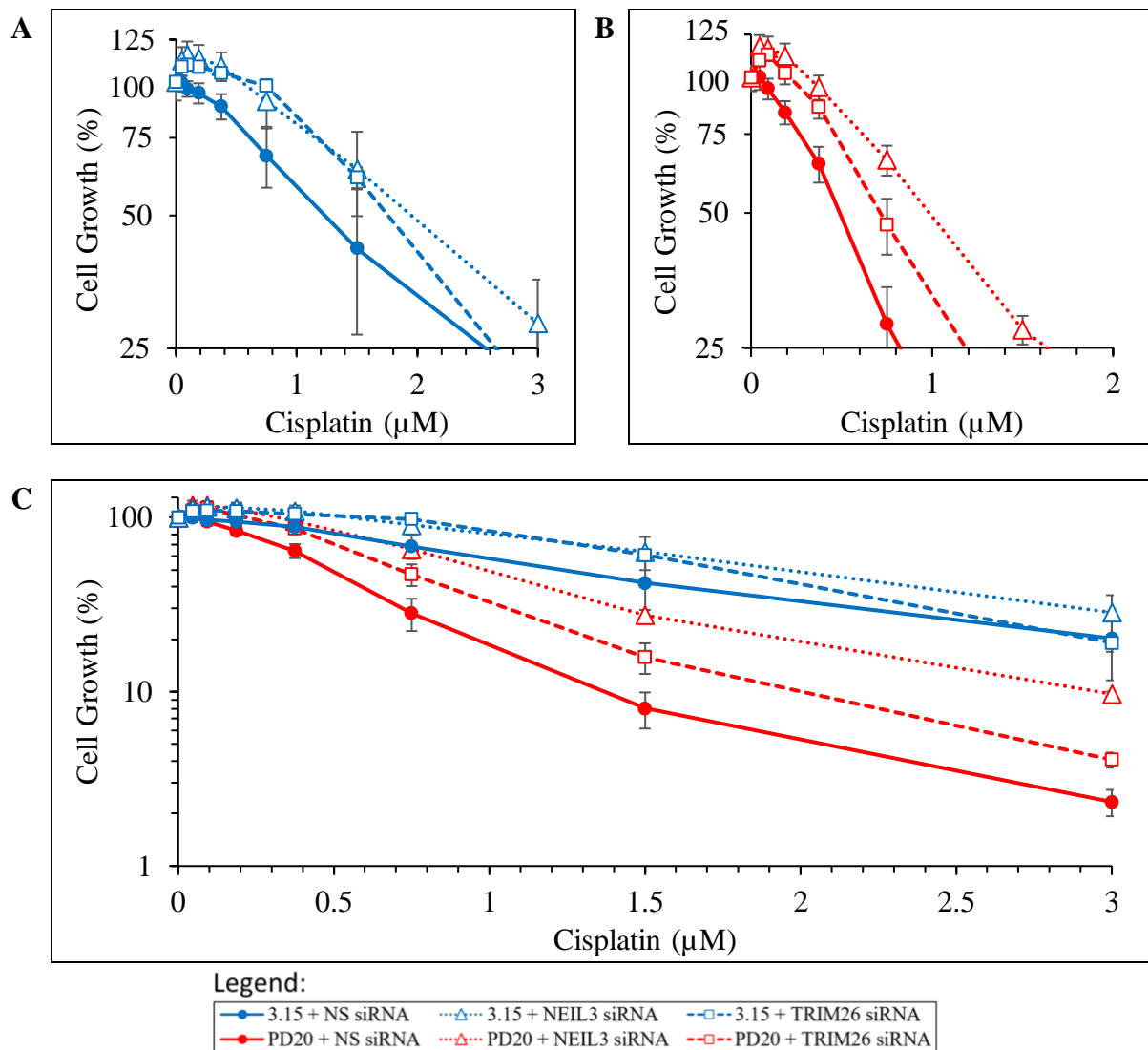


**D**

		IC <sub>50</sub> ± SD Values
3.15	+ NS siRNA	0.86 ± 0.19 μM
	+ NEIL3 siRNA	1.81 ± 0.63 μM
	+ TRIM26 siRNA	1.00 ± 0.01 μM
PD20	+ NS siRNA	0.14 ± 0.02 μM
	+ NEIL3 siRNA	0.24 ± 0.05 μM
	+ TRIM26 siRNA	0.10 ± 0.02 μM

**Figure 3.55: Growth inhibition of siRNA transfected (A) 3.15 (PD20 Corrected, blue) and (B) PD20 (FANCD2 deficient, red), and their comparison (C), following treatment with mitomycin C (MMC).**

**D)** IC<sub>50</sub> values for growth inhibition following treatment. Cells were transfected with non-specific (NS) siRNA, NEIL3 siRNA or TRIM26 siRNA. 3 x 10<sup>3</sup> cells per well, incubated for 72 h. Mean data was collected from triplicate technical and scientific repeats.



**D**

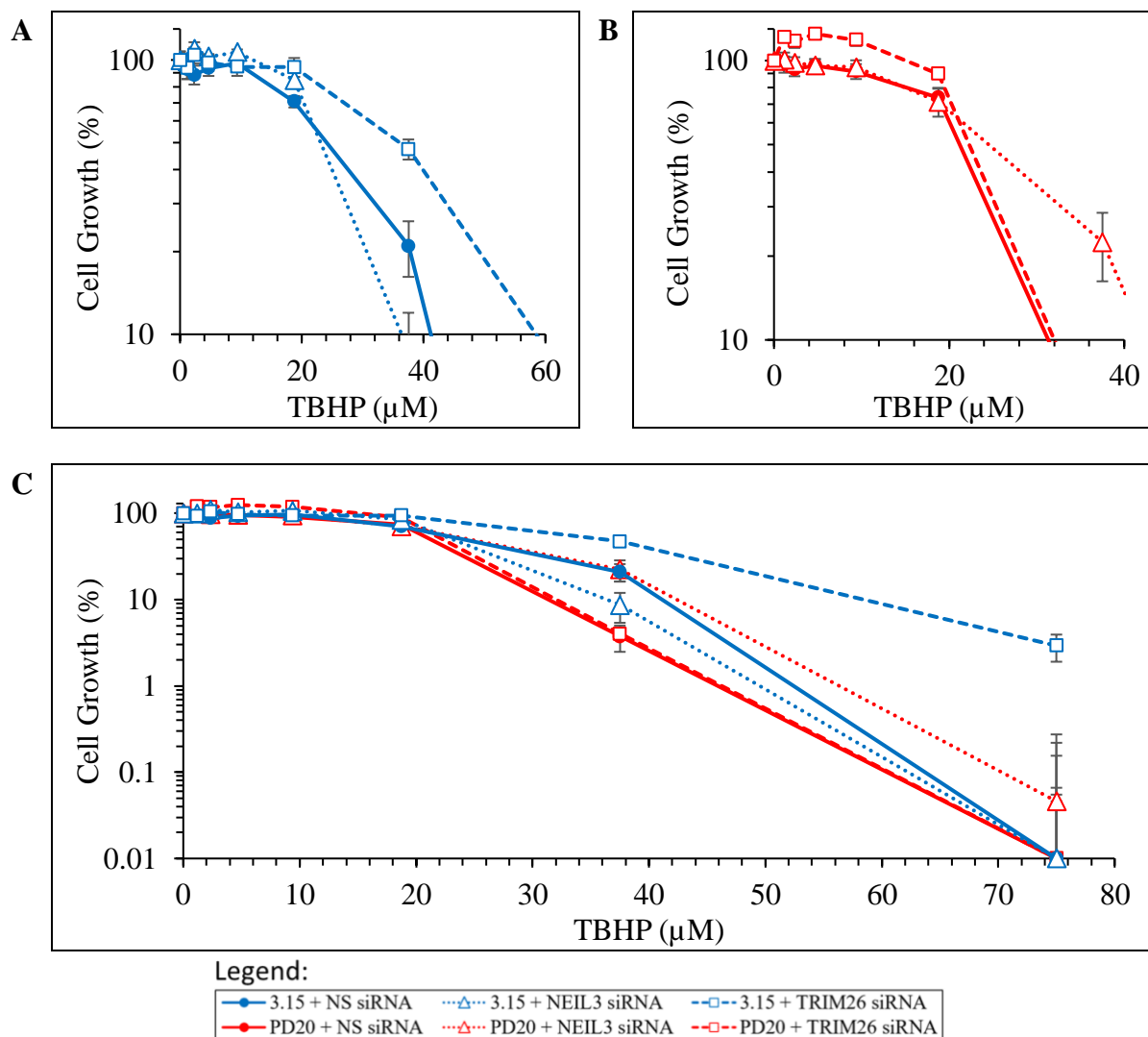
		IC <sub>50</sub> ± SD Values
3.15	+ NS siRNA	1.23 ± 0.26 μM
	+ NEIL3 siRNA	1.95 ± 0.60 μM
	+ TRIM26 siRNA	1.80 ± 0.11 μM
PD20	+ NS siRNA	0.48 ± 0.07 μM
	+ NEIL3 siRNA	1.02 ± 0.21 μM
	+ TRIM26 siRNA	0.74 ± 0.09 μM

**Figure 3.56: Growth inhibition of siRNA transfected (A) 3.15 (PD20 Corrected, blue) and (B) PD20 (FANCD2 deficient, red), and their comparison (C), following treatment with cisplatin.**

**D)** IC<sub>50</sub> values for growth inhibition following treatment. Cells were transfected with non-specific (NS) siRNA, NEIL3 siRNA or TRIM26 siRNA. 3 x 10<sup>3</sup> cells per well, incubated for 72 h. Mean data was collected from triplicate technical and scientific repeats.

As was expected in Figure 3.56, compared to the MTT assay results in Figure 3.11, the FANCD2 deficient cells (PD20) were observed as highly sensitive to the ICL-inducing agent cisplatin than the FANCD2 corrected cells (3.15). Compared to the IC<sub>50</sub> of the non-specific NS siRNA transfected cells, in Figure 3.56 the 3.15 cells showed increased resistance to cisplatin when TRIM26 was knocked down (IC<sub>50</sub> 1.23  $\mu$ M and 1.80  $\mu$ M). Similarly, when NEIL3 was knocked down, resistance was observed to have increased (IC<sub>50</sub> 1.95  $\mu$ M), though statistically, based on the standard deviation, it may not be a true difference. The PD20 cells also displayed a similar increase in resistance to cisplatin from the NS siRNA transfected cells when TRIM26 was knocked down (IC<sub>50</sub> 0.48  $\mu$ M and 0.74  $\mu$ M) and also when NEIL3 was knocked down (IC<sub>50</sub> 1.02  $\mu$ M). The results were consistent with each other, though the FANCD2 deficient cell line (PD20) displayed the most considerable change in resistance to cisplatin. Compared to the MMC results in Figure 3.55, knockdown of TRIM26 increased the FA and FA-corrected cells resistance to cisplatin, but knockdown of NEIL3 similarly increased cells resistance to the ICL-inducing agents. This further suggests that NEIL3 was not required for the excision MMC and cisplatin-induced ICLs, though possibly NEIL1 for cisplatin-induced ICLs.

Figure 3.57 shows the MTT assay results following treatment of the PD20 (FANCD2 deficient) and 3.15 (FANCD2 corrected) cell lines with the oxidative-inducing agent TBHP. As expected, there was very little difference in the IC<sub>50</sub> values between the two cell lines when transfected with the non-specific siRNA. The FANCD2 expressing cells (3.15) showed an intriguing observation of an increase in resistance to TBHP when TRIM26 was knocked down, but was not observed in the FANCD2 deficient cell line (PD20). This suggests that other processes may be dysfunctional in the FANCD2 deficient cell lines. When NEIL3 was knocked down, the 3.15 cells, even statistically, did not display a significant difference in TBHP resistance. However, an increase in resistance was observed in the FANCD2 deficient cell line (PD20) with NEIL3 siRNA. This may indicate that DNA repair processes in general are altered in the PD20 cell line. Interestingly in Figure 3.57C, the PD20 cells with NEIL3 knockdown appear almost parallel with the 3.15 cells transfected with NS siRNA. However, statistically, the difference in resistance to TBHP for the FANCD2 deficient (PD20) and corrected (3.15) cells when transfected with NEIL3 or TRIM26 siRNA would have been difficult to accept.



**D**

		IC <sub>50</sub> ± SD Values
3.15	+ NS siRNA	24.64 ± 3.08 μM
	+ NEIL3 siRNA	24.92 ± 2.87 μM
	+ TRIM26 siRNA	36.53 ± 3.55 μM
PD20	+ NS siRNA	22.41 ± 2.26 μM
	+ NEIL3 siRNA	24.77 ± 3.21 μM
	+ TRIM26 siRNA	24.98 ± 5.17 μM

**Figure 3.57: Growth inhibition of siRNA transfected (A) 3.15 (PD20 Corrected, blue) and (B) PD20 (FANCD2 deficient, red), and their comparison (C), following treatment with TBHP.**

**D) IC<sub>50</sub> values for growth inhibition following treatment.** Cells were transfected with non-specific (NS) siRNA, NEIL3 siRNA or TRIM26 siRNA.  $3 \times 10^3$  cells per well, incubated for 72 h. Mean data was collected from triplicate technical and scientific repeats.

## Chapter 4 Discussion

The FA-phenotypical cells were susceptible to the oxidative-inducing agent TBHP, but statistically, no real difference was observed compared to the non-FA phenotypical cells. NEIL1 overexpression studies statistically displayed no significant difference in genotoxin resistance in the FANCD2 deficient and WT/FANCD2 corrected cell lines, and therefore were not reproducible. The NEIL3 overexpression studies in the same cell lines displayed increased resistance to the genotoxic agents, but statistically, no significant difference was observed. Furthermore, truncated NEIL3 (NEIL3<sup>1506</sup>) expression was observed to have had equal to or improved genotoxin resistance compared to full-length sequenced NEIL3 (NEIL3<sup>FL</sup>) expressions, indicating this version of truncated NEIL3 was possible in entering the cell's nucleus. NEIL3 knockdown studies displayed an unexpected but intriguingly significant increase in resistance to the ICL-inducing agents MMC and cisplatin for the FA cells (PD20, FANCD2 deficient), though statistically, probably not as significant for the non-FA cells (3.15, corrected PD20). Similarly, the TRIM26 knockdown studies also displayed increased ICL-induced resistance, but no significant or statistical difference was observed, nor synthetic lethality as was presumably expected.

It was reported in Macé-Aimé *et al.* (2010) that overexpression of the DNA glycosylase NEIL1 in FA cells with FANCA or FANCC deficiency had increased resistance to the ICL-inducing agents MMC and 8-methoxypsoralen. This suggested that NEIL1 was either a potential substitute for ICL repair in FA cells or the preferred ICL incision mechanic in the FA pathway for the specific ICL induction. Furthermore, it displayed a potential association between the FA pathway and the base excision repair (BER) pathway. However, attempts to reproduce Macé-Aimé *et al.*'s (2010) result through their similar methodology for transfecting the FANCA-related cell lines HSC-72 (FANCA deficient) and HSC-72-Corrected with pcDNA3.1-hNEIL1-FLAG and treated with mitomycin C (MMC) could not be reproduced as the gifted cell lines were tested positive for mycoplasma contamination (Section 3.1, Figure 3.2), and therefore could not be confirmed. When reattempting the study with the FANCD2-related non-FA and FA cells (3.15/PD20, U2OS/-D2 and HeLa/-D2) instead, even with the additional antibiotic selection, the results from Section 3.4 (Figures 3.34, 3.35, 3.38, 3.39, 3.45, and 3.48) would consider the claim to be either not reproducible or not reproducible concerning FANCD2 deficiency. The Elder Laboratory discerned the preferences of DNA glycosylases NEIL1 and NEIL3 to the excision local of oxidised bases

along the DNA replication fork of double-stranded and single-stranded DNA, respectively (Martin *et al.*, 2017; Albelazi *et al.*, 2019). Furthermore, in relation to ICL repair, NEIL1 expression and especially NEIL3 overexpression were observed to excise ICLs induced from psoralen and cisplatin (Martin *et al.*, 2017; Martin, 2018). Therefore this study aimed to discern if DNA glycosylase NEIL3 would have the same association with the FA pathway as NEIL1 and could potentially indicate substituted or preferred ICL repair in FA-phenotype cells. Furthermore, extending the hypothesis to cancer cells, if the association of NEIL1 or NEIL3 to ICL repair were to be proven valid, the study could potentially consider these expressed DNA glycosylases as anti-cancer therapeutics.

The study was to be conducted with the use of MMC as the primary ICL-inducing reactive control for discerning FA from non-FA phenotypic cells, based on the continuation from the last FA cells tested in connection to NEIL1 expression and how FA was diagnosed (Mehta and Ebens, 2002; Macé-Aimé *et al.*, 2010), and the DNA crosslinking platinum compounds cisplatin and oxaliplatin as the causes of variability to bear in mind. Cisplatin had widely been used as a cancer chemotherapeutic drug for many years, and often as the first or subsequently combined chemotherapeutic drug, but often is resisted in various cancers (Dasari and Tchounwou, 2014). Though considered a DNA crosslinking agent, cisplatin mainly causes intrastrand crosslinks with a small percentage of ICLs (Jung and Lippard, 2007; Wang and Gautier, 2010). The cisplatin analog oxaliplatin contains a trans-1,2-diaminocyclohexane ligand bound to the amine groups, to which its bulkiness prevents DNA repair, and a bidentate oxalate group ligand bound to the platinum in place of the chlorides (Dasari and Tchounwou, 2014; Thiabaud *et al.*, 2020). Compared to cisplatin, oxaliplatin had been observed to increase DNA cross-linking induction in some colon cancer cells over others (Virag *et al.*, 2012), where p53 was reactivated in cisplatin-resistant and p53-mutated ovarian cancer cells through activation of the mitogen-activated protein kinase (MEK) 1 and 2 (Bhatt *et al.*, 2017), and had reduced side effects such as nephrotoxicity (Dasari and Tchounwou, 2014). However, initial attempts of MTS and MTT assays on oxaliplatin-treated cell growth did not display a statistically significant difference in susceptibility to oxaliplatin between FA and non-FA phenotypical cells (Appendix Figure 8). As well as the issues of resources and time and the protocols being refined at the time, oxaliplatin was no longer considered an alternative oxidative-inducing or ICL-inducing agent in place of TBHP or cisplatin.

As described in Section 1.2.2., all ICL-inducing agents also induce at least one additional DNA lesion and are used to treat preferred types of cancer. An ICL agent can also be used for other cancer types, but the treatment is based on the specific genes affecting the cancer cells compared to the non-cancerous cells within the patient and how the treatment was approached. Breast cancer with dysfunctional BRCA1/2 proteins would preferably be treated with a poly(ADP-ribose)polymerase (PARP) inhibitor such as Olaparib (Robson *et al.*, 2017) over an ICL-inducing agent. However, if the non-cancerous cells were also dysfunctional in BRCA1/2 proteins then the risk would increase as the same proteins are related to having a dysfunctional ICL-repair pathway (Chen *et al.*, 2014). Although, triple-negative breast cancer cells lacking the expression for the estrogen receptor (ER), progesterone receptor (PR) and human epidermal growth factor receptor 2 (HER2) proteins can be treated with an ICL-inducing agent such as cisplatin (Lee *et al.*, 2019). Interestingly, when an ICL-inducing agent is combined with another drug, such as cisplatin with the antidiabetic drug metformin to downregulate RAD51 expression in triple-negative breast cancer, the anticancer effect could be enhanced (Lee *et al.*, 2019, Boulikas *et al.*, 2008). However, drug resistance, such as cisplatin resistance, has been known to develop eventually from repeated treatment over time, and therefore alternative chemical derivatives or different treatments are considered (Boulikas *et al.*, 2008). Due to most types of cancers being internal to the body, and most chemotherapy treatments are administered intravenously (Amjad *et al.*, 2022), the anticancer drug is also limited concerning the required method of activation when administered. Gastrointestinal cancer that is sensitive to ICLs would be treated with MMC through intravenous administration but not by a psoralen agent due to the requirement of UV radiation through phototherapy for ICL activation, and therefore reserved for skin-related or surface layered carcinogens (Rathod *et al.*, 2022; Sinawe and Casadesus, 2022).

The issues throughout the present study could be summarised as (i) mycoplasma contamination and (ii) NEIL3 immunoblotting. The plasmid transfection and cell growth experiments were initially conducted on the FA cell lines HSC-72 (FANCA deficient) and HSC-72-Corrected, based on the practice described and results observed from Macé-Aimé *et al.* (2010). Following the successful conclusion of these experiments, it was intended to expand the project to either FA knockout or knockdown of colon cancer cells. However, as described in Section 3.1 and displayed in Figure 3.2, the gifted FA cell lines were contaminated with mycoplasma. Rescue of the contaminated cell lines was attempted, but either the mycoplasma developed a resistance to the treatment (Plasmocin) or the time

required for treatment was too long for it to be a viable option. Furthermore, there was always the chance that the Plasmocin treatment had altered the phenotype of the cells. Therefore, whatever experiments were performed and the results analysed and displayed in Section 3.1 were used as confirmatory controls for FA cells.

From a protein perspective, the detection of the DNA glycosylases NEIL1 and NEIL3 by immunoblotting was the most challenging issue. It was known that not many antibodies for specifically targeting hNEIL1 and especially hNEIL3 for immunoblotting were available. Although the solution to the issue would have been to consider producing monoclonal antibodies, the Elder Laboratory was not equipped with the necessary equipment and knowledge at the time, and monoclonal antibody production services were expensive and would have required up to nine months to produce the antibodies. Furthermore, the human NEIL3 protein structure was not known until recently by Rodriguez *et al.* (2020), and as of the publication of this thesis, a monoclonal and species-specific antibody for targeting hNEIL3 is still not available. At the time of the project, the commercial antibody that was considered most specific to NEIL3 was the anti-NEIL3 antibody described in Table 2.7. It had been used successfully by other lab members and was regarded as the best available to target hNEIL3. When the first issues concerning the western blot occurred, it was investigated whether it was the immunoblotting technique or the cell extraction procedure that might be the problem. However, based on the  $\beta$ -Actin and FANCD2 immunoblot results, the issue was not solely due to the western blot technique.

As displayed in Sections 3.4.1. and 3.4.3., the western blot results showed NEIL1 expression only in the pcDNA3.1-hNEIL1-FLAG plasmid-transfected cells (Figures 3.31, 3.33 and 3.44). No band for endogenous NEIL1 was observed in any cell lines, indicating a low level of expression, which was confirmed by the RT-PCR results (Figures 3.14 – 3.16). Similarly, in Sections 3.3.3. and 3.4.1., the western blot results showed no hNEIL3 expression except for the FANCD2 deficient cell line PD20 (Figure 3.17), of which it was also observed in the plasmid transfected PD20 cells at an increased expression (Figure 3.31) but was not confirmed as the recombinant protein. However, hNEIL3 protein expression eventually became an issue when trying to confirm over/underexpressed protein after plasmid or siRNA transfection, and it was not understood until investigated further.

An investigation was attempted into discerning the reason, however with the limited time and resources for continuing the project, hNEIL3 expression was determined through other options. Overexpression was determined based on the antibiotic selection after plasmid transfection (Section 3.4.3.), and underexpression was determined by RT-PCR image analysis (Section 3.5.1.), and the eventual MTT assays after the genotoxin-treated cell survival determined if the altered expression had affected the cells, and therefore certainty of altered expression. A possible reason why NEIL3 protein expression was visible at times was that the cells were affected by oxidative or inflammatory stress, which then upregulated NEIL3 protein expression (Fleming *et al.*, 2019), and only then were the cell extracts concentrated enough to display a visible band in western blot. This potential reason was only noticed during two incidents of faulty cell-culture incubators stressing the cells to the point of noting increased cell death, but the fault was unknown and had not been investigated, and it did not explain why the recombinant NEIL3 protein was not detected. However, upon finishing the project with what could have been salvaged, the company that sold the anti-NEIL3 antibody used for this thesis no longer registered the product as multispecies specific, but mouse and rat only, despite personal and Elder Laboratory experience, referenced articles, comments and answered questions stated the antibody worked in targeting hNEIL3. This potential reason was noticed during the confirmation of recombinant protein expression after antibiotic selection in Figure 3.43, where all but the anti- $\beta$ -Actin antibody were multispecies-specific and mouse-specific NEIL1 and NEIL3 proteins were detected.

There was an issue related to the MTT/MTS assays as a method of discerning the growth inhibition of cell cultures when treated with a genotoxic agent. It was considered to use clonogenic assay as the preferred method for analysing cell survival by clonogenicity when treated with a genotoxic agent, instead of the MTT/MTS assay analysing cell survival by metabolic activity (Buch *et al.*, 2012). The protocol may not have been appropriate for the FA and non-FA suspension cells (HSC-72/-Corrected and HSC-536/-Corrected, respectively) since the clonogenic assay is an adherent-cell-based protocol, but based on the cell growth analysis results of the FANCD2 deficient and WT/corrected cells (PD20/3.15, U2OS-D2/U2OS and HeLa-D2/HeLa, respectively) displayed in Section 3.2.1. (Figures 3.8 – 3.10), the protocol could have been used. For the PD20/3.15 cells, the clonogenic assay methodology would have required up to thirteen days to form colonies of approximately fifty cells (Kuhnert *et al.*, 2009), whereas the cells could be analysed after 72 h incubation with genotoxin treatment with the MTT assay, as it was used throughout this project.

However, it would have been more practical to have done both MTT and clonogenic assays for the plasmid or siRNA transfected studies to analyse the short and long-term effects after genotoxin treatment.

#### 4.1. NEIL1, NEIL3<sup>FL</sup>, and NEIL3<sup>1506</sup> Overexpression in FA cells

The MTS assay results in Figure 3.5 confirmed that the FA cells HSC-72 (FANCA deficient) were sensitive to the ICL-inducing agents MMC and cisplatin and, interestingly, were also sensitive to the oxidising agent TBHP, compared to the corrected (HSC-72-Corrected) or WT (HSC-93) cells. As expected in comparison, all of the MTT assay results confirmed that the FANCD2 deficient cells PD20, U2OS-D2 and HeLa-D2 were more sensitive than the corrected/WT counterparts 3.15, U2OS and HeLa to the MMC and cisplatin ICL-inducing agents, and a similar result was also observed when these cells were treated with the oxidising agent TBHP, as summarised in Figures 4.1 – 4.4. Although the difference in growth rate after TBHP treatment between the FA cells and WT/FA-Corrected cells was not consistently and as substantially different as the MMC and cisplatin-treated MTS and MTT assay results, it was still interesting to know that FA-phenotype cells were more sensitive to an oxidative agent than FA-corrected or WT cells. Furthermore, when comparing the cell growth after TBHP treatment results, the HSC-72 (FANCA deficient), HSC-72-Corrected, PD20 (FANCD2 deficient) and 3.15 (FANCD2 corrected) cells (Figures 3.5 and 3.11) had a higher growth rate and TBHP concentration range than the cancer cell lines U2OS (WT), U2OS-D2 (FANCD2 deficient), HeLa (WT) and HeLa-D2 (FANCD2 deficient; Figures 3.12 and 3.13, respectively).

**Table 4.1: Growth inhibition summary of FANCD2-deficient (PD20, U2OS-D2 and HeLa-D2) and WT/FANCD2 corrected (3.15, U2OS and HeLa) cell lines, following treatment with mitomycin C (MMC), cisplatin and TBHP.**

Cell Line	IC <sub>50</sub> ± SD Values		
	MMC	Cisplatin	TBHP
<b>3.15</b>	0.43 ± 0.02 µM	2.24 ± 0.14 µM	49 ± 1.01 µM
<b>PD20</b>	0.06 ± 0.00 µM	0.74 ± 0.04 µM	29 ± 0.86 µM
<b>U2OS</b>	103 ± 16.97 nM	1.57 ± 0.27 µM	4.56 ± 1.10 µM
<b>U2OS-D2</b>	36 ± 5.43 nM	0.40 ± 0.13 µM	3.34 ± 0.55 µM
<b>HeLa</b>	9.1 ± 0.81 nM	176 ± 5.83 nM	2.44 ± 0.19 µM
<b>HeLa-D2</b>	4.3 ± 1.51 nM	70 ± 4.88 nM	2.20 ± 0.51 µM

IC<sub>50</sub> values derived from Section 3.2.2., Figures 3.11 – 3.13. Mean data was collected from triplicate technical and scientific repeats.

According to the phenotype of the U2OS-D2 cells described in Table 2.1 (Section 2.1.1.) and through the cell line generation accomplished according to Schwab *et al.* (2015) were considered as *FANCD2*<sup>-/-</sup>, the FA-generated cancer cells U2OS-D2, and subsequently HeLa-D2, were confirmed through western blot as well as cell growth after cisplatin treatment only, and therefore no quantitative or RT-PCR confirmation. Therefore, the cells were expected not to display *FANCD2* expression. However, since the RT-PCR and western blots in Section 3.2.3. displayed some traces of *FANCD2* expression (Figures 3.27 – 3.29), it was logical to consider the *FANCD2*<sup>-/-</sup> generated cells U2OS-D2 and HeLa-D2 as rather *FANCD2* deficient or depleted. Furthermore, the FA-generated cancer cells U2OS-D2 and HeLa-D2 were confirmed to have an FA-phenotype similar to the actual FA cells HSC-72 (*FANCA* deficient) and PD20 (*FANCD2* deficient), based on the MTT results in summarised in Figure 4.1 when treated by ICL-inducing agents MMC and cisplatin.

**Table 4.2: Growth inhibition summary of plasmid transfected FANCD2-deficient (PD20, U2OS-D2 and HeLa-D2) and WT/FANCD2 corrected (3.15, U2OS and HeLa) cell lines, following treatment with mitomycin C (MMC), cisplatin and TBHP.**

		<b>IC<sub>50</sub> ± SD Values</b>		
<b>Cell Line</b>	<b>Plasmid Transfected</b>	<b>MMC</b>	<b>Cisplatin</b>	<b>TBHP</b>
<b>3.15</b>	<b>+ Empty Vector</b>	0.26 ± 0.01 μM	2.42 ± 0.16 μM	19.4 ± 0.51 μM
	<b>+ hNEIL1-FLAG</b>	0.25 ± 0.01 μM	2.53 ± 0.09 μM	24.8 ± 0.59 μM
	<b>+ hNEIL3<sup>FL</sup>-FLAG</b>	0.22 ± 0.01 μM	2.57 ± 0.09 μM	34.1 ± 1.09 μM
<b>PD20</b>	<b>+ Empty Vector</b>	0.05 ± 0.00 μM	0.87 ± 0.03 μM	19.5 ± 0.50 μM
	<b>+ hNEIL1-FLAG</b>	0.05 ± 0.00 μM	1.01 ± 0.04 μM	21.0 ± 0.61 μM
	<b>+ hNEIL3<sup>FL</sup>-FLAG</b>	0.04 ± 0.00 μM	0.94 ± 0.04 μM	21.5 ± 0.49 μM
<b>U2OS</b>	<b>+ Empty Vector</b>	0.08 ± 0.02 μM	1.30 ± 0.32 μM	1.45 ± 0.43 μM
	<b>+ hNEIL1-FLAG</b>	0.07 ± 0.01 μM	1.07 ± 0.15 μM	1.35 ± 0.38 μM
	<b>+ hNEIL3<sup>1506</sup>-FLAG</b>	0.08 ± 0.02 μM	1.38 ± 0.31 μM	2.25 ± 0.08 μM
<b>U2OS-D2</b>	<b>+ Empty Vector</b>	0.03 ± 0.00 μM	0.35 ± 0.08 μM	1.50 ± 0.38 μM
	<b>+ hNEIL1-FLAG</b>	0.03 ± 0.01 μM	0.22 ± 0.04 μM	1.30 ± 0.34 μM
	<b>+ hNEIL3<sup>1506</sup>-FLAG</b>	0.03 ± 0.00 μM	0.39 ± 0.06 μM	2.00 ± 0.68 μM
<b>HeLa</b>	<b>+ Empty Vector</b>	15.2 ± 0.65 nM	176 ± 13.87 nM	9.90 ± 0.47 μM
	<b>+ hNEIL1-FLAG</b>	15.5 ± 0.77 nM	178 ± 14.12 nM	>12.00 μM
<b>HeLa-D2</b>	<b>+ Empty Vector</b>	11.2 ± 0.69 nM	103 ± 8.04 nM	7.35 ± 0.50 μM
	<b>+ hNEIL1-FLAG</b>	11.6 ± 1.09 nM	109 ± 14.50 nM	7.56 ± 0.97 μM

IC<sub>50</sub> values derived from Section 3.4.2., Figures 3.33 – 3.41. Cells were transfected with empty vector, pcDNA3.1-hNEIL1-FLAG, pcDNA3.1-hNEIL3<sup>FL</sup>-FLAG or pcDNA3.1-hNEIL3<sup>1506</sup>-FLAG. Mean data was collected from triplicate technical repeats in one (3.15/PD20), two (U2OS/U2OS-D2) or three (HeLa/HeLa-D2) scientific repeats.

Following the preparation of the expression vectors, the prepared pcDNA3.1-hNEIL3<sup>FL</sup>-FLAG and pcDNA3.1-hNEIL3<sup>1506</sup>-FLAG plasmids were sent for DNA sequencing. The results indicated no mutations in the inserts and correct ligation to the plasmid DNA at the junctions (Figures 3.9 and 3.13). However, it could not be known if the prepared plasmids were functioning as expected until a plasmid transfection to a cell line was attempted. The initial plasmid-transfection attempts to the PD20 cells with the prepared plasmids in Section

3.4 displayed significant but also unexpected results (Figures 3.31A and 3.34) that seemed to agree with the hypothesis but also contradicted what was theorised based on the literature review. Although the western blots did not confirm the recombinant protein expression for the plasmid transfected PD20 cells (FANCD2 deficient, Figure 3.31A), the initial attempt of cell growth while treated with MMC did not display an increase in resistance to the ICL-inducing agent when transfected with pcDNA3.1-hNEIL1-FLAG (Figure 3.34, IC<sub>50</sub> 0.12 μM [+ Empty Vector] to 0.11 μM [+ hNEIL1-FLAG]), but did display a significant increase in resistance when transfected with pcDNA3.1-hNEIL3<sup>FL</sup>-FLAG or pcDNA3.1-hNEIL3<sup>1506</sup>-FLAG (Figure 3.34, IC<sub>50</sub> 0.36 μM and 0.25 μM, respectively). However as summarised in Figure 4.2, the plasmid transfected PD20 (FANCD2 deficient) and 3.15 (PD20 corrected) cells were not observed with the same significant difference in resistance to MMC. The attempts in recombinant protein expression confirmation and cell growth after MMC treatment with the plasmid-transfected U2OS and HeLa cells displayed results that raised doubts on the prepared plasmids. Upon investigating further through repeating the Sanger sequencing (Section 2.2.8.), as well as the pcDNA3.1-hNEIL1-FLAG plasmid (Appendix Figure 9), the inserts were reaffirmed as correct with no mutations, misalignment or insert orientations observed, as shown in Figures 3.9 and 3.13. Based on the reaffirmation, the issue was most likely due to the pcDNA3.1 vectors either being altered or damaged, possibly from repetitive cloning or being too old and no longer viable. Due to the lack of time in investigating further, the plasmid subcloning services GeneArt (Thermo Fisher Scientific) was hired in producing new plasmids with the same hNEIL3<sup>FL</sup>-FLAG and hNEIL3<sup>1506</sup>-FLAG inserts and pcDNA3.1 vector, with the only difference being the restriction enzyme sites in the positive (+) sequence order orientation (Figure 2.1). Apart from the results displayed in Figures 3.31A and 3.34 for the initial plasmid transfected PD20 cells, the rest of the plasmid transfection confirmation and cell growth MTT assay results in Section 3.4 were based on the new plasmids used.

**Table 4.3: Growth inhibition summary of antibiotic-selected and plasmid transfected FANCD2-deficient (U2OS-D2 and HeLa-D2) and WT/FANCD2 corrected (U2OS and HeLa) cell lines, following treatment with mitomycin C (MMC), cisplatin and TBHP.**

Cell Line	Plasmid Transfected	IC <sub>50</sub> ± SD Values		
		MMC	Cisplatin	TBHP
U2OS	+ Empty Vector	163 ± 20.24 nM	1.44 ± 0.09 µM	2.96 ± 0.14 µM
	+ hNEIL1-FLAG	209 ± 44.14 nM	1.88 ± 0.37 µM	4.55 ± 0.89 µM
	+ hNEIL3 <sup>1506</sup> -FLAG	255 ± 74.67 nM	1.95 ± 0.47 µM	4.31 ± 0.66 µM
U2OS-D2	+ Empty Vector	95 ± 17.97 nM	0.91 ± 0.11 µM	3.84 ± 0.24 µM
	+ hNEIL1-FLAG	89 ± 17.58 nM	0.92 ± 0.20 µM	4.50 ± 1.21 µM
	+ hNEIL3 <sup>1506</sup> -FLAG	136 ± 93.97 nM	1.77 ± 1.39 µM	>6.00 µM
HeLa	+ Empty Vector	13.4 ± 1.06 nM	97 ± 7.49 nM	6.46 ± 0.41 µM
	+ hNEIL1-FLAG	14.3 ± 0.81 nM	118 ± 7.16 nM	8.38 ± 0.41 µM
	+ hNEIL3 <sup>FL</sup> -FLAG	15.5 ± 1.06 nM	144 ± 7.38 nM	7.40 ± 0.32 µM
	+ hNEIL3 <sup>1506</sup> -FLAG	15.8 ± 0.57 nM	148 ± 6.72 nM	8.15 ± 0.35 µM
HeLa-D2	+ Empty Vector	14.9 ± 0.84 nM	170 ± 8.53 nM	7.59 ± 1.66 µM
	+ hNEIL1-FLAG	15.6 ± 0.61 nM	174 ± 8.53 nM	9.49 ± 0.04 µM
	+ hNEIL3 <sup>FL</sup> -FLAG	12.9 ± 0.70 nM	165 ± 8.44 nM	7.74 ± 0.84 µM
	+ hNEIL3 <sup>1506</sup> -FLAG	14.5 ± 0.57 nM	139 ± 9.37 nM	7.99 ± 0.57 µM

IC<sub>50</sub> values derived from Section 3.4.4., Figures 3.45 – 3.50. Cells were transfected with empty vector, pcDNA3.1-hNEIL1-FLAG, pcDNA3.1-hNEIL3<sup>FL</sup>-FLAG or pcDNA3.1-hNEIL3<sup>1506</sup>-FLAG. Mean data was collected from triplicate technical repeats in one (HeLa/HeLa-D2) or two (U2OS/U2OS-D2) scientific repeats.

The different plasmid-transfection methods between the prior and later half of Section 3.4 was due to the methodology based on Macé-Aimé *et al.* (2010), Edmonds *et al.* (2017), the Elder laboratory and subsequently Li *et al.* (2020), without an antibiotic-selection step. Although their methodologies had not stated if the plasmid-transfected cells were antibiotic

selected or not, the terminology of their methods and materials did not indicate a selective step after transfection but instead a high plasmid concentration to low or balanced cell concentration transfection. Understandably, this was to shorten the incubation time and have a higher certainty of transfection. However, though the results from Section 3.4.1. had confirmed recombinant protein expression and therefore plasmid transfection, especially for pcDNA3.1-hNEIL1-FLAG (Figures 3.31 and 3.33), the MTT assay results from Section 3.4.2. (summarised in Figure 4.2) suggested that the plasmid-transfection efficiency was low, and therefore the guarantee of all cells transfected was low. As described in Section 3.4.3., it was due to the recombinant protein expression results displayed in Figures 3.32 and 3.33 contradicting the MTT assay results displayed in Figures 3.39 – 3.41 (summarised in Figure 4.2) of the U2OS (WT) and U2OS-D2 (FANCD2 deficient) plasmid-transfected cells that suggested transfection was not absolute. Although the plasmid transfection was considered generally successful based on the western blot results of recombinant proteins hNEIL1-FLAG and hNEIL3<sup>1506</sup>-FLAG in Section 3.4.1., the cell growth of the plasmid transfected FANCD2 deficient (PD20, U2OS-D2 and HeLa-D2) and WT/FANCD2 corrected (3.15, U2OS and HeLa) cells after genotoxin treatment displayed no consistently significant differences compared to their empty vector transfected controls, as summarised in Figure 4.2. But there were notable differences of increased resistance observed from the plasmid transfected cancer cells (U2OS/-D2 and HeLa/-D2) when treated with cisplatin and especially TBHP (summarised in Figure 4.2), which questioned the plasmid transfection methodology as an inaccurate and imprecise protocol without antibiotic selection. Therefore, plasmid transfection was reattempted with the additional antibiotic step to increase the accuracy and precision of transfection, as described in Section 3.4.3., and the cell growth after genotoxin treatments results displayed in Section 3.4.4. (summarised in Figure 4.3) were different compared to Section 3.4.2. (summarised in Figure 4.2). Compared to the empty vector transfected controls, the WT cancer cells U2OS and HeLa displayed mostly a notable difference of increased resistance to the genotoxic agents when transfected with pcDNA3.1-hNEIL1-FLAG and antibiotic selected (summarised in Figure 4.3), compared to the non-antibiotic selected results displaying mostly a notable indifferent or decrease in resistance (summarised in Figure 4.2). It was similarly observed between the empty vector and pcDNA3.1-hNEIL1-FLAG transfected FA-generated cancer cells U2OS-D2 and HeLa-D2 when comparing the non-antibiotic (Figure 4.2) and antibiotic selected (Figure 4.3) plasmid transfected cells. However, in comparison between Figures 4.2 and 4.3, statistically there was no significant difference in resistance to genotoxin treatment when transfected with

pcDNA3.1-hNEIL1-FLAG. Similar observations were also noticed for the cancer cells transfected with NEIL3-expressing plasmids, with the truncated (NEIL3<sup>1506</sup>) notably better than the full-lengthed (NEIL3<sup>FL</sup>) sequenced NEIL3. But statistically, the only results that displayed a substantial and potentially significant difference in resistance were the WT and FANCD2 deficient U2OS cells (U2OS and U2OS-D2, respectively) transfected with pcDNA3.1-hNEIL3<sup>1506</sup>-FLAG and antibiotic selected, albeit when treated with TBHP.

The hNEIL1-FLAG protein expression contradicted with what was expected. Compared to the empty vector control, the first unexpected result was the contradiction of the pcDNA3.1-hNEIL1-FLAG transfected PD20 cells not increasing in resistance to MMC (Figure 3.34). This was unexpected as Macé-Aimé *et al.* (2010) described that FA cells with NEIL1 overexpression showed increased resistance to ICL-inducing agents, including MMC. However, it should be noted that this was based on cell survival data on the FANCA and FANCC-related cell lines HSC-72/Corrected and HSC-536/Corrected (respectively). More recently, PD20 cells containing a *NEIL1* knockout was more resistant to psoralen-induced ICL (Li *et al.*, 2020). However, this unexpected result was observed through most of the cell growth results throughout Section 3.4. Furthermore, the WT U2OS and HeLa cancer cells that presumably overexpressed hNEIL1-FLAG showed the expected MMC and cisplatin resistance. Subsequently, the WT and FANCD2-deficient U2OS and HeLa cancer cells that presumably overexpressed hNEIL1-FLAG also showed resistance to TBHP. This would suggest that NEIL1 is not the DNA glycosylase required for repairing MMC and cisplatin-induced ICLs, but could still repair oxidative-induced reactions.

Resistance against ICL- and oxidative-inducing agents with recombinant hNEIL3<sup>FL</sup>-FLAG and hNEIL3<sup>1506</sup>-FLAG proteins expressed were not observed consistently in all cells. It was previously shown in Martin *et al.* (2017) that truncated versions of NEIL3 recombinant proteins were more stable than the NEIL3<sup>FL</sup>, and that it promoted the notion of NEIL3 being the ideal protein for excising psoralen and cisplatin-induced ICLs. NEIL3<sup>FL</sup> overexpression in U2OS (WT) cells was shown in (Martin, 2018) to have a substantial increase in cisplatin resistance, and therefore, in theory, a truncated NEIL3 protein would promote the same or improved resistance to cisplatin. In Section 3.4.4. the WT and FANCD2-deficient U2OS cancer cells that presumably overexpressed hNEIL3<sup>1506</sup>-FLAG showed resistance to MMC, cisplatin and TBHP (summarised in Figure 4.3), and, apart from the WT cells to MMC and cisplatin, were more resistant to the genotoxic agents than the hNEIL1-FLAG expressed

cells. The WT HeLa cancer cells that presumably overexpressed hNEIL3<sup>1506</sup>-FLAG were more resistant to MMC, cisplatin and TBHP (summarised in Figure 4.3) than the presumably overexpressed hNEIL3<sup>FL</sup>-FLAG. However, the FANCD2 deficient cells (HeLa-D2) showed less resistance to MMC when presumably overexpressed with hNEIL3<sup>FL</sup>-FLAG and cisplatin when presumably overexpressed with hNEIL3<sup>FL</sup>-FLAG over hNEIL3<sup>1506</sup>-FLAG. Sequentially, HeLa-D2 displayed more resistance to TBHP when presumably overexpressed with hNEIL3<sup>1506</sup>-FLAG over hNEIL3<sup>FL</sup>-FLAG, but less than when overexpressed with hNEIL1-FLAG. Despite the novel idea of a recombinant NEIL3-truncated protein expressed *in vivo* in human cells increasing resistance to ICLs and oxidative damage, the MTT assay results summarised in Figure 34.3 suggests that NEIL3 is the DNA glycosylase required to excise MMC and cisplatin-induced ICLs and oxidative-induced reactions, more so for a truncated version of NEIL3, but not for any cancer cell with an FA phenotype.

#### 4.2. NEIL3 and TRIM26 Knockdown in PD20 and 3.15 Cells

It was known that the proteins involved in the base excision repair (BER) pathway were regulated by protein post-translational modifications such as ubiquitylation, but it was not known to which BER protein specifically (Carter and Parsons, 2016). Information on the E3 ubiquitin ligase tripartite motif-containing protein 26 (TRIM26) specifically was limited to examples of TRIM26 knockdown potentially decreasing efficiency to mouse induced pluripotent stem cell (iPSC) reprogramming (Zhao *et al.*, 2013) and overexpression leading to tumour suppression in papillary thyroid carcinoma (PTC) cells (Wang *et al.*, 2019). In relation to the BER pathway, the Elder laboratory (Edmonds *et al.* [2017], and subsequently Martin [2018]) recently determined that TRIM26 was observed to target NEIL1 and NEIL3, amongst other BER proteins, for degradation. Furthermore, it was observed that by knockdown of TRIM26, NEIL1 and NEIL3 protein stability was elevated, and cell survivability was increased when treated with cisplatin. Therefore, it was hypothesised that the knockdown of TRIM26 would result in a longer half-life of NEIL1 and especially NEIL3 *in vivo* and a corresponding increase in resistance to genotoxic agents. Indeed, this has been shown by several different groups, including the Elder laboratory (Edmonds *et al.*, 2017; Martin, 2018) and recently in Li *et al.* (2020). Therefore, the fact that this was not observed in the experiments carried out in this project is difficult to explain how or why. The FA original cells with the FANCD2 deficiency (PD20) or correction (3.15) and NEIL3 siRNA

displayed increased resistance to MMC and cisplatin, and with TRIM26 siRNA an increased resistance to cisplatin, but statistically the most significant differences were the PD20 cells with NEIL3 siRNA when treated with the ICL-inducing agents (summarised in Figure 4.4). However, it could be noted that the studies promoted and enforced the theory based on cell survival data on cancer cell lines, mostly U2OS cell lines, based on the resistance against cisplatin (Edmonds *et al.*, 2017; Martin, 2018) and psoralen (Martin, 2018; Li *et al.*, 2020) induced ICLs, and only one of the studies was related to FA but did not involve TRIM26 (Li *et al.*, 2020). Additionally, TRIM26 had never been associated with the FA pathway apart from this study, and recently being identified by Zhang *et al.* (2019). However, Zhang *et al.* (2019) could not determine the relation between TRIM26, amongst other identified proteins, with SLX4/FANCP in the DNA nuclease scaffolding complex.

**Table 4.4: Growth inhibition summary of siRNA transfected FANCD2-deficient (U2OS-D2 and HeLa-D2) and WT/FANCD2 corrected (U2OS and HeLa) cell lines, following treatment with mitomycin C (MMC), cisplatin and TBHP.**

Cell Line	siRNA Transfection	IC <sub>50</sub> ± SD Values		
		MMC	Cisplatin	TBHP
3.15	+ NS siRNA	0.86 ± 0.19 µM	1.23 ± 0.26 µM	24.64 ± 3.08 µM
	+ NEIL3 siRNA	1.81 ± 0.63 µM	1.95 ± 0.60 µM	24.92 ± 2.87 µM
	+ TRIM26 siRNA	1.00 ± 0.01 µM	1.80 ± 0.11 µM	36.53 ± 3.55 µM
PD20	+ NS siRNA	0.14 ± 0.02 µM	0.48 ± 0.07 µM	22.41 ± 2.26 µM
	+ NEIL3 siRNA	0.24 ± 0.05 µM	1.02 ± 0.21 µM	24.77 ± 3.21 µM
	+ TRIM26 siRNA	0.10 ± 0.02 µM	0.74 ± 0.09 µM	24.98 ± 5.17 µM

IC<sub>50</sub> values derived from Section 3.5.2., Figures 3.54 – 3.56. Cells were transfected with non-specific (NS) siRNA, NEIL3 siRNA or TRIM26 siRNA. Mean data was collected from triplicate technical and scientific repeats.

Although it was theoretically expected for cells with TRIM26 knockout, based on the studies stated previously, to have had an increase in resistance to cisplatin, it was surprising that the results were not as significantly diverse as expected, and it was not expected for the NEIL3 knockdown results to display increased resistance to cisplatin as well as MMC, as summarised and displayed in Figure 4.4. Compared to the presumed NEIL3 overexpression

results of PD20 and 3.15 cells in Section 3.4.2. (summarised in Figure 4.4), this could signify that NEIL3 was not required and may have been a burden to the cells when treated with MMC and cisplatin, but required for resistance against oxidative-induced treatment. Though unexpected, it could be deduced that neither NEIL1 nor NEIL3 were required to excise MMC-induced ICLs, or TRIM26 was required but NEIL3 may have been a liability to the cells when treated with MMC. This contradicts what was observed from the MTT assays of NEIL3-overexpressing U2OS cells after antibiotic-selection (summarised in Figure 4.3), though the hNEIL3<sup>FL</sup>-FLAG overexpressing cells were described in Section 3.4.3. and observed from Figures 3.43A and 3.44A as struggling to duplicate after plasmid transfection and antibiotic selection. As it was hypothesised that an FA cell line with an impaired BER pathway was hypersensitive to ICLs compared to an FA cell line's sensitivity to ICL-inducing agents, synthetic lethality was not observed in the MTT assay results (Figures 4.4).

## Chapter 5 Conclusion and Future Work

NEIL1 overexpression was confirmed by western blotting in the WT and FA-generated cancer cells U2OS and HeLa but had minor or inconsistent effects on resistance to crosslinking and oxidising agents. Overexpression of NEIL3, either a truncated protein version (NEIL3<sup>1506</sup>) lacking the C-terminal GRF domains, or the full-length protein, proved more difficult to confirm by western blotting. However, the MTT assays generally indicated a small increase in resistance irrespective of FA background, suggesting that NEIL3 overexpression was achieved in these cells. Unexpectedly, knockdown of NEIL3 showed increased resistance against ICL and oxidative agents independent of FA phenotype, while knockdown of TRIM26 showed no clear effect on the sensitivity of the FA cell line to the genotoxic agents tested, and therefore synthetic lethality, was not observed. In conclusion, the results indicate that the overexpression of NEIL1 or NEIL3 could not compensate for the loss of the FA pathway of ICL repair and had little reproducible effect on the resistance of these cell lines to crosslinking and oxidizing agents.

Despite the recombinant NEIL3<sup>1506</sup> protein not displaying a significant or statistically significant increased resistance to genotoxic agents repeatedly in all cell lines, there was still increased resistance in the U2OS cells, regardless of FA phenotype, and especially against an oxidative-inducing agent. Therefore, the truncated NEIL3 protein could be used for potential NEIL3 treatment, but would require further testing and analysis. NEIL3 expression was not consistently confirmed through western blot with the NEIL3-specific monoclonal antibody used in this study and, therefore, would require producing a monoclonal antibody or use a polyclonal antibody instead. Similarly, FLAG-tag was not consistently confirmed for the recombinant NEIL3 expression studies, possibly due to the protein folding structure of NEIL3 or the low binding capacity of the FLAG-tag. The alternative could have been to bind a 3xFLAG-tag on the N terminus of NEIL3 or use an alternative protein tag, such as the HaloTag for low protein expression confirmation (England *et al.*, 2015). As a confirmation, it is recommended that NEIL1 and NEIL3 overexpression and knockout studies be repeated in FA cell lines related to the FA core complex, such as lymphoblast cells HSC-72 (FANCA deficient) and HSC-536 (FANCC deficient), or a *FANCM*<sup>-/-</sup> generated cell line, and related to the FA incision complex, such as 1333 cells (FANCO/ERCC4/XPF deficient), for a better understanding of relation to the FA pathway. Furthermore, it is recommended that this study would be repeated for confirmation through

CRISPR/Cas9 knockout of TRIM26 or NEIL3 in alternative cell lines and cell lines with high NEIL3 expressions, such as acute lymphoblastic leukaemia cell lines CEM-C1 or CEM-C7. For genotoxic treatment, it would be recommended to repeat the study with MMC, cisplatin and TBHP as confirmational controls, and use diepoxybutane or psoralen as an alternative diagnosis for ICL sensitivity, a texaphyrin-platinum(IV) (Pt[IV]) version of oxaliplatin as an alternative to cisplatin and for platinum-compound resistant cells (Thiabaud et al., 2020), and hydrogen peroxide as the alternative oxidative-inducing agent.

## References

- Ahmad, A.S., Ormiston-Smith, N. and Sasieni, P.D. (2015) Trends in the lifetime risk of developing cancer in Great Britain: comparison of risk for those born from 1930 to 1960, *British Journal of Cancer*. 112(5), pp. 943–947. doi: 10.1038/bjc.2014.606.
- Albelazi, M.S., Martin, P.R., Mohammed, S., Mutti, L., Parsons, J.L. and Elder, R.H. (2019) The Biochemical Role of the Human NEIL1 and NEIL3 DNA Glycosylases on Model DNA Replication Forks, *Genes*, 10(4), p. 315. doi: 10.3390/genes10040315.
- Alcón, P. Shakeel, S., Chen, Z.A., Rappsilber, J., Patel, K.J., et al. (2020) FANCD2–FANCI is a clamp stabilized on DNA by monoubiquitination of FANCD2 during DNA repair, *Nature Structural & Molecular Biology*, 27(3), pp. 240–248. doi: 10.1038/s41594-020-0380-1.
- Amjad, M.T., Chidharla, A. and Kasi, A. (2022) Cancer Chemotherapy, in StatPearls [Internet]. Treasure Island (FL), USA: StatPearls Publishing, pp. 1–15. [Updated 3 March 2022] Available at: <https://www.ncbi.nlm.nih.gov/books/NBK564367/?report=classic> [Accessed: 7 June 2022].
- Auerbach, A.D. (2015) Diagnosis of Fanconi Anemia by Diepoxybutane Analysis, in *Current Protocols in Human Genetics*. Hoboken, NJ, USA: John Wiley & Sons, Inc., pp. 8.7.1-8.7.17. doi: 10.1002/0471142905.hg0807s85.
- Berney, M. and McGouran, J.F. (2018) Methods for detection of cytosine and thymine modifications in DNA, *Nature Reviews Chemistry*. 2(11), pp. 332–348. doi: 10.1038/s41570-018-0044-4.
- Bhatt, M., Ivan, C., Xie, X. and Siddik, Z.H. (2017) Drug-dependent functionalization of wild-type and mutant p53 in cisplatin-resistant human ovarian tumor cells, *Oncotarget*. 8(7), pp. 10905–10918. doi: 10.18632/oncotarget.14228.
- Bosshard, M., Markkanen, E. and van Loon, B. (2012) Base Excision Repair in Physiology and Pathology of the Central Nervous System, *International Journal of Molecular Sciences*, 13(12), pp. 16172–16222. doi: 10.3390/ijms131216172.
- Boulikas, T., Pantos, A., Bellis, E. and Christofi, P. (2008) 'Platinum Drugs', in Missailidis, S. (ed.) *Anticancer Therapeutics*. Chichester, UK: John Wiley & Sons, Ltd. pp.55-78 doi: 10.1002/9780470697047.
- Bradford, M.M. (1976) A rapid and sensitive method for the quantitation of microgram quantities of protein utilizing the principle of protein-dye binding, *Analytical*

- Biochemistry*. Academic Press, 72(1–2), pp. 248–254. doi: 10.1016/0003-2697(76)90527-3.
- Buch, K. Peters, T., Nawroth, T., Sanger, M., Schmidberger, H. and Langguth, P. (2012) ‘Determination of cell survival after irradiation via clonogenic assay versus multiple MTT Assay--a comparative study.’, *Radiation oncology (London, England)*, 7(1), p. 1. doi: 10.1186/1748-717X-7-1.
- Cadet, J. and Wagner, J.R. (2013) DNA Base Damage by Reactive Oxygen Species, Oxidizing Agents, and UV Radiation, *Cold Spring Harbor Perspectives in Biology*, 5, pp. 1–16. doi: 10.1101/cshperspect.a012559.
- Carter, R.J. and Parsons, J.L. (2016) Base Excision Repair, a Pathway Regulated by Posttranslational Modifications, *Molecular and Cellular Biology*. 36(10), pp. 1426–1437. doi: 10.1128/MCB.00030-16.
- Castillo, P., Bogliolo, M. and Surralles, J. (2011) Coordinated action of the Fanconi anemia and ataxia telangiectasia pathways in response to oxidative damage, *DNA Repair*. 10(5), pp. 518–525. doi: 10.1016/j.dnarep.2011.02.007.
- Ceccaldi, R., Sarangi, P. and D’Andrea, A.D. (2016) The Fanconi anaemia pathway: new players and new functions, *Nature Reviews Molecular Cell Biology*, 17(6), pp. 337–349. doi: 10.1038/nrm.2016.48.
- Chen, W., Balakrishnan, K., Kuang, Y., Han, Y., Fu, M., Gandhi, V., *et al.* (2014) ‘Reactive oxygen species (ROS) inducible DNA cross-linking agents and their effect on cancer cells and normal lymphocytes.’, *Journal of Medicinal Chemistry*. American Chemical Society, 57(11), pp. 4498–510. doi: 10.1021/jm401349g.
- Chen, H.-Y. and Lin, Y.-F. (2021) ‘DFT mechanistic study on the formation of 8-oxoguanine and spiroiminodihydroantoin mediated by iron Fenton reactions.’, *Dalton transactions (Cambridge, England : 2003)*. Royal Society of Chemistry, 50(28), pp. 9842–9850. doi: 10.1039/d1dt01508g.
- Cheung, R.S. and Taniguchi, T. (2017) Recent insights into the molecular basis of Fanconi anemia: genes, modifiers, and drivers, *International Journal of Hematology*, 106(3), pp. 335–344. doi: 10.1007/s12185-017-2283-4.
- Clamp, M., Fry, B., Kamal, M., Xie, X., Cuff, J., Lin, M., *et al.* (2007) Distinguishing protein-coding and noncoding genes in the human genome, *Proceedings of the National Academy of Sciences USA*, 104(49), pp. 19428–19433. doi: 10.1073/pnas.0709013104.
- Clement, C., Vassias, I., Ray-Gallet, D. and Almouzni, G. (2016) Functional Characterization of Histone Chaperones Using SNAP-Tag-Based Imaging to Assess De

- Novo Histone Deposition., *Methods in Enzymology*, 573, pp. 97–117. doi: 10.1016/bs.mie.2016.04.004.
- Dasari, S. and Tchounwou, P.B. (2014) Cisplatin in cancer therapy: Molecular mechanisms of action, *European Journal of Pharmacology*, 740, pp. 364–378. doi: 10.1016/j.ejphar.2014.07.025.
- Datta, A. and Brosh Jr., R.M. (2019) Holding All the Cards—How Fanconi Anemia Proteins Deal with Replication Stress and Preserve Genomic Stability, *Genes*, 10(2), p. 170. doi: 10.3390/genes10020170.
- Daya-Grosjean, L. (2008) Xeroderma Pigmentosum and Skin Cancer, in *Molecular Mechanisms of Xeroderma Pigmentosum*. New York, NY: Springer New York, pp. 19–27. doi: 10.1007/978-0-387-09599-8\_3.
- Deans, A.J. and West, S.C. (2013) DNA interstrand crosslink repair and cancer, *Nature Reviews Cancer*, 11(7), pp. 467–480. doi: 10.1038/nrc3088.DNA.
- Dizdaroglu, M. and Jaruga, P. (2012) Mechanisms of free radical-induced damage to DNA, *Free Radical Research*, 46(4), pp. 382–419. doi: 10.3109/10715762.2011.653969.
- Dolinnaya, N.G., Kubareva, E.A., Romanova, E.A., Trikin, R.M. and Oretskaya, T.S. (2013) Thymidine glycol: the effect on DNA molecular structure and enzymatic processing, *Biochimie*. 95(2), pp. 134–147. doi: 10.1016/j.biochi.2012.09.008.
- Edmonds, M.J., Carter, R.J., Nickson, C.M., Williams, S.C. and Parsons, J.L. (2017) ‘Ubiquitylation-dependent regulation of NEIL1 by Mule and TRIM26 is required for the cellular DNA damage response’, *Nucleic Acids Research*, 45(2), pp. 726–738. doi: 10.1093/nar/gkw959.
- England, C.G., Luo, H. and Cai, W. (2015) ‘HaloTag technology: a versatile platform for biomedical applications.’, *Bioconjugate Chemistry*. American Chemical Society, 26(6), pp. 975–86. doi: 10.1021/acs.bioconjchem.5b00191.
- Evans, M.D., Saparbaev, M. and Cooke, M.S. (2010) DNA repair and the origins of urinary oxidized 2'-deoxyribonucleosides, *Mutagenesis*, 25(5), pp. 433–442. doi: 10.1093/mutage/geq031.
- Fakouri, N.B., Hou, Y., Demarest, T.G., Christiansen, L.S., Okur, M.N., Mohanty, J.G., Croteau, D.L., *et al.* (2019) Toward understanding genomic instability, mitochondrial dysfunction and aging, *The FEBS Journal*, 286(6), pp. 1058–1073. doi: 10.1111/febs.14663.
- Fleming, A.M., Zhu, J., Howpay Manage, S.A. and Burrows, C.J. (2019) ‘Human NEIL3 Gene Expression Regulated by Epigenetic-Like Oxidative DNA Modification.’,

- Journal of the American Chemical Society*, 141(28), pp. 11036–11049. doi: 10.1021/jacs.9b01847.
- Garaycochea, J.I., Crossan, G.P., Langevin, F., Mulderrig, L., Louzada, S., Yang, F., *et al.* (2018) Alcohol and endogenous aldehydes damage chromosomes and mutate stem cells, *Nature*. 553(7687), pp. 171–177. doi: 10.1038/nature25154.
- Garcia-Higuera, I. Taniguchi, T., Ganesan, S., Meyn, M.S., Timmers, C., Hejna, J., *et al.* (1999) Fanconi Anemia Proteins FANCA, FANCC, and FANCG/XRCC9 Interact in a Functional Nuclear Complex, *Molecular and Cellular Biology*. American Society for Microbiology, 19(7), pp. 4866–4873. doi: 10.1128/MCB.19.7.4866/FORMAT/EPUB.
- Garcia-Higuera, I. Taniguchi, T., Ganesan, S., Meyn, M.S., Timmers, C., Hejna, J., *et al.* (2001) Interaction of the Fanconi anemia proteins and BRCA1 in a common pathway, *Molecular cell*. 7(2), pp. 249–62. doi: 10.1016/s1097-2765(01)00173-3.
- Hanahan, D. and Weinberg, R. A. (2011) ‘Hallmarks of cancer: the next generation.’, *Cell*. Elsevier Inc., 144(5), pp. 646–74. doi: 10.1016/j.cell.2011.02.013.
- Hassanpour, S.H. and Dehghani, M. (2017) Review of cancer from perspective of molecular, *Journal of Cancer Research and Practice*. 4(4), pp. 127–129. doi: 10.1016/j.jcrpr.2017.07.001.
- He, F. (2011) Bradford Protein Assay, *BIO-PROTOCOL*, 1(6). doi: 10.21769/bioprotoc.45.
- He, Y.-F., Li, B.-Z., Li, Z., Liu, P., Wang, Y., Tang, Q., *et al.* (2011) Tet-Mediated Formation of 5-Carboxylcytosine and Its Excision by TDG in Mammalian DNA, *Science*. 333(6047), pp. 1303–1307. doi: 10.1126/science.1210944.
- Hegde, M.L., Hegde, P.M., Bellot, L.J., Mandal, S.M., Hazra, T.K., Li, G.-M., *et al.* (2013) Prereplicative repair of oxidized bases in the human genome is mediated by NEIL1 DNA glycosylase together with replication proteins. *Proceedings of the National Academy of Sciences USA*, 110(33), pp. E3090-9. doi: 10.1073/pnas.1304231110.
- Hendrich, B., Hardeland, U., Ng, H.-H., Jiricny, J. and Bird, A. (1999) The thymine glycosylase MBD4 can bind to the product of deamination at methylated CpG sites, *Nature*, 401(6750), pp. 301–304. doi: 10.1038/45843.
- Hussain, S., Wilson, J.B., Medhurst, A.L., Hejna, J., Witt, E., Ananth, S., *et al.* (2004) Direct interaction of FANCD2 with BRCA2 in DNA damage response pathways, *Human Molecular Genetics*. 13(12), pp. 1241–8. doi: 10.1093/hmg/ddh135.
- Ishida, R. and Buchwald, M. (1982) Susceptibility of Fanconi’s anemia lymphoblasts to DNA-cross-linking and alkylating agents, *Cancer Research*, 42(10), pp. 4000–6.

Available at: <http://www.ncbi.nlm.nih.gov/pubmed/6809308>.

- Iyama, T. and Wilson, D.M. (2014) DNA Repair Mechanisms in dividing and non-dividing cells, *DNA Repair*, 12(8), pp. 620–636. doi: 10.1016/j.dnarep.2013.04.015.DNA.
- Jacobs, A.L. and Schär, P. (2012) DNA glycosylases: in DNA repair and beyond, *Chromosoma*, 121(1), pp. 1–20. doi: 10.1007/s00412-011-0347-4.
- Joenje, H., Levitus, M., Waisfisz, Q., D'Andrea, A., Garcia-Higuera, I., Pearson, T., *et al.* (2000) Complementation analysis in Fanconi anemia: assignment of the reference FA-H patient to group A, *American journal of human genetics*, 67(3), pp. 759–62. doi: 10.1086/303067.
- Jorde, L.B., Carey, J.C. and Bamshad, M.J. (2016) *Medical Genetics*. 5th edn. ISBN: 978-0-323-18835-7.
- Jung, Y. and Lippard, S.J. (2007) Direct Cellular Responses to Platinum-Induced DNA Damage, *Chemical Reviews*, 107(5), pp. 1387–1407. doi: 10.1021/cr068207j.
- Kavli, B., Sundheim, O., Akbari, M., Otterlei, M., Nilsen, H., Skorpen, F., *et al.* (2002) hUNG2 Is the Major Repair Enzyme for Removal of Uracil from U:A Matches, U:G Mismatches, and U in Single-stranded DNA, with hSMUG1 as a Broad Specificity Backup, *Journal of Biological Chemistry*, 277(42), pp. 39926–39936. doi: 10.1074/jbc.M207107200.
- Kimble, D.C., Lach, F.P., Gregg, S.Q., Donovan, F.X., Flynn, E.K., Kamat, A., *et al.* (2018) ‘A comprehensive approach to identification of pathogenic FANCA variants in Fanconi anemia patients and their families’, *Human Mutation*, 39(2), pp. 237–254. doi: 10.1002/humu.23366.
- Kino, K., Hirao-Suzuki, M., Morikawa, M., Sakaga, A. and Miyazawa, H. (2017) Generation, repair and replication of guanine oxidation products, *Genes and Environment*, 39(1), p. 21. doi: 10.1186/s41021-017-0081-0.
- Kino, K., Kawada, T., Hirao-Suzuki, M., Morikawa, M., Miyazawa, H. (2020) Products of Oxidative Guanine Damage Form Base Pairs with Guanine, *International Journal of Molecular Sciences*, 21(20), p. 7645. doi: 10.3390/ijms21207645.
- Klattenhoff, A.W., Thakur, M., Chu, C.S., Ray, D., Habib, S.L. and Kidane, D. (2017) Loss of NEIL3 DNA glycosylase markedly increases replication associated double strand breaks and enhances sensitivity to ATR inhibitor in glioblastoma cells, *Oncotarget*, 8(68), pp. 112942–112958. doi: 10.18632/oncotarget.22896.
- Krokan, H.E. and Bjoras, M. (2013) Base Excision Repair, *Cold Spring Harbor Perspectives in Biology*, 5(4), pp. a012583–a012583. doi: 10.1101/cshperspect.a012583.

- Kuhnert, V.M. Kachnic, L.A., Li, L., Purschke, M., Gheorghiu, L., Lee, R., *et al.* (2009) ‘FANCD2-deficient human fibroblasts are hypersensitive to ionising radiation at oxygen concentrations of 0% and 3% but not under normoxic conditions’, *International Journal of Radiation Biology*, 85(6), pp. 523–531. doi: 10.1080/09553000902883810.
- Lee, J.O., Kang, M.J., Byun, W.S., Kim, S.A., Seo, I.H., Han, J.A., *et al.* (2019) ‘Metformin overcomes resistance to cisplatin in triple-negative breast cancer (TNBC) cells by targeting RAD51’, *Breast Cancer Research*. *Breast Cancer Research*, 21(1), pp. 1–18. doi: 10.1186/s13058-019-1204-2.
- Li, N., Wang, J., Wallace, S.S., Chen, J., Zhou, J. and D'Andrea, A.D. (2020) ‘Cooperation of the NEIL3 and Fanconi anemia/BRCA pathways in interstrand crosslink repair.’, *Nucleic acids research*. Oxford University Press, 48(6), pp. 3014–3028. doi: 10.1093/nar/gkaa038.
- Liang, Y., Lin, S.-Y., Brunicardi, F.C., Goss, J. and Li, K. (2009) DNA Damage Response Pathways in Tumor Suppression and Cancer Treatment, *World Journal of Surgery*, 33(4), pp. 661–666. doi: 10.1007/s00268-008-9840-1.
- Lopez-Martinez, D., Liang, C.-C. and Cohn, M.A. (2016) Cellular response to DNA interstrand crosslinks: the Fanconi anemia pathway, *Cellular and Molecular Life Sciences*. 73(16), pp. 3097–3114. doi: 10.1007/s00018-016-2218-x.
- Lovell, M.A. and Markesbery, W.R. (2007) Oxidative DNA damage in mild cognitive impairment and late-stage Alzheimer’s disease, *Nucleic Acids Research*, 35(22), pp. 7497–7504. doi: 10.1093/nar/gkm821.
- Macé-Aimé, G., Couvé, S., Khassenov, B., Rosselli, F. and Saparbaev, M.K. (2010) The Fanconi anemia pathway promotes DNA glycosylase-dependent excision of interstrand DNA crosslinks, *Environmental and Molecular Mutagenesis*, 51(6), pp. 508–519. doi: 10.1002/em.20548.
- Maejima, Y., Zablocki, D. and Sadoshima, J. (2012) Oxidative Stress and Cardiac Muscle, *Muscle*. First Edit. pp. 309–322. doi: 10.1016/B978-0-12-381510-1.00023-5.
- Martin, P.R., Couvé, S., Zutterling, C., Albelazi, M.S., Groisman, R., Matkarimov, B.T., *et al.* (2017) The Human DNA glycosylases NEIL1 and NEIL3 Excise Psoralen-Induced DNA-DNA Cross-Links in a Four-Stranded DNA Structure, *Scientific Reports*, 7(1), pp. 1–13. doi: 10.1038/s41598-017-17693-4.
- Martin, P.R. (2018) *The Role of the Human Endonuclease VIII-Like 1 and 3 In the Repair of DNA Replication Blocking Lesions*. *PhD Thesis 2018*. The University of Salford. Available at: <http://usir.salford.ac.uk/id/eprint/49195/1/Thesis Peter Martin Final>

corrected 071218.pdf

- Massaad, M.J., Zhou, J., Tsuchimoto, D., Chou, J., Jabara, H., Janssen, E., *et al.* (2016) 'Deficiency of base excision repair enzyme NEIL3 drives increased predisposition to autoimmunity', *The Journal of Clinical Investigation*. American Society for Clinical Investigation, 126(11), p. 4219. doi: 10.1172/JCI85647.
- Maynard, S., Schurman, S.H., Harboe, C., de Souza-Pinto, N.C., Bohr, V.A. (2008) Base excision repair of oxidative DNA damage and association with cancer and aging, *Carcinogenesis*, 30(1), pp. 2–10. doi: 10.1093/carcin/bgn250.
- McCord, J.M. and Fridovich, I. (1968) The reduction of cytochrome c by hypoxanthine and xanthine oxidase, *Journal of Biological Chemistry*, 243(21), pp. 5753–5760. doi: 4972775.
- McHugh, P.J., Spanswick, V.J. and Hartley, J.A. (2001) 'Repair of DNA interstrand crosslinks: molecular mechanisms and clinical relevance.', *The Lancet. Oncology*, 2(8), pp. 483–90. doi: 10.1016/S1470-2045(01)00454-5.
- Mehta, P.A., Emoto, C., Fukuda, T., Seyboth, B., Teusink-Cross, A., Davies, S.M. (2019) 'Busulfan Pharmacokinetics and Precision Dosing: Are Patients with Fanconi Anemia Different?', *Biology of Blood and Marrow Transplantation*. NIH Public Access, 25(12), pp. 2416–2421. doi: 10.1016/j.bbmt.2019.07.014.
- Mehta, P.A. and Ebens, C. (2002) Fanconi Anemia (GeneReviews), in Adam, M.P., Ardinger, H.H., Pagon, R.A. and Wallace, S.E. (eds) GeneReviews® [Internet]. Seattle (WA), USA: University of Washington, Seattle, pp. 1–34. [Updated 3 June 2021] Available at: <http://www.ncbi.nlm.nih.gov/books/NBK1401/>. [Accessed 31 Aug. 2021].
- Nakabeppu, Y. (2014) Cellular Levels of 8-Oxoguanine in either DNA or the Nucleotide Pool Play Pivotal Roles in Carcinogenesis and Survival of Cancer Cells, *International Journal of Molecular Sciences*, 15(7), pp. 12543–12557. doi: 10.3390/ijms150712543.
- Neurauter, C.G., Luna, L. and Bjørås, M. (2012) Release from quiescence stimulates the expression of human NEIL3 under the control of the Ras dependent ERK–MAP kinase pathway, *DNA Repair*. 11(4), pp. 401–409. doi: 10.1016/j.dnarep.2012.01.007.
- O'Connor, M.J. (2015) Targeting the DNA Damage Response in Cancer, *Molecular Cell*. 60(4), pp. 547–560. doi: 10.1016/j.molcel.2015.10.040.
- Okonechnikov, K., Golosova, O. and Fursov, M. (2012) Unipro UGENE: a unified bioinformatics toolkit, *Bioinformatics*, 28(8), pp. 1166–1167. doi: 10.1093/bioinformatics/bts091.

- O’Neil, N. J., Bailey, M. L. and Hieter, P. (2017) ‘Synthetic lethality and cancer’, *Nature Reviews Genetics* 2017 18:10. Nature Publishing Group, 18(10), pp. 613–623. doi: 10.1038/nrg.2017.47.
- O’Reilly, E.M., Lee, J.W., Zalupski, M., Capanu, M., Park, J., Golan, T., *et al.* (2020) ‘Randomized, Multicenter, Phase II Trial of Gemcitabine and Cisplatin With or Without Veliparib in Patients With Pancreas Adenocarcinoma and a Germline BRCA/PALB2 Mutation.’, *Journal of clinical oncology : official journal of the American Society of Clinical Oncology*. American Society of Clinical Oncology, 38(13), pp. 1378–1388. doi: 10.1200/JCO.19.02931.
- Pang, Q. and Andreassen, P.R. (2009) Fanconi anemia proteins and endogenous stresses, *Mutation Research/Fundamental and Molecular Mechanisms of Mutagenesis*, 668(1–2), pp. 42–53. doi: 10.1016/j.mrfmmm.2009.03.013.
- Parsons, J.L. and Edmonds, M. J. (2016) ‘The Base Excision Repair Pathway’, in *Encyclopedia of Cell Biology*. Elsevier, pp. 442–450. doi: 10.1016/B978-0-12-394447-4.10046-X.
- Phaniendra, A., Jestadi, D.B. and Periyasamy, L. (2015) Free Radicals: Properties, Sources, Targets, and Their Implication in Various Diseases, *Indian Journal of Clinical Biochemistry*, 30(1), pp. 11–26. doi: 10.1007/s12291-014-0446-0.
- Pierce, B. A. (2014) Genetics: A Conceptual Approach. 5th edn. USA: Freeman, W.H. & Company. ISBN: 9781464109461.
- Rathod, D.G., Muneer, H. and Masood, S. (2022) Phototherapy, in StatPearls [Internet]. Treasure Island (FL), USA: StatPearls Publishing, pp. 1-10. [Updated 8 May 2022] Available at: <https://www.ncbi.nlm.nih.gov/books/NBK563140/> [Accessed: 7 April 2022].
- Regnell, C.E., Hildrestrand, G.A., Sejersted, Y., Medin, T., Moldestad, O., Rolseth, V., *et al.* (2012) ‘Hippocampal Adult Neurogenesis Is Maintained by Neil3-Dependent Repair of Oxidative DNA Lesions in Neural Progenitor Cells’, *Cell Reports*. Elsevier, 2(3), pp. 503–510. doi: 10.1016/J.CELREP.2012.08.008.
- Reis, A. and Hermanson, O. (2012) ‘The DNA glycosylases OGG1 and NEIL3 influence differentiation potential, proliferation, and senescence-associated signs in neural stem cells’, *Biochemical and Biophysical Research Communications*. Academic Press, 423(4), pp. 621–626. doi: 10.1016/J.BBRC.2012.04.125.
- Robson, M., Im, S., Senkus, E., Xu, B., Domchek, S., Masuda, N., *et al.* (2017) ‘Olaparib for Metastatic Breast Cancer in Patients with a Germline BRCA Mutation.’, *The New*

- England Journal of Medicine*, 377(6), pp. 523–533. doi: 10.1056/NEJMoa1706450.
- Rodriguez, A.A., Wojtaszek, J.L., Greer, B.H., Haldar, T., Gates, K.S., Williams, R.S., *et al.* (2020) ‘An autoinhibitory role for the GRF zinc finger domain of DNA glycosylase NEIL3’, *Journal of Biological Chemistry*. Elsevier, 295(46), pp. 15566–15575. doi: 10.1074/jbc.RA120.015541.
- Rolseth, V., Krokeide, S.Z., Kunke, D., Neurauter, C.G., Suganthan, R., Sejersted, Y., *et al.* (2013) Loss of Neil3, The major DNA glycosylase activity for removal of hydantoins in single stranded DNA, Reduces cellular proliferation and sensitizes cells to genotoxic stress, *Biochimica et Biophysica Acta - Molecular Cell Research*. 1833(5), pp. 1157–1164. doi: 10.1016/j.bbamcr.2012.12.024.
- Rolseth, V., Luna, L., Olsen, A.K., Suganthan, R., Scheffler, K., Neurauter, C.G., *et al.* (2017) ‘No cancer predisposition or increased spontaneous mutation frequencies in NEIL DNA glycosylases-deficient mice’, *Scientific Reports*, 7(1), p. 4384. doi: 10.1038/s41598-017-04472-4.
- Roy, L.M. Jaruga, P., Wood, T.G., McCullough, A.K., Dizdaroglu, M., and Stephen Lloyd, R., (2006) ‘Human Polymorphic Variants of the NEIL1 DNA Glycosylase’, *The Journal Of Biological Chemistry*, 103(21), pp. 15790–15798. doi: 10.1074/jbc.M610626200.
- Schwab, R.A. *et al.* (2015) The Fanconi Anemia Pathway Maintains Genome Stability by Coordinating Replication and Transcription, *Molecular Cell*. Elsevier, 60(3), pp. 351–361. doi: 10.1016/j.molcel.2015.09.012.
- Shinmura, K., Kato, H., Kawanishi, Y., Igarashi, H., Goto, M., Tao, H., *et al.* (2016) Abnormal Expressions of DNA Glycosylase Genes NEIL1, NEIL2, and NEIL3 Are Associated with Somatic Mutation Loads in Human Cancer, *Oxidative Medicine and Cellular Longevity*. 2016, pp. 1–10. doi: 10.1155/2016/1546392.
- Sinawe, H. and Casadesus, D. (2022) Mitomycin, in StatPearls [Internet]. Treasure Island (FL), USA: StatPearls Publishing, pp. 1-8. [Updated 29 July 2021]. Available at: <https://www.ncbi.nlm.nih.gov/books/NBK562249/> [Accessed: 7 April 2022].
- Smith, R.W.A., Monroe, C. and Bolnick, D.A. (2015) Detection of Cytosine Methylation in Ancient DNA from Five Native American Populations Using Bisulfite Sequencing, *PLOS ONE*. 10(5), p. e0125344. doi: 10.1371/journal.pone.0125344.
- Srivenugopal, K.S., Yuan, X., Friedman, H.S. and Ali-Osman, F. (1996) Ubiquitination-Dependent Proteolysis of O<sup>6</sup>-Methylguanine-DNA Methyltransferase in Human and Murine Tumor Cells following Inactivation with O<sup>6</sup>-Benzylguanine or 1,3-Bis(2-chloroethyl)-1-nitrosourea, *Biochemistry*, 35(4), pp. 1328–1334. doi:

10.1021/bi9518205.

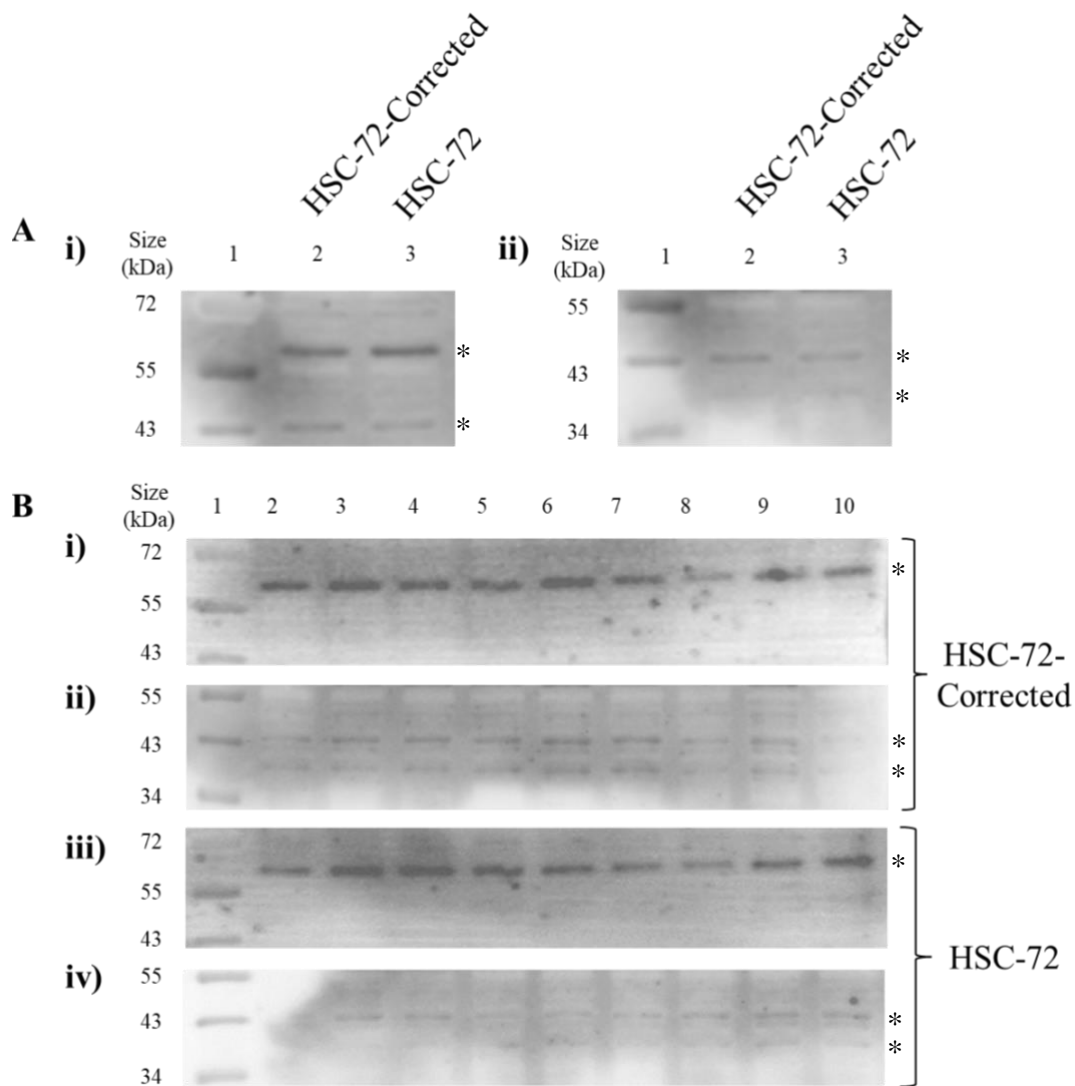
- Strachan, T. and Read, A. (2010) *Human Molecular Genetics*. 4th edn. New York, USA: Garland Science/Taylor & Francis Group. ISBN: 9780815341499.
- Taylor, S.J., Arends, M.J. and Langdon, S.P. (2020) ‘Inhibitors of the Fanconi anaemia pathway as potential antitumour agents for ovarian cancer’, *Exploration of Targeted Anti-tumor Therapy*, 1(1), pp. 26–52. doi: 10.37349/etat.2020.00003.
- Thiabaud, G., He, G., Sen, S., Shelton, K.A., Baze, W.B., Segura, L., *et al.* (2020) ‘Oxaliplatin Pt(IV) prodrugs conjugated to gadolinium-texaphyrin as potential antitumor agents.’, *Proceedings of the National Academy of Sciences of the USA*, 117(13), pp. 7021–7029. doi: 10.1073/pnas.1914911117.
- Timmers, C., Taniguchi, T., Hejna, J., Reifsteck, C., Lucas, L., Bruun, D., *et al.* (2001) Positional Cloning of a Novel Fanconi Anemia Gene, FANCD2, *Molecular Cell*, 7(2), pp. 241–248. doi: 10.1016/S1097-2765(01)00172-1.
- Tini, M., Benecke, A., Um, S.-J., Torchia, J., Evans, R.M. and Chambon, P. (2002) Association of CBP/p300 Acetylase and Thymine DNA Glycosylase Links DNA Repair and Transcription, *Molecular Cell*, 9(2), pp. 265–277. doi: 10.1016/S1097-2765(02)00453-7.
- Tran, O.T., Tadesse, S., Chu, C., Kidane, D. (2020) ‘Overexpression of NEIL3 associated with altered genome and poor survival in selected types of human cancer.’, *Tumour biology : the journal of the International Society for Oncodevelopmental Biology and Medicine*, 42(5), p. 1010428320918404. doi: 10.1177/1010428320918404.
- Tremblay, S. and Wagner, J.R. (2007) Dehydration, deamination and enzymatic repair of cytosine glycols from oxidized poly(dG-dC) and poly(dI-dC), *Nucleic Acids Research*, 36(1), pp. 284–293. doi: 10.1093/nar/gkm1013.
- Tsuiko, O., Jatsenko, T., Parameswaran Grace, L.K., Kurg, A., Vermeesch, J.R., *et al.* (2019) A speculative outlook on embryonic aneuploidy: Can molecular pathways be involved?, *Developmental Biology*, 447(1), pp. 3–13. doi: 10.1016/j.ydbio.2018.01.014.
- Tudek, B. (2003) Imidazole Ring-Opened DNA Purines and Their Biological Significance, *BMB Reports*, 36(1), pp. 12–19. doi: 10.5483/BMBRep.2003.36.1.012.
- Ubhi, T. and Brown, G. W. (2019) ‘Exploiting DNA Replication Stress for Cancer Treatment’, *Cancer Research*. American Association for Cancer Research Inc., 79(8), pp. 1730–1739. doi: 10.1158/0008-5472.CAN-18-3631.
- Vartanian, V., Lowell, B., Minko, I.G., Wood, T.G., Ceci, J.D., George, S., *et al.* (2006)

- 'The metabolic syndrome resulting from a knockout of the NEIL1 DNA glycosylase', *Proceedings of the National Academy of Sciences of the USA*. National Academy of Sciences, 103(6), p. 1864. doi: 10.1073/PNAS.0507444103.
- Virag, P., Perde-Schrepler, M., Fischer-Fodor, E., Tatomir, C., Dorneanu, S.A., Cernea, V.I., *et al.* (2012) Superior cytotoxicity and DNA cross-link induction by oxaliplatin versus cisplatin at lower cellular uptake in colorectal cancer cell lines, *Anti-cancer drugs*, 23(10), pp. 1032–8. doi: 10.1097/CAD.0b013e328355076f.
- Volk, D.E., Thiviyanathan, V., Somasunderam, A. and Gorenstein, D.G. (2007) Ab initio base-pairing energies of an oxidized thymine product, 5-formyluracil, with standard DNA bases at the BSSE-free DFT and MP2 theory levels, *Organic & Biomolecular Chemistry*, 5(10), p. 1554. doi: 10.1039/b702755a.
- Waisfisz, Q., de Winter, J.P., Kruyt, F.A.E., de Groot, J., van der Weel, L., Dijkmans, L.M., *et al.* (1999) A physical complex of the Fanconi anemia proteins FANCG/XRCC9 and FANCA, *Proceedings of the National Academy of Sciences*, 96(18), pp. 10320–10325. doi: 10.1073/pnas.96.18.10320.
- Wallace, B.D., Berman, Z., Mueller, G.A., Lin, Y., Chang, T., Andres, S.N., *et al.* (2017) APE2 Zf-GRF facilitates 3'-5' resection of DNA damage following oxidative stress, *Proceedings of the National Academy of Sciences USA*, 114(2), pp. 304–309. doi: 10.1073/pnas.1610011114.
- Wallace, S.S. (2002) Biological consequences of free radical-damaged DNA bases, *Free Radical Biology and Medicine*, 33(1), pp. 1–14. doi: 10.1016/S0891-5849(02)00827-4.
- Wallace, S.S. (2013) DNA glycosylases search for and remove oxidized DNA bases, *Environmental and Molecular Mutagenesis*, 54(9), pp. 691–704. doi: 10.1002/em.21820.
- Wang, J., Sarkar, T.R., Zhou, M., Sharan, S., Ritt, D.A., Veenstra, T.D., *et al.* (2010) CCAAT/enhancer binding protein delta (C/EBP $\delta$ , CEBPD)-mediated nuclear import of FANCD2 by IPO4 augments cellular response to DNA damage, *Proceedings of the National Academy of Sciences*, 107(37), pp. 16131–16136. doi: 10.1073/pnas.1002603107.
- Wang, K., Chai, L., Qiu, Z., Zhang, Y., Gao, H. and Zhang, X. (2019) Overexpression of TRIM26 suppresses the proliferation, metastasis, and glycolysis in papillary thyroid carcinoma cells, *Journal of Cellular Physiology*. 234(10), pp. 19019–19027. doi: 10.1002/jcp.28541.
- Wang, L.C. and Gautier, J. (2010) The Fanconi anemia pathway and ICL repair: implications

- for cancer therapy, *Critical Reviews in Biochemistry and Molecular Biology*, 45(5), pp. 424–439. doi: 10.3109/10409238.2010.502166.
- Whitaker, A.M., Schaich, M.A., Smith, M.R., Flynn, T.S. and Freudenthal, B.D. (2017) Base excision repair of oxidative DNA damage: from mechanism to disease, *Frontiers in bioscience (Landmark edition)*, 22, pp. 1493–1522. Available at: <http://www.ncbi.nlm.nih.gov/pubmed/28199214>.
- White, B., Tarun, M.C., Gathergood, N., Rusling, J.F. and Smyth, M.R. (2005) Oxidised guanidinohydantoin (Gh ox ) and spiroiminodihydantoin (Sp) are major products of iron- and copper-mediated 8-oxo-7,8-dihydroguanine and 8-oxo-7,8-dihydro-2'-deoxyguanosine oxidation, *Molecular BioSystems*, 1(5–6), pp. 373–381. doi: 10.1039/B511756A.
- Wilson, D.M. and Seidman, M.M. (2010) A novel link to base excision repair?, *Trends in Biochemical Sciences*. 35(5), pp. 247–252. doi: 10.1016/j.tibs.2010.01.003.
- Wolff, R.A., Abbruzzese, J. and Evans, D.B. (2003) 'Treatment of metastatic disease', in Kufe, D.W., Pollock, R.E., Weichselbaum, R.R., *et al.* (eds) *Holland-Frei Cancer Medicine*. 6th edn. [Internet] Hamilton (ON), USA. Available at: <https://www.ncbi.nlm.nih.gov/books/NBK14030/> [Accessed: 27 July 2022].
- Wu, R.A., Semlow, D.R., Kamimae-Lanning, A.N., Kochenova, O.V., Chistol, G., Hodson, M.R., *et al.* (2019) TRAIP is a master regulator of DNA interstrand crosslink repair, *Nature*. Springer US, 567(7747), pp. 267–272. doi: 10.1038/s41586-019-1002-0.
- Zhang, H., Chen, Z., Ye, Y., Ye, Z., Cao, D., Xiong, Y., *et al.* (2019) SLX4IP acts with SLX4 and XPF-ERCC1 to promote interstrand crosslink repair., *Nucleic Acids Research*. 47(19), pp. 10181–10201. doi: 10.1093/nar/gkz769.
- Zhao, W., Li, Q., Ayers, S., Gu, Y., Shi, Z., Zhu, Q., *et al.* (2013) Jmjd3 inhibits reprogramming by upregulating expression of INK4a/Arf and targeting PHF20 for ubiquitination, *Cell*. 152(5), pp. 1037–50. doi: 10.1016/j.cell.2013.02.006.
- Zhou, J., Liu, M., Fleming, A.M., Burrows, C.J. and Wallace, S.S. (2013) Neil3 and NEIL1 DNA Glycosylases Remove Oxidative Damages from Quadruplex DNA and Exhibit Preferences for Lesions in the Telomeric Sequence Context, *Journal of Biological Chemistry*, 288(38), pp. 27263–27272. doi: 10.1074/jbc.M113.479055.
- Zhou, J., Chan, J., Lambel , M., Yusufzai, T., Stumpff, J., Opresko, P.L., *et al.* (2017) NEIL3 Repairs Telomere Damage during S Phase to Secure Chromosome Segregation at Mitosis, *Cell Reports*, 20(9), pp. 2044–2056. doi: 10.1016/j.celrep.2017.08.020.

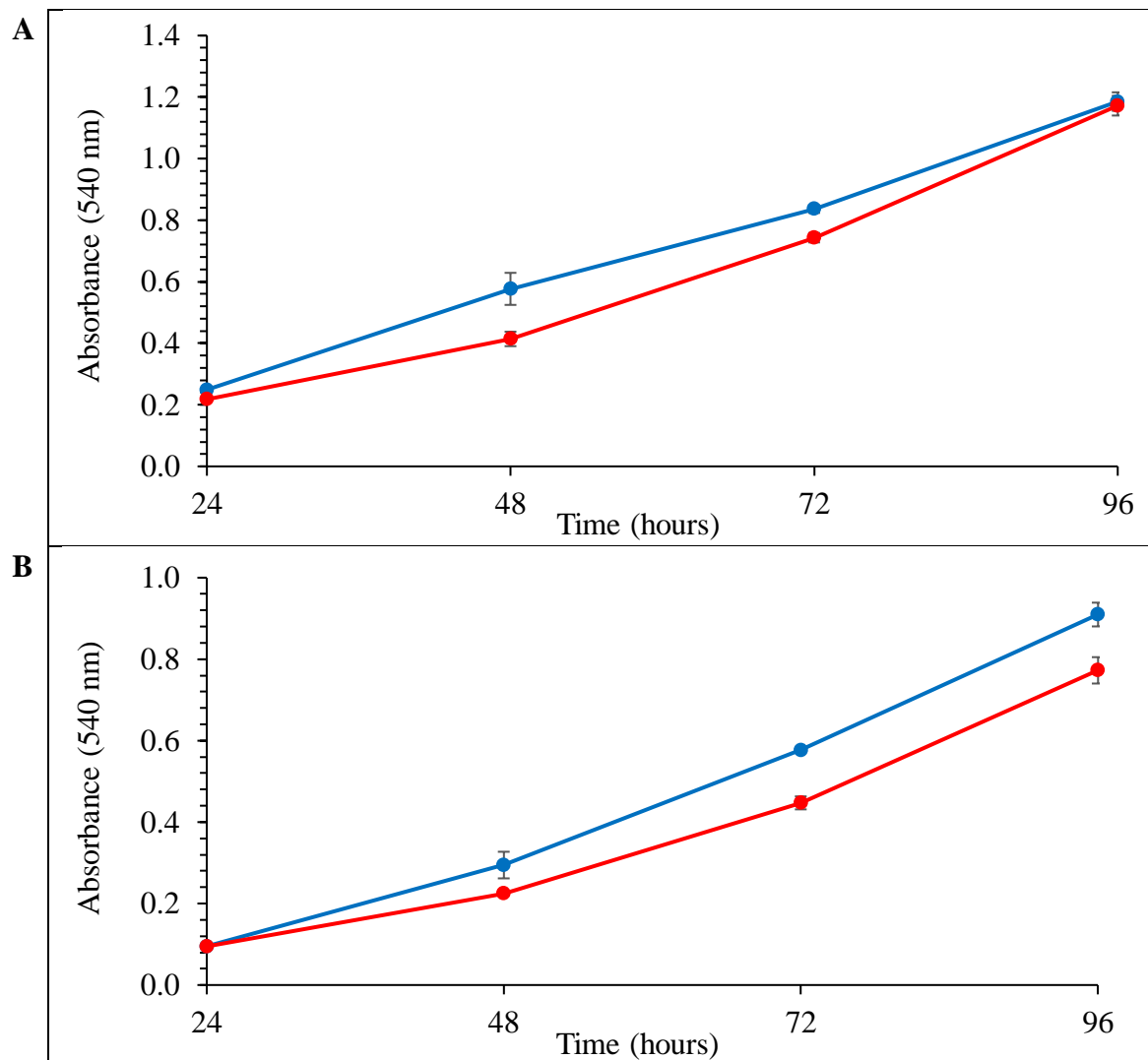
Zhou, J. Kang, Y., Chen, L., Wang, H., Liu, J., Zeng, S., *et al.* (2020) ‘The Drug-Resistance Mechanisms of Five Platinum-Based Antitumor Agents’, *Frontiers in Pharmacology*. Frontiers Media SA, 11. doi: 10.3389/fphar.2020.00343.

Appendix



**Appendix Figure 1: Western blots of HSC-72 (FANCA Deficient) and HSC-72-Corrected cell extracts following treatment with MMC. (A[i], B[i, iii]) NEIL3 and (A[ii], B[ii, iv]) NEIL1.**

(A) Lane 1, protein ladder; lane 2, HSC-72-Corrected control; lane 3, HSC-72 control. (B[i, ii]) HSC-72-Corrected cell extracts, (B[iii, iv]) HSC-72 cell extracts. Lane 1, protein ladder; lane 2 – 4, 1 h incubation treatment at 3  $\mu$ M, 0.3  $\mu$ M and 0.03  $\mu$ M MMC, respectively; lane 5 – 7, 8 h incubation treatment at 3  $\mu$ M, 0.3  $\mu$ M and 0.03  $\mu$ M MMC, respectively; lane 8 – 10, 24 h incubation treatment at 3  $\mu$ M, 0.3  $\mu$ M and 0.03  $\mu$ M MMC, respectively. Expected molecular weight: NEIL3, 68 kDa; NEIL1, 43 kDa. Cell extracts were from suspended and collected cells, protein extraction with a resuspension buffer and lysis buffer from Elder Laboratory stocks. (\*) Non-specific binding.

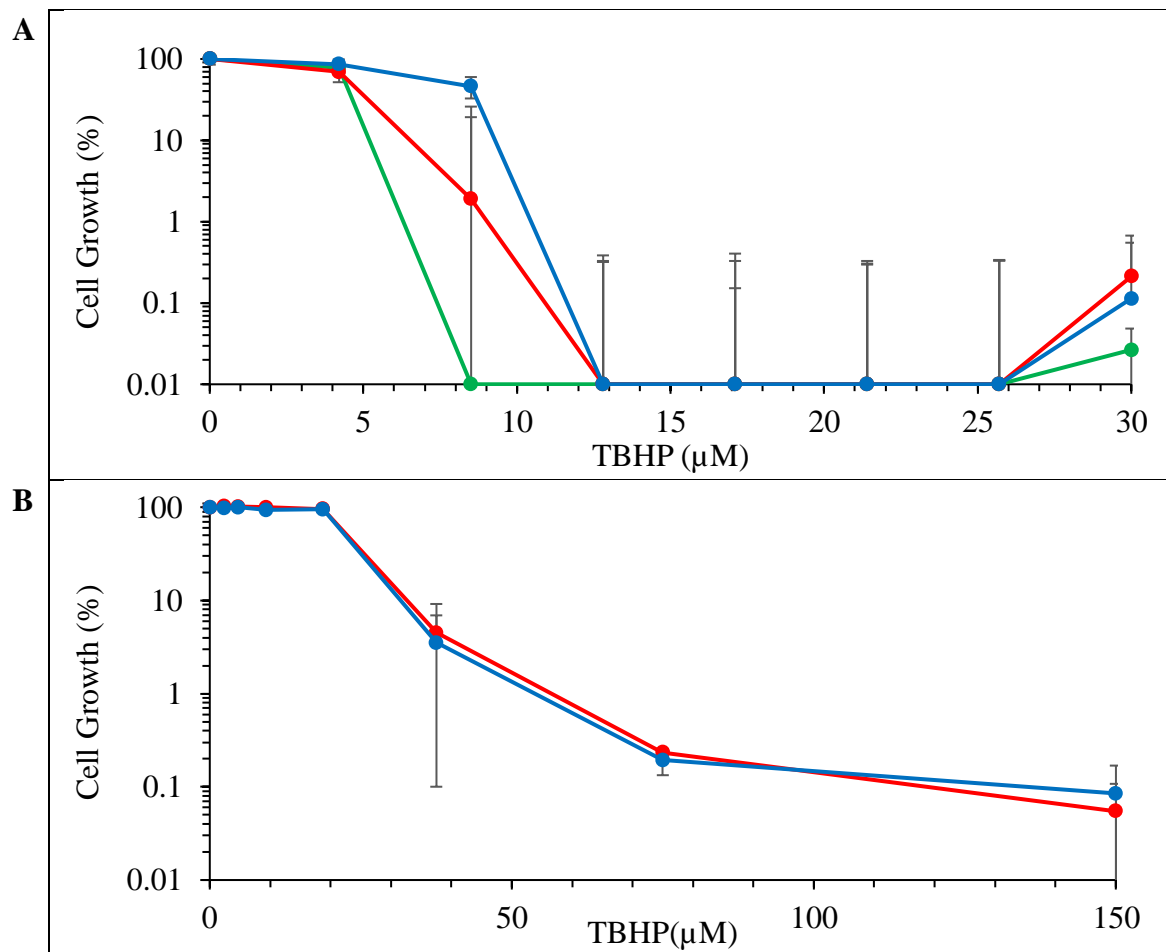


**D**

	Doubling Time		
	2 x 10 <sup>3</sup> cells	1 x 10 <sup>3</sup> cells	Mean ± SD
U2OS	33.01 min	22.36 min	27.68 ± 7.53 min
U2OS-D2	29.50 min	23.82 min	26.66 ± 4.01 min

**Appendix Figure 2: Growth of U2OS (WT, blue) and U2OS-D2 (FANCD2 deficient, red) cells determined using the MTT assay.**

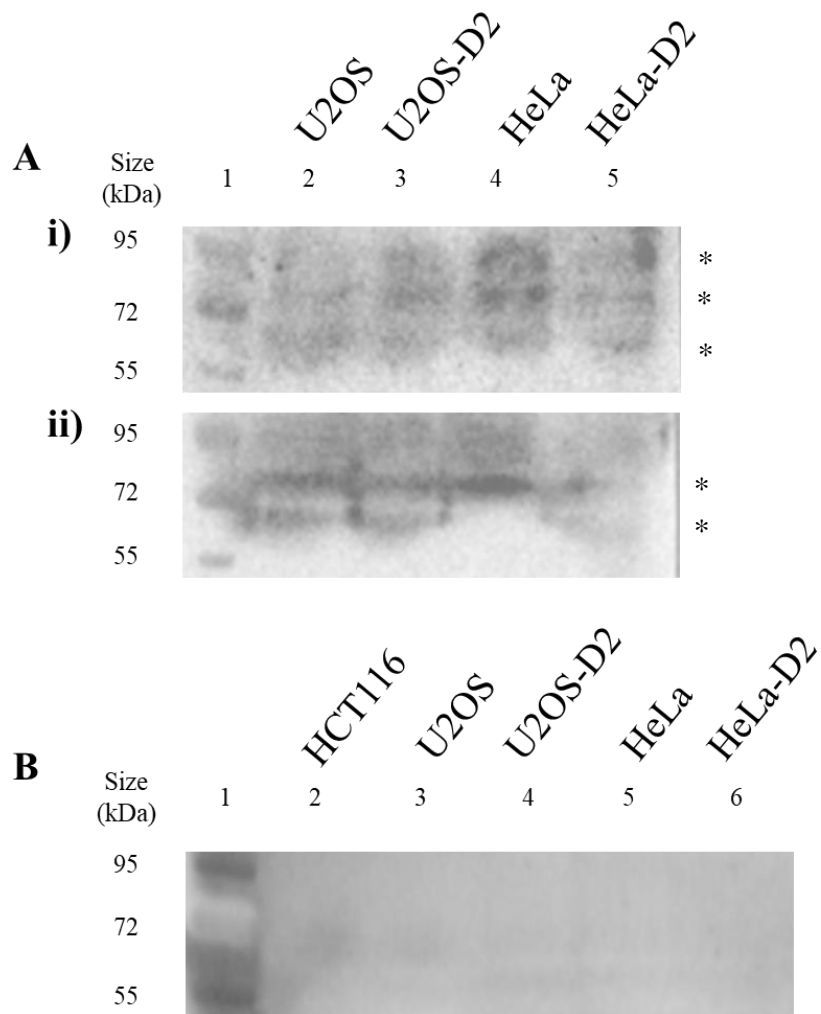
(A) 2 x 10<sup>3</sup> cells and (B) 1 x 10<sup>3</sup> cells per well. (C) Doubling times of U2OS and U2OS-D2 cells from cell seedings (A and B) between 24 h and 96 h. Mean data was collected from triplicate technical repeats.



	IC <sub>50</sub> ±SD Values
HSC-93	3.36 ± 0.25 μM
HSC-72-Corrected	8.61 ± 1.15 μM
HSC-72	3.44 ± 0.28 μM
3.15	25.67 ± 11.76 μM
PD20	26.52 ± 13.27 μM

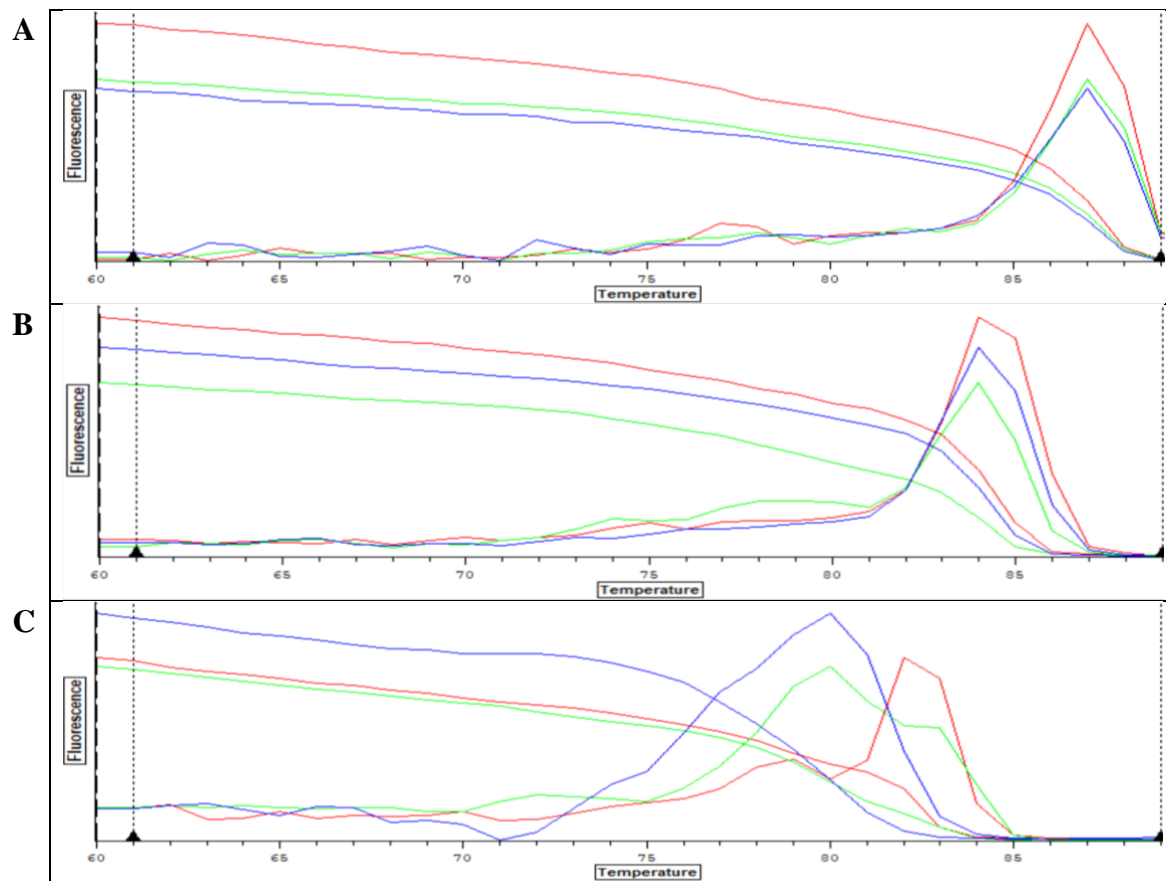
**Appendix Figure 3: Growth inhibition of (A) HSC-93 (WT, green), HSC-72 (FANCD2 deficient, red) and HSC-72-Corrected (blue), and (B) PD20 (FANCD2 deficient, red) and 3.15 (PD20 Corrected, blue), following treatment with TBHP.**

**B)** IC<sub>50</sub> values for growth inhibition following treatment. HSC-93/-72/-72-Corrected, 3-72-Corrected 1 x 10<sup>4</sup> cells per 96-well, incubated for 72 h. PD20/3.15, 3 x 10<sup>3</sup> cells per 96-well, incubated for 72 h. Mean data was collected from triplicate technical repeats.



**Appendix Figure 4: Western blots of cancer cell lines U2OS (WT), U2OS-D2 (FANCD2 Deficient), HeLa (WT), HeLa-D2 (FANCD2 Deficient) and HCT116 (WT) cell extracts for NEIL3.**

(A) Blocking buffer before primary antibody at (i) 4°C overnight or (ii) 37°C for 1 h. Lane 1, protein ladder; lane 2, U2OS; lane 3, U2OS-D2; lane 4, HeLa; lane 5, HeLa-D2. (B) Increased volumes of quantified cell extracts (up to 200 µg) loaded and blocking buffer at 4°C overnight. Lane 1, protein ladder; lane 2, HCT116; lane 3, U2OS; lane 4, U2OS-D2; lane 5, HeLa; lane 6, HeLa-D2. Expected molecular weight for NEIL3, 68 kDa. Cell extracts from suspended and collected cells, and protein extraction with a resuspension buffer followed by a lysis buffer from Elder Laboratory stocks. (\*) Non-specific binding.

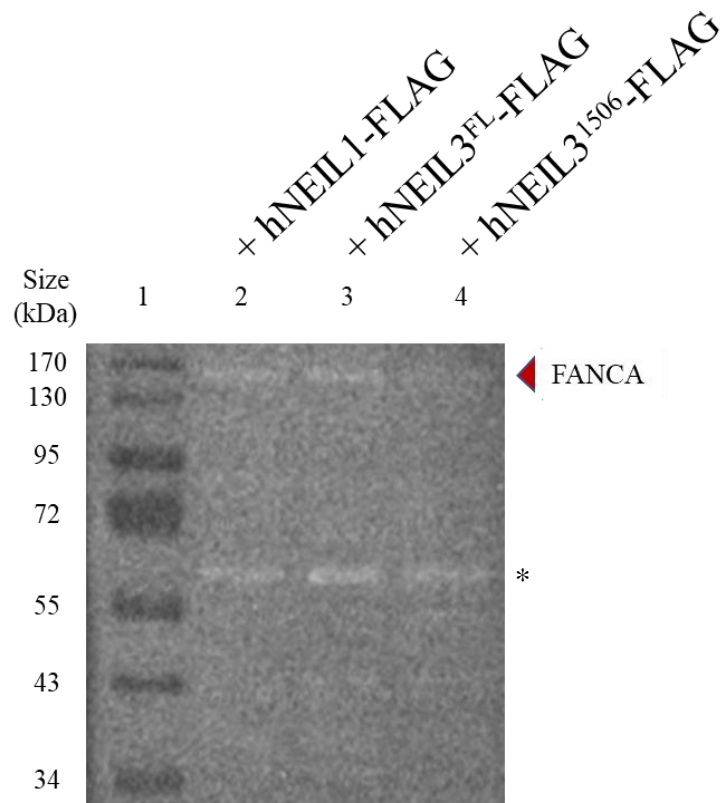


**D**

	Amplicon	Amplification Efficiency	C <sub>t</sub>	Mean ± SD Expression	
				Relative to <i>β-Actin</i>	Relative to <i>GAPDH</i>
<b>PD20</b>	<i>β-Actin</i>	105.37 %	27.66	1.00 ± 0.13	0.22 ± 0.03
		109.95 %	27.39		
	<i>GAPDH</i>	86.80 %	24.45	5.42 ± 4.26	1.20 ± 0.95
		120.92 %	26.26		
	<i>NEIL3</i>	109.51 %	30.23	0.16 ± 0.00	0.03 ± 0.00
		120.94 %	30.18		

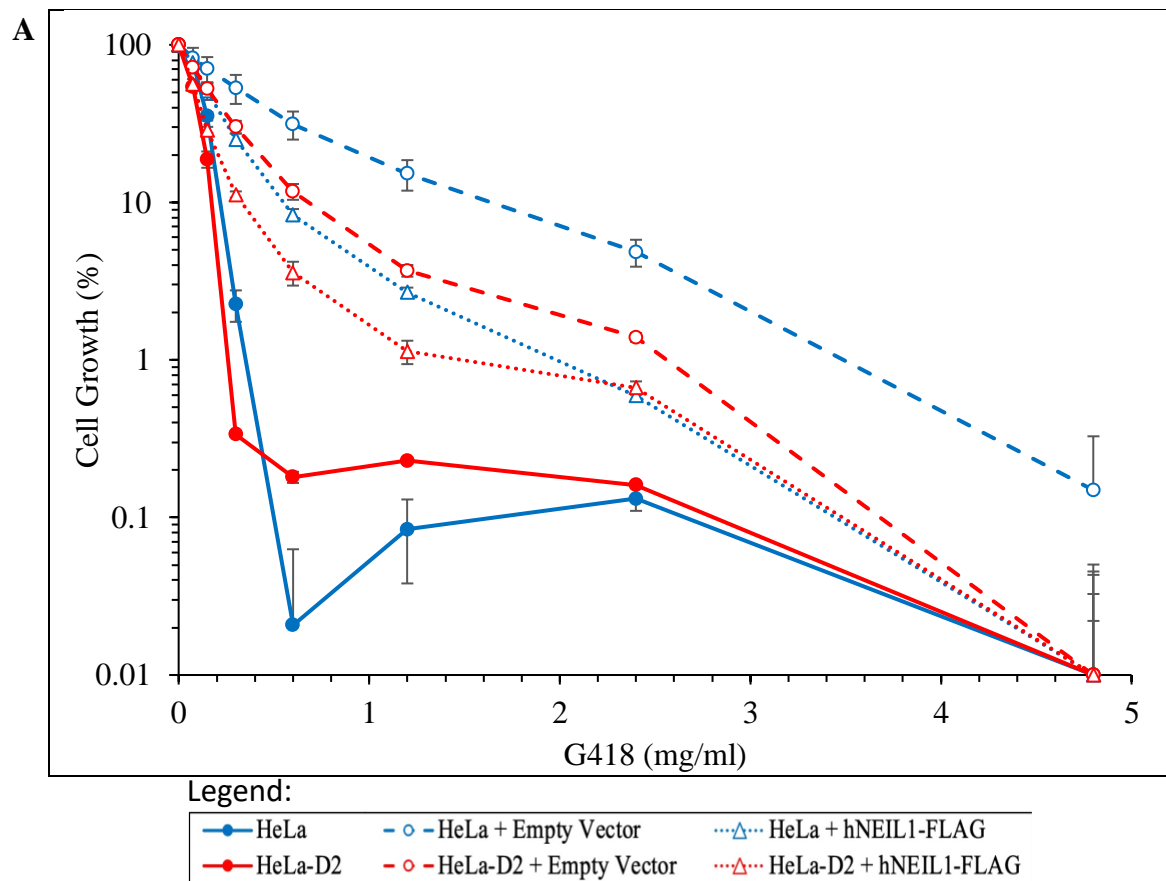
**Appendix Figure 5: Quantification of expression and melting curve of *β-Actin*, *GAPDH* and *NEIL3* from the cell line PD20 (FANCD2 deficient), by qRT-PCR.**

Melting curve of amplicons **A)** *β-Actin*, **B)** *GAPDH*, and **C)** *NEIL3* from triplicate technical repeats. **(D)** Best of two out of three quantified amplification efficiencies and cycle-thresholds (C<sub>t</sub>) from amplicons analysed in sections **A-C** and calculated amplicon expression relative to the cell's *β-Actin* or *GAPDH* amplification. Melting curves and quantified amplification efficiency and C<sub>t</sub> analysed through MJ OpticonMonitor analysis software version 3.1 (Bio-Rad). Protocol for qRT-PCR according to instruction with SensiFAST™ SYBR Lo-ROX kit (Bioline Meridian).



**Appendix Figure 6: Western blot of plasmid-transfected HSC-72-Corrected (FANCA expressing) cell extracts for FLAG-tag.**

Lane 1, protein ladder; lane 2, pcDNA3.1-hNEIL1-FLAG; lane 3, pcDNA3.1-hNEIL3<sup>FL</sup>-FLAG; lane 4, pcDNA3.1-hNEIL3<sup>1506</sup>-FLAG. Expected molecular weight: FANCA-FLAG, approximately 161 kDa; hNEIL3<sup>FL</sup>-FLAG, 69 kDa; hNEIL3<sup>1506</sup>-FLAG, 56 kDa; hNEIL1-FLAG, 44 kDa. (\*) Non-specific binding.

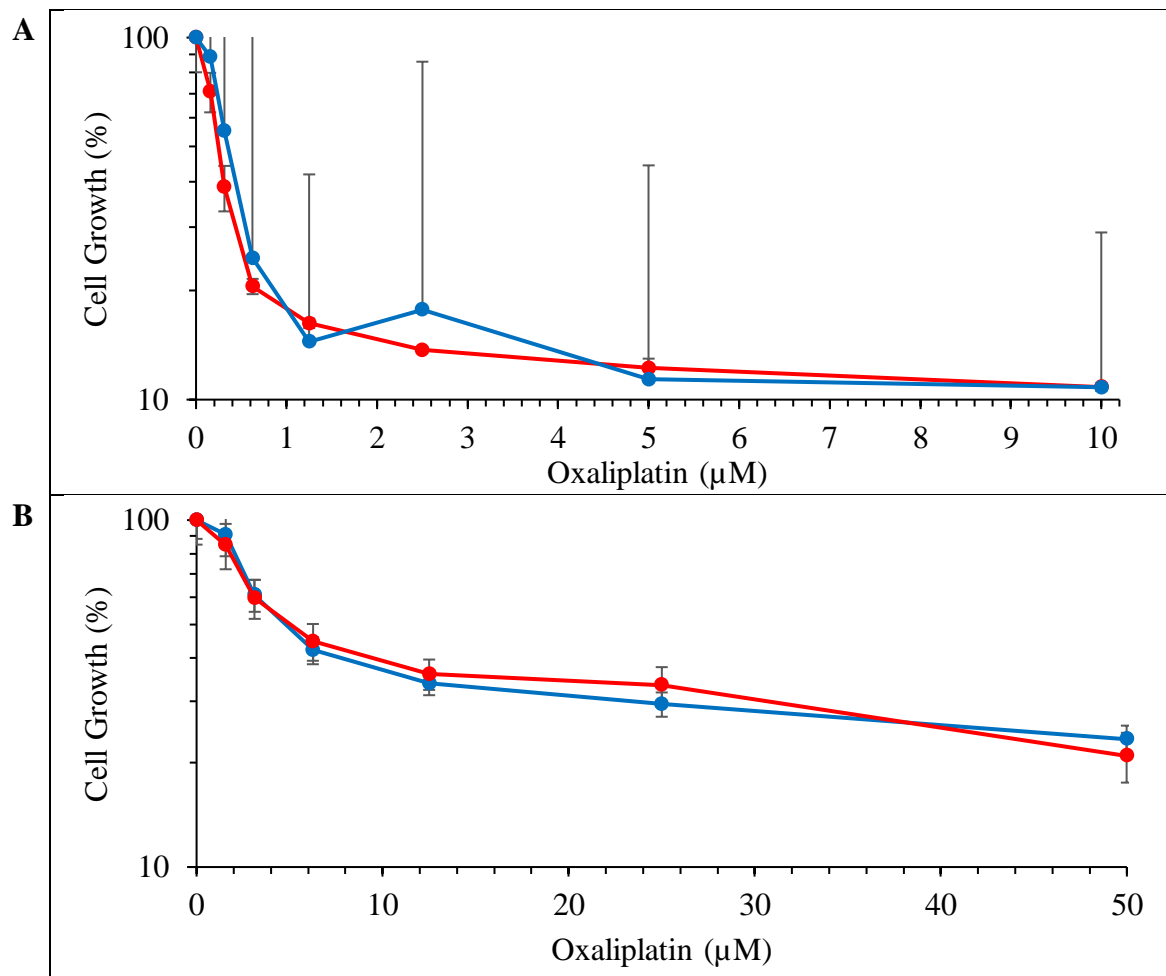


**B**

		IC <sub>50</sub> ± SD	Optimal Concentration for Antibiotic Selection for 168 h	Estimated Antibiotic Selection Concentration for 96 h
HeLa	Non-transfected	0.12 ± 0.00 mg/ml	0.6 mg/ml	1.8 mg/ml
	+ Empty Vector	0.31 ± 0.08 mg/ml	N/A	N/A
	+ hNEIL1-FLAG	0.15 ± 0.02 mg/ml	N/A	N/A
HeLa-D2	Non-transfected	0.08 ± 0.00 mg/ml	0.6 mg/ml	1.8 mg/ml
	+ Empty Vector	0.16 ± 0.02 mg/ml	N/A	N/A
	+ hNEIL1-FLAG	0.09 ± 0.01 mg/ml	N/A	N/A

**Appendix Figure 7: Growth inhibition and kill-curve of non-transfected and plasmid transfected HeLa (WT) and HeLa-D2 (FANCD2 deficient) cells, with antibiotic selector G418.**

**B)** IC<sub>50</sub> values for growth inhibition and optimal concentration values for antibiotic selection following treatment. Cells were non-transfected or transfected with empty vector or pcDNA3.1-hNEIL1-FLAG. 5 x 10<sup>2</sup> cells per well, incubated for 168 h with G418 (Gibco). Mean data was collected from triplicate technical and scientific repeats.



**C**

	IC <sub>50</sub> ± SD Values
HSC-72-Corrected	0.40 ± 0.11 µM
HSC-72	0.30 ± 0.07 µM
U2OS	3.87 ± 0.71 µM
U2OS-D2	4.93 ± 0.76 µM

**Appendix Figure 8: Growth inhibition of the FANCD2 deficient (red) and WT/Corrected (blue) cell lines (A) HSC-72/HSC-72-Corrected and (B) U2OS/U2OS-D2, following treatment with Oxaliplatin.**

**B)** IC<sub>50</sub> values for growth inhibition following treatment. HSC-72/HSC-72-Corrected, 1 x 10<sup>4</sup> cells per 96-well, incubated for 72 h. U2OS/U2OS-D2, 2 x 10<sup>3</sup> cells per 96-well, incubated for 72 h. Mean data was collected from triplicate technical repeats in (A) one or (B) three scientific repeats.

**A** hNEIL1-FLAG Forward Sanger-Sequence Result (From CMV\_fwd\_primer)  
 >461159601\_pcDNA31\_NEIL1\_CMVF\_pCDNA3\_A05  
 GAACCCACTGCTTACTGGCTTATCGAAAT **TAATACGACTCACTAATAGG**GAGACCCAAGCTGGCTAGCGTTTAAACGGGCC **CTAGAGCC**  
**CC**ATGCCTGAGGGCCCCGAGCTGCACCTGGCCAGCCAGTTTGTGAATGAGGCCTGCAGGGCGTGGTGTTCGGCGGCTGCGTGGAGAAG  
 TCCTCTGTCAGCCGCAACCCCTGAGGTGCCCTTTGAGAGCAGTGCCTACCGCATCTCAGCTTCAGCCCGCGGCAAGGAGCTGCGCTGATA  
 CTGAGCCCTCTGCTGGGGCCAGCCCCAACAGGAGCCACTGGCCCTGGTCTCCGCTTCGGCATGTCGGCTCTTTTCAGCTGGTGGCC  
 CGCGAGGAGCTGCCACGCCATGCCACCTGCGCTTTACACGGCCCCGCTGGCCCCCGGCTCGCCCTATGTTTCGTGGACATCCGCCGGT  
 TCGGCCGCTGGGACCTTGGGGGAAAGTGGCAGCCGGGCCCGGGCCCTGTGCTTGCAGGAGTACCAGAGTTCAGGGAGAATGTGTA  
 CGAAACCTAGCGGATAAGGCCTTTGACCGGCCATCTGCGAGGCCCTCTGGACCAGAGGTTCTTCAATGGCATTGGCAACTATCTGCGGG  
 CAGAGATCCTGTACCGGCTGAAGATCCCCCCTTTGAGAAGGCCCGCTCGGTCTGGAGGCCCTGCAGCAGCACAGGCCGAGCCCGGAG  
 CTGACCCTGAGCCAGAAGATAAGGACCAAGCTGCAGAATCCAGACCTGCTGGAGCTATGTCACCTAGTGCCTCAAGGAAGTGGTCCAGTT  
 GGGGGGCAAGGCTACGGGTCAGAGCGGGGAGGAGGACTTTGTGCTTTCAGCCTTCGAGCCTGGCTGCGCTGATGGCATGCCAGGCATGA  
 GCTCCCTGCAGGACCGGCATGGCCGTACCATCTGGTCCAGGGGATCCTGGACCCTGGACCCAAAGGGCGCAAGTCCCGCAAAAAG  
 AAATCAAGGCCACACAGCTGAGTCTGAGGACAGAGTGGAGGACGCTTTGCCTCAAGCAAGGCCCTTCCAGGACACGAAGGGCAA  
 AGAGAGACCTTCTAAGAGGACTGCAACCCAGCGGCTGAGGGGACCAGCCTCCAGCAGGACCCAGAAGCTCCACAGTGCCAAGAA  
 GGGGAGGAGGAAGGGGCGACAGGCAGCCTCTGGCCACTGCAGACCCCGGAAGGTCAAGGCTGA

**B** hNEIL1-FLAG Reverse Sanger-Sequence Result (From bGH\_rev\_primer)  
 >461159601\_pcDNA31\_NEIL1\_bGHR\_B05  
 GAGACCCAAGCTGGCTAGCGTTTAAACGGGCCCTCTAGAGCCACCATGCCTGAGGGCCCCGAGCTGCACCTGGCCAGCCAGTTTGTGAAT  
 GAGCCCTGCAGGGCGCTGGTGTTCGGCGGCTGCGTGGAGAAGTCCCTGTGTCAGCCGCAACCCCTGAGGTGCCCTTTGAGAGCAGTGCCTA  
 CCGCATCTCAGCTTCAGCCCGCGGCAAGGAGCTGCGCTGATACTGAGCCCTCTGCTGGGGCCAGCCCCAACAGGAGCCACTGGCCCT  
 GGTCTTCCGCTTCGGCATGTCGGCTCTTTTCAGCTGGTGCCTCGGAGGAGCTGCCACGCCATGCCACCTGCGCTTTTACACGGCCCCG  
 CCTGGCCCCGGCTCGCCTATGTTTCGTGGACATCCGCCGTTTCGGCCGCTGGGACCTTGGGGGAAAGTGGCAGCCGGGCCCGGGCC  
 TGTGCTTTCAGGAGTACCAGCAGTTTACGGGAGAATGTGCTACGAAACCTAGCGGATAAGGCCTTTGACCGGCCATCTGCGAGGCCCT  
 CTGGACCAGAGGTTCTTCAATGGCATTGGCAACTATCTGCGGGCAGAGATCTGTACCGGCTGAAGATCCCCCCTTTGAGAAGGCCCGCT  
 CGGTCTGGAGGCCCTGCAGCAGCACAGGCCGAGCCCGGAGCTGACCTGAGCCAGAAGATAAGGACCAAGCTGCAGAATCCAGACCTG  
 CTGGAGCTATGCTACTAGTGCCTCAAGGAAGTGGTCCAGTTGGGGGCAAGGCTACGGGTCAGAGAGCGGGGAGGAGGACTTTGCTGC  
 CTTTTCGAGCTGGCTGCGCTGCTATGGCATGCCAGGCATGAGCTCCCTGAGGACCGGCATGGCCGTACCATCTGGTTCCAGGGGGATCCT  
 GGACCCTGGACCCAAAGGGCGCAAGTCCCGCAAAAAGAAATCCAAGGCCACACAGCTGAGTCTGAGGACAGAGTGGAGGACGCTT  
 TGCCTCAAGCAAGGCCCTTCCAGGACACGAAGGGCAAGAGAGACCTTCTAAGAGGACTGCAACCCAGCGGCTGAGGGGACCAG  
 CCTCAGCAGGACCCAGAAGCTCCACAGTGCCTCAAGAAAGGGGAGGAGGAAGGGGCGACAGGCAGCCTCTGGCCACTGCAGACCCCG  
 AAGGTCAAGGCTGACATCCATCCTTGAACAGAGGGGACCTAGCCTCT **GACTACAAGGACGACGATGACAAGTGA****CCGGAAT****CA**  
 CCACACT

**C** hNEIL1-FLAG Overlapping Sanger-Sequence Result  
 GAACCCACTGCTTACTGGCTTATCGAAAT **TAATACGACTCACTAATAGG**GAGACCCAAGCTGGCTAGCGTTTAAACGGGCC **CTAGAGCC**  
**CC**ATGCCTGAGGGCCCCGAGCTGCACCTGGCCAGCCAGTTTGTGAATGAGGCCTGCAGGGCGTGGTGTTCGGCGGCTGCGTGGAGAAG  
 TCCTCTGTCAGCCGCAACCCCTGAGGTGCCCTTTGAGAGCAGTGCCTACCGCATCTCAGCTTCAGCCCGCGGCAAGGAGCTGCGCTGATA  
 CTGAGCCCTCTGCTGGGGCCAGCCCCAACAGGAGCCACTGGCCCTGGTCTCCGCTTCGGCATGTCGGCTCTTTTCAGCTGGTGGCC  
 CGCGAGGAGCTGCCACGCCATGCCACCTGCGCTTTTACACGGCCCCGCTGGCCCCCGGCTCGCCCTATGTTTCGTGGACATCCGCCGGT  
 TCGGCCGCTGGGACCTTGGGGGAAAGTGGCAGCCGGGCCCGGGCCCTGTGCTTGCAGGAGTACCAGCAGTTCAGGGAGAATGTGTA  
 CGAAACCTAGCGGATAAGGCCTTTGACCGGCCATCTGCGAGGCCCTCTGGACCAGAGGTTCTTCAATGGCATTGGCAACTATCTGCGGG  
 CAGAGATCCTGTACCGGCTGAAGATCCCCCCTTTGAGAAGGCCCGCTCGGTCTGGAGGCCCTGCAGCAGCACAGGCCGAGCCCGGAG  
 CTGACCTGAGCCAGAAGATAAGGACCAAGCTGCAGAATCCAGACCTGCTGGAGCTATGTCACCTAGTGCCTCAAGGAAGTGGTCCAGTT  
 GGGGGGCAAGGCTACGGGTCAGAGAGCGGGGAGGAGGACTTTGCTGCCTTTCGAGCCTGGCTGCGCTGCTATGGCATGCCAGGCATGA  
 GCTCCCTGCAGGACCGGCATGGCCGTACCATCTGGTCCAGGGGATCCTGGACCCTGGACCCAAAGGGCGCAAGTCCCGCAAAAAG  
 AAATCAAGGCCACACAGCTGAGTCTGAGGACAGAGTGGAGGACGCTTTGCCTCAAGCAAGGCCCTTCCAGGACACGAAGGGCAA  
 AGAGAGACCTTCTAAGAGGACTGCAACCCAGCGGCTGAGGGGACCAGCCTCCAGCAGGACCCAGAAGCTCCACAGTGCCAAGAA  
 GGGGAGGAGGAAGGGGCGACAGGCAGCCTCTGGCCACTGCAGACCCCGGAAGGTCAAGGCTGACATCCATCCTTGAACAGAGGGG  
 ACCTCAGCCTCT **GACTACAAGGACGACGATGACAAGTGA****CCGGAAT****CA**CCACACT

**Appendix Figure 9: Confirmation of pcDNA3.1-hNEIL1-FLAG through Sanger-sequencing.**

(A) Sequencing result with CMV forward primer; (B) sequencing result with bGH reverse primer; (C) overlap of sections A and B for the final sequenced result. Red highlight, T7 promoter sequence; green highlight, XbaI restriction digest site; grey highlight, Kozak consensus fragment; blue highlight, FLAG-tag; yellow highlight, EcoRI restriction digest site; red letters, sequence overlap.